SELECTIVE HYDROGENATION OF α,β-UNSATURATED ALDEHYDES AND BIOMASS PRODUCTS OVER SUPPORTED NOBLE METAL CATALYST

A THESIS

SUBMITTED TO THE

UNIVERSITY OF PUNE

FOR THE DEGREE OF

DOCTOR OF PHILOSOPHY

IN

CHEMISTRY

BY

SEEMALA BHOGESWARARAO

UNDER THE GUIDANCE OF

DR. D. SRINIVAS

CATALYSIS DIVISION

CSIR-NATIONAL CHEMICAL LABORATORY

PUNE – 411 008, INDIA

DECEMBER 2013

CERTIFICATE

This is to certify that the work incorporated in the thesis entitled **"Selective Hydrogenation of α,β-Unsaturated Aldehydes and Biomass Products over Supported Noble Metal Catalyst"** submitted by **Mr. Seemala Bhogeswararao,** to the University of Pune, for the degree of Doctor of Philosophy in Chemistry, was carried out by the candidate under my supervision at the Catalysis Division, CSIR-National Chemical Laboratory, Pune – 411 008, India. Such material as has been obtained from other sources has been duly acknowledged in the thesis. To the best of my knowledge, the present work or any part thereof has not been submitted to any other university for the award of any other degree or diploma.

Date: **Dr. D. Srinivas**

Place: Pune Research Guide

DECLARATION

I hereby declare that the work described in the thesis entitled "**Selective Hydrogenation of α,β-Unsaturated Aldehydes and Biomass Products over Supported Noble Metal Catalyst"** submitted for the degree of **Doctor of Philosophy** in **Chemistry** to the University of Pune, has been carried out by me at the Catalysis Division, CSIR-National Chemical Laboratory, Pune – 411 008, India, under the supervision of **Dr. D. Srinivas**. Such material as has been obtained from other sources has been duly acknowledged in this thesis. The work is original and has not been submitted in part or full by me for any other degree or diploma to this or any other university.

Date: **SEEMALA BHOGESWARARAO**

Place: Pune Research Scholar

.....dedicated to my

beloved parents

Acknowledgements

First of all, I would like to acknowledge my research guide, Dr. D. Srinivas, for his constant inspiration, invaluable guidance and constructive criticism which helped me a lot to focus my views in a proper perspective. I take this opportunity to express my intense reverence towards him for guiding me in the right direction throughout the course of this work. My deepest personal regards are due for him forever.

My heartfelt thanks are due to Dr. K. V. R. Chary, Dr. S. P. Mirajkar, Dr.T.Raja, Dr. K.R. Patil, Dr. Subhangi Umberkar, Dr. C. S. Gopinath, Dr. C.V.V. Satyanarayna, Dr. (Mrs.) S. S. Deshpande, Mr. R. K. Jha, Ms. Violet Samuel, Mr. Golap, Mr. Madhu, Mr. Milind and all other scientific and non-scientific staff for their valuable help and cooperation during my tenure as a research student.

I sincerely thank all my friends especially Jithendra, Rahul, Anuj, Mehejabeen, Joby, Unnikrishanan, Devadutta, Ravi, Bineesh, Pavan, Ajay, Narasimha, Hanumanth, Athul, Nishita, Rajesh, Srinivas, Ramesh, Edwin, Ashok, Laxmi and many friends who helped me during my research.

I am really thankful to my teachers, Prof. Syambabu, Dr. Subbarao, Prof. Jaya Prasad and Mr. Srinivas and my family members for their support, patience, encouragement and blessings.

It is indeed my privilege to thank the Director, CSIR-NCL and Chairman, Catalysis Division, CSIR-NCL, for giving me this opportunity and extending all possible infrastructural facilities at CSIR-NCL open for the research work.

Finally, I thank the Council of Scientific and Industrial Research, New Delhi for financial assistance.

Seemala Bhogeswararao

Table of Contents

List of Figures

List of Schemes

List of Tables

Chapter 1

General Introduction

1.1. Introduction

Addition of hydrogen to an organic molecule in presence of a catalyst is called catalytic hydrogenation. This addition followed by bond cleavage is termed as hydrogenolysis. Hydrogenation is the oldest and important process for production of bulk and fine chemicals. It is widely used in petrochemical process for various purifications methods e.g., selective reduction of trace amounts of acetylene in an ethylene stream, butene from butadiene stream, etc [1]. Hydrogenation is an exothermic reaction and the equilibrium usually lies far towards the hydrogenated product under most operating temperatures. Industrial hydrogenation requires a mean of limiting the temperature increase arising from the exothermic reaction. Higher temperature usually has a favourable effect on reaction rate, but may affect the selectivity and catalyst life unfavourably. Hydrogenation is influenced by a number of factors: (a) type of catalyst, (b) nature of solvent, (c) operating conditions, (d) purity of the starting chemicals, (e) reaction temperature, (f) H_2 pressure and (g) amount of catalyst. The influence of operating variables on selectivity is less straight forward but can often be linked to the effect of these and other variables on hydrogen availability at the catalyst surface. Hydrogenation can be carried out both in liquid- and gas-phases, but liquid-phase reactions are much common. In liquid-phase system, transport of hydrogen to catalyst surface is frequently the rate-limiting step. To react with substrate, hydrogen must move from gas to liquid-phase and then, to the solid catalyst surface. The concentration of hydrogen at the catalyst surface can vary widely and depends on the ratio of rate of hydrogen consumption to the rate of hydrogen supply and nature of the metal.

Catalytic hydrogenation is an important and widely investigated reaction in organic synthesis and in the manufacture of industrial chemicals. Cyclohexane, hexamethylene diamine (HMDA), toluene diamine (TDA), aniline and 1, 4-butanediol used in the production of polymers and plastics are prepared through hydrogenation processes. The indirect synthesis of hydrogen peroxide involves the step of hydrogenation of substituted anthraquinone to the corresponding hydroquinone. Sorbital employed in the manufacture of personal care items is produced via hydrogenation of glucose derived from corn starch [2]. In petroleum industry, hydrogenation is often the first step in the production of commodities such as gasoline. Hydrogenation is a vital step also in producing end products in fine chemicals and active pharmaceutical ingredients. Complete or partial hydrogenation of unsaturated fatty acids in vegetable oils producing margarine is a significant reaction in food industry. It is a crucial step also in upgradation of bio-oils / biocrudes leading to biofuels. In general, group VIII or group Ib/IIb metals in their pure state or in supported form are used as

catalysts in hydrogenation reactions. Although much understanding of the fundamentals and applications has been achieved, development of controlled and selective hydrogenation catalysts that operate at mild to moderate conditions is still a challenging task in this area of research. The effects of method of preparation, support-metal interactions, co-metals, additives, solvent etc., on the activity and selectivity of noble metal catalysts is yet to be fully understood. The work presented in this thesis addresses some of these aspects. Highly efficient, solid, supported noble metal catalysts have been prepared, characterized and investigated for chemoselective hydrogenation of two industrially relevant reactions viz., (1) hydrogenation of cinnamaldehyde (a representative α, β-unsaturated aldehyde) and (2) hydrogenation/hydrogenolysis/decarbonylation of furfural (a biomass-derived compound) to value-added chemicals.

Catalysis involving hydrogen directly or indirectly constitutes a very important part of modern developments in industrial catalysis. For example, much of petroleum refining may be regarded as a process for increasing H/C atomic ratio from 1.5-1.9 in the feedstocks to 1.8-2.1, needed more in transportation fuels. Production of hydrogen from coal, oil, or natural gas is in itself a major industrial process. Apart from the hydrogenation of nitrogen to ammonia and carbon monoxide to methanol, higher alcohols and hydrocarbons, hydrogenations and dehydrogenations form the basis of several other major processes in industries. Several processes in pharmaceuticals and fine chemicals are based on selective hydrogenation reactions. Table 1.1 lists a few industrial hydrogenation processes.

Table 1.1. Some industrial hydrogenation processes

S.No.	Reactant	Product	Catalyst	Temp. (°C)	Pressure (bar)
1	N_2	NH_3	Fe(111)	350	300
2	CO	CH_3OH	Cu/Zn/Al Oxides	250	50
3	Unsaturaed esters	Unsaturated alcohols	Cr/Cu Oxides	300	300
4	Benzene	Cyclehexane	Ni	80	30
5	Olefines/CO	Alcohols	Rh complex	80	20
6	Nitrobenzene	Aniline	Pd/C	80	70
7	Benzene	Cyclohexene	Rh(Zn)	80	10
8	Adiponitrile	Hexamethylene-diamine	Ni	100-130	30
9	Aldehydes	Alcohols	Cu/Cr oxides	160	60
10	Maleic anhydride	n-Butyrolactone	Cu/Cr Oxides	220	5

11	CO	Paraffin	Fe	300	60
12	Fat nitriles	Saturated amines	Ni	140	50
13	Phenol	Cyclohexanone	Ni	150-250	75-200
14	Oils	Unsaturated alcohols	Cu/Cr Oxides	200-300	100-300
15	Fats acids	Partially saturated acids	Cu/Cr Oxides	130-190	4
16	Diolefins/acetylene	Olefins	Pd	50-80	1-10
17	Dinitrotoluene	Diaminotoluene	Ni	100	50
18	Glucose	Sorbitol	Ni	140	170

1.1.1. Hydrogenation in Petrochemicals Sector

Catalyst plays an important role in the development of efficient processes for upgrading petroleum crude to chemical feedstocks and fuels such as gasoline, diesel, fuel oil, jet fuel and lubricants. The demand for petroleum refining catalyst has been increasing at 5.8% per year. More than 60% of petrochemical products and 90% of petrochemical processes are dependent on catalysts (National Research Council, 1992). The major catalytic hydrogenation processes in refining of petroleum crude are hydrotreating, hydrocracking and hydroisomerisation

1.1.1.1. Hydrotreating. It is a process that removes organic sulphur, nitrogen, oxygen and metals (Ni, V and Fe) from petroleum crudes at high hydrogen pressures. Hydrodesulfurization (HDS), hydrodenitrogenation (HDN), hydrodeoxygenation (HDO) and hydrodemetallization (HDM) are the reactions applied during the hydrotreating of heavy gas oil feedstocks containing various concentrations of organo sulfur, nitrogen and oxygen compounds and continued by hydrogenation of dialkenes, partial hydrogenation of alkenes and partial hydrogenation of polynuclear aromatics (Schemes 1.1 and 1.2). In hydrotreating process, no reduction in molecular size of the feedstock occurs, whereas in hydrorefining, the molecular weight of the feedstock is reduced up to 10%. In hydrocracking process, molecular size of the feed is reduced by 50% or more.

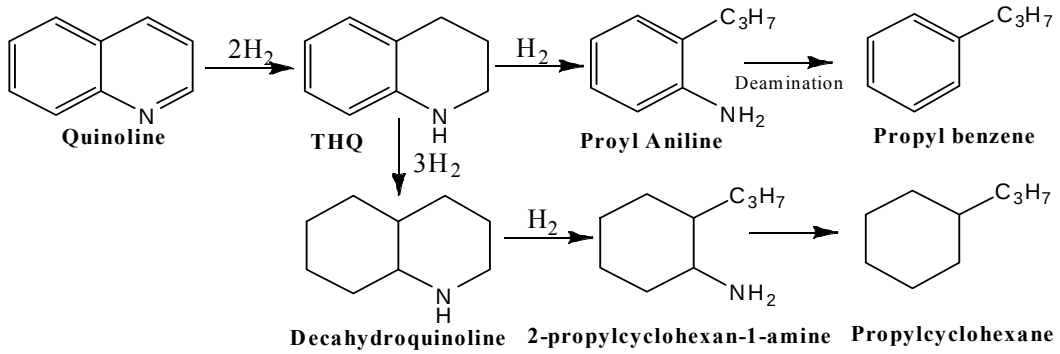

Scheme 1.1. Hydrodenitrogenation of quinoline to propylbenzene & propylcycloheaxane [3]

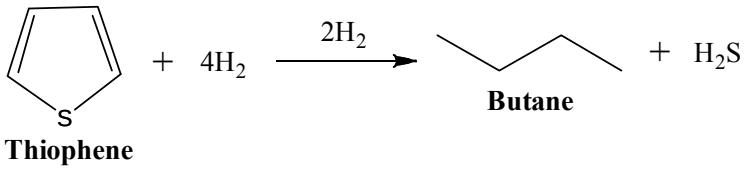

Scheme 1.2. Hydrodesulfurization of thiophene [4]

In a typical process for hydrotreating, the feed is first compressed and mixed with H_2 at 100 bar, following which it is preheated to about 350 °C. For hydrotreating, the most commonly used catalysts are sulfided CoMo and NiMo supported on γ-alumina. Promoters including boron, phosphorous, potassium and rare earth oxides may be added to lower the acidity of the catalyst and improve Mo sulfidability.

1.1.1.2. Hydrocracking. It is a process in which a low-value crude containing high percentage of polynuclear aromatics is simultaneously cracked and hydrogenated to produce high-value, low and middle distillates including gasoline and diesel fuel [5]. For this process the catalyst must be bi-functional, with acid sites to catalyze cracking reactions and active metal to catalyze hydrogenation. Hydrocracking of polynuclear aromatics has emerged as a route to production of diesel fuel, since it is necessary to reduce aromatic content to improve the quality of the fuel. The production of alkanes from the hydrogenation of the aromatics improves the cetane number, a measure of combustion efficiency for the diesel fuel. The hydrocracking catalysts have some designed parameters viz., (a) acidic strength, (b) hydrogenation activity and (c) surface area & porosity. Desirable reactions are naptha to LPG, light gas oil to gasoline and gas oil to Jet fuel.

1.1.1.3. Hydroisomerization. Light naptha from petroleum crude contains a small amount of butanes and high amount of n-pentanes and n-hexane. The octane number of these molecules, n-pentanes and n-hexane are 61.8 and 19, respectively. But their isomers 2-methylbutane and 2, 2-dimethylbutane have research octane numbers (RONs) of 99 and 89, respectively. So the fuel values could be increased by isomerizing the normal alkanes to the corresponding branched isomers, which then come under the gasoline pool [6]. Butane can be isomerized to the corresponding branched isomer, isobutene, which is then used for alkylating alkenes (Scheme. 1.3). Some H_2 is added to the reaction mixture to eliminate alkene coke precursors, but the reaction doesn't consume appreciable amounts of H_2. Because of the presence of H_2, this process is referred to as hydroisomerization. For this process, two types of catalysts are used to produce high RON alkanes: (1) highly active strong acids such as anhydrous $AlCl_3$ and (2) solid acids in combination with a transition metal e.g., Pt combined with Al_2O_3-SiO_2, zeolite such as mordenite and sulphated zirconia.

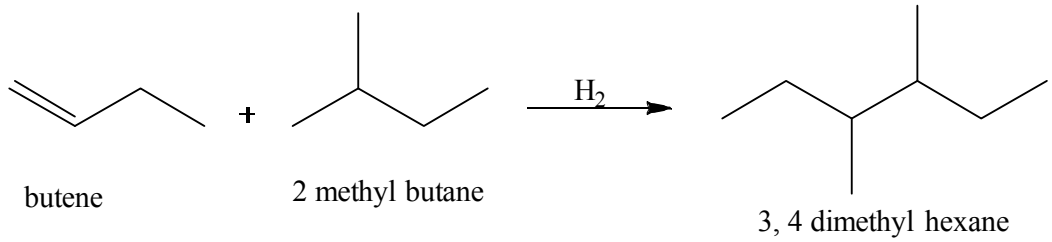

Scheme 1.3. Hydroisomerisation of butane and 2-methyl butane to 3, 4 dimethylhexane

1.1.2. Hydrogenation in Fine Chemicals Sector

Chemicals are classified into commodities, fine chemicals and speciality chemicals. Commodities are large-volume, low price and standardized chemicals produced in dedicated plants and used for large variety of applications. Petrochemicals, basic chemicals (ethylene, propylene, methanol, BTX, sulfuric acid, etc), heavy organics, monomers and some plastics come under commodities. Their prices are fully transparent and cyclic. Fine chemicals are complex, single, pure chemical substances. They are produced in limited quantities, less than 1000 metric tons per year. These are prepared using multipurpose plants by multistep batch chemicals and biotechnology processes. They are sold for more than $10 per kilogram. Speciality chemicals contain one or more fine chemicals as active ingredients. They are identified according to their performance properties, so that they are also called performance chemicals. They are usually sold under brand names and they should provide the product information. Some of the categories of speciality chemicals are adhesives, agrochemicals,

cleaning materials, cosmetic additives, construction chemicals, elastomers, flavours, food additives, fragrances, industrial gases, lubricants, polymers, surfactants, and textile auxiliaries. Catalytic hydrogenation in the fine chemicals industry is usually conducted with heterogeneous catalysts [7]. Selective catalytic hydrogenation of functional groups contained in organic molecules is one of the most useful and environmentally acceptable routes available for organic synthesis. In pharmaceutical and in the fine chemicals industry, many chemical conversions require stoichiometric amounts of reagents, and they generate large amounts of waste products [8]. This is in contrast to the production of bulk chemicals which mostly depend on catalysis. This difference can be explained by the higher complexity of pharmaceuticals and fine chemicals which makes catalysis more demanding. The driving forces for the development of new processes may be summarized as: (1) improved process economics, (2) advantage through superior technology, (3) quality of the product improvement, and (4) environmental safety. The e-factor was introduced by Sheldon and defined as a kilogram by-product by kilogram product from the reaction mixture (Table 1.2). Selective hydrogenation of carbon-carbon double bond and triple bond groups [9], nitro groups [10], carbonyl carbons [11] and aromatic groups [12] produces useful systems particular in flavour and fragrance chemicals and in fine chemicals and pharmaceutical products.

Table 1.2. The e-factor in various industries

S.No	Industry	Product (tonnage)	e-Factor
1	Oil refining	10^6 - 10^8	< 0.1
2	Bulk chemicals	10^4 - 10^6	1 to 5
3	Fine chemicals	10^2 - 10^4	5 to 50
4	Pharmaceuticals	10^1 - 10^3	> 100

1.2. Selectivity in Catalytic Hydrogenation

Selectivity is an important issue in catalytic hydrogenation. It is defined as the ratio of the amount of desired products obtained to the sum of the amounts of all the products formed in a particular reaction. Hydrogenation reactions are is classified into three types [13].

- ❖ Chemoselective hydrogenation
- ❖ Regioselective hydrogenation
- ❖ Stereoselective hydrogenation

Chemoselective hydrogenation of some of the reducible functionalities has been an important aspect in the field of heterogeneous catalysis**.** It is important when one functional group has to be hydrogenated in a molecule which has more than one functional groups present in it [14].

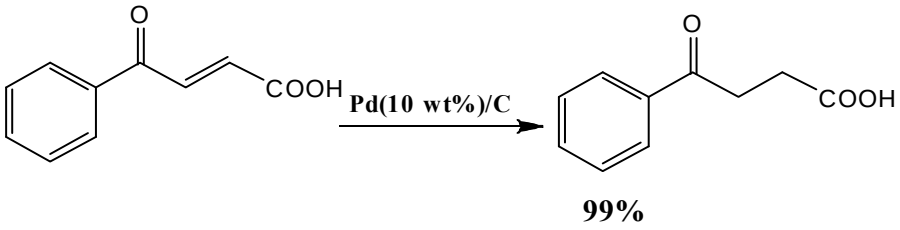

Scheme 1.4. Chemoselective hydrogenation of 4-oxo-4-phenylbut-2-enoic acid to 4-oxo-4-phenylbutanoic acid

Regioselective hydrogenation refers to hydrogenation of one functional group in presence of the same functional group present at a different position in an organic molecule [15].

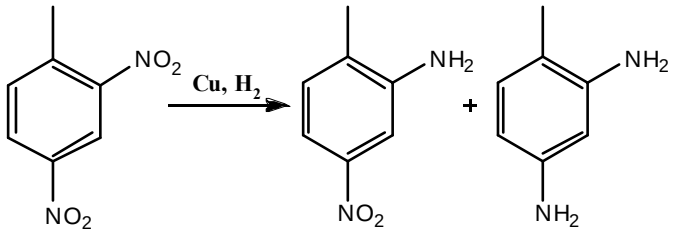

Scheme 1.5. Regioselective hydrogenation of 1-methyl-2, 4-dinitrobenzene

Stereoselective hydrogenation refers to formation of selectively one stereoisomer in presence of another by hydrogenation of the organic substrate. If the stereoisomers are enantiomers then such a transformation is called enanatioselective hydrogenation [16].

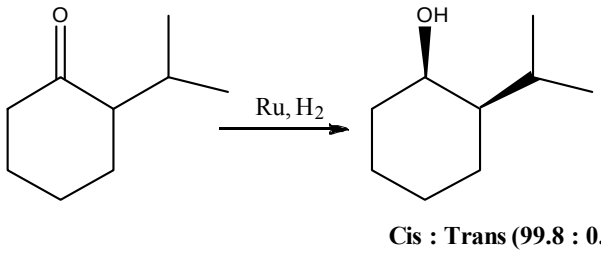

Scheme 1.6. Stereoselective hydrogenation of 2-isopropylcyclohexane-1-one

1.3. Supported Group VIII Metal Catalysts for Hydrogenation Reactions

Ni, Ru, Rh, Pd, Os, Ir and Pt are used as catalysts in hydrogenation reactions. Of these, Pd, Pt, and Ni have been used widely. Rh and Ru make excellent hydrogenation catalysts but their merits are not yet widely appreciated. Ir and Os have found less use. Noble metal catalysts are extremely important in large scale processes. These catalysts are divided into two categories: unsupported and supported [17]. The major issues with unsupported catalysts are synthesis, their characterization and sintering of the metals. Some of these problems were solved by supported catalysts. Supporting is a convenient technique for obtaining a large metal surface area which can control the sintering process during use or regeneration. Supported metal oxide catalysts consist of at least one active metal oxide component dispersed on the surface of a support [17]. The active oxides are often transition metal oxides, while the support may typically be alumina (preferentially γ- Al_2O_3), SiO_2, TiO_2, CeO_2, ZrO_2 or carbon.

Supported Pd is a versatile catalyst that can be used in hydrogenation (e.g., acetylene to olefins), dehydrogenation, decarbonylation, C-C bond coupling reactions and also in cracking reactions [18]. In 2010, palladium catalysed C-C coupling reactions were recognised by the Noble Prize in Chemistry. Supported noble metal catalysts were prepared by three methods. 1) dry-impregnation, 2) wet-impregnation and 3) ion-exchange methods. Supported palladium catalysts are particularly the most active catalyst in hydrogenation reaction than other noble and non-noble metals [19]. Pd is active in its metallic state so that before addition to reaction mixture, catalysts should be reduced under a flow of H_2 gas at 200 °C or by using reducing agents like $NaBH_4$, HCHO and HN=NH (hydrazine).

Supported platinum metal catalysts are highly suited for selective hydrogenation of various functional groups, hydrogenolysis and decarbonylation reactions [20]. Platinum can work under mild reaction conditions like low temperature and pressure. By using supported platinum catalysts, selectivity can be altered by changing supports and poisoning of some of the active sites or planes of the metal.

Supported nickel oxides require high temperatures for reduction than unsupported nickel oxides. Nickel is a preferred catalyst for oil hydrogenation reactions because the required products should be partially hydrogenated followed by isomerization [21]. Nickel is more active and selective when it was in partially reduced form than in completely reduced form. Recently, some reports have explained that the particle size of nickel plays a significant role in product selectivity [22].

In the case of supported metal catalysts, choice of support is more critical to prepare catalysts with high metal surface area. The supported catalysts have good resistance to sintering/poisoning of the active metal. The supports can also influence the product selectivity in organic reactions. Some of the issues with the supported metal catalysts include: metal agglomeration, metal particle size, metal dispersion and resistance to poisoning.

Metal dispersion (M_D) is one of the fundamental properties of supported metal catalysts. It can be defined as the ratio of number of active metal atoms exposed at the surface ($\mathbf{N_S}$) to the total number of metal atoms in a given amount of catalysts ($\mathbf{N_T}$) [23].

$$\mathbf{M_D = N_S/N_T}$$

Spillover phenomenon occurs due to dissociation of active species followed by transportation from one phase (donor) to another phase (acceptor). The process was first detected by Khoobiar [24] and observed on Pd and Pt metals. The major spillover phenomenon is the hydrogen spillover on the supports. Hydrogen atoms are formed by dissociation of molecular hydrogen on metal particle which then, migrate to another phase, hydrogen acceptor in the catalyst. Catalysts, which are highly active for initiating hydrogen spillover showed the best activities in hydrogenation reactions [25]. Promoters and co catalysts showed positive effect on hydrogen spillover by varying the degree of contacting between the initiating and hydrogen acceptor phases. They act as bridge between the two components of the catalysts facilitating hydrogen migration e.g., Pt-WO_3 system decreases the energy barrier to hydrogen spillover [26]. Spillover also depends on the nature of acceptor sites. In case of Al_2O_3 and SiO_2, it was found that the concentration support holds hydrogen closely matches with the surface hydroxyl groups. It infers that surface hydroxyl groups associated with acceptor sites for hydrogen on these supports showed higher hydrogen spillover.

The term support-metal interactions was introduced first at 1978 to explain the drastic changes in chemisorption properties of Group VIII noble metals. Particularly, these types of interactions are observed when the metal is supported on reducible catalysts (e.g., TiO_2, CeO_2, etc). Support-metal interactions can occur in different ways: (1) oxide support can invade the metal surface covering some portion of metal and generating separate active sites which can increase the catalytic activity. (2) Alternatively, metal spreads to increase its coverage of the oxide and importantly these metals interact directly with the reduced support cations. Support-metal interactions showed favourable results in a few reactions, e.g., selective reduction of trienes to dienes in fats and oils and hydrogenation of carbonyl groups [27, 28].

Promoter is a substance which is not catalytically active but improves the catalyst performance and enhances the selectivity of the desired product in the reaction [29]. It affects the electronic properties of catalysts and supported active metal phases, suppresses the undesired active sites on the catalysts further controlling the selectivity of the final product, controls the poisoning of the active sites and controls the growth of active catalyst particles.

1.4. CeO_2 and CeO_2-ZrO_2

Cerium with a $4f^2 5d^0 6s^2$ electronic configuration can exhibit both the +3 and +4 oxidation states; intermediate oxides can also be formed (Ce_2O_3). Thermodynamics data explain that cerium is unstable in the presence of oxygen and CeO_2 and Ce_2O_3 are easily formed. For example, cerium metal reacts easily with oxygen to form different oxides at about 10^{-93} atm of oxygen at 300 °C. CeO_2 crystallises in the fluorite structure, which is named after the mineral calcium fluoride. It has a face centred unit cell (fcc) with space group of Fm3m.

Reduction of CeO_2 results in the removal of O^{-2} ions from the ceria lattice generating anion vacant sites,

$$4Ce^{+4} + O^{-2} \longrightarrow 4Ce^{+4} + 2e^-/\square + 1/2O_2 \longrightarrow 2Ce^{+4} + 2Ce^{+3} + 1/2O_2 + \square$$

where the empty box represents the anion vacant site (O^{-2}). Two of the Ce^{4+} ions are reduced to Ce^{3+} ions. Ceria reduces at elevated temperatures and low oxygen pressures and forms oxygen-deficient non-stoichiometric oxides which upon cooling organise into highly ordered fluorite-related superstructures with complex stoichiometries (CeO_x; $1.714 < x < 2$).

Over the past several years, cerium oxide and CeO_2-containing materials have been widely studied as catalysts, supports and electronic promoters of heterogeneous catalytic reactions. For the last three decades, CeO_2 is in use in the automotive pollution control. The development of the Three-Way Catalysts (TWC) was determined by the need to simultaneously convert the hydrocarbons, CO and NO_x present in the automotive exhaust to H_2O, CO_2 and N_2. Ceria is also used to remove SO_x from the fluidized catalytic cracking (FCC) process [30] and several oxidation reactions [31]. CeO_2 is known to influence the dispersion of supported metals, promote the water gas shift and steam reforming reactions, increase the thermal stability of the support, promote noble metal reduction and oxygen store and release form surface and bulk vacancies and inter-metallic M-CeO_2 compounds.

The reductive behaviour of CeO_2 and their relations to catalysis have been studied widely by using different techniques viz., chemisorption [32], temperature-programmed

reduction (TPR) [33], electron spin resonance (ESR) [34], X-ray photoelectron spectroscopy (XPS) [35], extended X-ray absorption fine structure (EXAFS) [36, 37] and X-ray diffraction (XRD) [38]. Particularly, CeO_2 type reducible oxides are used as supports and additives for noble metal supported catalysts because it keeps the metal in more metallic nature and forms strong support-metal interactions (SMSI). For hydrogenation reactions and C-C coupling reactions, metal should be in pure metallic form.

In recent years, a special attention has been focused on the synthesis of CeO_2 structurally doped with ZrO_2. These materials showed enhanced thermal [39], redox [40] and catalytic properties. CeO_2-ZrO_2 materials are used widely in oxygen storage and in TWC technology. The causes for the enhanced redox properties and mechanism of the reduction process of CeO_2-ZrO_2 are still a matter of debate [41]. Incorporation of zirconia into ceria lattice enhances the reducibility of bulk ceria because of enhanced mobile lattice oxygen availability for reduction. Due to the facile redox properties, CeO_2-ZrO_2 mixed oxides find a wide variety of applications in catalysis.

Table 1.3. Classification of crystal phases of CeO_2-ZrO_2 binary system

Phase	Composition (Ce mol%)	Tetragonality (c/a)	Space group
Monoclinic (m)	0-10	-	$P2_1/C$
Tetragonal (t)	10-30	> 1	$P4_2/nmc$
Tetragonal (t')	30-65	> 1	$P4_2/nmc$
Tetragonal (t'')	65-80	1	$P4_2/nmc$
Cubic	80-100	1	Fm3m

As shown in Table 1.3, the phase diagram shows a monophase region of monoclinic (m) symmetry for CeO_2 in molar contents less than 10%, while the ceria content higher than 80% exhibits a cubic (c) phase [42]. At in between compositions (ceria molar ratio = 10-80%), the nature of CeO_2-ZrO_2 phase diagram is still unclear. In this region, indeed a number of stable and metastable phases of tetragonal symmetry are observed [43]. The three tetragonal phases are designated as t, t' and t'' and distinguished on the basis of powder XRD pattern and Raman characterization [44]. These phases can be prepared at high temperature by solid state synthesis. Upon cooling, the t-form, which is a stable one, can be formed through a diffusional phase decomposition. While the t'- form is obtained through a diffusionless transition and it is metastable. The t''-form is also a metastable phase and it is intermediate between t' and c. The t" phase shows no tetragonality of the cation sublattice and

it exhibits an oxygen displacement from ideal fluorite sites. It is often referred to as a cubic phase because its XRD pattern is indexed to the cubic Fm3m symmetry [45]. This is due to the fact that the cation sublattice prevalently generates the XRD pattern.

1.5. Selective Hydrogenation of α, β-Unsaturated Aldehydes

Selective hydrogenation of α, β-unsaturated carbonyl compounds is an important step in fine chemicals and flavour & fragrance chemistry [46]. In this study cinnamaldehyde is chosen as a representative α, β-unsaturated aldehyde. It is the main component of cassia (~90%) and ceylon cinnamon bark oils (~75%). It is present in smaller quantities in many other essential oils. Particularly, these products are used as intermediates for the synthesis of a few drugs in pharmaceuticals. The activity and the selectivity of the catalysts depend on the type of metal, support and additives [47]. Selective hydrogenation of olefin group is easier than carbonyl group because thermodynamics favour the C=C hydrogenation. So that most of the research work has been focussed on process for production of unsaturated alcohols. In homogenous procedures, selective hydrogenation of α, β-unsaturated aldehydes to unsaturated alcohols is carried out by using metal hydrides (Scheme 1.7). In these processes, a large amount of waste is formed which is environmentally hazardous. Moreover, hydride chemicals are difficult to handle compared to heterogeneous catalysts.

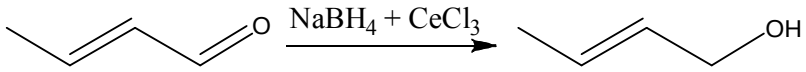

Scheme 1.7. Hydrogenation of crotonaldehyde to crotyl alcohol

Gallezot and Richard [47] published a detailed review explaining the factors influencing the activity and selectivity of catalysts in hydrogenation of α, β-unsaturated aldehydes. Hydrogenation of these compounds produces a variety of products (Scheme 1.8). 1, 2 Addition of hydrogen gives unsaturated alcohols; 3, 4-addition gives the saturated aldehyde; 1, 4-addition yields the enolic form which isomerizes into a saturated aldehyde. A consequent hydrogenation of C=C and C=O gives rise to saturated alcohols. In a few cases, unsaturated alcohols isomerize into saturated aldehydes in presence of a $Rh/AlPO_4$ catalyst [48]. Hydrogenation of α, β-unsaturated carbonyl compounds on metal surfaces occurs via Horiuti-Polyani mechanism involving di-$\sigma_{C=O}$ η^2, di-$\sigma_{C=C}$ η^2, or di-π η^2, (η^4) adsorbed states. From the theoretical studies of semiempirical Huckel calculations, Delbecq and Sautet [49] explained the adsorption of various α, β-unsaturated aldehydes (acrolein, crotonaldehyde, and cinnamaldehyde) on Pt and Pd crystal faces. According to their results, the mode of molecule

adsorption depends upon the nature of the active metal and the type of exposed plane. For example, di-σ form is preferred on Pt(111), a planar η^4 one on Pd(111) and Pt(100), and a $\pi_{C=C}$ one on Pt(110) and on the steps of Pt(111).

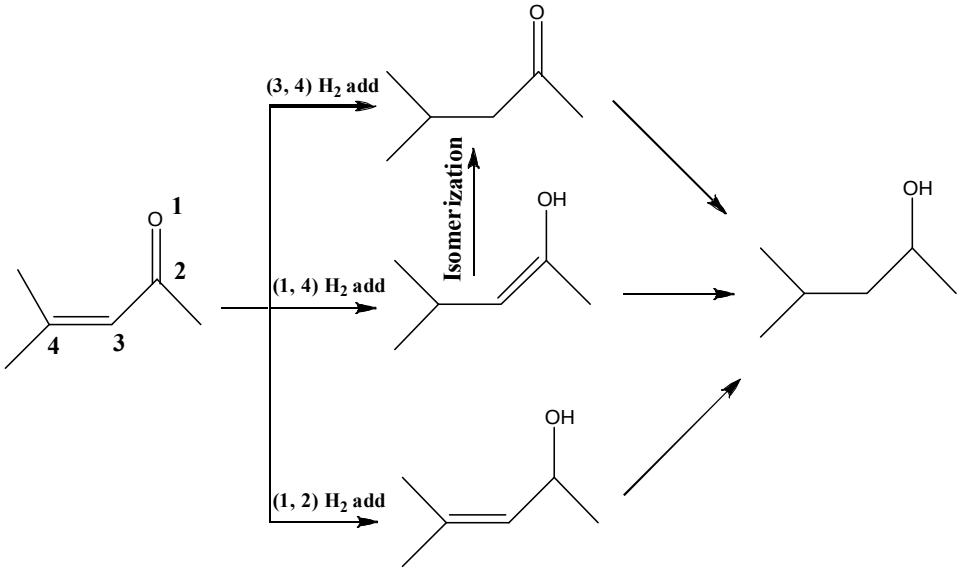

Scheme 1.8. Hydrogenation products of α, β-unsaturated aldehyde

The selectivity to unsaturated alcohols can be enhanced by the following factors:

- Selective adsorption of C=O bond on the catalyst surface compared to C=C bond or decreasing the binding energy of C=C bond by way of increasing the repulsive four electronic interactions with metal. This can happen when a substituent is present on C=C bond or by extended d-orbital containing metals (e.g., Os or Ir).
- Presence of Lewis-acid sites on the surface which could activate the carbonyl group
- Increasing the electron density on the metal by interaction with a support or ligand, and
- Higher abundance of (111) plane.

1.5.1. Influence of Nature of Metal

Selective hydrogenation of unsaturated aldehydes to unsaturated alcohols depends mainly on the nature of the metal. Delbecq and Sautet [49] explained based on theoretical studies that the metal selectivity is rationalized in terms of their d-band width. The larger the d-band width, stronger would be the four electron repulsive interactions with C=C bond and lower would be the probability of adsorption. The experimental results were well correlated with the d-band values. The d-band width of some metal increases in the order: Pd < Pt < Ir, Os. Palladium is highly selective for C=C group due to the preferred adsorption mode of conjugated (C=C) system on metal is η^4 which result in saturated aldehydes. Iridium and

osmium are rather selective; rhodium, and nickel are unselective; platinum, ruthenium, and cobalt are moderately selective [50].

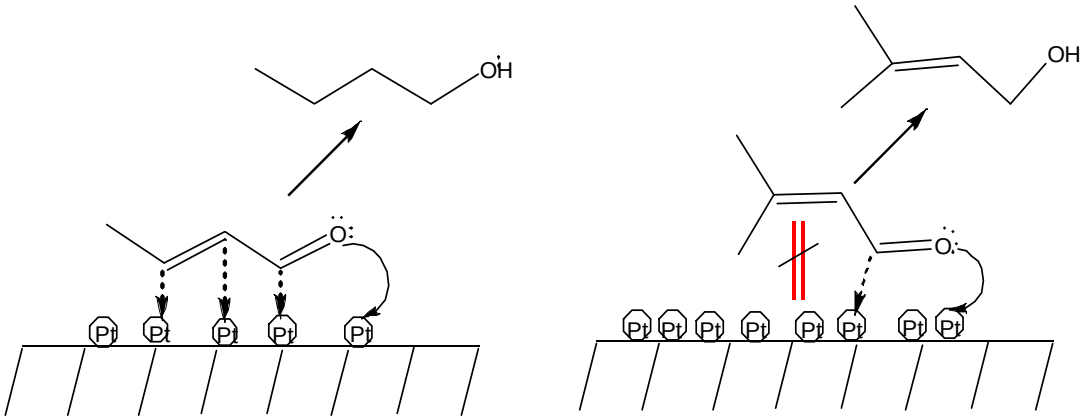

Fig. 1.1. Steric effect on hydrogenation of crotanaldehyde and 3-methyl crotanaldehyde

1.5.2. Steric Effects

Hydrogenation of crotanaldehyde and 3-methylcrotonaldehyde was conducted on Pt (111) surface [51]. In the case of 3-methylcrotanaldehyde, C=C hydrogenation decreased while the hydrogenation of C=O was unaltered. As a consequence higher apparent selectivity for C=O was observed by way of hindering adsorption of C=C due to presence of substituent at olefinic group (Fig. 1.1). In case of crotanaldehyde, hydrogenation took place at both C=C and C=O positions. Hydrogenation of 3-methylcrotonaldehyde was conducted also on Pt (111) and (110) planes. While Pt(111) mainly yielded unsaturated alcohols, Pt(110) resulted in saturated aldehydes and saturated alcohols at 80 °C. The close-packed structure of (111) plane surface induces steric hindrance for the methyl groups and as a consequence less adsorption of the C=C bond. Thus, the molecule is activated preferentially through the C=O group on Pt(111) surface. On the other hand, Pt (110) surface removes the steric hindrance and enables the activation of whole conjugated system and leads to formation of saturated aldehydes. Galvagno et al [52, 53] showed the affect of larger size (18 nm) ruthenium particles on selective synthesis of unsaturated alcohol. As the particle size increases the selectivity was also increased towards unsaturated alcohols.

1.5.3. Effect of Bimetal

Large number of studies has been reported on bimetallic (A-B) catalysts for selective hydrogenation reactions (Table 1.4). If the second metal (B) is more electropositive then, it favours the C=O hydrogenation. The electropositive metal B acts as an electron-donor ligand that increases the electron density on the first metal (A), thus decreasing the binding energies

of the C=C bond on metal surfaces and favouring the hydrogenation of the C=O with respect to the C=C bond.

Table 1.4. Effect of metals on selective synthesis of unsaturated alcohols

S. No	Metal	Second metal	Substrate	Selectivity	Ref
1	Pt	Fe	Cinnamaldehyde	85%	55
2	Pt	Co	Cinnamaldehyde	90%	56
3	Pt	Sn	Citral	60%	57
4	Pt	Sn	Crotonaldehyde	70%	58
5	Pt	Sn	Cinnamaldehyde	75%	59
6	Pt	Sn	Acrolein	60%	59
7	Pt	Ru	Cinnamaldehyde	80%	60
8	Pt	Sn	Furfural	80%	61
9	Pt	Ge	Cinnamaldehyde	64%	62
10	Pt	Ni	Crotonaldehyde	62%	63
11	Ru	Sn	Cinnamaldehyde	90%	64
12	Ru	Sn, Fe, Ge, Zn, Sb	Acrolein, 2-methyl propenal, 2-butenal, 3-methylbutenal.	70%	65
	Ru	Co	Cinnamaldehyde	64.5%	66
13	Rh	Sn	Citral	96%	67
14	Ni	Cu	Crotonaldehye	54%	68
15	Ni	Cu	Crotonaldehye	52%	69
16	Ag	Cd, Mn, La	Crotonaldehye	84%	70
17	Ag	Mn	Crotonaldehye	71.8%	70
18	Pt	-	Cinnamaldehyde	95.2%	73
19	Ru	-	CA	60%	74
20	Ir	Fe, Ge	Cirtal	95% (Fe), 100 (Ge)%	75
21	Co	Titania	CA	80%	76
22	Ir	-	Crotonaldehye	58%	77
23	Ru	-	Acorelin	75%	78

1.5.4. Electronic Effects of Supports

The selectivity of unsaturated alcohols from unsaturated aldehydes depends upon the mode of adsorption of molecule (either C=C or C=O) on the surfaces and electronic structure of the metal surface. The electronic structure of the metal can be affected by electron donating species which are directly interacting with the surface. From theoretical studies, it was concluded that higher electron density on metal particles increases the four electronic repulsive interactions with C=C group and also favours the back bonding interaction with the carbonyl group though π^*_{CO} orbital. Finally, it favours the C=O hydrogenation. Supports act as a macro-ligand interacting with the small metal particles [54]. In this case supports are acting as base molecules to donate electron to metal particles. Pt supported on graphite catalysts was highly selective for unsaturated alcohols than Pt/C (activated carbon) catalyst [54]. In presence of graphite support, the lattice was expanded due to the electron transfer taking place from support to the antibonding orbitals of the metal clusters [55]. The higher selectivity on graphite catalysts was attributed to higher electron density on the metal particles which cause decreasing probability of adsorption of C=C bond and hydrogenation.

1.5.5. Effects of Poisons on the Active Site

Selective poisoning of undesired sites which favour saturated aldehydes may suppress the hydrogenation of C=C group. Those active sites can be poisoned by using additives or other metals. In the case of crotanaldehyde hydrogenation on Cu/Al_2O_3 catalysts [56], absence of sulfur additive favours 1-butanol as a selective product whereas addition of thiophene alters the product selectivity towards to crotylalcohol. It was revealed that thiophene adsorption suppresses the undesired active sites which are favourable to C=C hydrogenation.

1.6. Lignocellulosic Biomass and Its Components

In recent years, the conversion of lignocellulosic biomass to value-added chemicals by heterogeneous catalysts has attracted renewed attention due to its environmental, economic, and strategic advantages. Depending on the type of biomass, biofuels are classified into two categories: a) First Generation Biofuel and b) Second Generation Biofuel [57].

The sources of first generation biofuels are sugarcane, wheat, sugar beet, corn starch, molasses and vegetable oils. Sugars present in biomass are fermented to produce bio-ethanol, an alcohol fuel which can be used directly in a fuel cell to produce electricity or serve as an additive to gasoline. Ethanol fuel is the most common biofuel worldwide. Ethanol can be used in petrol engines as a replacement for gasoline. It can be mixed with gasoline to any

percentage. Most existing car petrol engines can run on blends of up to 15% bio-ethanol with petroleum/gasoline. Ethanol has lower energy density than of gasoline so that it takes more fuel to produce the same amount of work. An advantage of ethanol is that it has higher octane rating than ethanol-free gasoline, which allows an increase of an engine's compression ratio for increased thermal efficiency. In high-altitude locations, some states mandate a mix of gasoline and ethanol as a winter oxidizer to reduce atmospheric pollution emissions. However, utilizing food-based resource for fuel production aggravates food shortage problem [57].

The sources of second generation biofuels are non-food-based biomass such as agricultural and municipality wastages. Mostly, it consists of lignocellulosic biomass which is not edible. From lignocellulosic biomass, large variety chemicals could be produced by various procedures. Due to technological issues, the alternative economical production of second generation biofuel is not at achieved completely. These issues are mainly due to chemical inertness and rigidity of lignocellulosic biomass. Lignocellulose biomass yields four different fractions; extractives (the wood extractives are fatty acids, resin acids, waxes and terpenes), cellulose, hemicellulose and lignin [58].

Cellulose. It is the world's largest organic raw material resource and it represents a huge reservoir of renewable carbon with an annual production estimated to 7.5 x 10^{10} tons [59]. Therefore, the catalytic conversion of cellulose plays a principal role in the production of a variety of valuable chemicals for further bio-refinery procedures. Due to the insolubility of cellulose, it needs to be hydrolyzed into water-soluble saccharides including oligomers and glucose in the first step, and subsequently converted to sugar alcohols and other chemicals through hydrogenation and/or hydrogenolysis (Scheme 1.9). [60]. In all these processes, the catalytic depolymerization of cellulose to glucose is a pre-requisite step from which transportation fuels and chemical platforms are then produced. Cellulose has been reported to be transformed into polyols in the presence of hydrogen over a supported noble metal catalyst such as Pt and Ru [61].

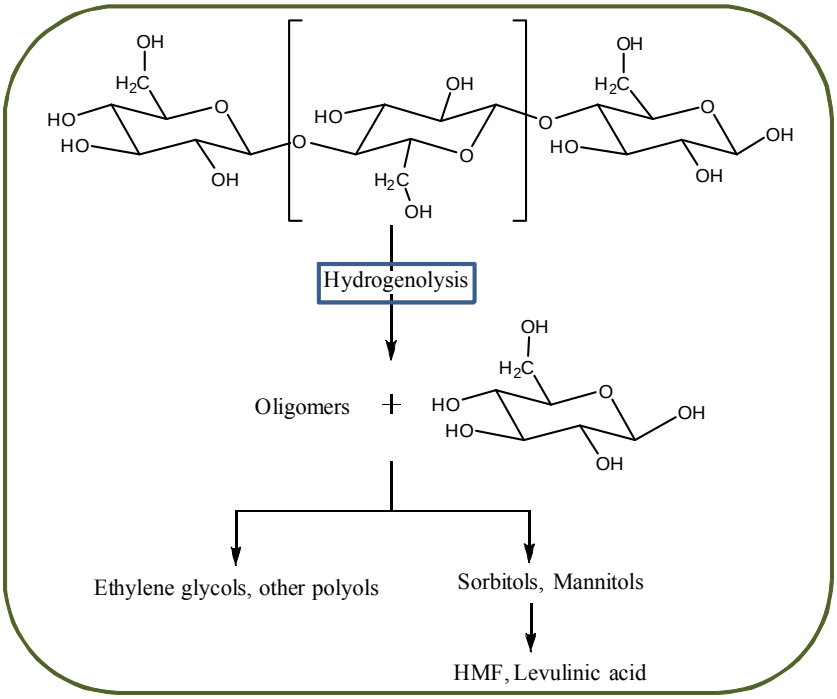

Scheme 1.9. Conversion of cellulose to polyols, HMF and levulinic acid

Hemicellulose. It is a mixture of polysaccharides containing xylose, arabinose, glucose, galactose, mannose, and other sugars, and is typically the second-most-abundant component of biomass, after cellulose. The hemicelluloses biomass contains mainly C5 and C6 sugars and the C5/C6 ratio always depends upon the nature of biomass source.

Lignin. It is second only to polysaccharides in natural abundance, contributing 24–33% and 19–28%, respectively, to dry wood weights of normal softwoods and temperate-zone hardwoods. It is also defined as an amorphous, polyphenolic material arising from enzymatic dehydrogenative polymerization of three phenylpropanoid monomers, namely, coniferyl alcohol, sinapyl alcohol and p-coumaryl alcohol (Fig 1.2). Normal softwood lignins are usually referred as guaiacyl lignins because the structural elements are derived principally from coniferyl alcohol (>90%), with the remainder consisting mainly of p-coumaryl alcohol-type units. Normal hardwood lignins, termed guaiacyl–syringyl lignins, are composed of coniferyl alcohol and sinapyl alcohol-type units in varying ratios. In hardwood lignins, the methoxyl content per phenylpropanoid unit is typically in the range 1.2–1.5 [62]. Grass lignins are also classified as guaiacyl–syringyl lignins. However, unlike hardwood lignins, grass lignins additionally contain small but significant amounts of structural elements derived from p-coumaryl alcohol. Grass lignins also contain p-coumaric, hydroxycinnamic, and ferulic acid residues attached to the lignin through ester and ether linkages [63].

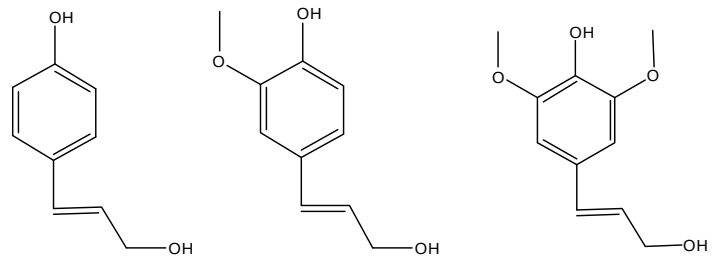

Fig. 1.2. Components of lignin

1.7. Furfural and Methods of Its Production

The only way to produce furfural (FAL) is acid catalyzed digestion of pentosan sugars from biomass (Scheme 1.10). Furfural is one of the most common industrial chemicals derived from the lignocellulose biomass, with an annual production volume of more than 200,000 tons [64]. At first in 1831, J. Dobereiner isolated a yellow oily substance when he treated carbohydrates with H_2SO_4 and MnO_2 [65]. After that, the same substance with molecular formula $C_5H_4O_2$ was prepared by G. Fownes by acid digestion and named furfural. Furfural is produced by two methods: low and high temperature processes. Most of the commercial units follow the low temperature process (<190 °C). Depending on the pentosan content, the final yield of furfural is always below 50% in these processes. The first process for production of furfural was started in 1921 by the Quaker Oats Company. In this process, dried oat hulls were mixed with aqueous sulfuric acid, maintaining the concentration of oat hulls as 0.02 wt%. After 5 h, the reaction is complete and the acid residue is separated into spent liquor and digested biomass [66]. After 50 years, Quacker Oats Company has developed a continuous process for production of furfural, with a full scale continuous plant at Belle Glade, Florida. The central part of this process was a brick-lined horizontal reactor which was fed with moisturized raw material. Admission of superheated steam and dilute sulfuric acid brought the contents to 184 °C. The Quaker Oats continuous process produced furfural with the same yield as the batch process, but without continuous steam stripping and with a fivefold decrease in residence time. This plant was operated for more than 30 years after that it was shut down because the cost of raw materials, labour, and maintenance given furfural production in the USA unprofitable. Other continuous process is Esher Wyss process [67]. In this process, continuous charge and discharge of the raw material and wide distribution of residence time causes the dramatic yield loss as compared to the other process. Hydrogenation and oxidation processes of furfural produce chemicals which are useful starting material in various industries (Scheme 1.11).

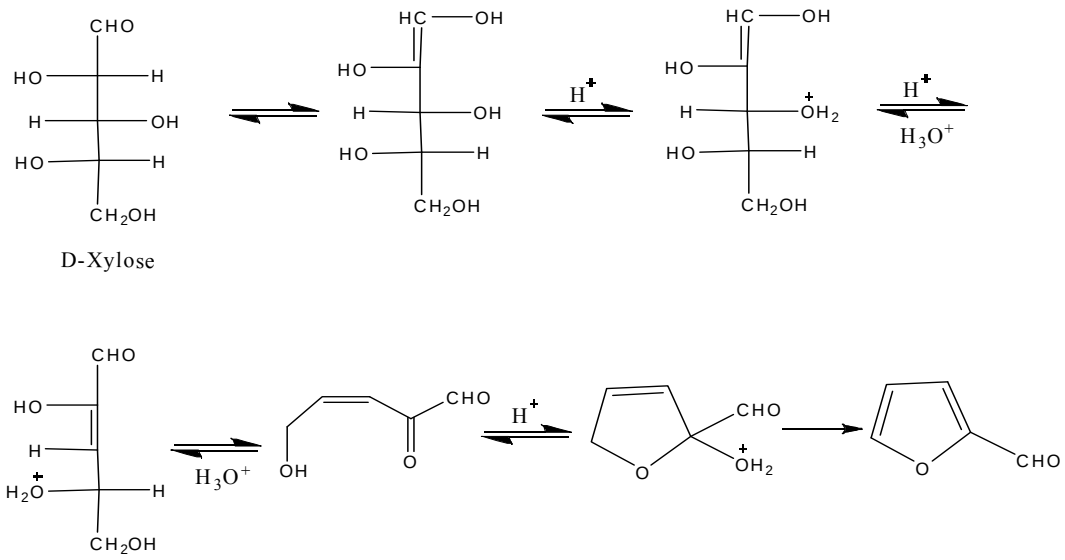

Scheme 1.10. Xylose to furfural reaction

Rosenlew Process [68]. This is also a continuous process for production of furfural and better than Esher Wyss process. It has a column type reactor. Raw material is charged at the top and discharged at the bottom, but the raw material is not mixed by fluidization. The narrow residence time favours the better furfural yields in this process. Both Rosenlew and Esher Wyss process were optimized without using the external acids (sulphuric acid). Reaction was catalyzed by carboxylic acids which were auto catalytically formed during the reaction.

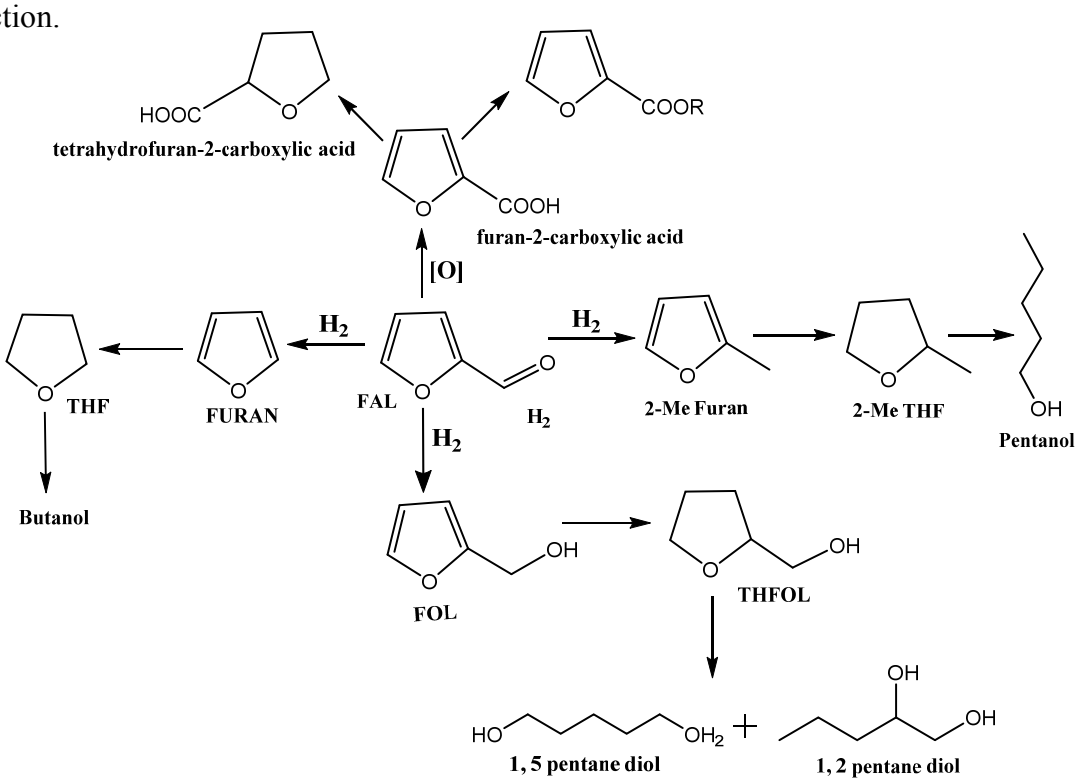

Scheme 1.11. Furfural to value added chemicals

Suprayield Process [69]. This process is operated at higher temperature and pressure conditions. By gradual decompression of reactor at higher temperature, the reaction mixture is boiled and continuously transferred to the vapour phase and in this manner furfural is removed from the reaction mixture by stripping. Superior yields (70%) are obtained in this process.

Half of the amount of furfural is converted to furfuryl alcohols and the remaining is used as a selective solvent in the refining of lubricating oils. In that, furfural is used as an extracting agent in petroleum industry for aromatics, polar components, mercaptans and other chemicals. It is also used in the synthesis of phenol-furfural resins which are stronger than phenol-formaldehyde (PF) resins [70]. To decrease the dependence of PF resins on formaldehyde, and their dangerous formaldehyde emissions, phenolic–furfural (PFu) resins have been developed [71]. PFu is a reactive solvent and excellent wetting agent for making of abrasive wheels, brake linings and refractory products for the steel industry. It is the feedstock of furan, methylfuran, acetylfuran, furfurylamine, and furoic acid. All these are oxygen contained heterocycles. Furfural contained crop guard is selective in suppressing parasitic nematodes. Crop guard reacts with the cuticle of the nematode. In this way nematodes are immobilized and destroyed. Crop guard finds application for the cultivation of tomatoes, groundnuts, peppers, and maize [72].

1.8. Chemicals Derived from Furfural

1.8.1. Furfuryl alcohol

Furfuryl alcohol (FOL) is made up of hydroxyl methyl group and furan ring. It is also known as 2-furancarbinol and 2-furylmethanol. The commercial catalyst used in FAL hydrogenation is a Cr_2O_3 promoted Cu-containing catalyst. FOL can be prepared either by vapour-phase or liquid-phase reaction. In vapour-phase, FAL is hydrogenated to FOL at 1 bar hydrogen pressure. In industries, the vapour-phase hydrogenation process is most widely employed. But, in this process of hydrogenation requires high molar ratio of H_2/furfural, so that large amounts of H_2 must be circulated. Hydrogenation of furfural in the liquid phase was first reported by Quaker Oats Company on Ni supported MgO catalyst [73]. By using Ni supported catalysts, furan ring hydrogenation also takes place so that to prevent the hydrogenation of the furan ring, copper chromium catalyst was applied at temperatures between 100 - 160 °C and H_2 pressures of 100 - 200 bar. Under these conditions furfuryl alcohol yields of 95–98% can be obtained in a solvent-free batch process. The selectivity of copper chromite catalyzed hydrogenation was further increased by addition of CaO as an additive. It controls the formation of resinification and etherification reactions. These type of

side reactions normally occur above 175 °C but in presence of CaO, these side reactions are controlled without loss in the furfuryl alcohol yield [74]. Due to environmental considerations and costs associated with chromium salts, chromium-free Cu hydrogenation catalysts have been developed. $CuFe/Al_2O_3$ and Cu/ZnO or MgO proved to be efficient catalysts [75]. Vapour-phase hydrogenation of furfural on copper chromite based catalysts was studied first time in 1927 at the temperature 140-150 °C [76] by Du Pont de Nemours. This catalyst deactivated after certain time on stream, so that the temperature of the catalyst bed was increased to 155 and 180 °C. At this temperature furfural produced not only the hydrogenation products but also the hydrogenolysis (methylfuran) products. By changing the catalysts to Cu on $Na_2O.xSiO_2$, instead of using copper chromite catalysts this problem was solved [77]. Sodium silicate lowers the hydrogenolysis product selectivity and increases the hydrogenation product selectivity up to 99% in the temperature range 135-175 °C. Pt catalysts on various supports have been reported for the vapour-phase hydrogenation of furfural [78]. Fig. 1.3 represents the process diagram of furfuryl alcohol production. Furfural is vaporised in a steam of hydrogen in a tubular vaporizer at 120 °C (A). After demisting (B), this stream is superheated before it enters the oil-heated multitubular reactor (D). The liquid furfural from the demister pad is recovered in tank C. After passage through the reactor, furfural conversion exceeds 99 %. The crude furfuryl alcohol is condensed from the reactor effluent and collected in tank (E). The hydrogen stream is passed through another demister (F) before it is recycled to the vaporizer (A). Some of the hydrogen is continuously vented as a bleed stream to prevent accumulation of impurities. The crude furfuryl alcohol from tank (E) is reheated and distilled in a vacuum column (G) to obtain furfuryl alcohol with a purity of more than 99%. The bottom fraction of the vacuum column consists of high-boiling oligomers, whereas water and methyl furan are withdrawn from the top of the column.

Furfuryl alcohol plays a major role in the production of foundary sand binders. For the last three decades, it has been extensively used to produce high quality cores and molds for metal casting. It finds application in corrosion-resistant fiber-reinforced plastics, in corrosion-resistant cements and mortars, in wood protection [79, 80], as reactive solvent for phenolic resins in the refractory industry, in paint stripper and cleaning compound formulation, as chemical building block for ranitidine type drug synthesis, as viscosity reducer for epoxy resins, and as chemical feedstock for tetrahydrofurfuryl alcohol and 3,4-dihydro- 2H-pyran.

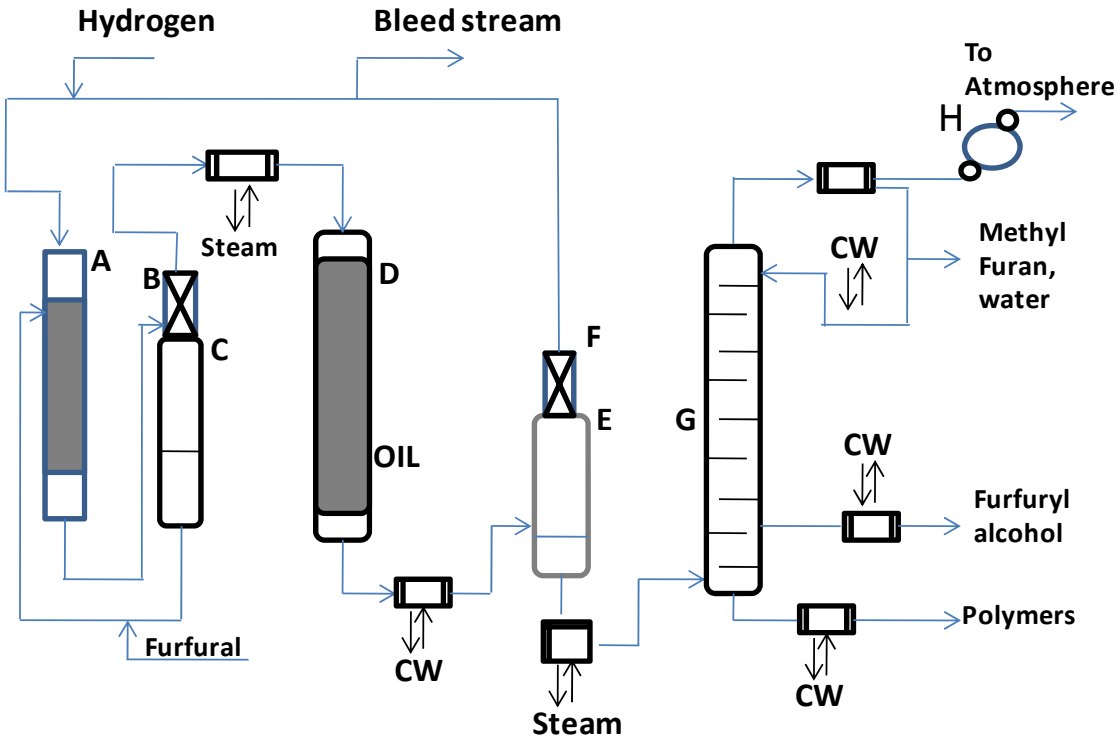

Fig. 1.3. Schematic diagram for furfural to furfuryl alcohol production

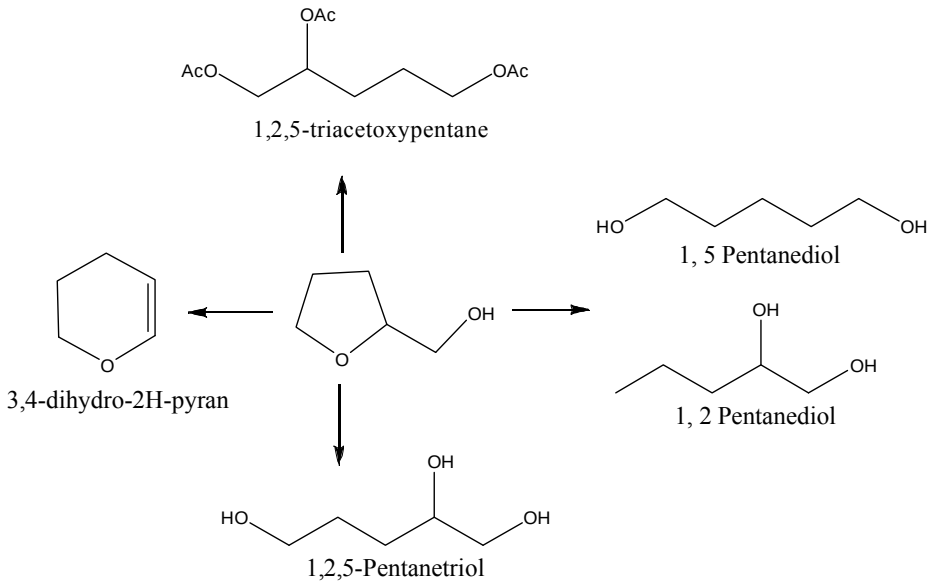

Scheme 1.12. Tetrahydrofurfuryl alcohols to value-added chemicals

1.8.2. Tetrahydrofurfuryl alcohol

Tetrahydrofurfuryl alcohol (THFOL) can be produced directly from furfural or from furfuryl alcohol. Supported Ni catalysts are preferred for this reaction. Nickel chromite catalysts were used for the production of THFOL from furfural in the liquid-phase in industries but the yields were only moderate (ca. 65%) [81]. With Raney Ni, THFOL is formed quite selectively from furfural, but excessive operating pressures and temperatures are needed (250 bar H_2, 150 °C) [82].

THFOL is known as a green solvent and it can be used as high-boiling solvent for dyes, printing inks, pesticides and herbicides, as paint-stripping agent, industrial cleaner and reactive diluent for epoxy resins. It is also used as intermediate chemical for the synthesis of disinfectant and antimetabolite drug. The main application of THFOL is to synthesize speciality chemicals such as 3, 4-dihydro-2H-pyran and tetrahydrofurfurylamine (Scheme 1.12).

1.8.3. Furan

Furan can be produced from decarbonylation of furfural on Pd supported catalysts [83] (Scheme 1.13). In 1959, Du Pont disclosed a route for synthesis of furan from furfural on Pd based catalysts without applying steam. Furfural is decomposed into furan and CO on Pd metal surfaces. In most of those methods, additives such as alkali metal carbonates have been used for decarbonylation of furfural on supported Pd catalysts. Due to the basic nature of the support, resinification of furfural was observed [84]. To control these side products, metal acetates were used as additives to increase the yield of furan. The Pd-catalyzed decarbonylation can also be performed in the vapour phase [85]. In a typical example, furfural is fed to Pd(0.3 wt%) on Al_2O_3 with a space velocity of furfural (WHSV) of 230 h^{-1} and with furfural/H_2 molar ratio close to one. Furan yield of 95% is obtained at 300 °C. Typical productivities of 10–15 kg of furan per gram of Pd can be reached before the catalyst needs to be regenerated. By using supported Pt and Rh catalysts these productivities can be increased [86]. Furan can also be produced by oxidation of 1, 3-butadiene over copper catalyst (Scheme 1.13) [87, 88]. It is a colourless liquid and highly volatile liquid with a boiling point of close to room temperature. It is used as a starting material for many speciality chemicals (Scheme 1.14).

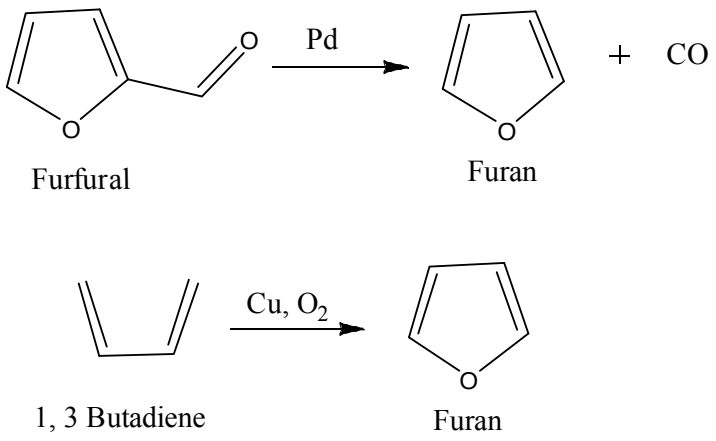

Scheme 1.13. Production of furan from furfural and 1, 3 butadiene

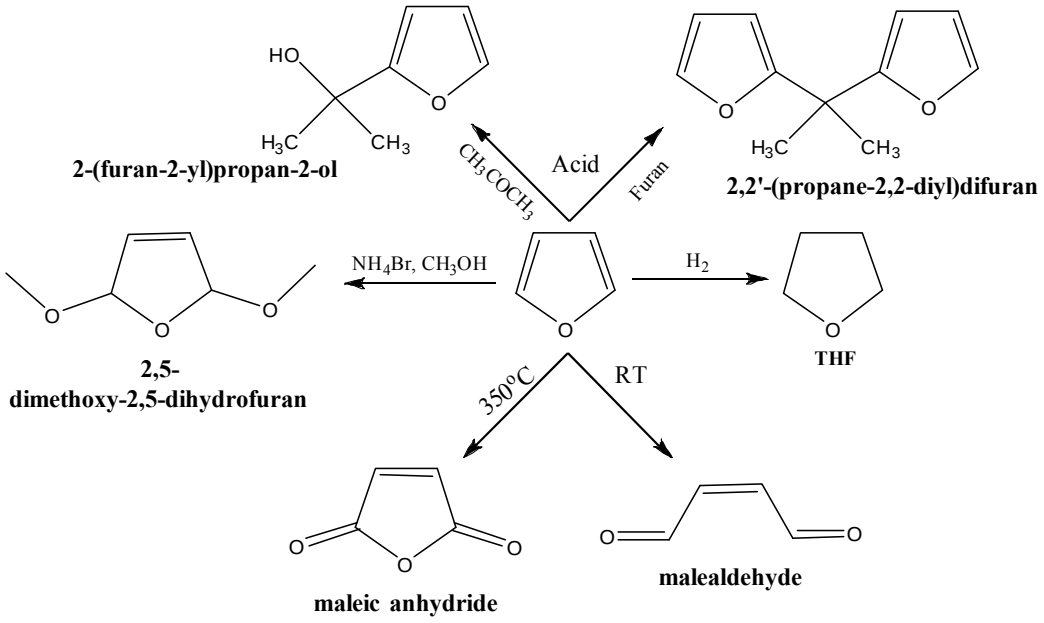

Scheme 1.14. Furan to value added chemicals

Furan is the important chemical for production of tetrahydrofuran (THF). It is also used in preparation of speciality chemicals like as 2, 5-dimethoxy-2, 5-dihydrofuran, 2, 2-difurylpropane, 2, 2-di(tetrahydrofurfuryl) propane, and pyrrole derivatives (Scheme 1.14).

1.8.4. Tetrahydrofuran

Tetrahydrofuran (THF) is an important starting chemical for a wide range of applications. About two hundred thousand tonnes of tetrahydrofuran are produced annually. THF is produced by various methods including Reppe process [89], butadiene acetoxylation process [90, 91], propylene oxide process [92] and maleic anhydride hydrogenation [93, 94].

Its production through pentose derived furfural [95] is highly attractive. In this process, furfural is the starting chemical for THF. Furfural to THF is a two step synthesis process. In the first step, furfural is decarbonylated to form furan, which in the second step is the hydrogenated to yield THF (Scheme 1.15).

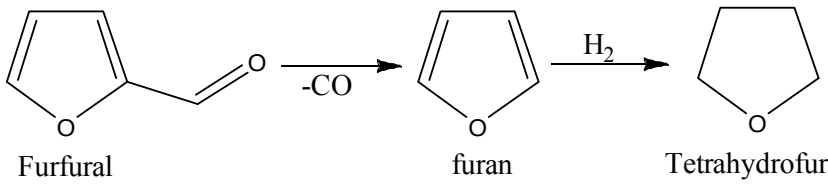

Scheme 1.15. Production of THF from furfural

THF is also used as a chemical intermediate in the manufacture of lysine, vitamin C, lubricants, dispersing agents and to obtain tetrahydrofurfuryl alcohol, among other applications [96].

1.9. Scope and Objective of the Present Work

The main objective of this work is to develop efficient and stable catalysts for selective hydrogenation of cinnamaldehyde (a representative α, β-unsaturated aldehyde) and furfural (a biomass-derived chemical) to value-added chemicals. As mentioned before, the structure and electronic properties of the metal can be tuned either by means of the support or additives. In this study, CeO_2-ZrO_2 which shows versatile applications in environmental catalysis is chosen as a support. Alkali is used as an additive/promoter. Pd, Pt and Ni are chosen as active metals for hydrogenation. In the case of Ni, a small quantity of Pt or Pd was also added as a second metal to promote the catalytic activity and selectivity of Ni. The influence of reaction parameters, composition of the support, type of the metal, promoter/additive, solvent, structural and textural features of the metal on the hydrogenation activity is investigated, for the first time. In reactions with fufural, other than hydrogenation, decarbonylation and hydrogenolysis/deoxygenation can also occur. One of the objective of this study to investigate the influence of reaction conditions, type of metal and support on the selectivity of these reactions with furfural as a reactant.

1.10. Organization of Thesis

The thesis is divided into seven chapters including **Chapter 1** on general introduction. **Chapter 2** describes the synthesis methodology of the catalysts and basic principle behind the characterization techniques used in this study. CeO_2, ZrO_2, CeO_2-ZrO_2 and Al_2O_3–supported Pt, Pd, Ni and Pt/Pd promoted Ni catalysts were prepared by impregnation method.

They were characterized by various physicochemical techniques including X-ray diffraction (XRD), N_2 adsorption–desorption, high resolution transmission electron microscopy (HRTEM), X-ray photoelectron spectroscopy (ESCA), Fourier-transform infrared spectroscopy (FTIR), temperature programmed desorption (TPD), diffused reflectance Fourier transform infrared (DRIFT) spectroscopy using NH_3 and pyridine as probe molecules, temperature programmed reduction (TPR) and chemisorption.

Chapter 3 describes the selective hydrogenation of cinnamaldehyde (a representative α,β-unsaturated aldehyde) to cinnamyl alcohols over Pt supported on CeO_2-ZrO_2 catalysts at 25 °C. Alkali addition (NaOH) enhanced the performance of the catalyst. The activity of this catalyst is superior to the hither to known catalysts for this reaction. Acidity of the support (due to the presence of ZrO_2 component) and higher metal dispersion and electron density at Pt (due to CeO_2 component) are responsible for the superior catalytic activity of Pt supported on CeO_2-ZrO_2 composite. Influence of reaction parameters, support, solvent and additive on catalytic activity is investigated in this chapter.

Chapter 4 investigates the hydrogenation activity of CeO_2, ZrO_2, CeO_2-ZrO_2-supported Pd(2 wt%) catalysts for liquid-phase hydrogenation of cinnamaldehyde. The Pd catalysts of the present study are selective for hydrogenation of C=C group in cinnamaldehyde. Support composition has a marked effect on the selectivity of the product. Support with CeO_2 : ZrO_2 = 1 : 1 molar composition exhibits superior performance. It is interesting to note that when the reactions are carried out in presence a small amount of alkali or when alkali is co-impregnated with Pd on the catalyst a surprising shift in selectivity from C=C to C=O hydrogenation is detected. Alkali addition influences the dispersion, electronic property and reducibility of Pd. These changes in molecular electronic structure of Pd are attributed to be responsible for the changes in the chemoselectivity brought about by alkali addition.

Chapter 5 describes chemoselective C=C hydrogenation of cinnamaldehyde over Ni(5 wt%)/CeO_2, ZrO_2 and CeO_2-ZrO_2 catalysts. The objective of the study in this chapter is to establish the effect of promoters on the activity and selectivity of Ni in liquid-phase hydrogenation of cinnamaldehyde. Ni supported on ZrO_2 and CeO_2-ZrO_2 show higher catalytic activity than Ni/CeO_2. When a small quantity of Pt or Pd (0.5 wt%) is co-impregnated with Ni(5 wt%) on CeO_2-ZrO_2 an enhancement in activity is detected. Detailed characterization studies reveal that increased metal dispersion is the cause for the enhanced activity of the noble metal promoted Ni catalysts. Under similar experimental conditions, the unpromoted catalyst is selective for hydrocinnamaldehyde product (C=C hydrogenation)

whereas the promoted catalyst yields 3-phenyl propanol (C=C and C=O hydrogenation product). The catalysts of this work are more active than the hitherto known Ni catalysts for C=C hydrogenation.

Chapter 6 describes the selective conversion of furfural (FAL; a biomass-derived compound) to several value-added chemicals viz., furfuryl alcohol (FOL), tetrahydrofurfuryl alcohol (THFOL), furan and tetrahydrofuran (THF). Catalytic hydrogenation of FAL to FOL and THFOL is carried out over Pt and Pd supported on γ-Al_2O_3, CeO_2, ZrO_2, CeO_2-ZrO_2, sulfated-ZrO_2, SiO_2, and MgO catalysts. The supported Pt catalysts are highly selective for furfuryl alcohols even at room temperature (25 °C) under H_2 pressure of 20 bar, while the supported Pd catalysts yield FOL as well as THFOL. This is the first report on selective hydrogenation of FAL to FOL and THFOL under such mild reactions conditions. Decarbonylation of FAL provides furan and further hydrogenation of furan yields THF. Decarbonylation is carried out at high temperature (200 – 260 °C) and in vapour-phase. One of the major issues is the catalyst stability under such conditions. In this work, a H_2-free decarbonylation process of FAL providing furan in high yields using Pd/Al_2O_3 catalyst is demonstrated. The reaction is carried out in presence of water-iso propanol (1 : 4) medium. FAL conversion of 100% and furan selectivity of 82% is achieved at 240 °C. The Pd/Al_2O_3 catalyst of this study is reusable in at least six recycling experiments without any loss in activity/selectivity. Further, the Al_2O_3-supported Pd catalysts show high activity for selective hydrogenation of furan to THF at room temperature and H_2 pressure of 60 bar. Nature of the support and its acidity has a major influence on the activity of supported Pd and Pt catalysts. Detailed investigations in terms of effects of process parameters on the yield of furan and THF are investigated.

Chapter 7 provides an overall summary and conclusions of the work presented in the thesis.

By and large, this thesis describes newer type and more effect supported noble metal catalysts for the selection hydrogenation of cinnamaldehyde (a representative α,β-unsaturated aldehyde) and furfural (a biomass-derived compound) to value-added industrial chemicals. Factors influencing the catalytic performance of noble metal catalysts are investigated.

1.11. References

[1] M. L. Derrien, Stud. Surf. Sci. Catal. 27 (1986) 613.

[2] K. van Gorp, E. Boerman, C.V. Cavenaghi, P.H. Berben, Catalysis Today 52 (1999) 349.

[3] J. C. Dermot, C. L. Edward and M. Raul, Applied Catalysis, 41 (1988) 81.

[4] A.V. David and D. William, J Organometallics 16 (1997) 1912.

[5] E. S. Bruce and R. K. James, Ind. Eng. Chem. Process Des. Develop., 11 (1972) 1.

[6] V. Calemma, S. Peratello, C. Perego, Applied Catalysis A: General 190 (2000) 207.

[7] R. A. Sheldon, H. Van Bekkum (2001) Fine Chemicals through Heterogeneous Catalysis. Weinheim, Germany: Wiley-VCH. (b) W. Bonrath, J. Medlock, J. Schütz, B. Wüstenberg and T. Netscher http://dx.doi.org/10.5772/48751. (c) W. Bonrath, T. Netscher, Applied Catalysis A: General 280 (2005) 55.

[8] A. L. Gemal, J. L. Luche, J. Am. Chem. Soc., 103 (1981) 5454.

[9] S. Katano, H. S. Kato, M. Kawai, and K. Domen, J. Phys. Chem. B, 107 (2003) 16.

[10] W. Jaime and K. Miriam, Ind. Eng. Chem. Prod. Res. Dev., 23 (1984) 1.

[11] S. Narayanan, Bulletin of the Catalysis Society of India 2 (2003)107.

[12] D. L. Shawn and M. A. Vannice, J. of Catal. 143 (1993) 539.

[13] F. Cavani, F. Trifiro, Catal. Today 34 (1997) 269.

[14] M. Akinori, M. Yumi, O. Eri, H. Tomoko, M. Tomohiro, and S. Hironao, Org. Lett., 8 (2006) 3279.

[15] W. H. Jones, W. F. Benning, P. Davis, D. M. Mulvey, P. I. Pollok, J. C. Schaeffer, R. Tull, L. M. Weinstock, Ann. N. Y. Acad. Sci. 158 (1969) 471.

[16] R. Noyori and T. Ohkuma. Pure Appl. Chem. 71 (1999) 1493.

[17] J. J. F. Scholten , A. P. Pijpers, A. M. L. Hustings, Catal. Rev. Sci. Eng., 27(1) (1985) 151.

[18] D Astruc, Inorg. Chem. 46 (2007) 1884.

[19] M. H. G. Prechtl, J. D. Scholten and J. Dupont, Molecules 15 (2010) 3441.

[20] X. Han, J. Li, Indian journal of chemistry Vol. 46A, (2007) 1747. (b) H. G. Manyar, B. Yang, H. Daly, H. Moor, S. McMonagle, Yu Tao, G. D. Yadav, A. Goguet, P. Hu, and C. Hardacre, ChemCatChem 5 (2013) 506.

[21] M. W. Balakos, E. E. Hernandez, Catalysis Today 35 (1997) 415.

[22] X. Chen, W. Sun, N. Xiao, Y. Yan, S. Liu, Chemical Engineering Journal 126 (2007) 5.

[23] A. Borodziński and M. Bonarowska, Langmuir 13 (1997) 5613.

[24] S. J. Khoobiar, J. Phys. Chem., 68 (1964) 41142.

[25] J. E. Benson, H. W. Kohn and M. Boudart, J. Catal., 5 (1966) 307.

[26] M. Boudart, M. A. Vannice, and J. E. Benson, Z. Phys. Chem. 64 (1969) 171.

[27] A. A. Wismeijer, A. P. G. Kieboom, H. Van Bekkum, React. Kinet. Catal. Lett. 29 (1985) 311.

[28] B. I. Rosen, US. Patent 4424163, (1984).

[29] J. Hagen in Industrial catalysis: a practical approach, Wiley-VCH, Weinheim, (1999) pp. 174. (b) I. Chorkendorff, J. M. Niemantsverdriet in Concepts of modern catalysis and kinetics, Wiley-VCH, Weinheim (2003) pp 335.

[30] A. A. Bhattacharyya, G. M. Woltermann, J. S. Yoo, J. A. Karch, and W. E. Cormier, Znd. Eng. Chem. Res., 27 (1988) 1356. (b) J. S. Yo and J. A. Jaecker, U.S. Patent 4,469,589 (1984). (c) R. J. Bertolacini, E. H. Hirschberg, and F. S. Modica, U.S. Patent 4,497,902 (1985).

[31] B. T. Kilbourn, J. Less Common Metals, 126 (1986) 101. (b) W. Liu and M. Flytzani-Stephanopoulos, J. Catal., 153 (1995) 304. (c) J. F. Brazdil and R. K. Grasselli, J. Catal., 79 (1983) 104. S. Imamura, Y. Uematsu, K. Utani, and T. Ito, Ind. Eng. Chem. Res., 30 (1991) 18.

[32] J. L. Duplan and H. Praliaud, Appl. Catal., 67 (1991) 325. (b) A. F. Diwell, R. R. Rajaram, H. A. Shaw, and T. J. Truex, Stud. Surf: Sci. Catal., 71 (1991) 139.

[33] S. Bernal, J. J. Calvino, G. A. Cifredo, J. M. Gatica, J. A. P. Omil, and J. M. Pintado, J. Chem. Soc. Faraday Trans., 89 (1993) 3499. (b) H. C. Yao and Y. F. Y. Yao, *J. Catal.,* 86 (1948) 254. (c) M. F. L. Johnson and J. Mooi, J. Catal., 103 (1987) 502. (d) C. Padeste, N. W. Cant, and D. L. Trimm, Catal. Lett., 18 (1993) 305. (e) J. Barbier, F. Marsollier, and D. Duprez, Appl. Catal. A: General, 90 (1992) 11. (f) L. A. Bruce, M. Hoang, A. E. Hughes, and T. W. Turney, Appl. Catal. A: General, 100 (1993) 51.

[34] J. L. G. Fierro, J. Soria, J. Sanz, and J. M. Rojo, J. Solid State Chem., 66 (1987) 154. (b) J. Cunningham, S. O'Brien, J. Sanz, J. M. Rojo, J. A. Soria, and J. L. G. Fierro, J. Mol. Catal., 57 (1990) 379.

[35] G. Munuera, A. Fernandez, and A. R. Gonzales-Elipe, Stud. Surf: Sci. Catal., 71 (1991) 207. (b) J. Z. Shyu, W. H. Weber, and H. *S.* Gandhi, J. Phys. Chem., 92 (1988) 4964. (c) F. Le Normand, L. Hilaire, K. Kili, G. Krill, and G. Maire, J. Phys.

Chem., 92 (1988) 2561. (d) J. Z. Shyu, K. Otto, W. L. H. Watkins, G. W. Graham, R. K. Belitz, and H. S. Gandhi, J. Catal., 114 (1988) 23. (e) Y. Zhou, M. Nakashima, and J. M. White, J. Phys. Chem., 92 (1988) 812. (f) A. Bensalem, F. Bozon-Verduraz, M. Delamar, and G. Bugli, Appl. Catal. A: General, 121 (1995) 81.

[36] L. Kepinski and M. Wolcyrz, Catal. Lett., 15 (1992) 329.

[37] T. Yumaguchi, N. Ikeda, H. Hattori, and K. Tanabe, J. Catal., 67 (1981) 324.

[38] C. Lamonier, G. Wrobel, and J. P. Bonnelle, J. Mater. Chem., 4 (1994) 1927.

[39] M. Pijolat, M. Prin, M. Soustelle, O. Touret, and P. Nortier, J. Chem. Soc. Faraday Trans. 91 (1995) 3941.

[40] P. Fornasiero, G. Balducci, R. Di Monte, J. Kaspar, V. Sergo, G. Gubitosa, A. Ferrero, and M. Graziani, J. Catal. 164 (1996) 173.

[41] M. Daturi, E. Finocchio, C. Binet, J. C. Lavalley, F. Fally, V. Perrichon, H. Vidal, N. Hickey and J. Kašpar, J. Phys. Chem. B 104 (2000) 9186.

[42] E. Tani, M. Yoshimura and S. Somiya, J.Amer. Ceram. Soc. 66 (1983) 506. (b) P. Duran, M. Gonzales, C. Moure, J. R. Jurdo, and C. Pascal, J. Mater. Sci. 25 (1990) 5001.

[43] S. Meriani, Mater Sci Eng 71 (1985) 369. (b) S. Meriani, Mater Sci Eng A-Struct Mater 109 (1989) 121.

[44] M. Yashima, K. Morimoto, N. Ishizawa, M. Yoshimura, J. Amer. Ceram. Soc. 76 (1993) 1745. (b) M. Yashima, H. Arashi, M. Kakihana, and M. Yoshimura, J. Amer. Ceram. Soc. 77 (1994) 1067.

[45] P. Fornasiero, G. Balducci, R. Di Monte, J. Catal. 164 (1996) 173.

[46] K. Bauer and D. Garbe, Common Fragrance and Flavor Materials, VCH, Weinheim, (1985). (b) K. Bauer and D. Garbe, in Ullman Encyclopedia, VCH, New York, (1988) 141. (c) K. Weissermel and H. J. Arpe, Industrial Organic Chemistry, Verlag Chemie, Weinheim, (1978).

[47] P. Gallezot, D. Richard, Catal. Rev. Sci. Eng., 40, (1998) 81.

[48] J. M. Campelo, A. Garcia, D. Luna, and J. M. Marinas, J. Catal., 113 (1988) 172.

[49] F. Delbecq and P. Sautet, J. Catal., 152 (1995) 217.

[50] P. N. Rylander, in Catalytic Hydrogenation in Organic Synthesis, Academic Press, New York, (1979), 72.

[51] P. Beccat, J. C. Bertolini, Y. Gauthier, J. Massardier, and P. Ruiz, J. Catal., 126, (1990) 451.

[52] S. Galvagno, G. Capanelli, G. Neri, A. Donato and R. Pietropaolo, J. Mol. Catal. 64, (1991) 237.

[53] S. Galvagno, C. Milone, G. Neri, A. Donato, and R. Pietropaolo, in Heterogeneous Catalysis and Fine Chemicals ZIZ (M. Guisnet, J. Barbier, J. Barrault, C. Bouchoule, D. Duprez, G. P. Crot, and C. Montassier, eds.), Studies in Surface Science and Catalysis Vol. 78, Elsevier, Amsterdam, 1993, p. 163.

[54] A. Giroir-Fendler, D. Richard, and P. Gallezot, in Heterogeneous Catalysis and Fine Chemicals (M. Guisnet, J. Barrault, C. Bouchoule, D. Duprez, C. Montassier, and G. Perot, eds.), Studies in Surface Science and Catalysis Vol. 41, Elsevier, Amsterdam, 1988, p. 171.

[55] D. Richard, P. Fouilloux, and P. Gallezot, in Proceedings ofthe 9th International Congress on Catalysis (M. J. Phillips and M. Ternan, eds.), Calgary, Canada, 1988, p. 1074.

[56] G. J. Hutchings, F. King, I. P. Okoye, and C. H. Rochester, Appl. Catal. A, 83 (1992) L7.

[57] L. G. Christiane, Animal Frontiers April 3 (2013) No. 2

[58] D. Montane, X. Farriol, J. Salvado, P. Jollez, E. Chornet J Wood Chem Technol 18 (1998) 171.

[59] A. D. French, N. R. Bertoniere, R. M. Brown, H. Chanzy, D. Gray, K. Hattori and W. Glasser, in Kirk-Othmer Encyclopedia of Chemical Technology, ed. A. Seidel, John Wiley & Sons, Inc., New York, 5th edn, 2004, vol. 5.

[60] A. D. French, N. R. Bertoniere, R. M. Brown, H. Chanzy, D. Gray, K. Hattori and W. Glasser, in Kirk-Othmer Encyclopedia of Chemical Technology, ed. A. Seidel, John Wiley & Sons, Inc., New York, 5th edn, 2004, vol. 5.

[61] A. Fukuoka, P. L. Dhepe, Angew. Chem. Int. Ed. 45 (2006) 5161; C. Luo, S. Wang and H. Liu, Angew. Chem. Int. Ed., 46 (2007) 7636.

[62] K. V. Sarkanen and H. L. Hergert, K. Sarkanen and C. Ludwig, eds., Lignins: Occurrence, Formation, Structure, and Reactions, Wiley-Interscience, New York, p. 43.

[63] N. G. Lewis, Science 275 (1997) 362.

[64] J. B. Binder, J. J. Blank, A. V. Cefali, and R. T. Raines ChemSusChem 3 (2010) 1268.

[65] H. E. Hoydonckx, W. M. Van Rhijn, W. Van Rhijn, D. E. De Vos, P. A. Jacobs,

Wiley-VCH Verlag GmbH & Co. KGaA, Weinheim, DOI: 10.1002/14356007.a12_119.

[66] C. S. Miner, H. J. Brownlee, Quaker Oats Co, US 1735084, 1922.

[67] E. Schinn, Escher Wyss G.M.B.H., US 3035962, 1962.

[68] K. Kiminki, R. Kulmala, S. Sipila, W. Oy. A. B. Rosenlew, US 4029515, 1975.

[69] K. J. Zeitsch: ‘‘Sugar Series’’, in The Chemistry and Technology of Furfural and its Many By-products, vol. 13, 1st ed., Elsevier Science, Amsterdam 2000.

[70] F. B. Oliveira, C. Gardrat, C. Enjalbal, E. Frollini, A. Castellan, Journal of Applied Polymer Science, 109 (2008) 2291.

[71] A. Pizzi, E. Orovan, F. A. Cameron, Holz Roh Werkstoff 42 (1984) 467.

[72] www.cropguard.co.za

[73] F. N. Peters, Quaker Oats Co., US 1906873, 1928.

[74] L. J. Franier, H. H. Fineberg, Ashland Oil Inc., US 4251396, 1979. (b) L. J. Franier, H. H. Fineberg, Ashland Oil Inc., US 4302397, 1980.

[75] M. Bunji, US 4252689, 1979.

[76] E. Ricard, H. M. Guinot US 1739919, 1927. (b) Du Pont de Nemours, US 2077422, 1931.

[77] S. Swadesh, Quaker Oats Co., US 2754304, 1952.

[78] A. B. Merlo, V. Vetere, J. F. Ruggera, M. L. Casella, Catal Comm 10 (2009) 1665. (b) R. S. Rao, R. Terry, K. Baker and M. A. Vannice, Catal. Lett. 60 (1999) 51. (c) J. Kijeński, P. Winiarek, T. Paryjczak, A. Lewicki, A. Mikołajska, Applied Catalysis A: General 233 (2002) 171.

[79] J. Kijenski, P. Winiarek, T. Paryjczak, A. Lewicki, A. Mikolajska, Appl. Catal. A 233 (2002) 171.

[80] B. M. Nagaraja, V. Siva Kumar, V. Shasikala, A. H. Padmasri, B. Sreedhar, B. David Raju, K. S. Rama Rao, Catal. Comm. 4 (2003) 287.

[81] X. Chen, W. Sun, N. Xiao, Y. Yan, S. Liu Chemical Engineering Journal 126 (2007) 5.

[82] Y. Nakagawa, H. Nakazawa, H. Watanabe, and K. Tomishige, ChemCatChem 4 (2012)1791.

[83] H. B. Copelin, D. I. Garnett , Du Pont de Nemours & Co., US 3007941, 1959.

[84] A. P. Dunlop, G. W. Huffman, Quaker Oats Co., US 3257417, 1963.

[85] R. D. Srivastava and A. K. Guha J. of. Catal 91 (1985) 254.

[86] M. Fischer, M. Irgang, L. Wambach, BASF Ag., US 4780552, 1988.

[87] R. B. Pinkerton, Du Pont de Nemours & Co., US 4387236, 1982.

[88] J. M. Fremont, D. I. Garnett, Du Pont de Nemours & Co., US 4243593, 1980.

[89] J. Schneiders, BASF, DE 1 043 342, 1957.

[90] T. Onoda Mitsubishi Chem., US 3 922 300, 1975.

[91] J. Toriya, K. Shirago, Mitsubishi Chem., US 4 010 197, 1977.

[92] T. Shimizu, T. Yasui Kurary, US 4 567 305, 1986.

[93] J. Kanetaka T. Asano, S. Masamune, Ind. Eng. Chem. 62 (1970) 24.

[94] T.A. Bither, Du Pont US 4 442 226, 1982.

[95] S. Sitthisa, D. E. Resasco, Catal. Lett. 141 (2011) 784.

[96] B. M. Nagaraja, A. H. Padmasri, B. David Raju, K. S. Rama Rao, J. Mol. Catal. A: Chem. 265 (2007) 90.

Chapter 2

Experimental Methods and Characterization Techniques

2.1. Introduction

This chapter describes the synthesis of supported catalysts used in this study. It also provides the techniques employed for characterization of the catalysts, generalized reaction procedures and the methods of product analysis. The support materials were prepared by precipitation method and desired metals, in required quantities, were deposited on those supports by impregnation method. The following supported metal catalysts were prepared.

Pd/CeO_2, Pd/ZrO_2, Pd/CeO_2-ZrO_2, Na-Pd/CeO_2-ZrO_2

Pt/CeO_2, Pt/ZrO_2, Pt/CeO_2-ZrO_2

Ni/CeO_2, Ni/ZrO_2, Ni/CeO_2-ZrO_2, Ni-Pt/CeO_2-ZrO_2, Ni-Pd/CeO_2-ZrO_2

Pt/Al_2O_3, Pd/Al_2O_3, Pt/MgO, Pt/SiO_2, Pt/SO_4-ZrO_2

These catalysts were characterized by chemical composition [atomic absorption spectroscopy (AAS) and inductively coupled plasma-optical emission spectroscopy (ICP-OES)], powder X-ray diffraction (XRD), nitrogen-physisorption, high-resolution transmission electron microscopy (HRTEM), X-ray photoelectron spectroscopy (XPS), Fourier transform infrared (FTIR) spectroscopy (of adsorbed pyridine and CO), temperature-programmed desorption (TPD of NH_3 and CO_2), temperature-programmed reduction (with H_2, TPR-H_2) and chemisorption (of H_2 and CO) techniques. Catalytic activities of these materials were tested for selective hydrogenation of cinnamaldehyde (CA; a representative α,β-unsaturated aldehyde) and furfural (FAL; a biomass-derived compound) to important industrial chemicals.

2.2. Catalyst Preparation

2.2.1. Support Materials

2.2.1.1. CeO_2. In a typical synthesis, 6.31 g of cerous nitrate [$Ce(NO_3)_3.6H_2O$, Semco] was dissolved in 180 ml of distilled water taken in a triple-necked, glass, round-bottom flask (2 l) fitted with a water-cooled condenser, pH electrode and burette containing 0.1 M aqueous NaOH solution and placed in an temperature controlled oil bath. The contents of the flask were heated to 80 °C. NaOH solution was added drop-wise with stirring and the pH of the solution was maintained at 10. Cerium precipitated in the form of its hydroxide. The suspension was digested at 80 °C for 3 h while stirring. Then, it was cooled to 25 °C. The precipitate formed was separated, washed with distilled water (until all the Na^+ ions were removed), dried at 110 °C for 6 h and finally, calcined at 450 °C for 2.5 h to get the yellow coloured CeO_2 support.

2.2.1.2. ZrO_2. 4.71 g of zirconyl nitrate [$ZrO(NO_3)_2.xH_2O$, Loba Chemie] was dissolved in 145 ml of distilled water taken in a triple-necked, glass, round-bottom flask (2 l)

and subjected to precipitation as described in section 2.2.1.1. Zirconium hydroxide, thus formed was dried at 110 °C for 6 h and then, calcined at 450 °C for 2.5 h to get the ZrO_2 support. Colour: white.

2.2.1.3. CeO_2-ZrO_2. This support with Ce:Zr molar ratio of 1:1 was prepared by co-precipitation method using cerious nitrate and zirconyl nitrate as sources of ceria and zirconia, respectively. $Ce(NO_3)_36H_2O$ (7.35 g, Semco) and $ZrO(NO_3)_2.xH_2O$ (2.8 g, Loba Chemie) were dissolved separately in 168 and 120 ml of distilled water, respectively. They were taken in a triple-necked, glass, round-bottom flask. Temperature was raised to 80 °C and 0.1 M aqueous NaOH solution was added to it drop-wise for 1 h with constant stirring; pH of the contents was maintained at about 10. Stirring was continued for another 3 h, and then it was stopped and cooled to 25 °C. Cations precipitated in the form of their hydroxides. The precipitate was separated and washed with distilled water until all the Na^+ ions were removed. It was then, dried at 110 °C for 6 h, powdered and calcined at 450 °C for 2.5 h to get the final yellow coloured product. CeO_2-ZrO_2 mixed oxides with Ce:Zr molar ratios of 1:2 and 1:4 were prepared in the same manner taking required amounts of ceria and zirconia sources.

2.2.2. Supported Metal Catalysts

2.2.2.1. Pd(2 wt%)/CeO_2-ZrO_2, Pd(2 wt%)/CeO_2 and Pd(2 wt%)/ZrO_2. Palladium (2 wt%) supported on CeO_2–ZrO_2 (Ce: Zr = 1:1) was prepared by dry-impregnation method. In a typical preparation, 0.570 g of tetraamminepalladium(II) nitrate [$Pd(NH_3)_4(NO_3)_2$, 10 wt% aqueous solution, Aldrich] was added drop-wise to 1 g of CeO_2–ZrO_2 taken in a beaker. It was thoroughly mixed at 25 °C, dried at 120 °C for 5 h till all the water evaporated and then, calcined at 400 °C for 2 h. Colour: brown.

Pd(2 wt%)/CeO_2 and Pd(2 wt%)/ZrO_2 were prepared in a similar manner taking 0.570 g of tetraamminepalladium(II) nitrate and 1 g of CeO_2 or ZrO_2 supports, respectively.

2.2.2.2. Na-Pd(2 wt%)/CeO_2-ZrO_2. 0.262 g of NaOH dissolved in 1 ml of water and 0.570 g of 10 wt% aqueous solution of tetraamminepalladium(II) nitrate were mixed and added slowly to 1 g of CeO_2–ZrO_2 (Ce:Zr = 1:1) while mixing thoroughly at 25 °C. The slurry was dried at 120 °C for 5 h till all the water got evaporated. It was then, calcined at 400 °C for 2 h. Colour: brown

2.2.2.3. Pd(0.5 wt%)/CeO_2-ZrO_2. In this case, palladium metal loading was done by wet-impregnation method. 0.0704 g of $Pd(NH_3)_4(NO_3)_2$ (10 wt% aqueous solution) was taken in a beaker containing 10 ml of de-ionized water. This solution was added to 1 g of CeO_2–ZrO_2 (Ce:Zr = 1:1). It was thoroughly mixed. Water was removed over a rotary evaporator.

The solid obtained was recovered, dried at 120 °C for 6 h and calcined at 500 °C for 2 h. Prior to use, the sample was reduced in a flow of H_2 (30 ml/min) at 250 °C for 2.5 h. Colour: brown.

2.2.2.4. Pd(2, 5 and 10 wt%)/Al_2O_3. Commercial γ-Al_2O_3 was activated at 150 °C for 2 h. Then, required amounts of Pd were loaded onto it by wet-impregnation method. In typical preparations, tetraamminepalladium(II) nitrate [$Pd(NH_3)_4(NO_3)_2$, 10 wt% aqueous solution, Aldrich: 0.5749 g for 2 wt% Pd, 1.408 g for 5 wt% Pd and 2.8169 g for 10 wt% Pd] was taken in 10 ml of distilled water and added to 1 g of activated γ-Al_2O_3 contained in a glass, round-bottom flask. It was mixed thoroughly and dried at 80°C over a rotary evaporator. The solid obtained was recovered, dried at 100 °C for 6 h in an oven and calcined at 400 °C for 2 h. Color: brown.

2.2.2.5. Pt(5 wt%)/CeO_2-ZrO_2, Pt(5 wt%)/CeO_2 and Pt(5 wt%)/ZrO_2. These samples were prepared by wet-impregnation method. Tetraaminoplatinum(II) nitrate [$Pt(NH_3)_4(NO_3)_2$, 3 wt% aqueous solution, Aldrich; 1.767 g] was taken in a beaker containing 10 ml of de-ionized water. It was added to 1 g of CeO_2–ZrO_2 (Ce:Zr = 1:1) contained in a glass, round-bottom flask. It was mixed thoroughly and dried at 80 °C over a rotary evaporator. The solid obtained was recovered and dried at 100 °C for 6 h in an electric oven. Then, it was calcined at 400 °C for 2 h. Colour: brown.

Catalyst samples with Pt loadings of 0.5, 1, and 2 wt% were prepared in the same manner taking appropriate amounts of the platinum precursor (0.1675 g for 0.5 wt% Pt; 0.3367 g for 1 wt% Pt and 0.6803 g for 2 wt% Pt loading).

Pt(5 wt%)/CeO_2 and Pt(5 wt%)/ZrO_2 were prepared following the same wet-impregnation procedure taking 1.767 g of tetraaminoplatinum(II) nitrate (3 wt% aqueous solution) in 10 ml of de-ionized water and 1 g of CeO_2 and ZrO_2 supports, respectively.

2.2.2.6. Al_2O_3, SO_4-ZrO_2, MgO and SiO_2-supported Pt. Commercial γ-alumina was activated at 150 °C for 2 h. Then, it was cooled to 25 °C keeping in a desiccator. A required amount of solid tetraaminoplatinum(II) nitrate (Aldrich; 0.0816, 0.1052 and 0.222 g for 2, 5 and 10 wt%, respectively) was dissolved in 10 ml of de-ionized water which was then, added drop-wise to 1 g of activated γ-alumina taken in a glass, round-bottom flask. It was thoroughly mixed. Then, water was removed at 80 °C using a rotary evaporator. The solid formed was dried at 100 °C for 6 h in an oven and then, calcined at 400 °C for 2 h.

Commercial sulphated-zirconia, MgO and SiO_2 were activated at 120 °C for 2 h and then, Pt(5 wt%) was loaded by wet-impregnation as described above for Pt/Al_2O_3. Colour:

Pt(2, 5 and 10 wt%)/Al_2O_3 and Pt(5 wt%)/MgO: grey; Pt(5 wt%)/SO_4-ZrO_2: white; Pt(5 wt%)/SiO_2: black.

2.2.2.7. Ni(5 wt%)/CeO_2-ZrO_2, Ni(5 wt%)/CeO_2 and Ni(5 wt%)/ZrO_2. Nickel supported on ceria and zirconia catalysts were prepared by wet-impregnation method. 0.2597 g of $Ni(NO_3)_2.6H_2O$ (Thomas Baker) was dissolved in 10 ml of de-ionized water and added to 1 g of CeO_2–ZrO_2 (Ce:Zr = 1:1). It was then, dried at 80°C over a rotary evaporator. The solid was recovered and dried at 120°C for 6 h in an electric oven. Then, the material was calcined at 500 °C for 2 h.

Ni(5 wt%) supported on CeO_2 and ZrO_2 were prepared in the same manner taking 0.2597 g of the nickel precursor and 1 g of CeO_2 and ZrO_2, respectively.

Catalysts with 3, 10 and 15 wt% of Ni supported on ZrO_2 were prepared taking 0.1525, 0.5478 and 0.8710 g of the Ni source and 1 g of ZrO_2 support, respectively. Colour: brown.

2.2.2.8. Ni(5 wt%)-(Pd/Pt)(0.5 wt%)/CeO_2-ZrO_2. 0.2597 g of $Ni(NO_3)_2.6H_2O$ and 0.0704 g of $Pd(NH_3)_4(NO_3)_2$ (10 wt% aqueous solution) were dissolved in a 10 ml of de-ionized water and added to 1 g of CeO_2–ZrO_2 (Ce:Zr = 1:1) taken in a glass, round-bottom flask. Then, it was dried at 80 °C over a rotary evaporator. The solid formed was recovered, dried at 120 °C for 6 h and calcined at 500 °C for 2 h.

For Ni-Pt catalyst, 0.005 g of solid $Pt(NH_3)_4(NO_3)_2$, 0.2597 g of the nickel source and 1 g of CeO_2-ZrO_2 were taken. Colour: brown.

2.3. Characterization Techniques and Sample Preparation

2.3.1. Powder X-ray Diffraction

XRD is an important tool to determine the crystallinity, phase purity, crystal structure and crystallite size of catalyst materials [1]. The XRD method involves interaction between the incident monochromatized X-rays (CuK_α or MoK_α) with the atoms of a periodic lattice. X-rays scattered by the atoms in an ordered lattice interfere constructively as described by the Bragg's law: $n\lambda = 2d \sin\theta$, where, λ is the wavelength of X-rays, d is the distance between two lattice planes (interplanar distance), θ is the angle between incoming X-rays and normal to the reflecting lattice plane and *n* is an integer known as the order of reflection [1, 2]. XRD of the powdered samples were recorded in the 2θ range of 10 - 80° at a scan rate of 2.3°/min on an Xpert Pro PANalytical X-ray diffractometer with Ni-filtered CuK_α radiation (40 kV, 30 mA). Material in the form of films was prepared on glass plates and investigated by XRD. Crystallite size of the materials was determined using the Scherrer equation:

$$L = K\lambda/\beta\cos\theta \quad (1)$$

where, θ and λ are Brag angle and wavelength of incident X-ray radiation, respectively. K is a constant approximately taken as 0.9; β is the line width on the 2θ scale in radians. The inter-planar spacing (d) in case of tetragonal lattice is related to unit cell parameters (a, b and c) as follows:

$$1/d^2 = h^2/a^2 + k^2/b^2 + l^2/c^2 \quad (2)$$

2.3.2. Nitrogen Physisorption

The most common method for measuring surface area and textural characteristics of catalyst materials is that based on the theory developed by Brunauer, Emmett and Teller (BET), considering the multilayer adsorption. The BET equation can be represented as:

$$P/V(P_o\text{-}P) = 1/cV_m + [(c\text{-}1)/cV_m]\ (P/P_o), \quad (3)$$

where P is adsorption equilibrium pressure, P_o is saturation vapour pressure of the adsorbate at the experimental temperature, V is volume of N_2 adsorbed at a pressure P, V_m is volume of adsorbate required for monolayer coverage, and c, a constant that is related to the heat of adsorption and liquefaction [3-5]. A linear relationship between $P/V(P_o\text{-}P)$ and P/P_o is required to obtain the quantity of nitrogen adsorbed. The monolayer volume, V_m is given by $1/(S+I)$, where S is the slope which is equal to $(c\text{-}1)/cV_m$ and I is intercept equal to $1/cV_m$. The surface area of the material (S_{BET}) is related to V_m, by the equation:

$$S_{BET} = (V_m/22414)N_a\sigma, \quad (4)$$

where N_a is Avagadro number and σ is mean cross sectional area covered by one adsorbate molecule. The value of σ generally accepted for N_2 is 0.162 nm^2. Several computational procedures are available for the derivation of pore size distribution from physisorption isotherms. Most popular among them is the Barrett-Joyner-Halenda (BJH) model, which is based on speculative emptying of the pores by a step-wise reduction of P/P_o. Allowance is made for the contraction of the multilayer in those pores already emptied by the condensate [3]. The pore size distribution is usually expressed as a plot of $\Delta V_p/\Delta r_p$ versus r_p, where V_p is pore volume and r_p is pore radius. Adsorption of nitrogen measured by the Brunauer-Emmett-Teller (BET) equation at low pressure (10^{-4} Torr) and liquification temperature of N_2 (-196 °C) is the standard method for determination of surface area, pore volume and pore size distribution of nanoporous materials. All these measurements were conducted on a NOVA 1200 Quanta Chrome instrument. Specific surface area was determined by total surface area of the sample by sample weight. About 100 mg of sample was taken in a quartz cell and evacuated at 200 °C for 1 h. After that, the quartz cell was dipped in a liquid nitrogen container up to the sample level and then, started passing nitrogen through it. Adsorption and desorption of nitrogen was measured in the P/P_o range of 0.1 to 0.

2.3.3. High Resolution Transmission Electron Microscopy

Transmission electron microscopy (TEM) is typically used for high resolution imaging of thin films of a solid sample for micro structural and compositional analysis. It reveals that particle size distribution, metal dispersion, morphology and chemical composition of the supported metal particles. The technique involves: (i) irradiation of a very thin sample by a high-energy electron beam, which is diffracted by the lattices of a crystalline or semi-crystalline material and propagated along different directions, (ii) imaging and angular distribution analysis of the forward scattered electrons (unlike scanning electron microscopy where backscattered electrons are detected) and (iii) energy analysis of the emitted X rays [6]. In detail, a primary electron beam of high energy and high intensity passes through a condenser to produce parallel rays, which impinges on the sample. As the attenuation of the beam depends on the density and thickness, the transmitted electrons form a two-dimensional projection of the sample mass, which is subsequently magnified by the electron optics to produce the so-called bright field image. The dark field image is obtained from the diffracted electron beams, which are slightly off angle from the transmitted beam. Typical operating conditions of TEM instruments are 100-200 keV electrons, 10^{-6} mbar vacuum, 5 nm resolution and magnification of about 3 x 10^5 or 10^6. For high resolution transmission electron microscopy (HRTEM), the operating conditions are: 100 – 300 keV electrons, 10^{-6} vacuum, 0.5 nm resolution, magnification of about 3 x 10^5 (or) 10^6. The topographic information obtained by TEM in the vicinity of atomic resolution can be utilized for structural characterization and identification of various phases [7]. TEM also provides real space image on the atomic distribution in the bulk and surface of a nano-crystal. TEM of the samples were recorded using a JEOL-model 1200 EX instrument operating at 100 KV.

If N_S is the total number of metal atoms present on the surface and N_T is the total number of metal atoms (surface and bulk). Then, the metal dispersion can be expressed as;

$$D = N_s/N_T \quad (5)$$

For spherical particles, useful relationship between the metal dispersion, surface area and mean particle diameter can be established by making assumption on the nature of the crystal plane exposed on the metal surface [8-10]. Assuming equal proportion of the three low index planes (111), (110) and (100) on the polycrystalline surface of a face-centered cubic (fcc) metal, the crystal data, number of atoms per unit area in these planes and mean number of atoms n_s can be calculated. Surface area (a_m) occupied by an atom 'm' on a polycrystalline surface is equal to $1/n_s$. The volume (v_m) occupied by an atom m in the bulk metal is given by

$$v_m = M/\rho N_A \quad (6)$$

where, M = atomic mass, ρ = mass density and N_A = Avogadro's number. The relation between mean metal particle (d_{VA}) and metal dispersion (D) is given as follows:

$$d_{VA} = 6 \sum n_i V_i / \sum n_i A_i = 6\ v_m N_T / a_m N_s \quad (7)$$

where, $A_i = \pi d_i^2$, $V_i = \pi d_i^3/6$ and $D = 6\ (v_m/a_m)/d_{VA}$. Specific surface area (S_{sp}) is expressed as:

$$S_{sp} = \sum n_i A_i / \rho \sum n_i V_i = 6/\rho d_{VA} \quad (8)$$

With d_{VA} expressed in nanometers, ρ in $g.cm^{-3}$ and S_{SP} in $m^2.g^{-1}$, then the above equation becomes

$$S_{SP} = 6000/\rho d_{VA} \quad (9)$$

0.001-0.005 g of the sample was transferred in to a beaker containing 5 ml of iso-propanol solvent. It was kept for sonication for 0.5 h at room temperature. Only, a drop of isopropanol-dispersed sample was placed on a copper grid (200 mesh, ICON Analytical), dried for 4 h at room temperature and then used in HRTEM experiments.

2.3.4. X-ray Photoelectron Spectroscopy

The nature, oxidation state and dispersion of surface metal species were estimated by XPS, also known as Electron Spectroscopy for Chemical Analysis (ESCA) [11]. The spectra were obtained by irradiating a material with a beam of X-rays and simultaneously measuring the kinetic energy and number of electrons that escape from the top of the surface composition being analyzed. XPS spectra of the samples were acquired on a VG Microtech Multilab ESCA 3000 with Mg Kα radiation (hυ = 1253.6 eV). Base pressure in the analysis chamber was maintained at 3-6 x 10^{-10} mbar. The energy resolution of the spectrometer was set at 0.8 eV at pass energy of 20 eV. The peak corresponding to carbon 1s (at 284.2 eV) was taken as a reference in estimating binding energy (BE) values of various elements in the material and the error in all binding energy values reported is ± 0.1 eV. XPS spectral deconvolution enabled the relative percentage concentration of metal in different oxidation states present on the surface of the material. Sensitivity factor of an element (S) and percentage metal concentration (C_X) were estimated using the following equations.

$$S = f\ \sigma\ D\ \lambda \quad (10)$$

where, f = X-ray flux, σ = photoelectron cross-section, D = detector efficiency and λ = electron mean free path, and

$$C_X = (A_i/S)/\sum(A_i/S_i) \quad (11)$$

where, C = concentration of element X, A_i = area of metal photo emission peak and S = sensitivity factor of a particular metal. Samples were prepared as pellets so as to accelerate out gassing and remove carbon from the surface, before performing the XPS measurements.

2.3.5. Fourier Transform Infrared Spectroscopy

FTIR spectra of pyridine adsorbed on catalysts were recorded on a Shimadzu FTIR-8201 PC spectrophotometer in the wave number range of 400 – 4000 cm^{-1} with an accumulation of 100 scans and at a spectral resolution of 4 cm^{-1}.

FTIR spectra of adsorbed CO were recorded on a Bruker IFS 88 spectrometer with DTGS detector using OPUS software at a resolution of 4 cm^{-1} over 64 scans. Samples were made in the form of self-supporting wafers (12 mg/cm^2) of thickness suitable for transmission IR experiments [12]. Samples were directly treated in a specially designed quartz cell equipped with KBr windows, suitable for activation and in situ IR studies.

2.3.6. Temperature-Programmed Desorption

Probe molecules were adsorbed at 40 °C and their desorption with increasing temperature was monitored to characterize the surface properties of the catalysts. In the present work, NH_3 [13] and CO_2 [14, 15] were used as probe molecules to determine the acidity and basicity of different catalyst samples. The studies were done on a Micromeritics Auto Chem 2910 instrument. In a typical experiment, 0.1 g of the catalyst sample was taken in a U-shaped, flow-thru, quartz sample tube. Prior to measurements, the catalyst was pretreated in He (30 ml/min) at 400 °C for 1 h. A mixture of NH_3 in He or CO_2 in Ar (10 vol%) was passed (30 ml/min) at 40 °C for 1 h. Then, the sample was, subsequently flushed with He (30 ml/min) at 100 °C for 1 h. The TPD measurements were carried out in the range 100 – 800 °C at a heating rate of 10 °C/min. NH_3 or CO_2 concentration in the effluent was monitored with a gold-plated, filament thermal conductivity detector. The amount of desorbed ammonia or carbon dioxide was determined based on the area under the peak.

2.3.7. Temperature-Programmed Reduction

H_2-TPR is a technique in which a chemical reaction is monitored between metal particles and hydrogen gas while the temperature increases in a programmed manner with time [16, 17]. 0.05 g of the catalyst was placed in a quartz tube and treated with He gas (20 ml/min) at 200 °C for 1 h. A gas mixture of H_2(5%) – Ar(95%) was then passed (20 ml/min) through the quartz reactor at 40 °C for 1 h. The temperature was raised to 950 °C at a heating rate of 10°/min and held at that temperature for 10 min. The amount of hydrogen consumed was estimated and the reduction capacity of the catalyst was determined. A standard CuO powder was used to calibrate the amount of H_2 consumption. These studies were done on a Micromeritics Auto Chem 2920 instrument.

2.3.8. H_2 and CO Pulse Chemisorptions

Metal dispersion (MD), metal specific surface area (MSS) and average metal particle size (D_a) were determined by H_2 and CO pulse chemisorptions techniques [18]. Pulse chemisorptions studies (CO, H_2) were done on an Auto Chem 2910 Micromeritics (USA) instrument. 0.1 g of sample was placed in a sample cell holder and then the sample was heated under the flow of He gas at 200 °C for 1 h. By this treatment, the sample surface was cleaned and the moisture was completely removed. Prior to chemisorption study, catalyst was reduced in a flow of hydrogen (50 ml/min) at 300 °C for 3 h and flushed with He gas for 1 h at 300 °C. Then, the sample was cooled to ambient temperature in the same helium stream. Hydrogen and CO uptake was determined by injecting H_2 or CO pulses from a calibrated on-line sampling valve into helium stream passing over the reduced samples at 30 °C. The volume of adsorbed H_2 or CO was estimated at STP and metal dispersion, metal specific surface area and mean particle size were calculated by using the equations given below.

$$MSS = V_m \,.\, N_a \,/\, S_f \,.\, S_d \,.\, L \qquad (12)$$

$$MD = V_m \,.\, A_w \, 10^4 \,/\, \%W \,.\, S_f \qquad (13)$$

$$D_a = 10^3 \,.\, F/\, MSS \,.\, D_m \qquad (14)$$

Here, V_m = volume of hydrogen gas adsorbed at monolayer coverage (moles/g-catalyst), S_d = metal surface density (number of atoms per square meter), S_f = stoichiometric factor, A_w = atomic weight, L = grams of metal per gram of catalyst, %W = weight percentage of metal in the catalyst, D_m = metal density i.e., grams per metal unit volume

2.4. Reaction Procedure

All the hydrogenation experiments were carried out in a 300 ml capacity autoclave supplied by Parr Instruments or 100 ml stainless-steel Parr micro bench-top reactor (Parr 4875) Co., USA, which was equipped with a heating arrangement, overhead stirrer, thermo well, internal cooling coil, gas inlet and outlet, liquid sampling valve, safety rupture disc, pressure gauge and a transducer for digital pressure display

2.4.1. Hydrogenation of Cinnamaldehyde

2.4.1.1. Over Pt/CeO_2, Pt/ZrO_2 and Pt/CeO_2-ZrO_2. Prior to reactions, the catalysts were freshly reduced at 300 °C, for 2.5 h, in a flow of hydrogen (30 ml/min). Upon reduction, the color of the catalyst changed from dark brown to black. The temperature was brought down to 25 °C. Without exposing to atmosphere, 0.05 g of reduced catalyst was transferred into a Parr reactor (300 ml) containing cinnamaldehyde (4 g, Aldrich Co) and iso-propanol solvent (40 ml, s. d. fine Chem Ltd., India). The reactor was initially flushed and then

pressurized with hydrogen to a desired value (1 – 30 bar). The reaction was conducted for 2 or 8 h at 25 °C while stirring at a speed of 500 revolutions per minute.

2.4.1.2. Over Pd/CeO_2, Pd/ZrO_2 and Pd/CeO_2-ZrO_2. Prior to reactions, the catalyst was reduced under a flow of hydrogen (30 ml/min) at 200 °C for 2 h. Upon reduction, the color of the catalyst changed from dark brown to black. It was cooled to 25 °C. Without exposing to atmosphere, 0.05 g of the reduced catalyst was transferred into a Parr reactor (300 ml) containing cinnamaldehyde (4 g) and ethanol solvent (40 ml). The reactor was initially flushed and then pressurized with hydrogen to a desired value (2, 5, 10 or 20 bar). The temperature of the reactor was also raised to a desired value (50, 80, 120 or 150°C) and the reaction was conducted while stirring (500 revolutions per minute) for 8 h.

2.4.1.3. Over Ni/CeO_2, Ni/ZrO_2 and Ni or Ni-(Pd or Pt)/CeO_2-ZrO_2. Prior to hydrogenation reactions, the catalyst was reduced at 400 °C under a flow of hydrogen (30 ml/min). The color of the catalyst changed from dark brown to black. Without exposing to atmosphere, 0.05 g of the reduced catalyst was transferred into a 100 ml stainless-steel Parr micro bench-top reactor (Paar 4875 power controller and 4871 process controller) containing cinnamaldehyde (1 g) and iso-propanol (25 ml). The reactor was initially flushed and then, pressurized with hydrogen to 5 – 30 bar. Temperature of the reactor was raised to 75 – 150 °C and the reaction was conducted for 0.5 to 8 h while stirring at a speed of 600 revolutions per minute.

2.4.2. Hydrogenation/Decarbonylation of Furfural/Furan over Pd or Pt/Al_2O_3

Prior to reaction, the catalyst was reduced (at 250 and 350 °C for Pd/Al_2O_3 and Pt/Al_2O_3, respectively) in a flow of H_2 (30 ml/min). Without exposing to atmosphere, 0.05 g of the reduced catalyst was transferred into a 100 ml stainless-steel Parr micro bench-top reactor containing furfural (FAL; 1 g, Thomas Baker) or furan (1 g, Spectrochem Ltd., India) and iso-propanol (20 ml, s. d. fine Chem Ltd., India). The reactor was initially flushed and then, pressurized with hydrogen or nitrogen to 5 – 30 bar. Temperature of the reactor was raised to 25 – 240 °C and the reaction was conducted for 0.5 to 8 h while stirring at a speed of 600 revolutions per minute.

2.5. Product Analysis

2.5.1. Cinnamaldehyde Hydrogenation

Products of cinnamadehyde hydrogenation were analyzed by gas chromatography (GC) [(Varian 3400; column - CP-SIL 5 CB (30 m-long and 0.53 mm i.d x 0.25 μm)] and identified by GC-MS [Shimadzu GCMS-QP5050A; column -HP-5 (30 m-long x 0.25 mm i.d.

x 0.25 μm thickness)] techniques using a program: 40 – 120 °C at 15°/min and 1 min hold; 120 – 200 °C at 5°/min and 1 min hold; 200 – 260 °C at 20°/min and 1 min hold.

2.5.2. Hydrogenation/Decarbonylation of Furfural/Furan

The liquid products were analysed by GC [Varian 3400; column - CP-SIL 8CB (60 m-long and 0.25 mm-i.d x 0.25 μm)] and identified by GC-MS [Shimadzu GCMS-QP5050A; column -HP-5 (30 m-long x 0.25 mm i.d. x 0.25 μm thickness)] using a program: 80 – 120 °C at 10°/min and 1 min hold; 120 – 200 °C at 5°/min and 1 min hold and 200 – 260 °C at 20°/min and 1 min hold.

2.6. References

[1] W.H. Bragg, W.L. Bragg, The Crystalline State, Vol. 1, McMillan, New York (1949).

[2] G. Bergeret, in: Handbook of Heterogeneous Catalysis, Vol. 2, Eds: G. Ertl, H. Knozinger, J. Weitkamp, Wiley-VCH, Weinheim, pp. 464 (1997).

[3] S. Brunauer, P.H. Emmett, E. Teller, J. Am. Chem. Soc. 60 (1938) 309.

[4] E.P. Barrett, L.G. Joyner, P.P. Halenda, J. Am. Chem. Soc. 73 (1951) 373.

[5] G. Ertl, H. Knözinger, F. Schüth, J. Weitkamp, Handbook of Heterogeneous Catalysis Vol 2 (2008) Wiley-VCH, Weinheim.

[6] J. R. Fryer, Chemical Applications of Transmission Electron Microscopy, Academic Press, San Diego (1979).

[7] J.M. Thomas, O. Terasaki, P.L. Gai, W. Zhou, J. Gonzalez-Calbet, Acc. Chem.Res. 34 (2001) 583.

[8] B. E. Sundquist, Acta Metall. 12 (1964) 67.

[9] J. R. Anderson, Structure of Metallic Catalysts, Academic Press, London, 1975, p. 296.

[10] J. F. Scholten, in Preparation of Catalysts II: Scientific Bases for the Preparation of Heterogeneous Catalysts, B. Delmon, P. Grange, P. Jacobs, G. Poncelet, (Eds.), Elsevier, Amsterdam, 1979, p. 685.

[11] K. Siegbahn, C. Nordling, A. Fahlmann, R. Nordberg, K. Hamrin, J. Hedman, G. Johannson, T. Bergmark, S. E. Karlsson, I. Lindgren, B. Lindberg, ESCA – Stomic, Molecular and Solid State Structure Studied by Means of Electron Spectroscopy, Almquist and Wicksell, Uppsala, 1967.

[12] V.B. Kartha, "Spectroscopic Methods in Heterogeneous Catalysis" Eds N.M. Gupta, V.B. Kartha and R.A. Rajadhyaksha, Tata McGraw Hill, pp.1 (1991).

[13] J. Shen, R. D. Cortright, Y. Chen, J. A. Dumesic, Catal. Lett. 26 (1994) 247.

[14] G. Busca, V. Lorenzelli, Mater. Chem. 7 (1982) 89.

[15] M. Kantschewa, E. V. Albano, G. Ertl, H. Knözinger, Appl. Catal. Gen. 8 (1983) 71.

[16] S. D. Robertson, B. D. McNicol, J. H. de. Baas, S. C. Kloet, J. W. Jenkins, J. Catal. 37 (1975) 424.

[17] A. Jones, B. D. McNicol, Temperature Programme Reduction for Solid Material Characterization, Marcel Dekker, New York, 1986.

[18] T. E. Whyte Jr. Catal. Rev., 8 (1973) 117.

Chapter 3

Selective Hydrogenation of C=O in Cinnamaldehyde over Pt/CeO_2-ZrO_2 Catalysts

3.1. Introduction

Selective hydrogenation of cinnamaldehyde (CA) is of fundamental and industrial importance [1, 2]. In this compound, hydrogenation can occur either at the olefinic (C=C) or carbonyl (C=O) groups (Scheme 3.1). While the hydrogenation of olefinic group forms hydrocinnmaldehyde (HCA), that of the carbonyl group (C=O) yields cinnamyl alcohol (CAL, an unsaturated alcohol). Both these products of CA-a representative α, β-unsaturated aldehyde hydrogenation are widely used in pharmaceuticals, perfumes and flavors [4, 5]. Thermodynamics favor the hydrogenation of C=C group. Selective hydrogenation of the C=O group to achieve the corresponding unsaturated alcohol in high yield is a challenging task [1-3]. Stoichiometric reducing agents like metal hydrides, metal chlorides, aluminium isopropoxide, etc., accomplish this selective reduction to unsaturated alcohols [1, 4]. But those homogeneous processes involve costly chemicals or co-produce large amount of waste. Heterogeneous catalysts offer several advantages. A large number of supported Os, Ir, Pt, Rh, Ru, Au and Co catalysts have been reported for this transformation [6-10]. However, high selectivity at high conversion levels particularly at ambient conditions and catalyst reusability are still issues to be resolved. This is a highly demanding task due to the complexity of the system involving a rather complicated reaction mechanism, including competitive/non-competitive and dissociative/non-dissociative adsorption, side reaction, adsorption of solvent, etc [2, 4, 11]. In order to prevent consecutive hydrogenations to form 3-phenylpropanol (PPL, a saturated alcohol) and the isomerization of the allylic alcohol (Scheme 3.1), the catalyst has to suppress these reactions. The selectivity to unsaturated alcohol (CAL) must be controlled by changes in the rate constants of both competitive reactions and in adsorption constants of the components [1]. However, the key factors that control the activity and selectivity in the hydrogenation of CA are still unclear. Support material and particle size of the metals, selective poisoning, presence of a second metal, preparation method, catalyst precursor, temperature of reduction, pressure, etc., have been proposed to influence the intra-molecular hydrogenation selectivity [1].

The selectivity for the unsaturated alcohol can be enhanced by polarizing the C=O group or by hindering the adsorption of the substrate through the C=C group. This can be achieved by a right choice of the support which can interact with the supported metal [12 – 14], addition of a more electropositive metal such an iron, tin or zinc [15 – 17] or by steric and electronic effects provided by the support [1, 18]. Recently, Ramos-Fernández et al [19] have reported the effect of the support, Al_2O_3 and SiO_2, on the catalytic behavior of Cr-ZnO promoted Pt catalysts. The SiO_2 support enabled high dispersion of the promoter, which in

turn facilitated high selectivity (>95%) towards unsaturated alcohol in the hydrogenation of cinnamaldehyde. However, high temperature (110 °C), high pressure (70 bar) and long reaction times (> 10 h) were needed to obtain high conversion of CA over those catalysts. Teddy et al [20] studied the influence of alloying in carbon nanotube-supported Pt-Ru catalysts for the selective hydrogenation. High selectivity (94%) towards CAL together with high activity (CA conversion = 70%) was obtained through high temperature treatment (110 °C) of the catalyst. Coq et al [21] studied zirconia-supported Ru catalysts and proposed the formation of Ru-ZrO_x sites at the periphery of the Ru particles to explain the enhanced selectivity for CAL. Although many studies have been conducted on this or other α, β-unsaturated aldehydes using Pt supported on different oxides, a more efficient and selective catalyst *active even at room temperature and low pressures of H_2* is still not known.

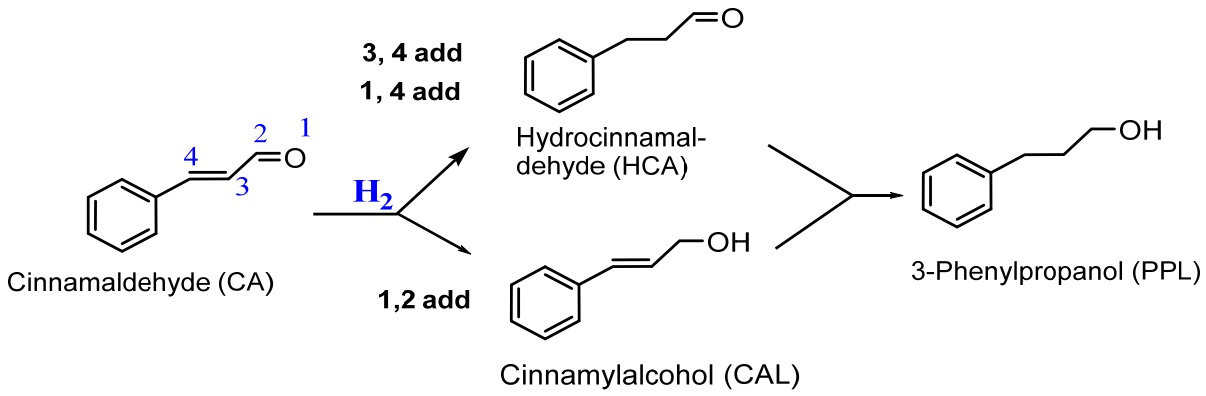

Scheme 3.1. Hydrogenation products of cinnamaldehyde.

The application of Pt/CeO_2-ZrO_2 catalysts for this reaction is studied in this work. Ceria is a reducible oxide. It facilitates dispersion of Pt and provides good support-metal interactions. Ceria-zirconia solid solutions provide thermal stability and prevent sintering of the supported metals. Presence of zirconia enhances oxygen storage capacity of ceria. All these superior characteristics of CeO_2-ZrO_2 support are expected to impart higher activity and selectivity in hydrogenation reactions. In this study, it is found that the support, electronic structure of the metal and alkali ion addition influence the conversion and product selectivity. CAL (formed via C=O hydrogenation) is the major product.

3.2. Experimental

CeO_2-ZrO_2-supported Pt catalysts were prepared and characterized as reported in Chapter 2 (sections 2.2.2.5 and 2.3). Metal dispersions were estimated from CO adsorption studies. Fourier transform infrared (FTIR) spectra of adsorbed CO were recorded on a Bruker IFS 88 spectrometer with DTGS detector using OPUS software at a resolution of 4 cm^{-1} over

64 scans. Samples were made in the form of self-supporting wafers (ca. 12 mg/cm^2) of thickness suitable for transmission IR experiments. Samples were directly treated in a specially designed quartz cell equipped with KBr windows, suitable for activation and in situ IR studies. The samples were degassed while increasing the temperature to 450 °C at slow heating rate (ca. 1 – 2°/min), treated with 100 torr of oxygen pressure at 450 °C for 1 h and followed by degassing at that temperature to clean any pre-adsorbed molecules at the active sites. Reduction was carried out under hydrogen (60 torr) for 1 h after bringing down the temperature to 250 °C. Subsequently, hydrogen was degassed at this temperature and cooled slowly to 25 °C. Spectra were recorded by gradually increasing the CO equilibrium pressure in the range of 0.001 to 5 mbar. Spectra were recorded by injecting increasing dosage of known small amounts of CO starting from 0.07 µmol till as high as 50 µmol using a pirani vacuum gauge (Oerlikon Leybold Vakuum Thermovac) after calibrating the glass linings. The catalyst spectrum collected before CO dosage was used as reference for obtaining the reported background-subtracted spectra. Spectra were normalized with respect to pellet thickness. The particle size of Pt metal was calculated from the dispersion values (CO-FTIR) by considering surface density of Pt atoms.

Details of reaction procedure and methods used in product identification and quantification are described in Chapter 2 (sections 2.4.1 and 2.5.1).

3.3. Results and Discussion

3.3.1. Structural Characterization

3.3.1.1. XRD. CeO_2- ZrO_2 (Ce:Zr = 1:1) showed a typical XRD pattern which could be assigned to the presence of both cubic and tetragonal phases, with the cubic phase being more predominant than the tetragonal phase (Fig. 3.1). Recently, Li et al [22] have also observed a mixed crystalline phase for CeO_2-ZrO_2 prepared at lower temperatures (< 500 °C). Neat CeO_2 showed a cubic fluorite structure [23]. The unit cell parameter (a_{cubic}) of "neat" CeO_2-ZrO_2 was smaller (0.537 nm) than "neat" CeO_2 (0.542 nm), suggesting formation of a CeO_2-ZrO_2 solid solution. The ionic radius of Zr^{4+} (0.084 nm) is smaller than that of Ce^{4+}(0.097 nm)/Ce^{3+}(0.112 nm) and hence, a decrease in unit cell parameter of CeO_2-ZrO_2 was observed [24]. The unit cell parameter decreased (from 0.537 to 0.512 nm) also when Pt was impregnated (Table 3.1). Samples reduced in a flow of hydrogen showed three additional peaks of low intensity at 39.7, 46.1 and 67.7° (Fig. 3.1) corresponding to reflections from (111), (200) and (220) planes of metallic platinum, respectively. The intensity of (111) reflection for all these supported Pt samples [Pt(5 wt%)/CeO_2, Pt(5

wt%)/ZrO_2 and Pt(5 wt%)/CeO_2-ZrO_2) was higher than that of the other two indicating that these planes were preferentially oriented to the others. Jung et al [25] found a preferential orientation of (111) plane when Pt was supported on herringbone carbon nanofibres and of (220) plane when it was supported on alumina. Support and the method of preparation can, therefore, influence the orientation of metal crystallites. Using Debye-Scherrer formula and the XRD peak corresponding to (111) reflection, the average crystallite size of X-ray detectable metallic Pt on CeO_2, CeO_2-ZrO_2 and ZrO_2 was estimated and it was found to be 57.2, 50.5 and 34.2 nm, respectively.

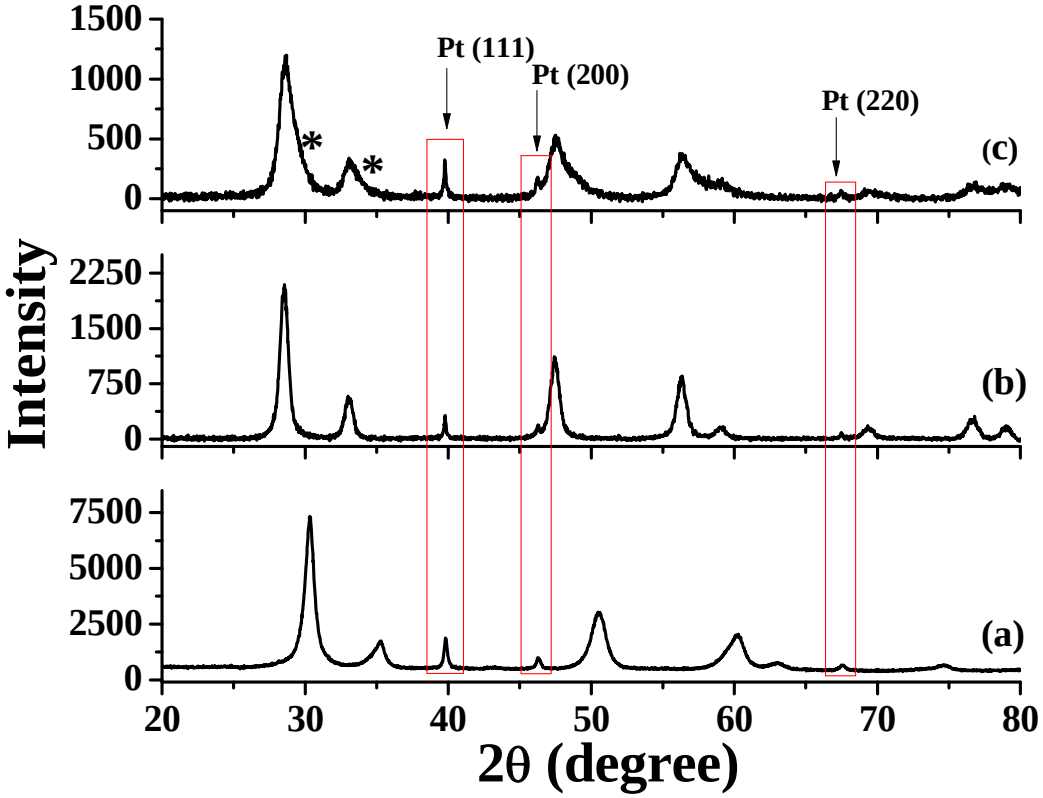

Fig. 3.1. XRD patterns of reduced a) Pt(5 wt%)/ZrO_2, b) Pt(5 wt%)/CeO_2 and c) Pt(5 wt%)/CeO_2-ZrO_2 samples. Asterisk (*) indicates peaks due to the tetragonal phase

Table 3.1. Physicochemical properties of Pt (5 wt%) supported on CeO_2-ZrO_2

Sample	XRD			N_2 adsorption - desorption			Acidity (NH_3-TPD, mmol/g)	H_2 Uptake – Pt (TPR, mmol/g)
	Support		Average crystallite size of Pt (nm)	S_{BET} (m^2/g)	Pore volume (cm^3/g)	Average pore diameter (nm)		
	Lattice parameter (a_{cubic}, nm)	Average crystallite size (nm)						
CeO_2-ZrO_2	0.537	7.72 (cubic) 7.314 (tetra)	-	115	0.17	6.1	0.179	-
Pt(5 wt%)/CeO_2	0.512	14.07	57.2	91	0.157	6.91	0.295	0.270
Pt(5 wt%)/ZrO_2	0.509	11.9	34.2	107	0.161	6.02	0.440	0.236
Pt(5 wt%)/CeO_2-ZrO_2	0.512	10.97 (cubic), 6.5(tetragonal)	50.5	94	0.139	5.87	0.367	0.376

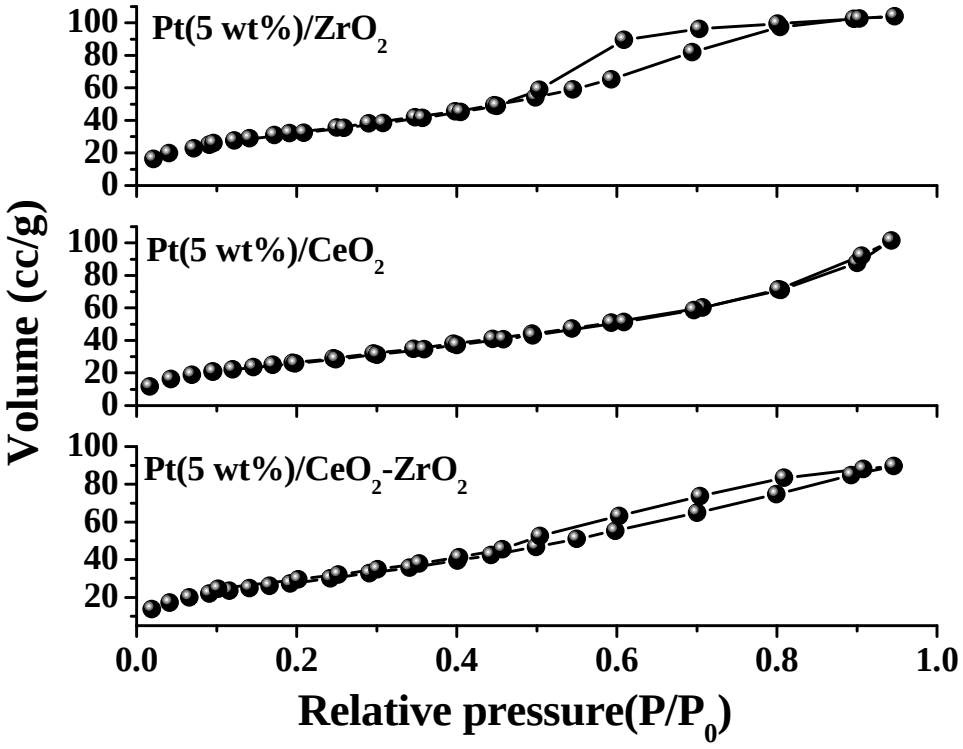

Fig. 3.2. N_2 adsorption-desorption isotherms of 5 wt% Pt supported on ZrO_2, CeO_2 and CeO_2-ZrO_2

3.3.1.2. N_2-Physisiorption. All these materials showed typical type IV isotherms with H_3 hysterisis loops (Fig. 3.2). The specific surface area (S_{BET}) of different catalysts decreased in the order: Pt(5 wt%)/ZrO_2 (107 m^2/g) > Pt(5 wt%)/CeO_2-ZrO_2 (94 m^2/g) > Pt(5 wt%)/CeO_2 (91 m^2/g) (Table 3.1). Upon Pt impregnation, S_{BET} of CeO_2-ZrO_2 decreased from 115 to 107 m^2/g.

3.3.1.3. HRTEM. Representative HRTEM images of Pt(5 wt%) supported on CeO_2 ZrO_2 and CeO_2-ZrO_2 are shown in Fig. 3.3. From these micrographs, the particle size of Pt was determined to be in the range of 5 – 12 nm. There are a few particles which are of 40 nm size. The values of Pt crystallite sizes determined from XRD measurements are higher than those estimated from HRTEM. The Pt peak profile in XRD can be separated into two contributions, that corresponding to large crystallites in the thin part of the Pt peaks and to small crystallites in the tails of the diffraction line. The values reported from XRD are those for the large crystallites. From the lattice fringes it was found that the (111) plane of Pt is preferentially exposed which agrees well with the inference derived from the XRD results.

3.3.1.4. X-ray Photoelectron Spectroscopy. The electronic structure of Pt was determined using X-ray photoelectron spectroscopy. Fig. 3.4 shows the binding energy (B.E.) peaks arising from the 4f core levels of reduced Pt(5 wt%) supported on CeO_2, ZrO_2 and CeO_2-ZrO_2. The peaks at 70.7 and 74.1 eV for Pt(5 wt%)/CeO_2 are corresponded to $4f_{7/2}$ and $4f_{5/2}$ levels of Pt^0. The positions of these peaks are in agreement with the values reported by others [23]. Deconvolution of those peaks revealed the presence of an oxidized form of platinum (Pt^{2+}) with XP peaks at 72.4 and 75.5 eV, very small in percentage of concentration (Table 3.2). Pt(5 wt%)/ZrO_2 showed the peaks due to Pt^0 at 70.9 and 74.6 eV. These for Pt(5 wt%)/CeO_2-ZrO_2 occurred at 71.3 and 74.6 eV.

Table 3.2. Binding energy values (in eVs) of supported Pt catalysts

Sample	Pt^0		Pt^{2+}	
	$4f_{7/2}$	$4f_{5/2}$	$4f_{7/2}$	$4f_{5/2}$
Pt (5 wt%)/CeO_2	70.7	74.1	72.4	75.5
Pt (5 wt%)ZrO_2	70.9	74.6	72.2	75.7
Pt (5 wt%)/CeO_2-ZrO_2	71.3	74.6	72.5	75.8

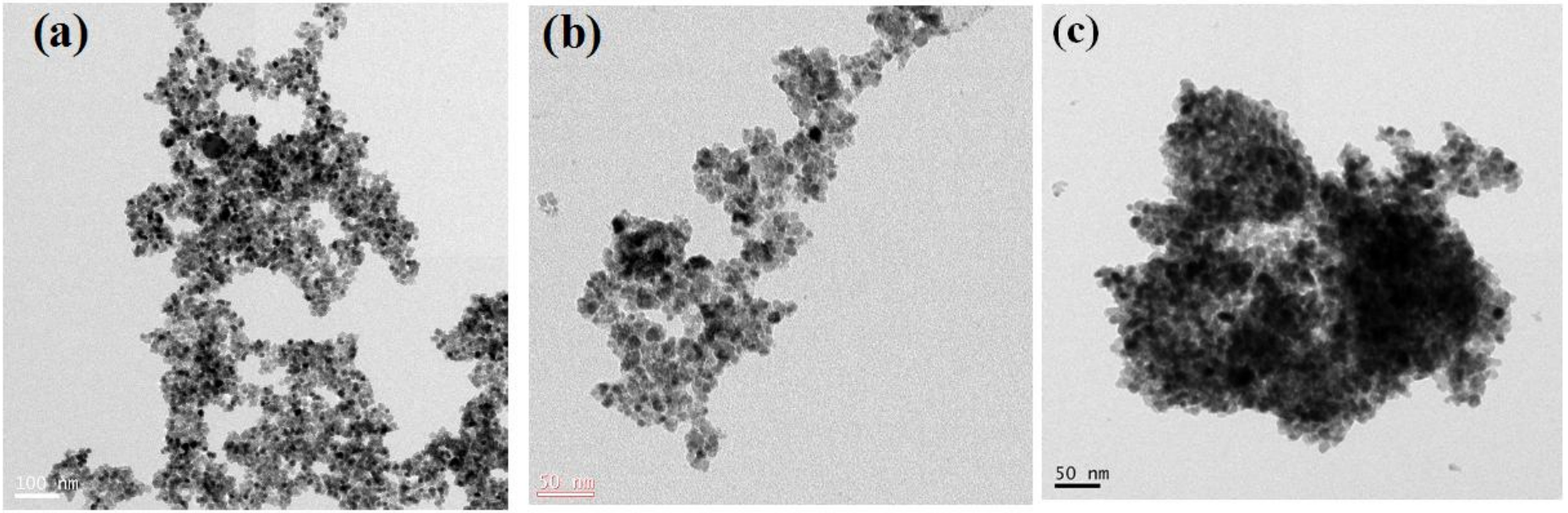

Fig. 3.3. HRTEM images of Pt(5 wt%) supported on a) CeO_2, b) CeO_2-ZrO_2 and c) ZrO_2

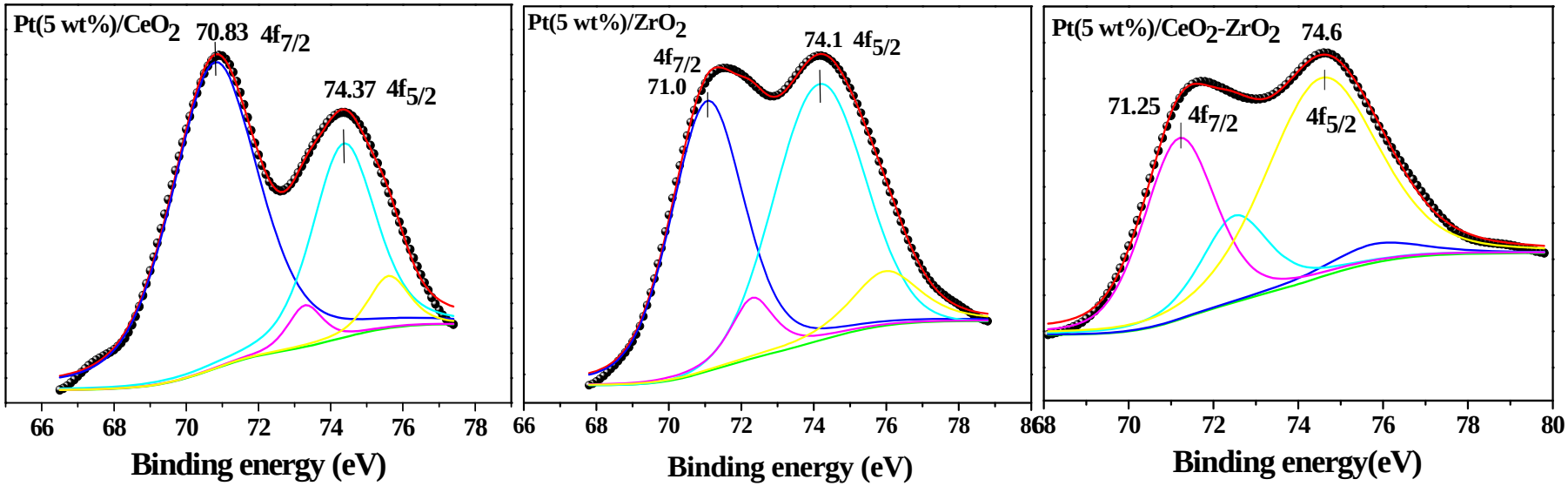

Fig. 3.4. XPS of 5 wt% Pt supported on CeO_2, ZrO_2 and CeO_2-ZrO_2

Based on these peaks positions it can be concluded that Pt on CeO_2 is relatively rich in electron density than that supported on ZrO_2 and CeO_2-ZrO_2. It is also likely that the crystallites of Pt are smaller on CeO_2-ZrO_2 than on "neat" ZrO_2 and CeO_2 [25, 26].

3.3.1.5. DRIFT Spectra of Adsorbed Pyridine. The nature and the type of acid sites on CeO_2-ZrO_2 were determined by DRIFT spectroscopy using pyridine as probe molecule (Fig. 3.5). The sample showed IR peaks of adsorbed pyridine at 1608, 1597, 1485 and 1440 cm^{-1} (Fig. 3.5). The peaks at 1608 and 1440 cm^{-1} are attributed to H-bonded pyridine and those at 1597 and 1485 cm^{-1} are assigned to pyridine-coordinated to weak Lewis acid sites [27]. Generally, strong Lewis acid IR peaks are observed at 1623 and 1455 cm^{-1} whereas Brönsted acid peaks are observed at 1639 and 1546 cm^{-1}, both were absent in present case. Upon impregnation of Pt, the relative concentration of these acidic sites has changed.

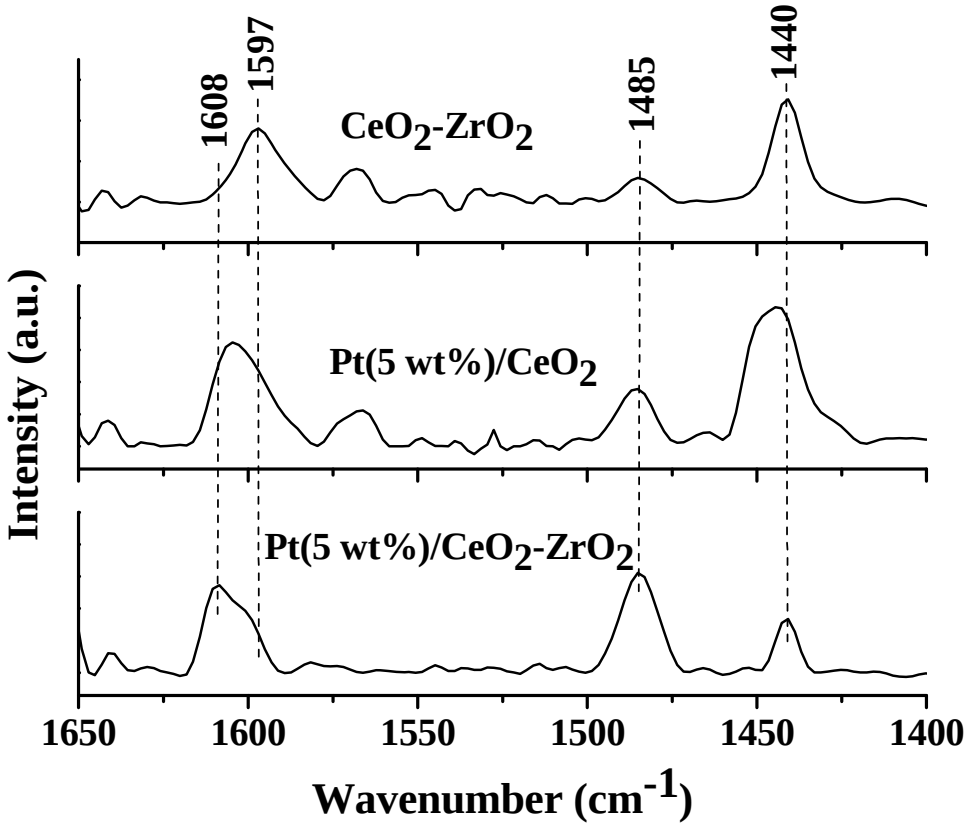

Fig. 3.5. DRIFT spectra of adsorbed pyridine of neat CeO_2-ZrO_2 and 5 wt% Pt loaded on CeO_2-ZrO_2 and CeO_2

3.3.1.6. NH_3–TPD. The density of acid sites on supported Pt catalysts was quantified by NH_3-TPD measurements (Fig. 3.6, Table 3.1). Two overlapping, broad desorption peaks were observed in the temperature range 100 – 400 °C. While the peak at 150 – 175 °C is

attributed to NH_3 desorbed from the surface hydroxyl groups that at 250 – 275 °C is corresponded to weak Lewis acid sites [12]. Metal impregnation enhanced the acidity (Table 3.1). The acidity (NH_3 desorption) of the supported Pt catalysts increased in the order: Pt(5 wt%)/CeO_2 (0.295 mmol/g) < Pt(5 wt%)/CeO_2-ZrO_2 (0.367 mmol/g) < Pt(5 wt%)/ZrO_2 (0.440 mmol/g).

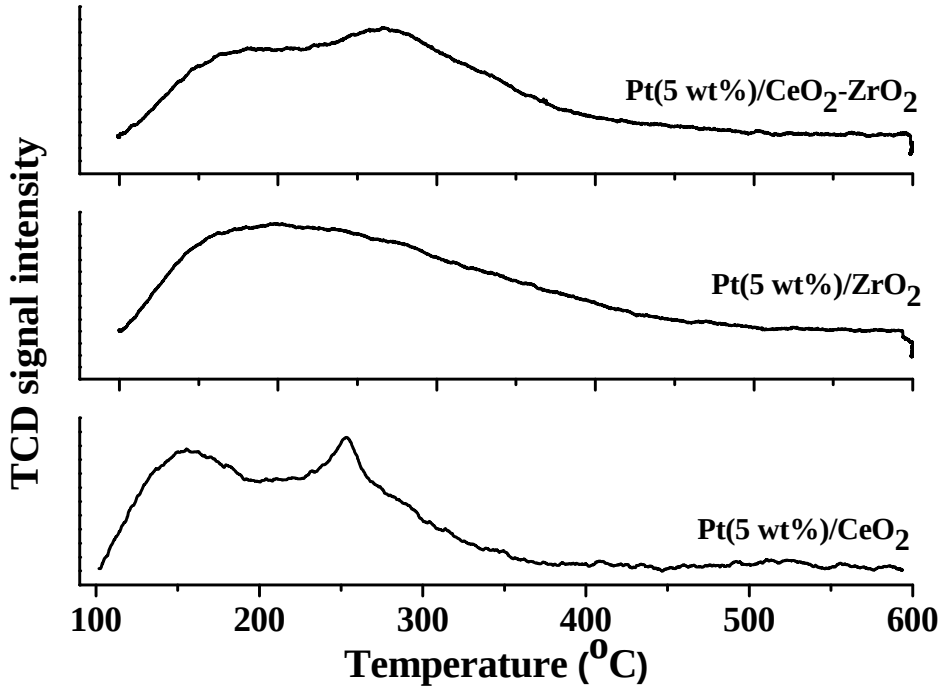

Fig. 3.6. NH_3-TPD profiles of 5 wt% Pt supported catalysts

3.3.1.7. Temperature-Programmed Reduction with Hydrogen. H_2-TPR provided knowledge on support-metal interactions. It revealed the reduction temperatures of metal and the support. Bulk platinum showed a hydrogen uptake peak in TPR at 130 – 160 °C. This peak in the case of Pt(5 wt%) supported on CeO_2 (70 and 106 °C) and CeO_2-ZrO_2 (80 and 149 °C) occurred at lower temperatures possibly due to support-metal interactions and variation in crystallite/particle sizes (Fig. 3.7). CeO_2 is a reducible oxide and keeps the metal in lower oxidation state. While the peak at 80 °C in the case of Pt(5 wt%)/CeO_2-ZrO_2 is attributed to Pt strongly interacting with the support, that at 149 °C is attributed to relatively larger size of Pt crystallites. These hydrogen uptake peaks in the case of Pt supported on ZrO_2 were observed at 98 and 184 °C, respectively. Neat CeO_2 showed a broad reduction peak centred at 850 °C. In CeO_2-ZrO_2, this peak due to CeO_2 reduction shifted to lower temperatures (376 and 494 °C) due formation of a CeO_2-ZrO_2 solid solution. These experiments, thus, provided definite evidence that the reduction peaks observed below 184

°C in the case of supported Pt catalysts are due to metal only and not because of the support oxide. The amount of hydrogen uptake by these catalysts was found to decrease in the order: Pt(5 wt%)/CeO_2-ZrO_2 (0.376 mmol/g) > Pt(5 wt%)/CeO_2 (0.270 mmol/g) > Pt(5 wt%)/ZrO_2 (0.236 mmol/g) (Table 3.1). This observation indicates that the extent of dispersion and the amount of exposed Pt is higher on CeO_2-ZrO_2 than on the other supports.

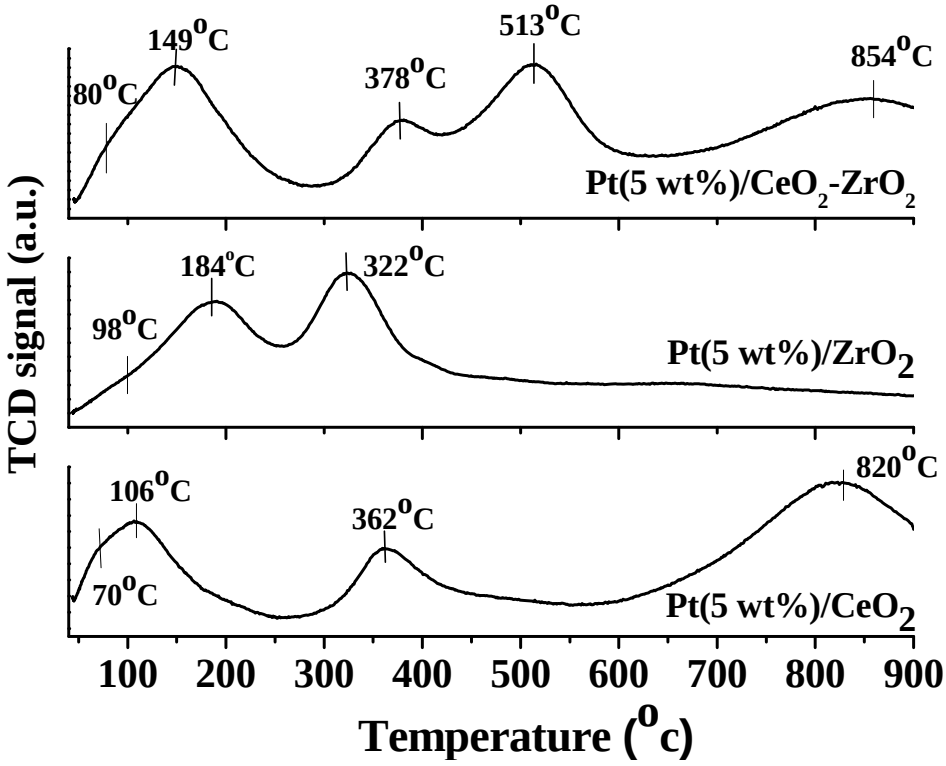

Fig. 3.7. Temperature-programmed reduction (H_2) profiles of Pt(5 wt%) supported on CeO_2, ZrO_2 and CeO_2-ZrO_2

3.3.1.8. FTIR Spectra of Adsorbed CO. Metal dispersion and average metal particle diameter were estimated from the in situ DRIFT spectra of adsorbed CO. Representative CO adsorption profiles for Pt(5 wt%)/CeO_2-ZrO_2 at different CO dosages are shown in Fig. 3.8. It was assumed that one mole of surface Pt adsorbs one mole of CO. It was also presumed that the surface Pt was very sensitive to gas molecules at ambient temperatures and the adsorption is irreversible. Based on these assumptions, Pt will adsorb CO irrespective of the CO partial pressure, i.e., as long as free surface Pt sites are available it will keep on adsorbing CO until all CO present is consumed. Based on this, small doses of calculated amount of CO were injected into the vacuum line and the spectra were recorded. Unless all the surface of Pt is consumed upon each injection the resultant partial pressure in the line shows zero reading. Once each surface Pt atom is consumed in Pt-CO bond formation, further injection of CO

leads to no further increase in CO adsorption as indicated by no (or negligible) drop of pressure and thus no significant increase of integrated intensity of the absorption band (bands). Thus, a plot of integrated intensity verses CO dosage (Fig. 3.8, right panel) shows a straight line passing through origin (i.e. until no surface Pt is left unsatisfied) and an almost horizontal line to X-axis. The extrapolation of these two lines gives the point i.e. amount of CO required for consumption by surface Pt atoms. Thus, by counting the amount of CO, the amount of surface Pt atoms was calculated.

Two overlapping IR bands at 2058 and 2078 cm^{-1} were observed (Fig. 3.8). Based on earlier reports [28, 29], the former is attributed to CO linearly bonded to low-coordinated, open Pt atoms and the latter to Pt adsorbed at terrace sites. The position of the former shifted to 2064 cm^{-1} as the dosing of CO was increased. Also, a weak band was observed at 1854 cm^{-1} attributable to bridge bonded CO. Observation of this peak indicates that there are also a few number of small size metallic Pt particle on the surface of CeO_2-ZrO_2. In other words, the CO adsorption studies, in concurrence with HRTEM, reveal the presence of different types of Pt particles whose concentration determines the hydrogenation selectivity. Based on these CO adsorption studies, metal dispersion on different supports was estimated to increase in the order: Pt(5%)/ZrO_2 (16.2%) < Pt(5%)/CeO_2 (20.3%) < Pt(5%)/CeO_2-ZrO_2 (40.5%). Incorporation of ZrO_2 in CeO_2 promoted the dispersion of Pt by nearly two times. This is a quite high dispersion value, indicating that approximately half of the platinum atoms is located at the surface. However, the crystallite size, as measured from Scherrer equation (XRD) indicated quite large crystal size (50.5 nm). These large crystal sizes strongly indicate that the dispersion of platinum is low, much lower than 40.5%. HRTEM (Fig. 3.3), on the other hand, showed the presence of a large number of platinum particles of dimension 5 – 12 nm along with some particles of much larger size. Croy et al [30] and Dömök et al [31] demonstrated that the binding energy (BE) values of photoelectrons ejected from metal particles depend on the metal particle size. The smaller the species the higher would be the binding energy. The BE values of Pt supported on CeO_2-ZrO_2 were higher than those of CeO_2 and ZrO_2 (Table 3.2). This experimental observation also points out the presence of a large number of smaller Pt particles on CeO_2-ZrO_2 support. The observed metal dispersion from CO-adsorption studies (40.5% for Pt(5%)/CeO_2-ZrO_2) is due to a stoichiometric average of crystals of smaller as well as larger dimensions.

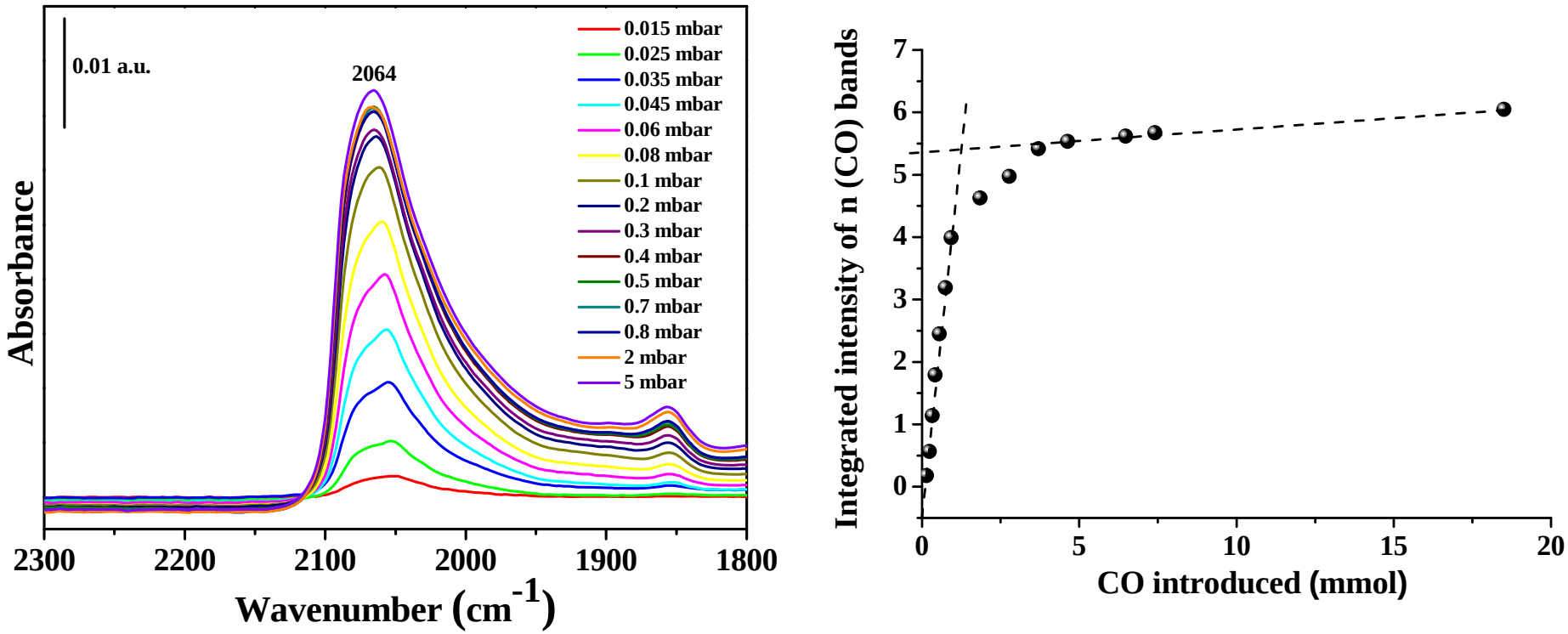

Fig. 3.8. FTIR spectra of adsorbed CO on Pt (5 wt%)/CeO_2-ZrO_2 catalyst

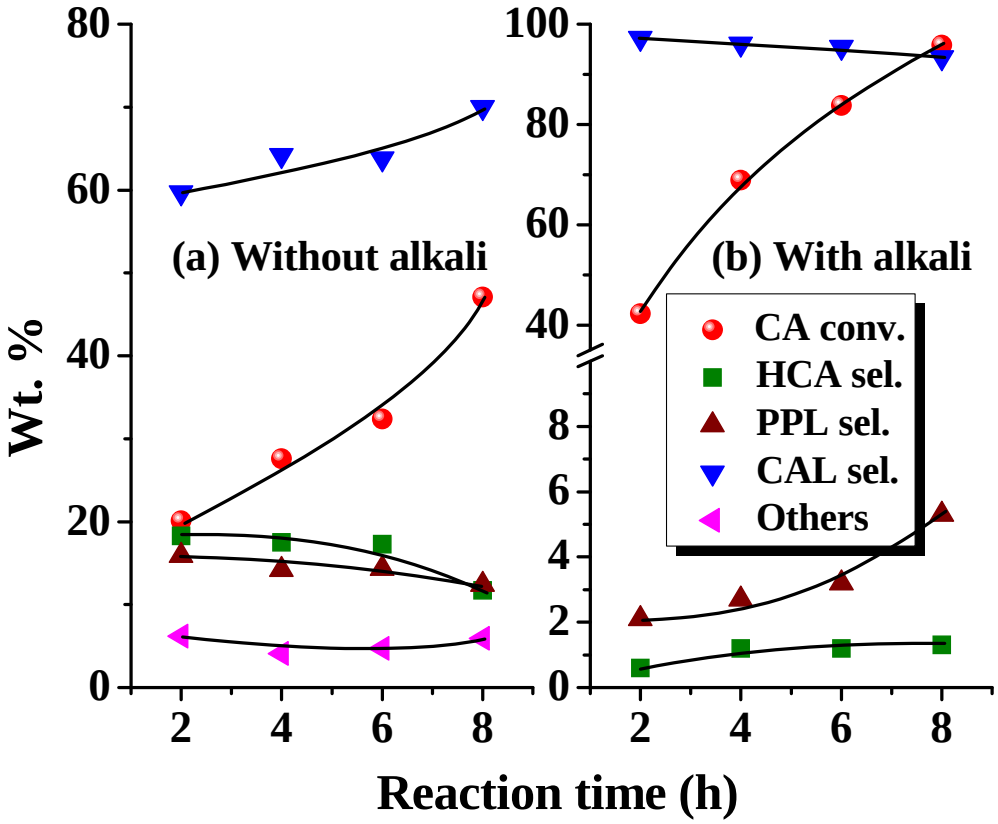

Fig. 3.9. Influence of alkali addition on hydrogenation of cinnamaldehyde over Pt(5 wt%) supported CeO_2-ZrO_2 catalysts. *Reaction conditions*: Catalyst (reduced at 300 °C for 2 h) = 0.05 g, cinnamaldehyde (CA) = 4 g, solvent (iso-propanol) = 40 ml, alkali solution = 0.02 g of NaOH in 10 ml water (p^H = 13), H_2 pressure = 20 bar, reaction temperature = 25 °C, stirring speed = 500 rpm. HCA = hydrocinnamaldehyde, PPL = 3-phenylpropanol, CAL = cinnamyl alcohol, other products include acetals.

3.3.2. Catalytic Activity

Supported Pt catalysts of the present study are highly active even at room temperature (25 °C) for the hydrogenation of cinnamaldehyde (CA). Fig. 3.9 (left panel) shows the variation of CA conversion and products selectivity as a function of reaction time for Pt(5 wt%)/CeO_2-ZrO_2 catalyst. This reaction usually yields different hydrogenated products as shown in Scheme 3.1. Hydrogenation of the carbonyl group (1, 2-addition) results in unsaturated alcohol – cinnamyl alcohol (CAL) and of the olefinic bond (3, 4-addition) gives the saturated aldehyde – hydrocinnamaldehyde (HCA). The 1, 4-addition gives enol which

isomerizes into HCA. Further hydrogenation leads to formation of 3-phenylpropanol (PPL) and subsequently, propylbenzene (PB). Also CAL can get reduced to PPL. In the present study, over supported Pt catalysts, 1, 2-addition is more selective than 3, 4 and 1, 4-additions. Over Pt(5 wt%)/CeO_2-ZrO_2, CAL formed with a selectivity of 60 – 70%, while HCA + PPL together formed with a selectivity of 23 – 33% (Fig. 3.9; left panel). Formation of a minor quantity of acetal side product (selectivity = 4 – 6%) was also detected. At the end of 8 h, CA conversion was 47.1%. Formation of PB was not detected.

3.3.2.1. Effect of Alkali Addition. When alkali (0.02 g of NaOH in 10 ml of water) was added to the reaction medium, a significant enhancement in catalytic activity was observed (Fig. 3.9; right panel). At 8 h, CA conversion increased from 47.1 to 95.8%, turnover frequency (TOF; moles of CA converted per mole of exposed Pt per hour) increased from 343 to 698 and CAL selectivity increased from 70 to 93.4%. Side reactions (acetal formation) got completely suppressed. Several bases including NaOH, KOH, $Cs(OH)_2$, $NaHCO_3$, Na_2CO_3, $(COONa)_2$ and Na_2SO_4 were examined. Among all these, NaOH was found to provide high catalytic activity and CAL selectivity (Table 3.3).

Table 3.3. Influence of base type on hydrogenation of cinnamaldehyde over Pt(5 wt%)/CeO_2-ZrO_2

Base	CA conversion (wt%)	TOF (h^{-1})	Product selectivity (%)		
			HCA	PPL	CAL
NaOH	42.3	1233	0.6	2.1	97.3
Na_2CO_3	36.3	1058	26.4	12.0	61.6
$NaHCO_3$	36.5	1064	18.8	8.9	72.3
$(COONa)_2$	40. 6	1184	14.6	8.9	76.5
Na_2SO_4	39.7	1158	16.0	9.7	74.3
KOH	36.0	1050	17.2	8.8	74.0
$Cs(OH)_2$	27.9	813	16.2	11.0	72.8

Reaction conditions: Catalyst (Pt (5 wt%)/CeO_2-ZrO_2 reduced at 300 °C for 2 h) = 0.05 g, cinnamaldehyde (CA) = 4 g, solvent (iso-propanol) = 40 ml, promoter = 0.02 g of base in 10 ml water, H_2 pressure = 20 bar, reaction temperature = 25 °C, reaction time = 2 h, stirring speed = 500 rpm. Turnover frequency (TOF) = moles of CA converted per mole of exposed Pt (derived from CO adsorption studies) per hour.

Table 3.4. Influence of solvent on hydrogenation of cinnamaldehyde over Pt(5 wt%)/CeO_2-ZrO_2

Solvent	Solvent properties				CA conversion (wt%)	TOF (h^{-1})	Product selectivity (%)			
	Polarity index	Dielectric constant (Debye)	Miscibility in water (%)	Gutmann acceptor number			HCA	PPL	CAL	Others
Isopropanol	3.9	17.9	100	33.8	20.1	586	18.3	15.9	59.7	6.2
Acetonitrile	5.8	36.6	100	18.9	4.9	143	42.6	11.8	45.5	0
Toluene	2.4	2.38	0.051		3.0	87	47.1	27.2	25.7	0
Dioxane	4.8	2.25	100	10.3	10.6	309	24.1	12.5	63.4	0
Ethanol	5.2	24.3	100	37.9	28.9	843	9.9	8.1	47.3	34.7
Tert.-butanol	4.0	18	0.43	36.8	10.0	292	19.9	10.9	69.1	0

Reaction conditions: Catalyst (reduced at 300 °C for 2 h) = 0.05 g, cinnamaldehyde (CA) = 4 g, solvent = 40 ml, promoter alkali = nil, H_2 pressure = 20 bar, reaction temperature = 25 °C, reaction time = 2 h, stirring speed = 500 rpm.

3.3.2.2. Effect of Solvent. Further, the nature of solvent was found to have a profound influence on CA conversion and CAL selectivity (Table 3.4). The reactions were conducted in non-polar (toluene) and polar – aprotic (dioxane and acetonitrile) and protic (ethanol, iso-propanol and tert.-butanol) solvents. CA conversion was much higher in ethanol and iso-propanol than in other solvents (TOF = 843 and 586, respectively). However, formation of undesired acetal products was detected in the presence of alcohol solvents. Extent of this was lower in iso-propanol than in ethanol (Table 3.4). As noted from Table 3.3, when base (NaOH) was added to the reaction mixture, side reactions were suppressed and CAL formed selectively. In toluene and acetonitrile solvents, hydrogenation of olefinic bond was preferred to the carbonyl bond of CA. In view of higher apparent activity and CAL selectivity, iso-propanol was chosen as the solvent of choice in further studies.

3.3.2.3. Effect of Pt Loading. Metal loading was essential to get high yields of CAL. As seen from Table 3.5, CA conversion increased with increasing amount of Pt loading. Conversion of CA increased from 70.4 to 95.8% when the Pt loading on CeO_2-ZrO_2 was increased from 0.5 to 5 wt%. Only a marginal variation in CAL selectivity (89 – 93.4%) was observed. This suggests a uniform dispersion of Pt on CeO_2-ZrO_2 support up to a metal loading of at least 5 wt%.

Table 3.5. Influence of percentage metal loading on hydrogenation of cinnamaldehyde

Pt loading (wt%)	CA conversion (wt%)	Product selectivity (%)			
		HCA	PPL	CAL	Others
0.5	70.4	1.9	2.0	89.1	7.0
1	78.2	3.4	2.8	82.5	11.3
2	85.0	1.1	2.5	90.5	5.9
5	95.8	1.3	5.3	93.4	0

Reaction conditions: Catalyst (reduced at 300 °C for 2 h) = 0.05 g, cinnamaldehyde (CA) = 4 g, solvent (iso-propanol) = 40 ml, alkali solution = 0.02 g of NaOH in 10 ml water (pH = 13), H_2 pressure = 20 bar, reaction temperature = 25 °C, reaction time = 8 h, stirring speed = 500 rpm.

3.3.2.4. Effect of Reaction Temperature. The effect of reaction temperature was studied in the absence of alkali promoters as the conversions were lower without alkali addition and the effect of temperature on the reaction can be monitored better. The reactions

were conducted at 25, 50, 75 and 100 °C. As seen from Table 3.6, CA conversion increased from 20.1 to 63.4% in 2 h as the temperature was raised from 25 to 100 °C. Increase in CAL selectivity from 60 to 71% at the expense of HCA+PPL products selectivity was also noted. This study thus reveals that although Pt is effective even at 25 °C for the selective hydrogenation of carbonyl group of CA, temperature further facilitates this selective transformation.

3.3.2.5. Effect of Hydrogen Pressure. Hydrogen pressure was varied from 1 to 30 bar while keeping the other parameters constant. CA conversion and CAL selectivity increased with increasing hydrogen pressure (Table 3.7). A pressure of 20 bar was found optimum to yield CA conversion of 95.8% and CAL selectivity of 93.4% at the end of 8 h at 25 °C.

Table 3.6. Effect of reaction temperature on the hydrogenation of cinnamaldehyde over Pt(5 wt%)/CeO_2-ZrO_2

Temperature (°C)	CA conversion (wt%)	TOF (h^{-1})	Product selectivity (%)			
			HCA	PPL	CAL	Other products
25	20.1	586	18.3	15.9	59.7	6.2
50	39.3	1146	14.3	12.7	64.9	8.1
75	43.5	1268	15.3	11.3	66.9	6.5
100	63.4	1849	10.8	13.1	71.1	5.0

Reaction conditions: Catalyst (reduced at 300 °C for 2 h) = 0.05 g, cinnamaldehyde (CA) = 4 g, solvent (iso-propanol) = 40 ml, alkali addition = nil, H_2 pressure = 20 bar, reaction time = 2 h, stirring speed = 500 rpm. Turnover frequency (TOF) = moles of CA converted per mole of exposed Pt (derived from CO adsorption studies) per hour.

Table 3.7. Effect of H_2 pressure: Hydrogenation of cinnamaldehyde over Pt(5 wt%)/CeO_2-ZrO_2

H_2 pressure (bar)	CA conversion (wt%)	TOF (h^{-1})	Product selectivity (%)			
			HCA	PPL	CAL	Others
1	17.0	124	28.5	4.8	66.8	0
5	40.0	292	11.6	6.4	82.0	0
10	80.7	588	3.2	3.2	89.6	4.1
20	95.8	698	1.3	5.3	93.4	0
30	99.2	723	0.1	10.2	89.6	0

Reaction conditions: Catalyst (reduced at 300 °C for 2 h) = 0.05 g, cinnamaldehyde (CA) = 4 g, solvent (iso-propanol) = 40 ml, alkali solution = 0.02 g of NaOH in 10 ml water (pH = 13), reaction temperature = 25 °C, reaction time = 8 h, stirring speed = 500 rpm.

Table 3.8. Influence of catalyst amount on hydrogenation of cinnamaldehyde over Pt(5 wt%)/CeO_2-ZrO_2

Catalyst amount (g)	CA conversion (wt%)	TOF (h^{-1})	Product selectivity (%)			
			HCA	PPL	CAL	Others
0.025	33.7	491	11.8	5.9	82.3	0
0.050	40.0	292	11.7	6.4	82.0	0
0.075	42.2	205	17.8	7.7	74.5	0
0.1	75.0	273	10.6	6.1	75.9	7.5
0.15	86.4	210	20.5	9.3	68.8	1.4

Reaction conditions: Catalyst = Pt (5 wt%)/CeO_2-ZrO_2 reduced at 300 °C for 2 h, cinnamaldehyde (CA) = 4 g, solvent (iso-propanol) = 40 ml, alkali solution = 0.02 g of NaOH in 10 ml water (pH = 13), H_2 pressure = 5 bar, reaction temperature = 25 °C, reaction time = 8 h, stirring speed = 500 rpm.

3.3.2.6 Effect of Catalyst Amount. CA conversion increased (Table 3.8) with increasing amount catalyst from 0.025 to 0.15 g. However, the selectivity for CAL had decreased. At higher amounts of the catalyst, acidity of the medium increased which facilitated activation of olefinic bonds and formation of acetal products. An amount of 0.05 g of catalyst was found ideal at our reaction conditions. The selectivity to CAL verses conversion plots, as varied by changing the amount of catalyst in the reactor (Table 3.8) and by changing the reaction time (Fig. 3.9) showed a similar trend. The selectivity to CAL decreased with increasing conversion. At the same time some increase in the selectivity to PPL (formed via further hydrogenation of CAL) was observed. This variation in product selectivity with conversion followed the trend proposed in the reaction Scheme 3.1.

3.3.2.7 Effect of Support. Fig. 3.10 demonstrates the influence of support on the catalytic activity and product selectivity of the Pt supported catalysts. CeO_2-ZrO_2 was found to be a better support than neat CeO_2 and neat ZrO_2. While CA conversion was 95.8% with CAL selectivity of 93.4% at the end of 8 h, by using Pt(5%)/CeO_2-ZrO_2, the conversion was only 88.9 and 81.8% on Pt(5 wt%)/CeO_2 and Pt(5 wt%)/ZrO_2, respectively. In the presence of zirconia, the activity and selectivity (for CAL) of ceria had increased. Table 3.9 compares the catalytic activity of Pt/CeO_2-ZrO_2 with those of other reported catalysts. High amount of catalyst and temperature are the requirements with most of the known catalysts. They are either poorly active or less selective. The catalyst of the present study shows efficient activity and selectivity even at ambient temperature (25 °C).

3.4. Structure-Activity Correlations

The catalysts of the present work are highly active and selective for the hydrogenation of CA even at 25 °C and H_2 pressures as low as 20 bar. Cinnamyl alcohol is the major product. CA conversion at the end of 8 h over these catalysts increased in the order: Pt(5 wt%)/ZrO_2 (81.8%) < Pt(5 wt%)/CeO_2 (88.9%) < Pt(5 wt%)/CeO_2-ZrO_2 (95.8%); and the selectivity for CAL increased in the order: Pt(5 wt%)/ZrO_2 (73.6%) < Pt(5 wt%)/CeO_2 (85.6%) < Pt(5 wt%)/CeO_2-ZrO_2 (93.4%). The selectivity in the hydrogenation of cinnamaldehyde was affected by the metal particle size. An increase in metal particle size (>3 nm) favored selectivity towards the unsaturated alcohols (CAL). Gallezot and Richard [1] explained this on the basis of steric effects wherein with large metal particles, the aromatic ring restrains a close approach of the C=C bond to the metal surface. But on small metal particles, the aromatic ring can lie aside of the metal particle and the C=C bond can be hydrogenated. Originally, Loffreda et al [40, 41] and Serrano-Ruiz et al [42] explained based on theoretical calculations, that the α, β-unsaturated aldehydes adsorb in a different way on

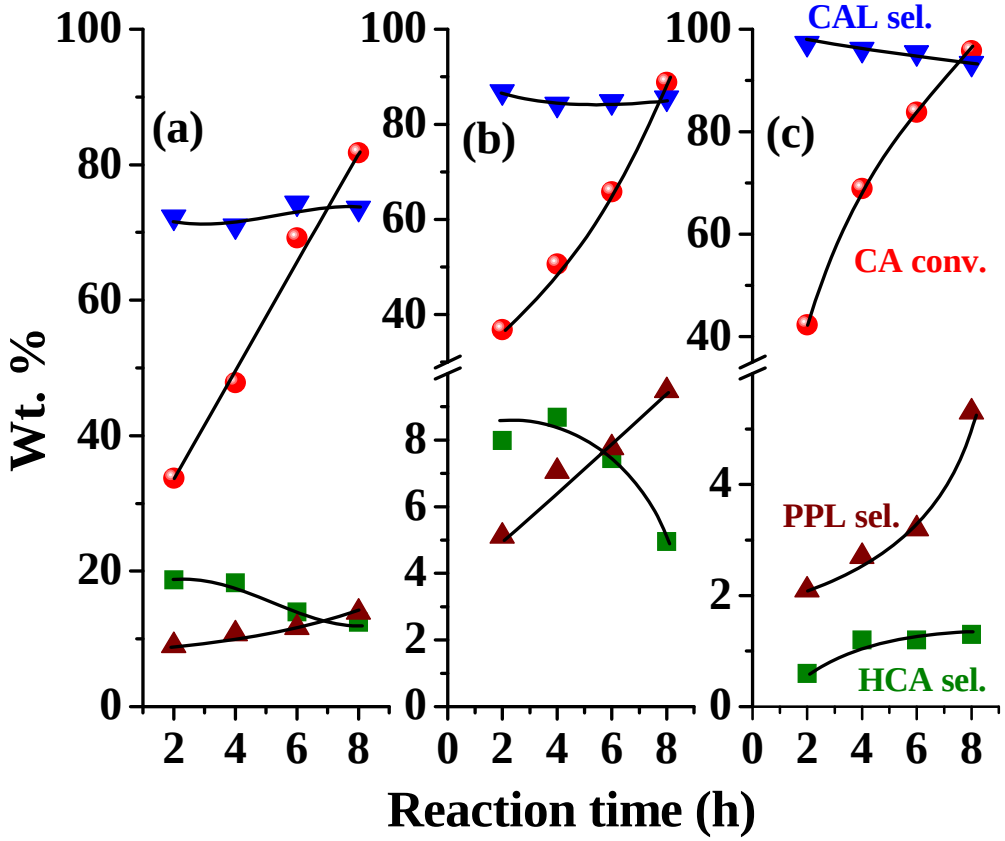

Fig. 3.10. Influence of support on hydrogenation of cinnamaldehyde: (a) Pt(5 wt%)/ZrO_2, (b) Pt(5 wt%)/CeO_2 and (c) Pt(5 wt%)/CeO_2-ZrO_2. *Reaction conditions:* Catalyst reduced at 300 °C for 2 h = 0.05 g, cinnamaldehyde (CA) = 4 g, solvent (iso-propanol) = 40 ml, alkali solution = 0.02 g of NaOH in 10 ml water (p^H = 13), H_2 pressure = 20 bar, reaction temperature = 25 °C, stirring speed = 500 rpm.

Table 3.9. Catalytic activity of different supported Pt catalysts for hydrogenation of cinnamaldehyde

Catalyst	Reaction conditions (amount of catalyst, temperature, H_2 pressure, reaction time)	CA conversion (%)	CAL selectivity (%)	Reference
Pt (14%)/zeolite-Y	0.4 g, 60 °C, 40 bar, 2 h	75	96	[32]
Pt(5%)/K-10 montmorillonite	0.02 g, 25 °C, 4 bar, 17 h	70	99	[33]
Pt(2%)/modified montmorillonite	0.3 g, 100 °C, 5 bar, 5 h	89	80	[34]
Pt(3%)/potassium titanate nanotube	0.05 g, 40 °C, 10 bar, 4 h	70	83	[35]
Pt(4%)-$FeCl_2$(0.2%)/charcoal	0.4 g, 60 °C, 40 bar, 2 h	75	87	[36]
Pt(2.2%)carbon nano fibre	0.1 g, 100 °C, 50 bar	90	68	[25]
Pt(5%)Fe(0.8%)Zn(0.4%)/mesoporous carbon	0.3 g, 100 °C, 16 bar, 12 h	96	86	[36]
Pt(3%)/multi-walled carbon nanotubes	0.4 g, 80 °C, 20 bar, 9 h	100	88	[30]
Pt(5%)/Cr-ZnO	0.3 g, 110 °C, 70 bar, 2 h	100	96	[19, 37]
$PtSn_{0.8}/SiO_2$	0.2 g, 90 °C, 10 bar, 4 h	60	80	[38]
Pt(1%)/Al_2O_3	0.4 g, 60 °C, 40 bar, 2 h	90	64	[39]
Pt(5%)/CeO_2-ZrO_2	0.05 g, 25 °C, 20 bar, 8 h	97.4	91.5	This work

different crystal planes and steps. While on Pt (111) plane, CA prefers to adsorb through η^1(C=O) coordination, on Pt (100) the adsorption is through both η^2(C=C) and η^1(C=O) modes. With increasing crystallite size, the fraction of steps and corners decreases and (111) planes are preferentially oriented. The particle size of Pt in the catalysts of present work is 5 – 12 nm. A few particles of 40 nm were also observed (HRTEM). Hence, as expected, (111) plane is more exposed (XRD and HRTEM) and thereby the catalysts of this study are more selective for the CAL product.

As seen from CO adsorption studies, support influenced to a great extent the Pt dispersion. Dispersion of Pt is more on CeO_2-ZrO_2 (40.5%) than on CeO_2 (20.3%) and ZrO_2 (16.2%). It is interesting to note that variation in catalytic activity (CA conversion; Fig. 3.10) is in line with the variation in metal dispersion.

The acidity of different catalysts increased in the order: Pt(5 wt%)/CeO_2 (0.295 mmol/g) < Pt(5 wt%)/CeO_2-ZrO_2 (0.367 mmol/g) < Pt(5 wt%)/ZrO_2 (0.440 mmol/g). This led to unwanted side reactions (acetals formation). Lewis acidity facilitated adsorption of CA through its carbonyl group and enabled selective formation of CAL product. As seen from the XPS data (Table 3.2), CeO_2 (a reducible metal oxide) promoted electron density at the site of Pt. Higher electron density on metal facilitates π^*_{CO} back-bonding and thereby, an enhancement in selectivity to CAL during the hydrogenation of CA is observed. The factors of acidity of the support (due to the presence of ZrO_2 component) and higher electron density at Pt (due to CeO_2 component) are responsible for the higher catalytic activity and selectivity of Pt supported on CeO_2-ZrO_2 composite material. Addition of base to the reaction medium suppressed the side reactions. Apart from altering the electronic structure of metal [22], alkali ions (Na^+) have also facilitated the adsorption of CA through their carbonyl groups and enhanced the catalytic activity and CAL selectivity.

The physical properties of solvents used in the present study are listed in Table 3.4 along with the catalytic activity data. Solvents showed a marked effect on catalytic activity. Dielectric constant and miscibility with water are a measure of polarity of the solvent. Gutmann's acceptor number (AN) determines the Lewis acidity of the solvent. A comparison of these physical parameters and catalytic activity data reveal that the polarity of solvent alone is not sufficient but higher value of AN is also essential to get good activity and selectivity. Ethanol and iso-propanol have higher values of AN associated with high miscibility in water. Hence, they are the right choice of solvents to get high catalytic activity. Acetonitrile, in spite of being more polar and miscible with water, has lower value of AN and hence, is not a good choice of solvent. Madon et al [43], in hydrogenation of cyclohexene,

found a dependence of turnover rates (at a given H_2 pressure) on the chemical entity of the solvent used. The concentratoin of dissolved H_2 is the crucial parameter that determined the reaction rate. The rate increased with the increasing liquid phase H_2 concentration which depends on the nature of the solvent. Later, Madon and Iglesia [44] explained this solvent-induced non-ideal behavior effect in terms of transition state theory. They reported that the rates of catalytic reactions in the presence of solvents depend only when it influences the activated complexes involved in the kinetically significant steps in the catalytic cycle. Possibly, the same explanation holds good even in the present study. Delbecq and Sautet [10] reported that metal selectivities can be rationalized in terms of the different radial expansion of their d bands; the larger, the band the stronger the four-electron repulsive interactions with the C=C bond and lower the probability of its adsorption. Indeed, d band width increases in the series Pd < Pt < Ir, Os which accounts well for the selectivities observed over Pd and Pt catalysts. Crystallite size (5 – 12 nm), preferential exposure of (111) plane, high dispersion (40.5%), high electron density, strong metal-support interactions and facile low-temperature reducibility of Pt are the unique features that made Pt(5 wt%)/CeO_2-ZrO_2 as a highly efficient and selective hydrogenation catalyst.

3.5. Conclusions

Intramolecular liquid-phase hydrogenation of cinnamaldehyde was investigated over Pt(5 wt%) supported on CeO_2, ZrO_2 and CeO_2-ZrO_2. Cinnamyl alcohol was obtained as the selective product at 25 °C and 20 bar H_2 pressure. Structural and electronic factors, alkali promoters and solvent influenced the catalytic properties. Acidity of the support (due to the presence of ZrO_2 component) and higher electron density at Pt (due to CeO_2 component) are responsible for higher catalytic activity and selectivity of Pt supported on CeO_2-ZrO_2 composite material. These catalysts were highly active and selective even at 25 °C and found to be superior to most of the hitherto known supported Pt catalysts.

3.6. References

[1] P. Gallezot, D. Richard, Catal. Rev. Sci. Eng. 40 (1998) 81.

[2] P. Claus, Topic Catal. 5 (1998) 51.

[3] U.K. Singh, M.A. Vannice, Appl. Catal. A: Gen. 213 (2001) 1.

[4] P. Mäki-Arvela, J. Hájek, T. Salmi, D.Y. Murzin, Appl. Catal. A: Gen. 292 (2005) 1.

[5] K. Weissermel, H. J. Arpe, Industrial Organic Chemistry**,** Verlag Chemie,

Weinheim, 1978.

[6] J. C. Serrano-Ruiz, J. Luettich, A. Sepúlveda-Escribano, F. Rodríguez-Reinoso, J. Catal. 241 (2006) 45.

[7] P. Kluson, L. Cerveny, Appl. Catal. 128 (1995) 13.

[8] X. F. Chen, H. X. Li, Y. P. Xu, M. H. Wang, Chinese Chem. Lett. 13 (2002) 107.

[9] P. Claus, A. Brülckner, C. Mohr, H. Hofmeister, J. Am. Chem. Soc. 122 (2000) 11430.

[10] F. Delbecq, P. Sautet, J. Catal. 152 (1995) 217.

[11] T. Vergunst, F. Kapteijn, J. A. Moulijn, Catal. Today 66 (2001) 381.

[12] A. Dandekar, M. A. Vannice, J. Catal. 183 (1999) 344.

[13] B. Campo, M. Volpe, S. Ivanova, R. Touroude, J. Catal. 242 (2006) 162.

[14] K. Liberkova, R. Touroude, D. Y. Murzin, Chem. Eng. Sci. 57 (2002) 2519.

[15] S. Galvagne, A. Donato, G. Neri, R. Pietrepaele, C. Capannolli, J. Mol. Catal. 78 (1993) 227.

[16] S. Galvagne, C. Milone, A. Donato, G. Neri, R. Pietropaolo, Catal. Lett. 17 (1993) 55.

[17] J. Q. Wang, Y. Z. Wang, S. H. Zhe, M. H. Qiao, H. X. Li, K. N. Fan, Appl. Catal. A: Gen. 272 (2004) 29.

[18] D. Richard, J. Ockelford, A. Giroir-Fendler, P. Gallezot, Catal. Lett. 3 (1989) 53.

[19] E. V. Romos-Fernández, J. Ruiz-Martínez, J. C. Serrano-Ruiz, J. Silvestre-Albero, A. Sepúlveda-Escribano, F. Rodriguez-Reinoso, Appl. Catal. A: Gen. 402 (2011) 50.

[20] J. Teddy, A. Falqui, A. Corrias, D. Carta, P. Lecante, I. Gerber, P. Serp, J. Catal. 278 (2011) 59.

[21] B. Coq, P. S. Kubhar, C. Moreau, P. Moreau, F. Figueras, J. Phys. Chem. 98 (1994) 10180.

[22] G. Li, B. Zhao, Q. Wang, R. Zhou, Appl. Catal. B: Env. 97 (2010) 41.

[23] A. Trovarelli, Catal. Rev. 38 (1996) 439.

[24] A. Martínez-Arias, M. Fernández-García, V. Ballesteros, L. N. Salamanca, J. C. Conesa, C. Otero, J. Soria, Langmuir 15 (1999) 4796.

[25] A. Jung, A. Jess, T. Schubert, W. Schütz, Appl. Catal. A: Gen. 362 (2009) 95.

[26] Z. -T. Liu, C. -X. Wang, Z. –W . Liu, J. Lu, Appl. Catal. A: Gen. 344 (2008) 114.

[27] E. Bekyarova, P. Fornasiero, J. Kašpar, M. Graziani, Catal. Today 45 (1998) 179.

[28] P. Hollins, Surf. Sci. Rep. 16 (1992) 51.

[29] A. Martínez-Arias, J. M. Coronado, R. Cataluňa, J. C. Conesa, J. Soria, J. Phys.

Chem. B. 102 (1998) 4357.

[30] J. R. Croy, S. Mostafa, L. Hickman, H. Heinrich, B. Roldan Cuenya, Appl. Catal. A: Gen. 350 (2008) 207.

[31] M. Dömök, A. Oszkó, K. Baán, I. Sarusi, A. Erdöhelyi, Appl. Catal. A: Gen. 383 (2010) 33.

[32] P. Gallezot, A. Giroir-Fendler, D. Richard, Catal. Lett. 5 (1990) 169.

[33] G. Szöllösi, B. Török, L. Baranyi, M. Bartók, J. Catal. 179 (1998) 619.

[34] D. Manikandan, D. Divakar, T. Sivakumar, Catal. Commun. 8 (2007) 1781.

[35] C. -Y. Hsu, T. -C. Chiu, M. -H. Shih, W. -J. Tsai, W. -Y. Chen, C. -H. Lin, J. Phys. Chem. C 114 (2010) 4502.

[36] N. Mahata, F. Conçalves, M. Fernando, R. Pereira, J. L. Figueiredo, Appl. Catal. A: Gen. 339 (2008) 159.

[37] E. V. Ramos-Fernández, A. F. P. Ferreira, A. Sepúlveda-Escribano, F. Kapteijn, F. Rodríguez-Reinoso, J. Catal. 258 (2008) 52.

[38] A. J. Plomp, D. M. P. van Asten, A. M. J. van der Eerden, P. Mäki-Arvela, D. Y. Murzin, K. P. de Jong, J. H. Bitter, J. Catal. 263 (2009) 145.

[39] A. Giroir-Fendler, D. Richard, P. Gallezot, Catal. Lett. 5 (1990) 175.

[40] D. Loffreda, F. Delbecq, F. Vigné, P. Sautet, Angew. Chem. Ind. Ed. 44 (2005) 5279.

[41] D. Loffreda, F. Delbecq, F. Vigné, P. Sautet, J. Am. Chem. Soc. 128 (2006) 1316.

[42] J. C. Serrano-Ruiz, A. López-Cudero, J. Solla-Gullón, A. Sepúlveda-Escribano, A. Aldaz, F. Rodríguez-Reinoso, J. Catal. 253 (2008) 159.

[43] R. J. Madon, J. P. O-Connell, M. Boudart, AIChE J. 24 (1978) 904.

[44] R. J. Madon, E. Iglesia, J. Mol. Catal. A: Chem. 163 (2000) 189.

Chapter 4

Chemoselective Hydrogenation of Cinnamaldehyde over Pd/CeO_2-ZrO_2 Catalysts

4.1. Introduction

Selective hydrogenation of α, β-unsaturated aldehydes is one of the most important areas in catalysis research [1]. Cinnamaldehyde is a vinyologue of benzaldehyde. In such compounds, hydrogenation can occur either at olefinic (C=C) or carbonyl (C=O) groups. While the former leads to saturated aldehydes of industrial and biological importance, the latter results in unsaturated alcohols (Scheme 3.1). All these selective hydrogenation products of cinnamaldehyde are widely used in perfumery industry. Recently, hydrocinnamaldehyde was found be an important intermediate in the preparation of pharmaceuticals used in the treatment of HIV [2]. Supported Pt, Ru, Co, Au and Ir catalysts [3-8] were reported to selectively hydrogenate the carbonyl group resulting in cinnamyl alcohol. On the contrary, supported Pd catalysts were selective for hydrogenation of the olefinic group resulting in hydrocinnamaldehyde [9]. In view of the industrial importance of the hydrogenation products, design and development of more efficient and selective catalysts is still remaining as a challenging task. For this, a detailed study revealing the influence of the nature of metal and support metal-interaction is essential. A study on the catalytic activity of Pd(2 wt%) supported on CeO_2, ZrO_2 and CeO_2-ZrO_2 is reported here, for the first time. The influence of various reaction parameters and in particular, alkali (NaOH) addition on product selectivity is investigated. It is known that by incorporation of Zr ions into ceria lattice, the redox behaviour of ceria is enhanced [10]. Zirconia incorporation also increases the thermal stability of CeO_2 and improves the metal–CeO_2 interactions. CeO_2-ZrO_2-supported Pd has been used as three-way catalysts [11-16], in natural gas combustion [17], total oxidation of hydrocarbons [18], methanol decomposition [19], vapor phase hydrogenation of phenol [20] and in several other reactions [21]. The chemoselective hydrogenation activity of these novel catalysts is reported in this chapter.

4.2. Experimental Procedure and Characterization Techniques

Pd(2 wt%)/CeO_2, Pd(2 wt%)/ZrO_2, Pd(2 wt%)/CeO_2-ZrO_2 (Ce : Zr = 1:1 molar ratio) and Na-Pd(2 wt%)/CeO_2-ZrO_2 (Ce : Zr = 1:1 molar ratio) catalysts are synthesized and characterized as reported in Chapter 2 (sections 2.2.2. and 2.3). Prior to use in reactions, the catalysts were freshly reduced at 200 °C in a flow of H_2 (30 ml/min) for 2.5 h. Procedures used in catalytic activity studies are reported in Chapter 2 (section 2.4.1.2).

4.3. Results and Discussion

4.3.1. Structural Properties

4.3.1.1. XRD. The ceria-zirconia mixed oxides are formed in different crystalline structures depending on their chemical composition. According to the $Ce_{1-x}Zr_xO_2$ phase

diagram [22], for $x \leq 0.15$, a cubic fluorite-type phase is known to form and for $x \geq 0.85$, a monoclinic phase is formed. At intermediate compositions, various phases (t, t', t'', κ and t*) have been identified [22-24]. Oxygen deficient structures, such as the pyrochlore structure ($A_2B_2X_7$) may also be formed [25-29]. For ceria-zirconia mixed oxides, the pyrochlore structure is generally reported to be formed under severe reduction conditions. However, there is an evidence of its formation even during low temperature reduction of the sample [29]. In other words, ceria-zirconia material exhibits complex structural characteristics. Neat ceria of the present study showed XRD peaks in the 2θ range of 28 – 80° indicating a distinct, cubic, fluorite structure [30]. On the contrary, CeO_2-ZrO_2 composite exhibited XRD pattern typical of a mixture of cubic and tetragonal phases with the former being more predominant (Fig. 4.1; the peaks due to the tetragonal phase are marked by asterisk). Recently, Li et al [31] have also reported such a mixed crystallite phase in CeO_2-ZrO_2 materials prepared by calcining at lower temperatures (< 500 °C). In the materials prepared in this work, the presence of pyrochlore structure was not detected.

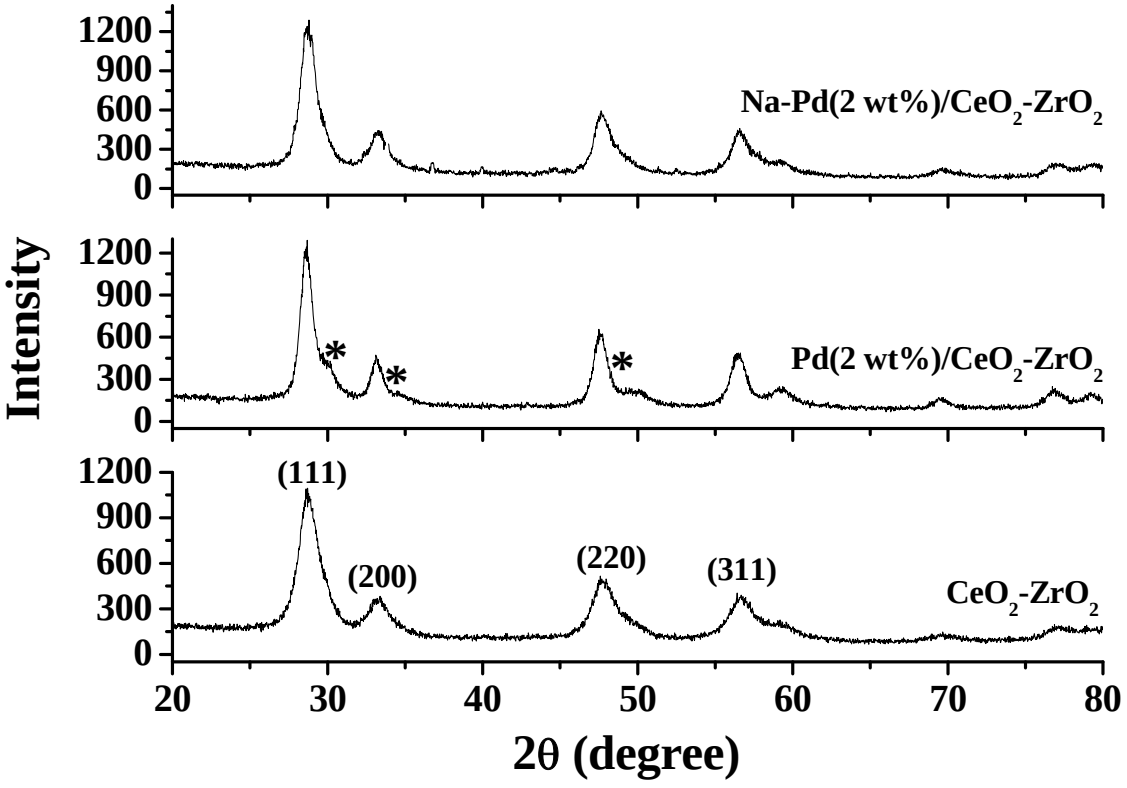

Fig. 4.1. X-ray diffractograms of CeO_2-ZrO_2 (1:1 molar ratio) and supported Pd catalysts

The unit cell parameter of the cubic phase (a_{cubic}) of CeO_2-ZrO_2 is smaller (0.539 nm) than CeO_2 (0.542 nm), suggesting formation of a CeO_2-ZrO_2 solid solution [note: ionic radius of Zr^{4+}(0.084 nm) is smaller than that of Ce^{4+}(0.097 nm)/Ce^{3+}(0.112 nm)] [32]. Palladium and sodium impregnation did not alter the structure except for shift in peaks to higher 2θ value by 0.1 – 0.3°. At 2 wt% of Pd loading, no separate PdO phase was detected indicating that it is highly dispersed. Representative XRD profiles of CeO_2-ZrO_2, Pd(2 wt%)/CeO_2-ZrO_2 and Na-Pd(2 wt%)/CeO_2-ZrO_2 are depicted in Fig. 4.1. The average crystallite size of the materials was determined from the linewidth of the XRD peak corresponding to (111) reflection (2θ ≈ 28.7°) using Debye-Scherrer equation (Table 4.1). It varied for different supports in the order: ZrO_2 (21.5 nm) > CeO_2 (15.8 nm) > CeO_2-ZrO_2 (9.3 nm) indicating that zirconia incorporation renders materials with low crystallite size. The crystallite size of CeO_2-ZrO_2-supported Pd was higher (9.6 nm) than the corresponding support oxide (9.3 nm). Alkali impregnation (leading to Na-Pd(2 wt%)/CeO_2-ZrO_2) decreased the crystallite size to 6.7 nm.

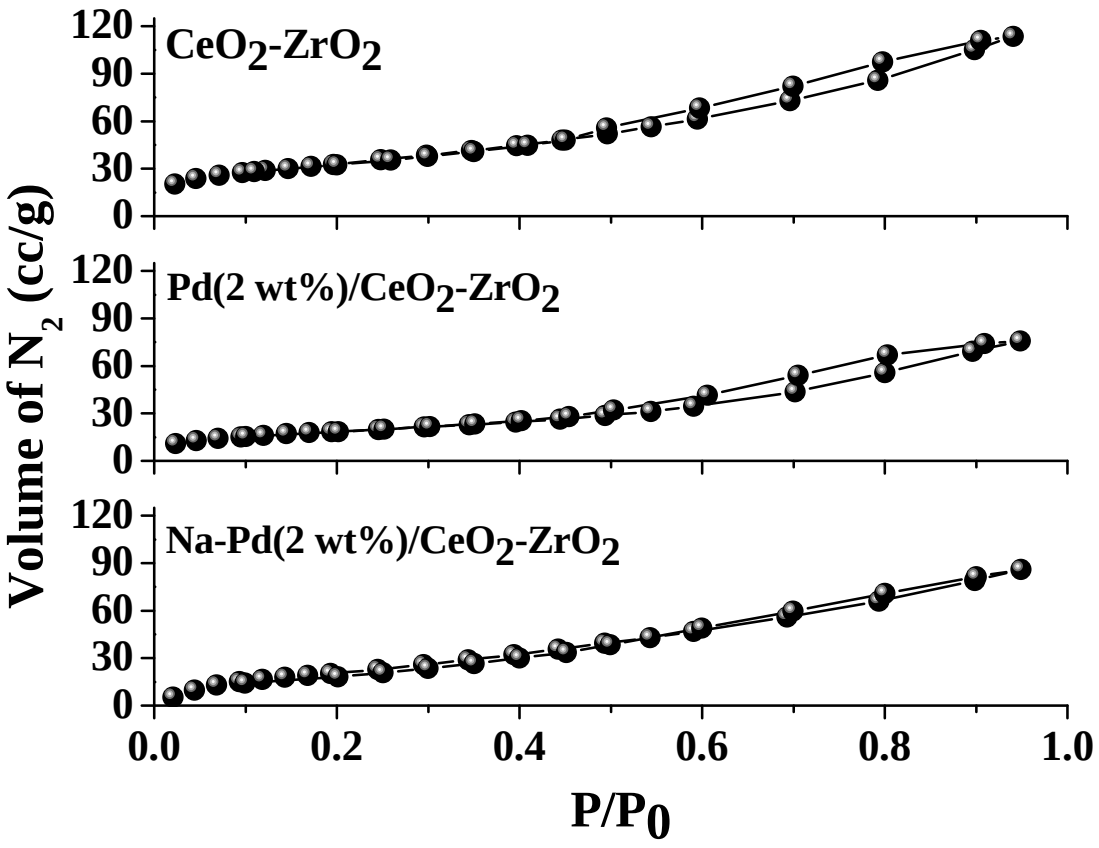

Fig. 4.2. N_2 adsorption-desorption isotherms of CeO_2-ZrO_2 (1:1 molar ratio) and supported Pd(2 wt%) catalysts

Table 4.1. Physicochemical properties of CeO_2-ZrO_2-supported Pd(2 wt%) catalysts

Sample	XRD		N_2 adsorption - desorption			Acidity (NH_3-TPD, mmol/g)	H_2 Uptake (TPR, mmol/g)	
	Lattice parameter (a_{cubic}, nm)	Average crystallite size (nm)	S_{BET} (m^2/g)	Pore volume (cm^3/g)	Average pore diameter (nm)		Overall	Pd
CeO_2	0.542	15.8	97	0.12	3.2	-	-	-
ZrO_2	0.512	21.5	112	0.183	4.5	-	-	-
CeO_2-ZrO_2	0.539	9.3	115	0.17	6.1	0.179	-	-
Pd(2 wt%)/CeO_2	0.537	12.6	75	0.13	2.2	0.231	-	-
Pd(2 wt%)/ZrO_2	0.512	28.1	83	0.169	4.1	0.390	-	-
Pd(2 wt%)/CeO_2-ZrO_2 (1:1)	0.541	9.6	65	0.11	7.2	0.308	0.179	0.044
Na-Pd(2 wt%)/CeO_2-ZrO_2 (1:1)	0.537	6.7	121	0.14	4.3	0.034	0.330	0.059

4.3.1.2. N_2-Physisiorption. The textural properties of CeO_2-ZrO_2, Pd(2 wt%)/CeO_2-ZrO_2 and Na-Pd(2 wt%)/CeO_2-ZrO_2 were determined by N_2 adsorption-desorption technique (Fig. 4.2 and Table 4.1). All these materials showed typical type IV isotherms with H_3 hysterisis loop. The specific surface area (S_{BET}) and pore volume of the supported Pd(2 wt%) catalysts are lower (65 m^2/g and 0.11 ml/g, respectively) that the support composite oxide (115 m^2/g and 0.17 ml/g, respectively). When sodium was also present the material exhibited highest S_{BET} (121 m^2/g). However, the average pore diameter of it was lower (4.3 nm) than CeO_2-ZrO_2 (6.1 nm) and Pd/CeO_2-ZrO_2 (7.2 nm). It is worth noting that the variation in S_{BET} (obtained from N_2 adsorption-desorption measurements) follows the variation in crystallite size of these materials (determined from XRD studies).

4.3.1.3. High Resolution Transmission Electron Microscopy. HRTEM images of Pd(2 wt%)/CeO_2, Pd(2 wt%)/ZrO_2 and Pd(2 wt%)/CeO_2-ZrO_2 are shown in Fig. 4.3. Palladium is in a dispersed state on CeO_2-ZrO_2 support. Agglomeration of particles was detected on "neat" ceria and zirconia supports. The crystallite size of the support (5 – 12 nm from HRTEM) is in agreement with that determined from XRD.

4.3.1.4. X-ray Photoelectron Spectroscopy. Representative XP spectra of Pd supported catalysts in Pd 3d region are shown in Figs. 4.4(a) and 4.4(b). The binding energy values are reported in Table 4.2. The binding energies of Pd^0, Pd^{2+} and Pd^{4+} states are 335 and 340.6, 337.5 and 342.9 & 338.4 and 343.5 eV, respectively corresponding to the $3d_{5/2\text{-}3/2}$ spin-orbit doublet [33-36]. The binding energy of Zr3p also falls in the same range. Therefore, the B.E. peaks of Zr3p overlap with those of Pd3d. From the binding energy values (Table 4.2) it is concluded that Pd on CeO_2-ZrO_2 is in a +2 oxidation state. The binding energy value of Pd ($3d_{5/2}$) on pure ZrO_2 is higher than that observed over pure CeO_2 support consistent with the facile reducibility of the latter than the former support. The $3d_{5/2}$ peak of Pd in Na-Pd(2 wt%)/CeO_2-ZrO_2 appeared at lower binding energy value (336.5 eV) than that of Pd(2 wt%)/CeO_2-ZrO_2 (336.8 eV) revealing that Pd in the former is in a reduced +(2-δ) oxidation state while that in the latter is in a "formal" +2 oxidation state. In other words, alkali affected the electronic structure of Pd. The peaks corresponding to Pd in Na-Pd(2 wt%)/CeO_2-ZrO_2 are broader than those for Pd(2 wt%)/CeO_2-ZrO_2 due to the presence of different metal oxidation states [+2 and +(2-δ)]. This led to differences in the relative intensity of Zr and Pd peaks in these two samples (Fig. 4.4). The B.E. values of Ce $3d_{5/2}$ and Zr $3d_{5/2}$ are also included in Table 4.2 and are consistent with the reported values [33].

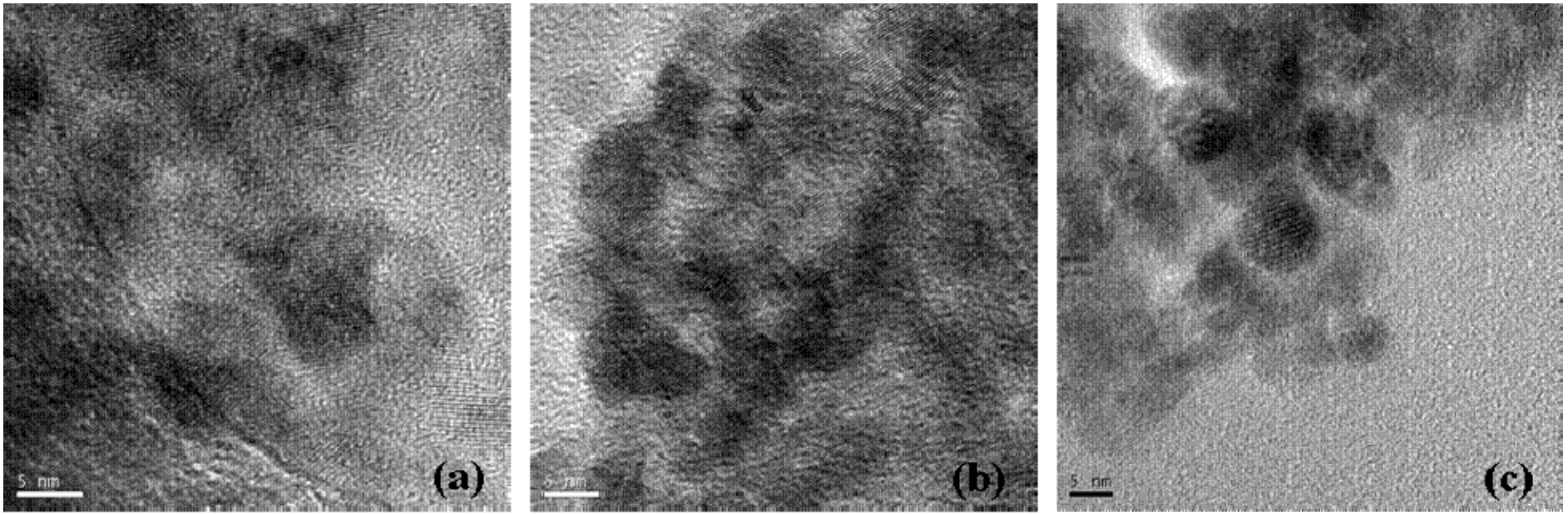

Fig. 4.3. High resolution transmission electron micrographs: (a) Pd(2 wt%)/CeO_2, (b) Pd(2 wt%)/ZrO_2, and (c) Pd(2 wt%)/CeO_2-ZrO_2 (Ce : Zr molar ratio = 1 : 1)

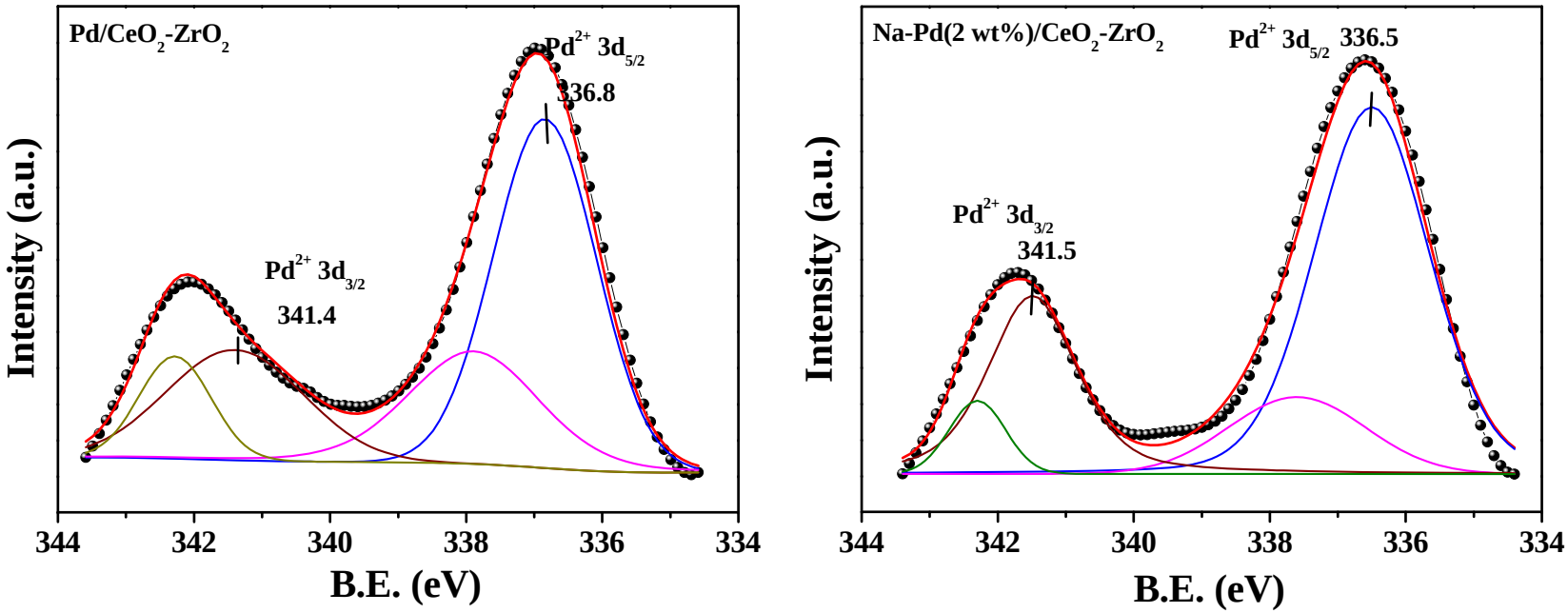

Fig. 4.4(a). XPS of Pd 3d region of supported palladium catalysts

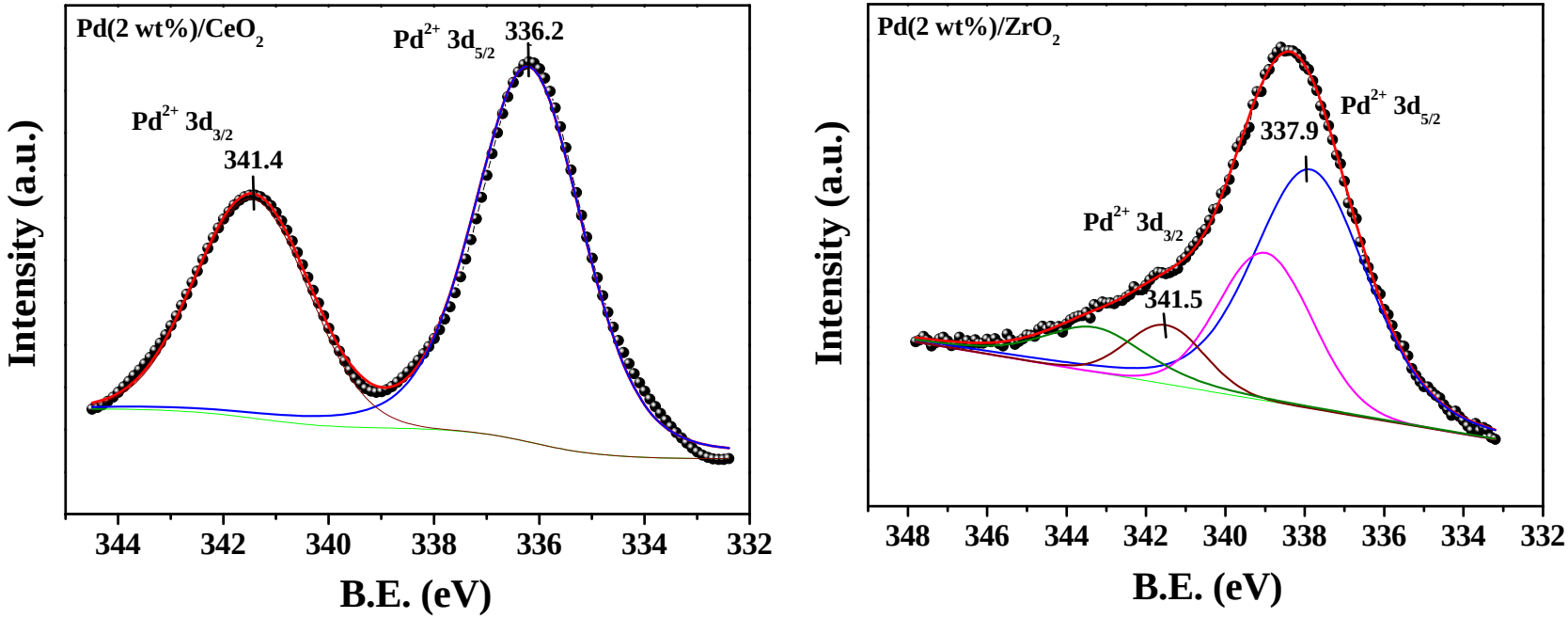

Fig. 4.4(b). XPS of Pd 3d region of supported palladium catalysts

Table 4.2. Binding energy values (in eVs) for supported Pd(2 wt%) catalysts

Sample	Pd $3d_{5/2}$	Ce $3d_{5/2}$	Zr $3d_{5/2}$	Na 1s
Pd(2 wt%)/CeO_2	336.2	881.3	-	-
Pd(2 wt%)/ZrO_2	337.9	-		-
Pd(2 wt%)/CeO_2-ZrO_2	336.8	881.0	181.3	-
Na-Pd(2 wt%)/CeO_2-ZrO_2	336.5	881.2	181.0	1070.1

4.3.1.5. DRIFT Spectroscopy of Adsorbed Pyridine and NH_3-TPD. CeO_2-ZrO_2 is a weakly acidic oxide. The nature and type of acid sites on CeO_2-ZrO_2 were determined by DRIFT spectroscopy using pyridine as probe molecule (Fig. 4.5). The sample showed IR peaks of adsorbed pyridine at 1592, 1575, 1484 and 1440 cm^{-1} (Fig. 4.5). While the peaks at 1592 and 1440 cm^{-1} are attributed to H-bonded pyridine, those at 1575 and 1484 cm^{-1} are corresponded to pyridine-coordinated to weak Lewis acid sites [37]. It is known that strong Lewis acid sites show adsorbed pyridine-IR peaks at 1623 and 1455 cm^{-1} and Brönsted sites at 1639 and 1546 cm^{-1}. However, these peaks are not observed in the spectrum of CeO_2-ZrO_2 indicating that such strong acidic sites are absent. The pyridine-IR peaks broadened and decreased in intensity as the desorption temperature increased from 200 to 400 °C (Fig. 4.5).

The number of acidic sites on CeO_2-ZrO_2 and supported Pd catalysts were quantified by NH_3-TPD measurements (Fig. 4.6 and Table 4.1). CeO_2-ZrO_2 showed a broad desorption peak in the temperature region 100 – 500 °C (Fig. 4.6, right panel). Based on the knowledge gained from pyridine-IR studies, this broad NH_3 desorption is attributed to surface acidic hydroxyl and weak Lewis acid (Ce and Zr) sites. In the case of Pd catalysts, a shoulder peak was also observed at around 110 – 150 °C which could be attributed to NH_3 desorption from PdO species (Fig. 4.6). The amount of NH_3 desorbed from different supported Pd(2 wt%) catalysts decreased in the following order: Pd(2 wt%)/ZrO_2 (0.390 mmol/g) > Pd(2 wt%)/CeO_2-ZrO_2 (0.308 mmol/g) > Pd(2 wt%)/CeO_2 (0.231 mmol/g). The amount of NH_3 desorbed from support CeO_2-ZrO_2 was found to be 0.179 mmol/g. These results indicate that ZrO_2 is more acidic than CeO_2. Incorporation of ZrO_2 into the CeO_2 lattice enhances the acidity of the support. The alkali impregnated supported Pd catalyst [Na-Pd(2 wt%)/CeO_2-ZrO_2] did not show NH_3 desorption peak. In other words, alkali impregnation suppressed the acidity of the catalysts.

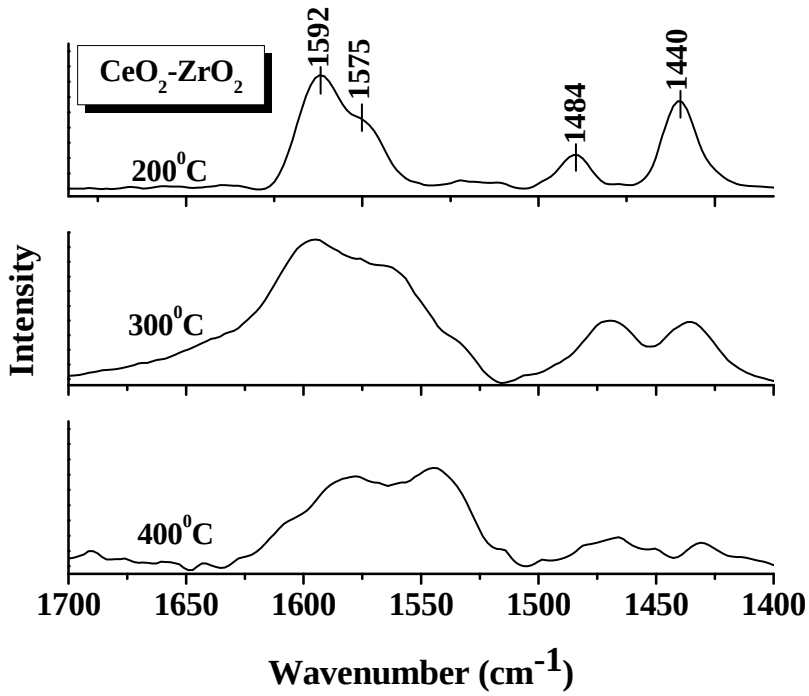

Fig. 4.5. DRIFT spectra of adsorbed pyridine on CeO_2-ZrO_2

4.3.1.6. Temperature-Programmed Reduction. The H_2 consumption profiles during temperature-programmed reduction (TPR) of supported Pd catalysts are shown in Fig. 4.7. Pd(2 wt%)/CeO_2-ZrO_2 showed two reduction peaks: (1) a sharp, low-temperature peak with maximum at 62 °C and (2) a broad, high temperature peak at 347 °C. While the former is attributed to reduction of PdO, the latter corresponds to reduction of CeO_2. Bulk CeO_2 shows reduction peak at around 550 °C [37]. Its shift to 347 °C as observed in the present study is due to interaction with zirconia in the solid solution and metal (Pd)-support interactions [37]. When Na is also present, the reduction peaks shifted to higher temperatures (Fig. 4.7). Reduction of PdO occurred at 97 °C in Na-Pd(2 wt%)/CeO_2-ZrO_2 instead of 62 °C in Pd(2 wt%)/CeO_2-ZrO_2. The reduction of CeO_2 occurred at 494 °C instead of 347 °C. This shift in reduction peak to higher temperature is a consequence of support-metal interactions. Thus, Na impregnation not only alters the textural and acidic properties but also influences the reduction behaviour. The overall H_2 uptake by Pd(2 wt%)/CeO_2-ZrO_2 and Na- Pd(2 wt%)/CeO_2-ZrO_2 was estimated to be 0.179 and 0.330 mmol/g. H_2 uptake exclusively by palladium in Pd(2 wt%)/CeO_2-ZrO_2 and Na- Pd(2 wt%)/CeO_2-ZrO_2 was estimated to 0.044 and 0.061 mmol/g, respectively. The higher amount of H_2 consumption in Na-Pd(2 wt%)/CeO_2-ZrO_2 than in Pd(2 wt%)/CeO_2-ZrO_2 indicates higher dispersion of palladium in the former catalyst.

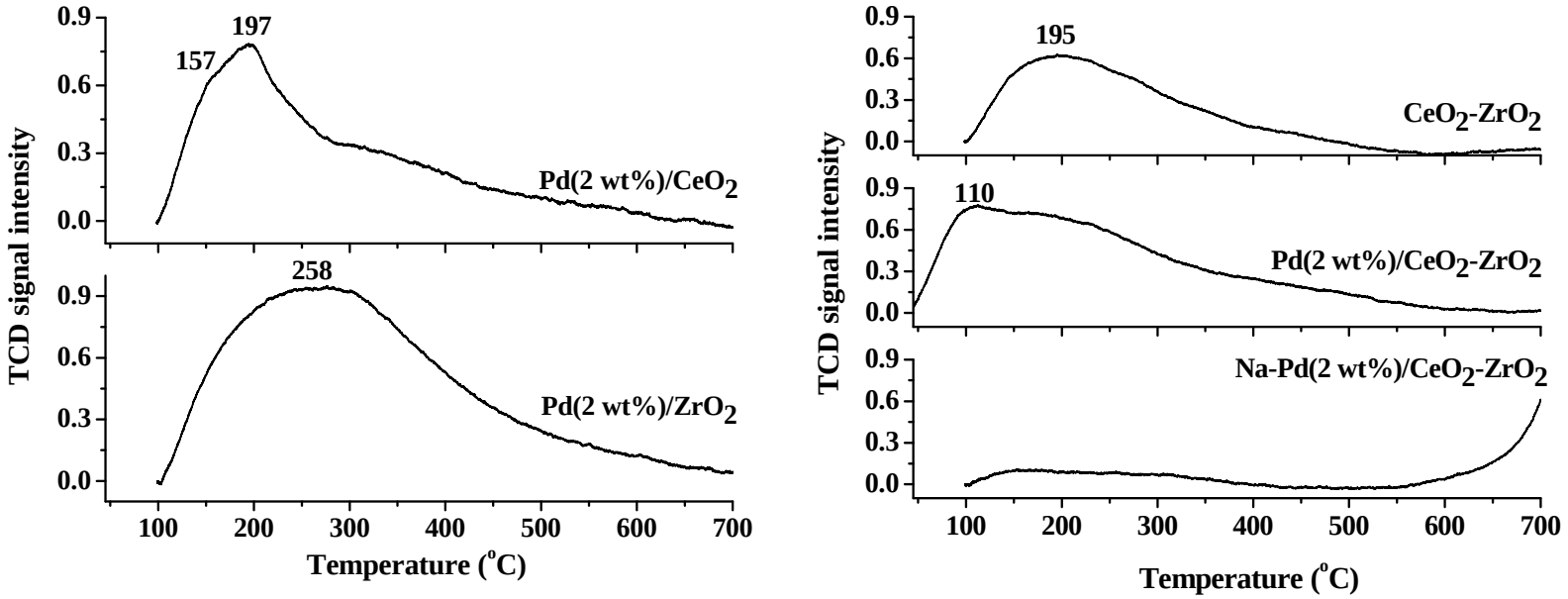

Fig. 4.6. NH_3-TPD profiles of CeO_2-ZrO_2 and supported Pd catalyst

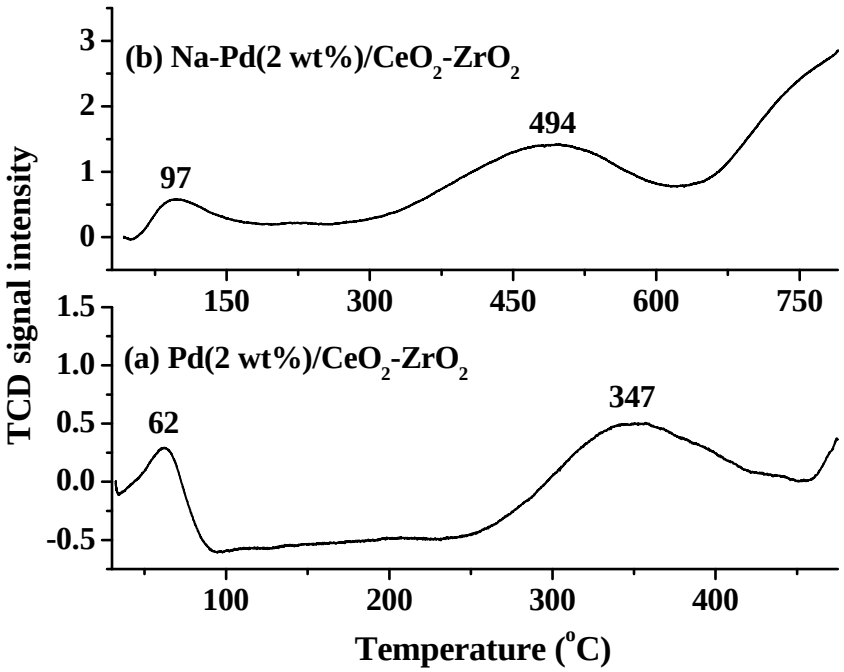

Fig. 4.7. H_2–temperature-programmed reduction of supported Pd catalysts

4.3.2. Catalytic Activity

Hydrogenation of cinnamaldehyde (CA) yields different products as shown in Scheme 3.1. Hydrogenation of the carbonyl group (1, 2-addition) yields the unsaturated alcohol – cinnamyl alcohol (CAL). Hydrogenation of the olefinic bond (3, 4-addition) gives the saturated aldehyde – hydrocinnamaldehyde (HCA). The 1, 4-addition gives enol which isomerizes into HCA. Further hydrogenation leads to the formation of 3-phenylpropanol (PPL) and subsequently, propylbenzene (PB). Also CAL can get reduced to PPL. Hydrogenation of α, β-unsaturated aldehydes on metal surfaces proceeds via the Horiuti–Polayni mechanism involving adsorbed states: di-σC=Oη^2, di-σC=Cη^2, or di-πη^2(η^4) [38-40]. In the present study, over Pd/CeO_2-ZrO_2 catalysts, 3, 4 and 1, 4-additions are more predominant than the 1, 2-addition. Formation of PB could not be detected at the reaction conditions used in this study.

4.3.2.1. Influence of Support. The type and nature of the support have a marked influence on CA conversion and product selectivity (Table 4.3). CA conversion is higher with Pd supported on ZrO_2 than on CeO_2 (compare entry nos. 4 and 5; Table 4.3). In the case of Pd supported on CeO_2-ZrO_2, an increase in conversion of CA was observed with increasing amount of ZrO_2 in the mixed oxide composition (compare entry nos. 1 and 3, Table 4.3). However, PPL selectivity (obtained via hydrogenation of carbonyl group) was relatively higher over Pd supported on CeO_2 (18%) than on ZrO_2 (11.3%). Even in the case of CeO_2-ZrO_2 catalysts, the PPL selectivity was found higher when there was an increase in the

composition of CeO_2 in the mixed oxide. In other words, while ZrO_2 support leads to higher conversion and HCA product formation (via 3, 4 and 1, 4 additions), CeO_2 support results in higher amount of PPL formation. CeO_2 is an easily reducible oxide and hence, a part of Pd can be in δ+ state. On the other hand, Pd on ZrO_2 (a weakly reducible oxide) will be in zero state only. An electron depleted $Pd^{\delta+}$ on CeO_2 will polarize the electron rich carbonyl group instead of electron deficient olefinic group and thereby results in preferential 1, 2-addition of hydrogen and formation of PPL. $Pd^{\delta+}$ would be less reactive than Pd^0 and hence, lower conversion of CA was observed over Pd(2 wt%)/CeO_2 than over Pd(2 wt%)/ZrO_2.

Table 4.3. Hydrogenation of cinnamaldehyde over supported Pd catalysts

Catalyst (Ce : Zr molar ratio)	CA conversion (wt%)	Product selectivity (%)		
		HCA	PPL	Others
Pd/CeO_2-ZrO_2 (1:1)	69.6	82.5	16.7	0.7
Pd/CeO_2-ZrO_2 (1:2)	68.1	86.0	13.9	0.1
Pd/CeO_2-ZrO_2 (1:4)	79.6	90.0	10.0	0
Pd/CeO_2	91.0	82.0	18.0	0
Pd/ZrO_2	95.5	88.7	11.3	0

Reaction conditions: Catalyst (0.05 g), cinnamaldehyde (CA, 4 g), solvent – toluene (40 ml), H_2 pressure = 20 bar, reaction time = 8 h.

4.3.2.2. Effect of Temperature. Hydrogenation of CA increased with increasing reaction temperature (Table 4.4). Complete conversion of CA was observed at 80 °C itself. Hydrocinnamaldehyde (HCA) was the major product (82.5 – 90%). 3-Phenylpropanol (PPL) was detected with selectivity in the range 10.0 – 16.7%. A small amount of other products including ethers and acetals (0 – 0.7 wt%) was also detected. With increasing temperature the selectivity of HCA increased at the expense of PPL and other products.

4.3.2.3. Effect of Solvent. The reaction was conducted in non-polar toluene and cyclohexane and polar ethanol solvents (Table. 4.4). In general, CA conversion is much higher in ethanol than in toluene and cyclohexane. Fig. 4.8 shows the conversion verses time plots in different solvents. While HCA is the selective product (82.5 – 84.6%) in non-polar solvents, HCA (50.7%) along with significant amounts of PPL (10.8%) and other products (acetals + ethers; 38.5%) formed in polar ethanol solvent. Unlike in non-polar solvents, hydrogenation of the carbonyl group of CA yielding PPL is more pronounced in ethanol. As PPL is formed in higher amounts, it participates in further reactions at higher temperatures leading to acetals and ethers (selectivity = 38.5% at 50 °C and 74% at 150 °C).

Table 4.4. Influence of temperature on hydrogenation of cinnamaldehyde over Pd(2 wt %)/CeO_2-ZrO_2 (Ce : Zr molar ratio = 1 : 1)

Temperature (°C)	Solvent = toluene, additive = nil				Solvent = ethanol, additive = nil				Solvent = ethanol, additive = 16 mg NaOH in 10 ml water			
	CA conversion (wt%)	Product selectivity (%)			CA conversion (wt%)	Product selectivity (%)			CA conversion (wt%)	Product selectivity (%)		
		HCA	PPL	Others		HCA	PPL	Others		HCA	PPL	Others
50	69.6 (60.4)[a]	82.5 (84.6)[a]	16.7 (15.0)[a]	0.7 (0.4)[a]	89.9	50.7	10.8	38.5	99.4	67.3	29.7	2.9
80	100	87.7	11.6	0.7	100	37.0	19.9	43.1	100	60.1	32.7	7.3
120	100	88.1	11.3	0.6	100	21.0	14.5	64.5	100	42.1	30.7	27.2
150	100	90.0	10.0	0	100	12.3	12.3	74.0	100	29.5	37.9	32.6
150									100[b]	35.0[b]	40.4[b]	23.3[b]
150									100[c]	20.0[c]	63.4[c]	16.6[c]

Reaction conditions: Catalyst (0.05 g), cinnamaldehyde (CA, 4 g), solvent (40 ml), H_2 pressure = 20 bar, reaction time = 8 h. HCA = hydrocinnamaldehyde, PPL = 3-phenylpropanol, other products include ethers and acetals.

[a]Data in parentheses corresponds to experiments in cyclohexane instead of toluene.

[b]H_2 pressure = 10 bar, additive = 0.018 g of NaOH in 30 ml water.

[c]H_2 pressure = 10 bar, additive = 0.054 g of NaOH in 30 ml water.

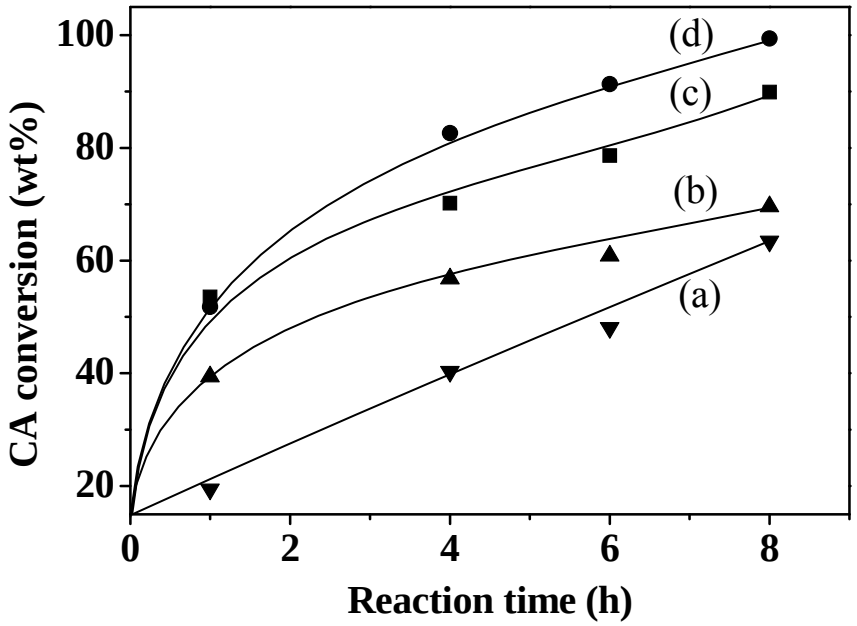

Fig. 4.8. Conversion vs time plots for hydrogenation of cinnamaldehyde (CA) in different solvents. (a) cyclohexane, (b) toluene, (c) ethanol and (d) ethanol + additive (10 mg of NaOH in 10 ml water). *Reaction conditions:* Pd(2 wt%)/CeO_2-ZrO_2 (Ce : Zr molar ratio = 1 : 1) = 0.05 g, CA = 4 g, solvent = 40 ml, H_2 pressure = 20 bar, reaction temperature = 50 °C.

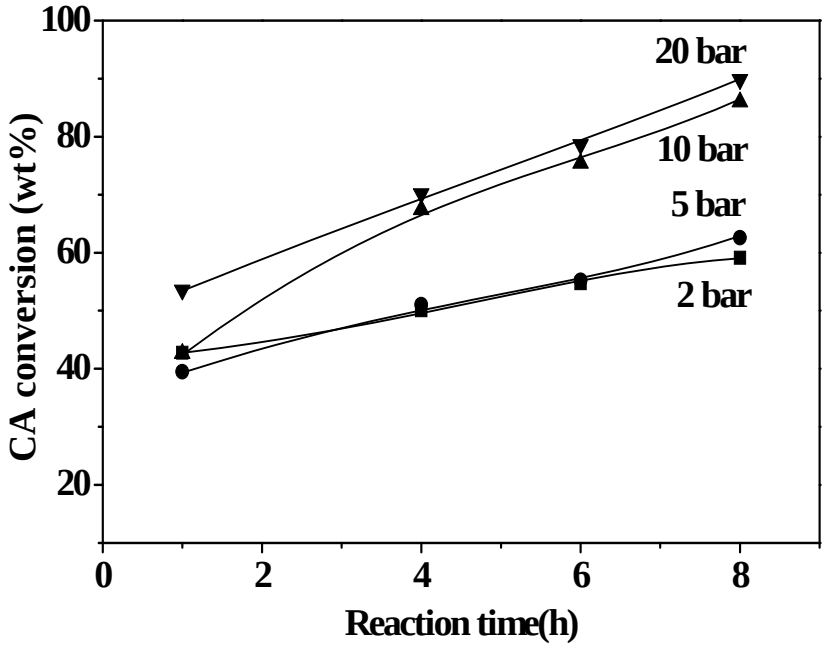

Fig. 4.9. Conversion of cinnamaldehyde (CA) at various pressures over Pd (2 wt%)/CeO_2-ZrO_2 (Ce : Zr molar ratio = 1 : 1) catalyst. *Reaction Conditions:* catalyst = 0.05 g, CA = 4 g, ethanol = 40 ml, reaction temperature = 50 °C.

H_2 pressure influenced CA conversion and products selectivity (Table 4.5, Fig. 4.9). The conversion of CA increased from 59.1 to 89.9% by increasing the pressure from 2 to 20 bar. Also a significant reduction in the formation of other products (from 73.6 to 38.5%) was observed at higher temperatures. The reaction occurs even on "bare" CeO_2-ZrO_2. But CA conversion and HCA and PPL selectivity were much higher when Pd was also present. Pd to some extent blocks the acidic sites leading to side reactions on the CeO_2-ZrO_2 surface and thereby enhances the selectivity of the desired products.

Table 4.5. Effect of pressure and alkali on hydrogenation of cinnamaldehyde over Pd(2 wt%)/CeO_2-ZrO_2 (Ce : Zr molar ratio = 1 : 1)

Catalyst	H_2 pressure (bar)	CA conversion (wt%)	Product selectivity (%)		
			HCA	PPL	Others
CeO_2-ZrO_2	20	58.8	30.4	4.3	65.3
Pd/CeO_2-ZrO_2	20	89.9	50.7	10.8	38.5
	10	86	39.2	9.5	51.3
	5	62.6	38.4	8.8	52.8
	2	59.1	24.5	1.9	73.6
Na-Pd/CeO_2-ZrO_2	20	72.3	89.0	8.9	2.1

Reaction conditions: Catalyst (0.05 g), cinnamaldehyde (CA, 4 g), solvent – ethanol (40 ml), reaction temperature = 50 °C, reaction time = 8 h.

4.3.2.4. Effect of Alkali Addition. The formation of acetals and ethers (other products) are catalyzed by acid sites on the catalyst surface. Pyridine-IR (Fig. 4.5) and NH_3-TPD (Fig. 4.6) experiments revealed the presence of Lewis acid sites on CeO_2-ZrO_2-based catalysts. In order to suppress these side reactions forming undesired products, alkali was impregnated on the catalysts and then, calcined to prepare Na-Pd(2 wt%)/CeO_2-ZrO_2. NH_3 desorption was little (0.034 mmol/g) from Na-Pd(2 wt%)/CeO_2-ZrO_2 indicating that the catalyst was nearly neutral. The selectivity for the acetals and ethers decreased from 38.5 to 2.1% by using this alkali-modified catalyst (Table 4.5).

In other experiments, NaOH solution was added in different concentrations to the reactions over Pd/CeO_2-ZrO_2 in ethanol conducted at 150 °C and 10 bar H_2 pressure (Table 4.4). Suppression of other products and change in selectivity for hydrogenation of C=C (yielding HCA) to C=O (yielding PPL) was noted. An enhancement in PPL product

selectivity from 37.9 to 63.4% was observed when 0.054 g of NaOH in 30 ml water was added.

4.4. Structure-Activity Correlations

Alkali has a positive effect on the rate of hydrogenation (Fig. 4.8). It activates the C=O group of α, β-unsaturated aldehydes and facilitates hydrogenation yielding unsaturated alcohols (CAL). The enhanced activation of the C-O bond could be interpreted by the polarization of C=O bond resulting from the interaction of the alkali cation with the lone-pair electrons of the oxygen atom of the C-O group. This unsaturated alcohol (CAL) is further hydrogenated to a saturated alcohol (PPL) in presence of Pd(2 wt%)/CeO_2-ZrO_2 catalyst by 1, 4 addition. Finally, the saturated alcohol percentage increases with increasing alkali percentage and the formation of acetals and ethers is reduced. Mahmoud et al [2] reported that hydrogenation of HCA to PPL does not occur significantly at normal temperatures over Pd/SiO_2 catalyst. However, the hydrogenation of CAL proceeds very fast (30 times faster than the hydrogenation of CA to CAL) [2]. These sequential reactions, thereby, enhance the selectivity of PPL in the product. A similar behaviour occurs even in our experiments. The Na ions in Na-Pd(2 wt%)/CeO_2-ZrO_2 are involved mainly in the reduction of acid sites on the support surface. On the other hand, in the experiments with alkali solutions, the alkali ions have not only suppressed the acidity of the catalyst but at the same time involved in polarising the C=O group of CA leading to differences in product selectivity.

The catalytic activity of Pd(2 wt%)/CeO_2-ZrO_2 is significantly higher than that of carbon nanofiber and activated carbon-supported Pd(5 wt%) catalysts. With less amount of Pd in the former catalyst, complete conversion of CA at 80 °C was achieved in just 1 h while it requires nearly 30 h over the latter catalysts [41]. Pd(1 wt%)/SiO_2 required higher temperature (100 instead of 80 °C), pressure (30 instead of 20 bar) and amount of catalyst (200 instead of 0.050 g) to achieve similar conversions of CA. In other words, the Pd catalysts of the present study are more efficient and the support has a significant role in the improved activity of these catalysts. Pd catalysts are known for selective hydrogenation of C=C. However, in this study, it is demonstrated that by adding a small quantity of alkali, the electronic and redox properties of Pd can be fine-tuned and the selectivity for hydrogenation (between C=C and C=O of cinnamaldehyde) can be controlled.

4.5. Conclusions

Chemoselective hydrogenation of cinnamaldehyde over CeO_2-ZrO_2 supported Pd catalysts is reported for the first time. Cinnamaldehyde has two functional groups (C=C and C=O) for hydrogenation. In general, the hydrogenation of C=C is preferred over Pd catalysts. However, by adding a small quantity of alkali the selectivity for hydrogenation can be changed / altered. Alkali addition influenced the dispersity, electronic property and reducibility of Pd. These changes in molecular electronic structure of Pd are responsible for the changes in the chemoselectivity brought about by alkali addition.

4.6. References

[1] M. Boudart, Nature 372 (1994) 320.

[2] S. Mahmoud, A. Hammoudeh, S. Gharaibeh, J. Melsheimer, J. Mol. Catal. A: Gen. 178 (2002) 161.

[3] J. C. Serrano-Ruiz, J. Luettich, A. Sepúlveda-Escribano, F. Rodríguez-Reinoso, J. Catal. 241 (2006) 45.

[4] P. Kluson, L. Cerveny, Appl. Catal. 128 (1995) 13.

[5] X. F. Chen, H. X. Li, Y. P. Xu, M. H. Wang, Chinese Chem. Lett. 13 (2002) 107.

[6] P. Claus, A. Brülckner, C. Mohr, H. Hofmeister, J. Am. Chem. Soc. 122 (2000) 11430.

[7] P. N. Rylander, Catalytic Hydrogenation in Organic Synthesis, Academic Press, New York, (1979) p. 72.

[8] L. Zhang, J. M. Winterbottom, A. P. Boyes, S. Raymahasay, J. Chem. Technol. Biotechnol. 72 (1998) 264.

[9] F. Delbecq, P. Sautet, J. Catal. 152 (1995) 217.

[10] G. Ranga Rao, J. Kašpar, R. Di Monte, S. Meriani, M. Graziani, Catal. Lett. 24 (1994) 107.

[11] B. Zhao, G. Li, C. Ge, Q. Wang, R. Zhou, Appl. Catal. B: Env. 96 (2010) 338.

[12] M. Shen, J. Wang, J. Shang, Y. An, J. Wang, W. Wang, J. Phys. Chem. C. 113 (2009) 1543.

[13] M. Shen, M. Yang, J. Wang, J. Wen, M. Zhao, W. Wang, J. Phys. Chem. C. 113 (2009) 3212.

[14] G. W. Graham, H. W. Jen, R. W. McCabe, A. M. Straccia, L. P. Haack, Catal. Lett. 67 (2000) 99.

[15] M. Zhao, S. Chen, X. Zhang, M. Gong, Y. Chen, J. Rare Earths. 27 (2009) 728.

[16] P. Bera, K. C. Patil, V. Jayaram, G. N. Subbanna, M. S. Hegde, J. Catal. 186 (2000) 293.

[17] S. Specchia, P. Palmisano, E. Finocchio, G. Busca, Chem. Eng. Sci. 65 (2010) 186.

[18] G. Wang, M. Meng, Y. Zha, T. Ding, Fuel (2010) doi: 10.1015/j.fuel.2010.03.031.

[19] H. Wang, Y. Chen, Q. Zhang, Q. Zhu, M. Gong, M. Zhao, J. Natural Gas Chem. 18 (2009) 211.

[20] S. Velu, M. P. Kapoor, S. Inagaki, K. Suzuki, Appl. Catal. A: Gen. 245 (2003) 317.

[21] L. Vivier, D. Duprez, ChemSusChem. 3 (2010) 654.

[22] M. Yashima, T. Hirose, S. Katano, Y. Suzuki, M. Kakihana, M. Yoshimura, Phys. Rev. B: Condens Matter 51 (1995) 8018.

[23] S. Otsuka-Yao-Matsuo, T. Omata, N. Izu, H. Kishimoto, J. Solid State Chem. 138 (1998) 47.

[24] T. Omata, H. Kishimoto, S. Otsuka-Yao-Matsuo, N. Ohtori, N. Umesaki, J. Solid. State Chem. 147 (1999) 573.

[25] J. B. Thomson, A. R. Armstrong, P. G. Bruse, J. Am. Chem. Soc. 118 (1996) 11129.

[26] T. Montini, A. Speghini, L. De Rogatis, B. Lorenzut, M. Bettinelli, M. Graziani, P. Fornasiero, J. Am. Chem. Soc. 131 (2009) 13155.

[27] P. R. Shah, T. Kim, G. Zhou, P. Fornasiero, R. J. Gorte, Chem. Mater 18 (2006) 5363.

[28] T. Montini, N. Hickey, P. Fornasiero, M. Graziani, M. A. Bañares, M. V. Martinez-Huerta, I. Alessandri, L. E. Depero, Chem. Mater 17 (2008) 1157.

[29] T. Montini, M.A. Bañares, N. Hickey, R. Di Monte, P. Fornasiero, J. Kašpar, M. Graziani, Phys. Chem. Chem. Phys. 6 (2004) 1.

[30] A. Trovarelli, Catal. Rev. 38 (1996) 439.

[31] G. Li, B. Zhao, Q. Wang, R. Zhou, Appl. Catal. B: Env. 97 (2010) 41.

[32] A. Martínez-Arias, M. Fernández-García, V. Ballesteros, L. N. Salamanca, J. C. Conesa, C. Otero, J. Soria, Langmuir 15 (1999) 4796.

[33] C. A. Franchini, D. V. Cesar, Catal. Lett. 137 (2010) 45.

[34] A. Dolbecq, J. D. Compain, P. Mialane, J. Marrot, F. Secheresse, B. Keita, L. R. B. Holzie, F. Miserque, L. Nadjo, Chem. Eur. J. 15 (2009) 733.

[35] V. I. Parvulescu, V. Parvulescu, U. Endruschat, G. Filoti, F. G. Wagner, C. Kubel, R. Richards, Chem. Eur. J. 12 (2006) 2343.

[36] S. Roy, A. Marimuthu, M. S. Hegde, G. Madras, Catal. Commun. 9 (2008) 811.

[37] E. Bekyarova, P. Fornasiero, J. Kašpar, M. Graziani, Catal. Today 45 (1998) 179.

[38] K. Bauer, D. Garbe, Common Fragrance and Flavor Materials, VCH, Weinheim. (1985).

[39] S. I. Fukuzawa, T. Fujuami, S. Yamuchi, S. Sakai, J. Chem. Soc. Perkin Trans I. (1986) 1929.

[40] R. Touroude, J. Catal. 65 (1980) 110.

[41] C. Pham-Huu, N. Keller, G. Ehret, L. J. Charbonniere, R. Ziessel, M. J. Ledoux, J. Mol. Catal. A: Chem. 170 (2001) 155.

Chapter 5

Selective Hydrogenation of C=C in Cinnamaldehyde over Noble Metal Promoted Ni/CeO_2-ZrO_2 Catalysts

5.1. Introduction

Selective hydrogenation of α, β-unsaturated aldehydes is an organic transformation of fundamental and industrial importance (Scheme 3.1) [1-3]. In such compounds, hydrogenation occurs at both C=C and C=O functional groups. While hydrogenation of the olefinic group leads to saturated aldehydes, the carbonyl group hydrogenation yields unsaturated alcohols. Both these hydrogenation products of cinnamaldehyde (CA) - a representative α, β-unsaturated aldehyde are widely used in pharmaceuticals, perfumes and flavours [4]. Hydrocinnamaldehyde was found as an important intermediate in the preparation of a drug used in the treatment of HIV [4]. Supported Ni catalysts are selective for C=C hydrogenation in CA. Although, hydrogenation of C=C compared to C=O is easy, development of still more efficient catalysts that operate at moderate conditions is desirable. Catalytic application CeO_2-ZrO_2-supported Ni for the liquid-phase hydrogenation of CA is investigated, for the first time, in this chapter. The influence of noble metal (Pd and Pt) and alkali (NaOH) promoters on the catalytic activity and product selectivity of the supported Ni is studied. Enhancement in hydrogenation activity of some catalysts when a small amount of noble metal was added (Cu-Pt, Co-Pt, Ru-Pt, Fe-Pt and Sn-Pt) has already been reported [5-11]. The present study confirms such an enhancement even in the case of supported Ni catalysts. Detailed characterization studies revealed that increased metal dispersion is the cause for the enhanced activity of the promoted catalysts. The catalysts of this work are more active than the hitherto known Ni catalysts for C=C hydrogenation.

5.2. Experimental Procedure and Characterization Techniques

Ni(5 wt%)/CeO_2, Ni(3, 5, 10 and 15 wt%)/ZrO_2, Ni(5 wt%)/CeO_2-ZrO_2 (Ce:Zr = 1:1 molar ratio) and Ni(5 wt%)-(Pd or Pt, 0.5 wt%)/CeO_2-ZrO_2 (Ce:Zr = 1:1 molar ratio) catalysts were synthesized and characterized as reported in Chapter 2 (sections 2.2.2. and 2.3). Prior to use in reactions, the catalysts were freshly reduced at 400 °C in a flow of H_2 (30 ml/min) for 2.5 h. Procedures used in catalytic activity studies are reported in Chapter 2 (section 2.4.1.3).

5.3. Results and Discussion

5.3.1. Structural Properties

5.3.1.1. XRD. Catalyst samples reduced in hydrogen atmosphere showed two characteristic XRD peaks at 44.5° and 52° arising from (111) and (200) planes of metallic Ni having a face-centered cubic structure (JCPDS Card No. 04-0850). Intensities of these peaks increased with increasing Ni content (Fig. 5.1). In the case of Ni(5wt%)/CeO_2 and Ni(5wt%)/ZrO_2, a decrease in unit cell parameter of the support ($a_{Support}$) was noted when Ni

was present, revealing that a portion of Ni is possibly substituted in lattice sites of the CeO_2 and ZrO_2 [$a_{Support}$: 0.542 nm (for "neat" CeO_2), 0.512 nm (for "neat" ZrO_2), 0.540 nm (for Ni(5wt%)/CeO_2) and 0.508 nm (Ni(5wt%)/ZrO_2)] [12]. No such decrease in unit cell parameter ($a_{Support}$) was observed for Ni supported on CeO_2-ZrO_2 solid solutions suggesting that most of the Ni in those samples is located on the surface of the support only. This surface-rich Ni on CeO_2-ZrO_2 cubic fluorite structure thereby showed more intense metallic Ni peaks than Ni(5 wt%)/CeO_2 and Ni(5 wt%)/ZrO_2 (Fig. 5.1).

The XRD peaks corresponding to Ni were much smaller compared to those of the supports (Fig. 5.1). However, by using ORIGIN-8 software and expanding and blowing up the XRD patterns, the full-width at half height of Ni(111) reflection was estimated, which in turn enabled determination of the average crystallite size of Ni using Debye-Scherrer formula. The crystallite size of Ni on CeO_2-ZrO_2 was found larger (24.6 nm) than that on ZrO_2 (17.8 nm) and CeO_2 (3.7 nm, Table 5.1). This variation of Ni crystallite size agrees well with the available metal content on the surface of support and enhanced metal dispersion property of CeO_2. The crystallite sizes of Ni for 5, 10 and 15 wt% Ni/ZrO_2 were estimated to be 17.8, 28.0 and 25.6 nm, respectively. The size of metal crystals on Ni(3 wt%)/ZrO_2 was below the X-ray detection limit. Co-presence of Pt and Pd decreased the mean crystallite size of Ni from 24.5 [for Ni(5 wt%)/CeO_2-ZrO_2] to 21.5 nm [for Ni(5 wt%)-Pt(0.5 wt%)/CeO_2-ZrO_2] and 10.7 nm [for Ni(5 wt%)-Pd(0.5 wt%)/CeO_2-ZrO_2]. It may be noted that the Ni contents (nominal value – 5 wt% and actual value determined by AAS – 4.5, 4.3 and 4.4 wt%; Table 5.1) of these three compositions - Ni(5 wt%)/CeO_2-ZrO_2, Ni(5 wt%)-Pt(0.5 wt%)/CeO_2-ZrO_2 and Ni(5 wt%)-Pd(0.5 wt%)/CeO_2-ZrO_2, respectively, were nearly the same. H_2-temperature-programmed reduction experiments showed individual reduction peaks of Ni and noble metal suggesting that Ni-Pt and Ni-Pd exist as bimetallic components and not as alloys. Raab and Lercher [13] reported a similar observation for Pt promoted dispersion of Ni supported on TiO_2 used for gas-phase hydrogenation of crotanaldehyde.

5.3.1.2. N_2-Physisorption. Upon Ni loading, the specific surface area (S_{BET}) of CeO_2-ZrO_2 decreased from 115 to 65 m^2/g. While platinum had little effect, co-presence of Pd increased the surface area of Ni/CeO_2-ZrO_2 from 65 to 77 m^2/g (Table 5.1). The reason for this increase is however, not clear at this point of time.

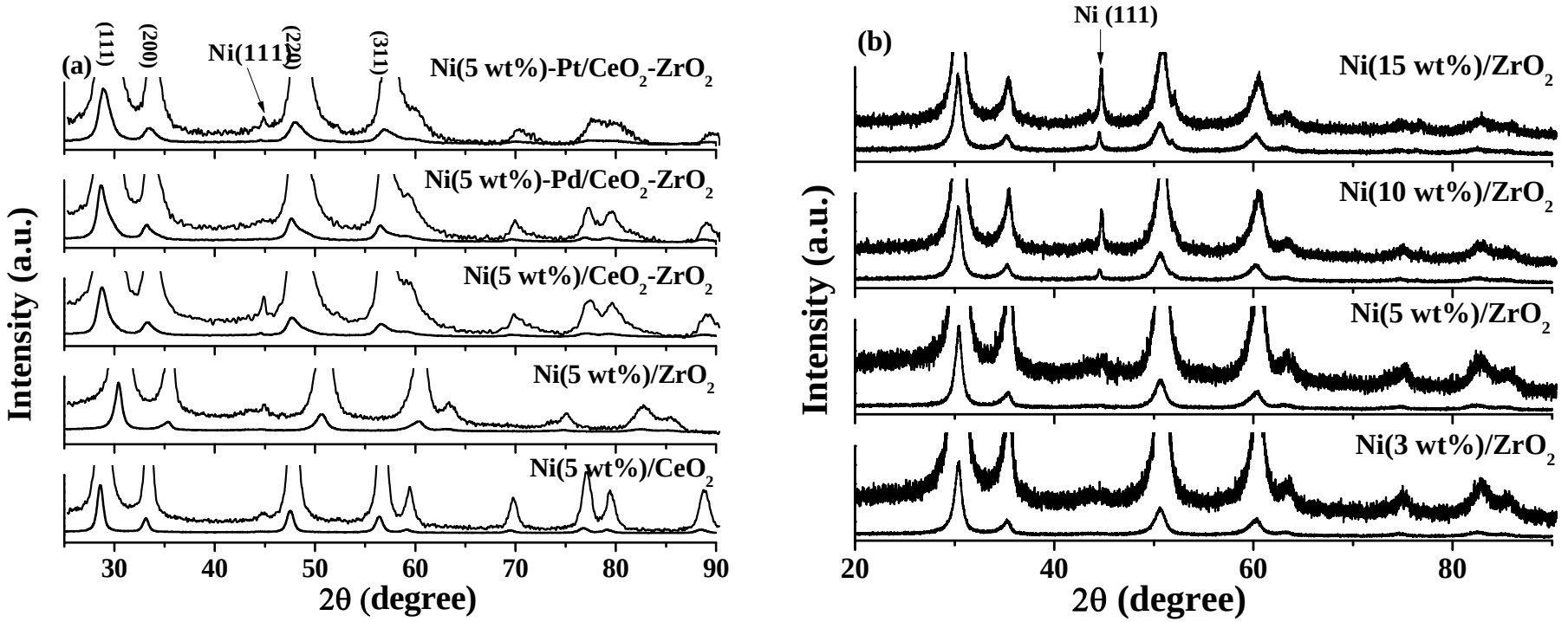

Fig. 5.1. XRD profiles of (a) CeO_2-ZrO_2-supported Ni catalysts. Nominal values of Pd and Pt were 0.5 wt%. (b) Different loadings of Ni supported on ZrO_2

Table 5.1. Physicochemical characteristics of CeO_2-ZrO_2-supported Ni catalysts

Sample[a]	Ni content (output, wt%; AAS)	Structural properties (XRD)			Specific surface area (S_{BET}; m^2/g)	Acidity (mmol/g; NH_3-TPD)	Basicity (mmol/g; CO_2-TPD)	Binding energy values (eV, XPS)		
		Unit cell parameter ($a_{Support}$; nm)	Average crystallite size (nm)					Ce ($3d_{5/2}$)	Zr ($3d_{5/2}$)	Ni ($2p_{3/2}$)
			Support	Ni						
CeO_2-ZrO_2	-	0.537	7.7	-	115	0.180	0.220	-	-	-
Ni(5wt%)/CeO_2-ZrO_2	4.5	0.537	7.8	24.6	65	0.208	0.248	881.7	181.3	852.4
Ni(5wt%)/CeO_2	4.3	0.540	12.9	3.7	63	0.175	0.234	881.3	-	852.1
Ni(5wt%)/ZrO_2	4.4	0.508	10.7	17.8	88	0.302	0.255	-	181.8	852.0
Ni(5wt%)-Pt(0.5wt%)/CeO_2- ZrO_2	4.3	0.533	8.4	21.5	67	-	-	881.1	181.4	851.2
Ni(5wt%)-Pd(0.5wt%)/CeO_2- ZrO_2	4.4	0.540	13.5	10.7	77	-	-	880.9	181.2	851.4

[a]Input values of metals used in synthesis are denoted in parentheses.

5.3.1.3. HRTEM. Representative HRTEM images (Fig. 5.2) revealed that Ni is uniformly distributed on the support. From the XRD data (Table 5.1) it appeared that in some cases, the size of Ni crystallites is bigger than that of the support crystallites. However, it should be noted that XRD provides crystallite size information of only those crystals which are above the X-ray detection limit. HRTEM images show that Ni is uniformly distributed on the support surface. Hence, it is likely that the crystallites of Ni which are bigger in size are only a few in numbers, while a majority of Ni crystals are smaller than the size of the support crystallites and are finely dispersed and located on the support surface.

5.3.1.4. XPS. Binding energy (BE) values of Ce ($3d_{5/2}$), Zr ($3d_{5/2}$) and Ni ($2p_{3/2}$) determined from XPS are listed in Table 5.1. The BE values of Ni $2p_{3/2}$ for different catalysts decreased in the order: Ni(5 wt%)/CeO_2 (852.5 eV) > Ni(5 wt%)/CeO_2-ZrO_2 (852.1 eV) > Ni(5 wt%)/ZrO_2 (852.0 eV) (Fig. 5.3.). Noble metal incorporation lowered the BE value still further [Ni(5 wt%)/CeO_2-ZrO_2 (852.1 eV) > Ni(5 wt%)-Pd(0.5 wt%)/CeO_2-ZrO_2 (851.5 eV) > Ni(5 wt%)-Pt(0.5 wt%)/CeO_2-ZrO_2 (851.4 eV)]. Croy et al [14] and Dömök et al [15] reported that BE values of photoelectrons ejected from metal particles depend on the metal particle size. The smaller the particle, the higher would be the binding energy. Hence, the average particle size of Ni on different supports is expected to decrease in the order: Ni(5 wt%)/ZrO_2 > Ni(5 wt%)/CeO_2-ZrO_2 > Ni(5 wt%)/CeO_2. Pt and Pd enhanced the dispersion of Ni in Ni(5 wt%)-Pt(0.5 wt%)/CeO_2-ZrO_2 and Ni(5 wt%)-Pd(0.5 wt%)/CeO_2-ZrO_2, respectively. This agrees well with the XRD and TEM results. Ni on ZrO_2 support is more metallic in nature (lower BE value) than that on CeO_2 and CeO_2-ZrO_2. Noble metals (especially Pd) enhanced the metallic nature of Ni. The observed shift in BE values is also because of weaker metal-support interactions in the case of ZrO_2 than in CeO_2-ZrO_2 and CeO_2. Shifts in energy can be explained in terms of charge transfer to the metal particle from the support due to delocalized electron distributions arising from oxygen vacancies [16, 17]. Shift to higher binding energy values is an indication of strong interaction between support and metal particle. In the case of Ni(5 wt%)/ZrO_2, the Ni $2p_{3/2}$ peak appeared at lower BE value of 852.0 eV compared to that of Ni(5 wt%)/CeO_2-ZrO_2 (at 852.1 eV) and Ni(5 wt%)/CeO_2 (at 852.5 eV). Hence, it can be concluded that support-metal interactions are weaker in the case of Ni(5 wt%)/ZrO_2 than in Ni(5 wt%)/CeO_2-ZrO_2 and Ni(5 wt%)/CeO_2. Similar observations were found by Croy et al [17] for Pt supported on several oxides. "Neat" CeO_2 shows a main line for $3d_{5/2}$ at 882.2 eV. In the case of CeO_2 and CeO_2-ZrO_2-supported Ni(5 wt%) catalysts, this line appeared at 881.8 and 882.0 eV, respectively.

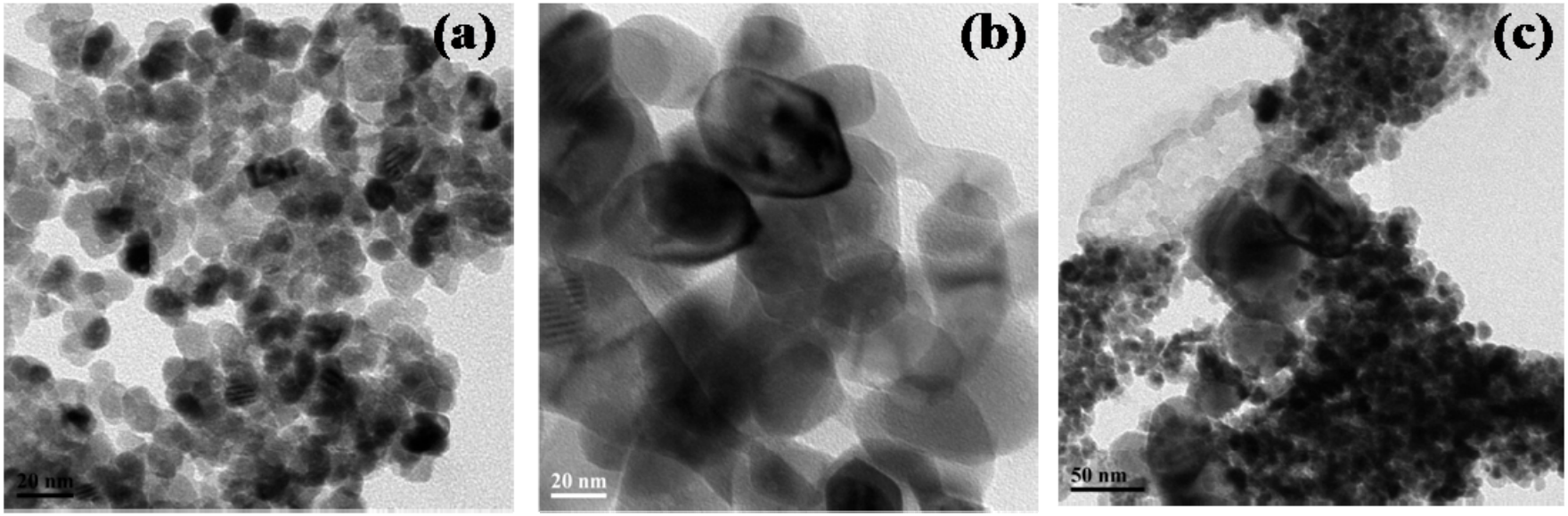

.

Fig. 5.2. HRTEM images of (a) Ni(5 wt%)/CeO_2, (b) Ni(5 wt%)/ZrO_2 and (c) Ni(5 wt%)/CeO_2-ZrO_2

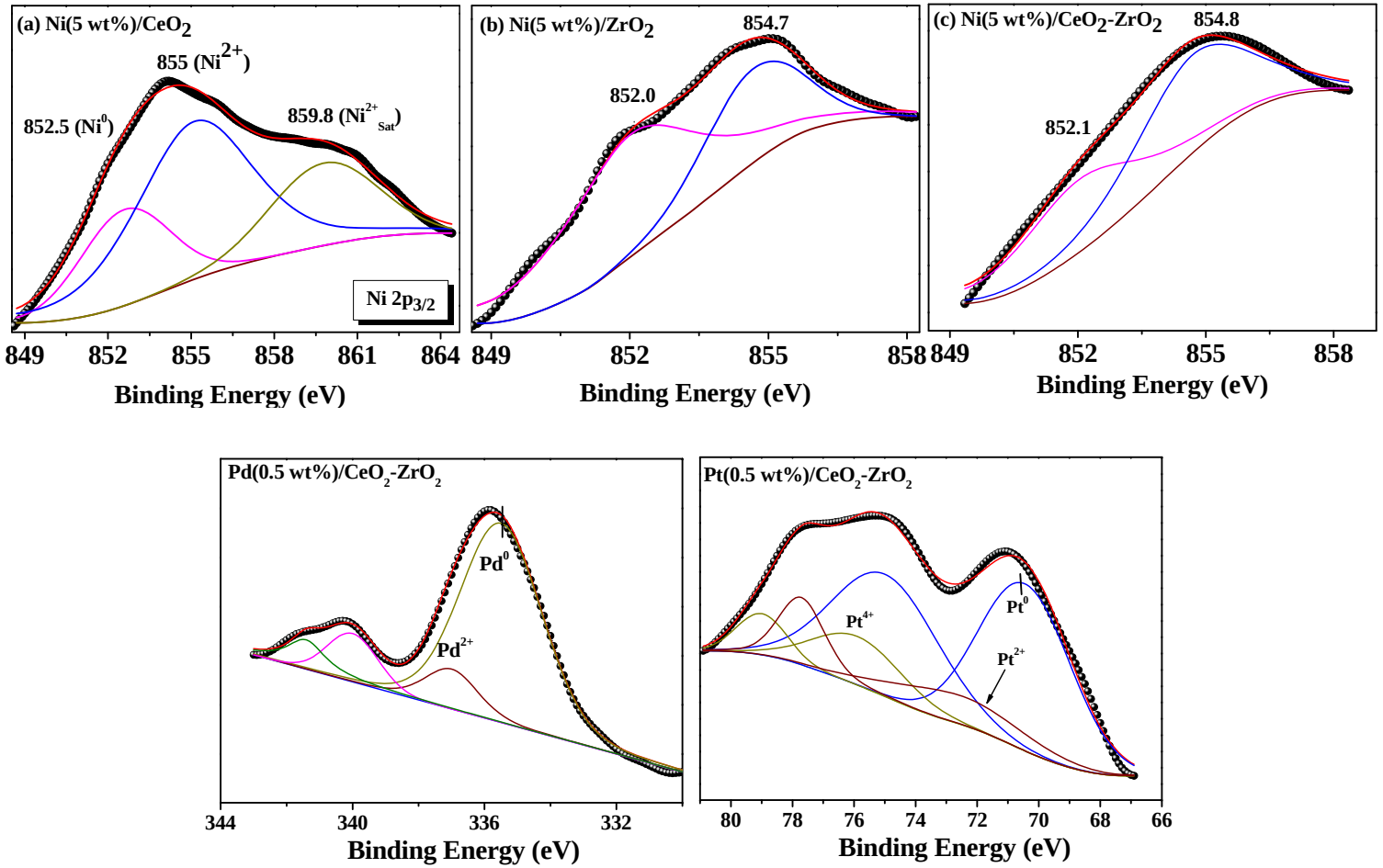

Fig. 5.3. XPS of Ni(5 wt%) supported on ZrO_2, CeO_2 and CeO_2-ZrO_2 and core level spectra of (0.5 wt%) Pt, (0.5 wt%) Pd supported on CeO_2, ZrO_2 catalysts

Shift in line position of $3d_{5/2}$ is due to changes in the electronic structure of Ce^{4+} as a consequence of support-metal interactions. XPS revealed that a part of Ni in the catalysts is in +2 oxidation states showing a main $2p_{3/2}$ line at around 855 eV and its corresponding satellite line at 859.8 eV (Fig. 5.3). Spectral deconvolution enabled the relative percentage concentrations of zero and +2 valent Ni species (sensitivity factor of Ni in concentration estimations was considered as 4.5), which were (69, 31), (43.2, 56.8), (28.1, 71.9), (18, 72) and (63, 37) for Ni(5 wt%)/ZrO_2, Ni(5 wt%)/CeO_2-ZrO_2, Ni(5 wt%)/CeO_2, Ni(5 wt%)-Pt(0.5 wt%)/CeO_2-ZrO_2 and Ni(5 wt%)-Pd(0.5 wt%)/CeO_2-ZrO_2, respectively. This indicates that ZrO_2 and CeO_2-ZrO_2 supports, in presence of Pd, keep most of the Ni in metallic state. Such effects of support on the electronic properties of Ni are found to have profound influence on the activity of these catalysts.

The chemical states of Pt and Pd in reduced catalysts, Pt(0.5 wt%)/CeO_2–ZrO_2 and Pd(0.5 wt%)/CeO_2–ZrO_2, respectively were determined from their corresponding core level spectra (Fig. 5.3). Pt was present in zero, +2 and +4 oxidations states with their compositions being 65.8, 15.8 and 18.4 %, respectively. The $4f_{7/2}$ peak of Pt^0 was observed at 70.5 eV. The main line of Pt^{2+} and Pt^{4+} appeared at 71.9 and 75.6 eV, respectively. Pd was present in zero and +2 oxidation states with composition being 88.2 and 11.8 %, respectively. The main line for metallic Pd ($3d_{5/2}$) appeared at 335.5 eV and of Pd^{2+} (as PdO) appeared at 337.0 eV. The BE values of Pt^0 and Pd^0 were well within the expected range [18].

5.3.1.5. NH_3-TPD and CO_2-TPD. As shown in Figs. 5.4(a) and 5.4(b), the TPD curves of the catalysts are broad and asymmetric and point out the presence of more than one type of acid and base centers. While the desorption peaks with peak maximum at about 150 °C in NH_3 and CO_2-TPD are due to weak acid and base sites, respectively, those at higher temperatures 250 – 350 °C in NH_3-TPD and 300 – 350 °C in CO_2-TPD are due to stronger acidic and basic sites. Support influenced the position of the high temperature desorption peak. The overall basicity of the catalysts (Table 5.1) is nearly the same [0.234 – 0.255 mmol/g, Fig. 5.4(b)]. However, acidity was affected by the support. Acidity of different catalysts decreased in the order: Ni(5 wt%)/ZrO_2 (0.302 mmol/g) > Ni(5 wt%)/CeO_2-ZrO_2 (0.208 mmol/g) > Ni(5 wt%)/CeO_2 (0.175 mmol/g) [Fig. 5.4(a)]. CeO_2-ZrO_2-supported Ni(5 wt%) has higher acidity (0.208 mmol/g) than "neat" CeO_2-ZrO_2 (0.180 mmol/g). Pure zirconia is acidic in nature. When metal gets incorporated into its lattice, additional acid sites were generated and thereby an enhancement in overall acidity of the catalyst was observed.

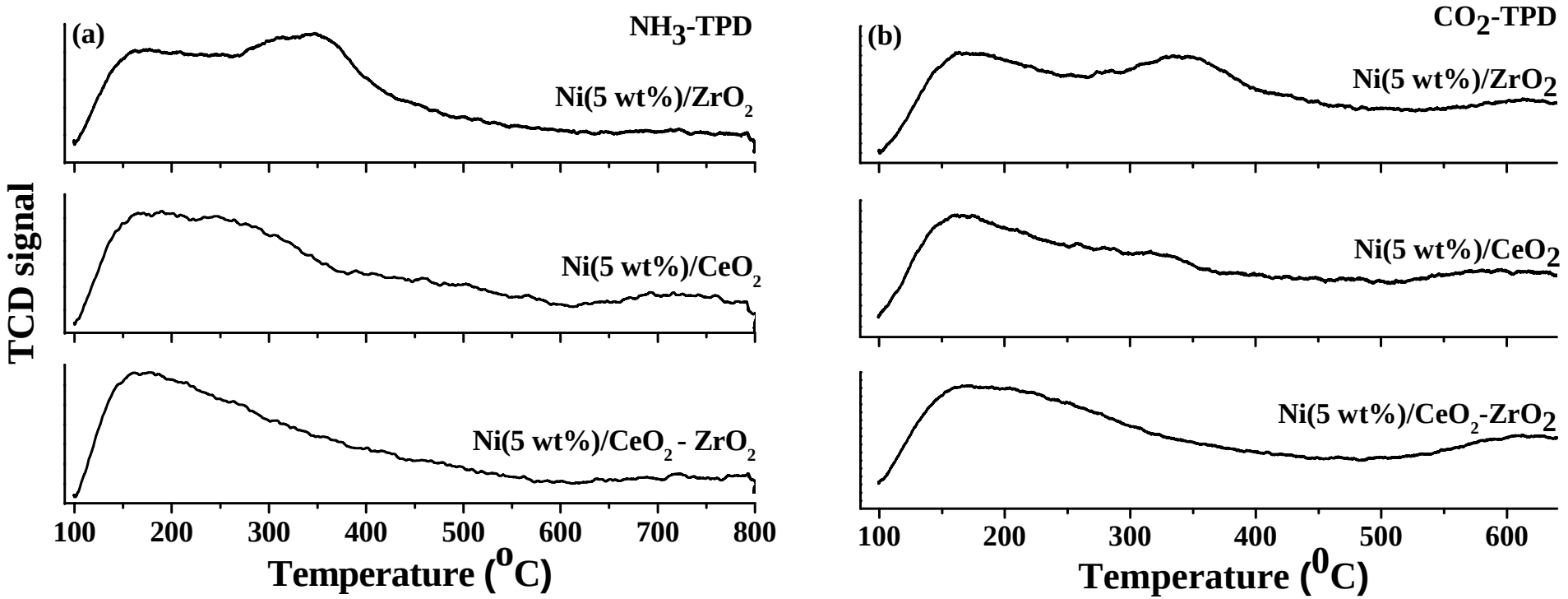

Fig. 5.4. (a) NH_3-TPD and (b) CO_2-TPD profiles of CeO_2-ZrO_2- supported Ni catalysts

5.3.1.6. H_2-TPR. Fig. 5.5(a) represents the temperature programmed reduction profiles of the supported Ni catalysts. Usually, NiO reduces at around 350 – 400 °C. ZrO_2-supported NiO showed reduction peaks at 212, 300 and 471 °C, while the peaks at 212 and 300 °C are attributed to NiO weakly interacting with the support that at 471 °C is corresponded to strongly interacting and framework substituted NiO [19]. CeO_2-supported NiO showed reduction peaks at 152, 187, 276 and 705 °C. The high temperature peak at 705 °C is corresponded to reduction of bulk ceria [20]. The remaining peaks are corresponded to NiO. While the peak at 276 °C is due to weakly interacting NiO with support, those at 152 and 187 °C are due to dispersed NiO strongly interacting with CeO_2 support. Ceria is a reducible oxide and hence, facilitates reduction of the supported metal. CeO_2-ZrO_2-supported NiO showed peaks at 180, 265 and 370 °C. XRD studies pointed out that the crystals of Ni on this support are larger than those on ZrO_2 and CeO_2. The peak at 370 °C is therefore corresponded to large crystallites of NiO and the ones at 265 and 180 °C are corresponded to smaller crystallites and NiO strongly interacting with the support. It is known, that when a part of Ni occupies the lattice sites, oxygen vacancies are created [21]. Adsorbed oxygen at those sites during the pretreatment process gets reduced at lower temperatures. Overlap of these peaks with the reduction peaks of NiO cannot be ruled out. Based on the reduction temperature values, it can be concluded that the reducibility of Ni on different supports decreases in the order: Ni(5 wt%)/CeO_2 > Ni(5 wt%)/CeO_2-ZrO_2 > Ni(5 wt%)/ZrO_2. In the case of Ni(5 wt%)/CeO_2-ZrO_2, the H_2 uptake values below 450 °C will have contributions also from the support oxide. By subtracting this contribution of CeO_2-ZrO_2 support (0.69 mmol/g) from the total (1.54 mmol/g), the H_2 uptake value of Ni(5 wt%) supported on CeO_2-ZrO_2 becomes smaller (0.85 mmol/g) than those of Ni(5 wt%)/CeO_2 (1.04 mmol/g) and Ni(5 wt%)/ZrO_2 (1.02 mmol/g). It may be noted that in the case of the latter two catalysts, the supports do not show reduction peaks in this temperature region and hence, the hydrogen uptake values are solely due to Ni only. In view of this, it could be stated that the actual dispersion of Ni is higher on CeO_2 and ZrO_2 than on CeO_2-ZrO_2. In the case of Ni(5 wt%)/CeO_2 and Ni(5 wt%)/ZrO_2, not all Ni is located on the surface as a small quantity of it also goes into the support lattice locations. However, in the case of Ni(5 wt%)/CeO_2-ZrO_2, metal is located mainly on the surface. This could be yet another reason for the higher dispersion of Ni on CeO_2 and ZrO_2 than on CeO_2-ZrO_2 supports.

Bulk PtO showed hydrogen uptake peak in TPR at 130 – 160 °C. Pt(0.5 wt%) supported on CeO_2-ZrO_2 showed reduction peaks at 111 and 165 °C. While the latter peak is

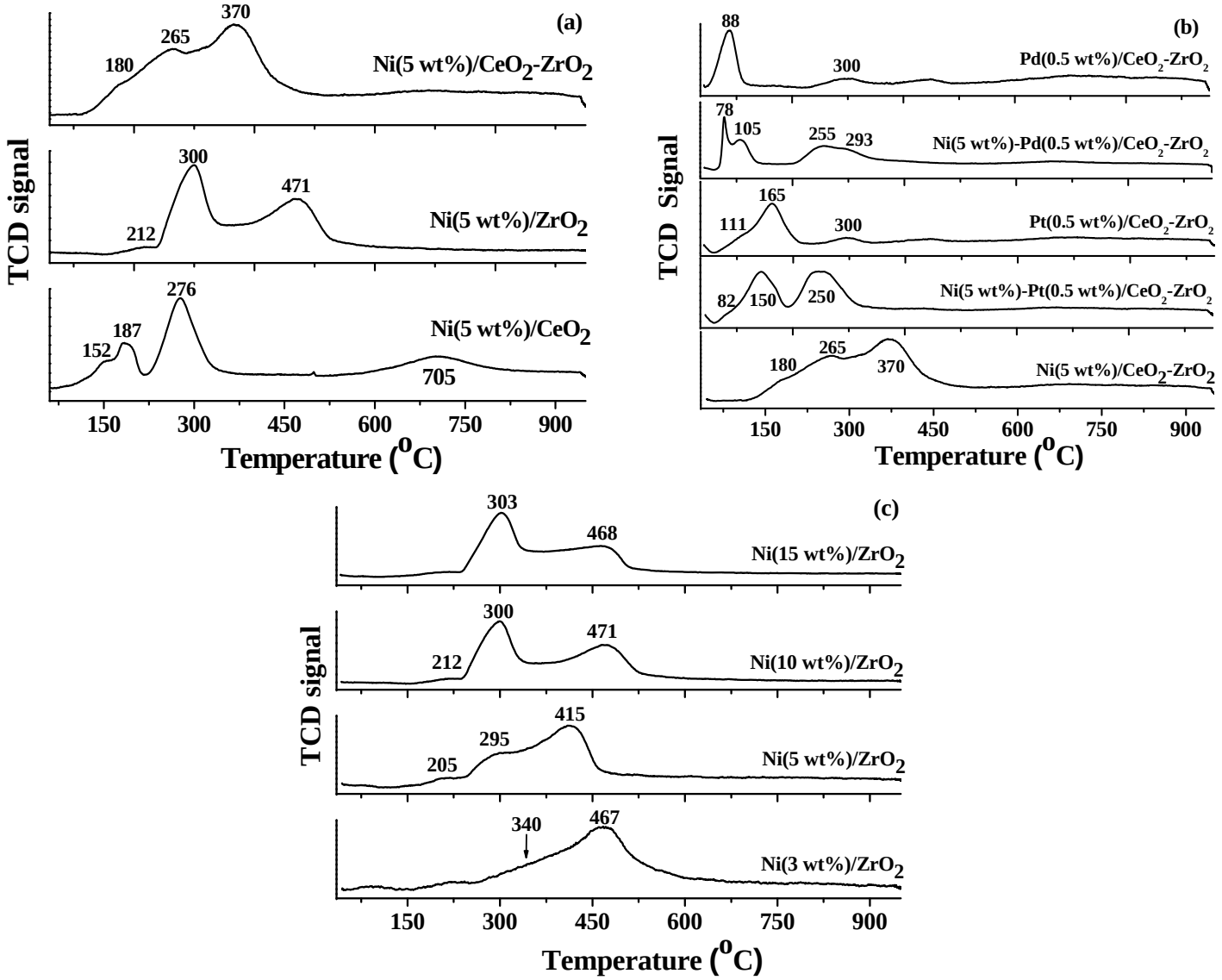

Fig. 5.5. H_2-TPR profiles of supported Ni catalysts

attributed PtO of large crystallites that at 111 °C is corresponded to PtO strongly interacting with the support. CeO_2-ZrO_2-supported Pd(0.5 wt%) showed TPR peaks at 88 and 300 °C. The peak at 300 °C common in both Pt and Pd catalysts is due to defect sites of the support CeO_2-ZrO_2 mixed oxide. The peak at 88 °C is due to reduction of PdO.

When both Ni and noble metal were present, a decrease in reduction temperature of both the metals was observed as a consequence of synergistic effect (Fig. 5.5(b)). In the case of Ni(5 wt%)-Pt(0.5 wt%)/CeO_2-ZrO_2, the reduction peaks of NiO and PtO were observed at 250, 150 and 82 °C. In the case of Ni(5 wt%)-Pd(0.5 wt%)/CeO_2-ZrO_2 catalysts, those peaks were observed at 255, 105 and 78 °C. Although the apparent H_2 uptake value of Ni(5 wt%)-Pt(0.5 wt%)/CeO_2-ZrO_2 was nearly the same as that of Ni(5 wt%)/CeO_2-ZrO_2, this value had contributions from both Ni and Pt. Fig. 5.5(c) shows TPR profiles of different amounts Ni loaded on ZrO_2. At 3 wt% of Ni loading, a peak at 467 °C was prominent. Weak shoulders were observed at 340 and 205 °C. As described previously, the peak at 467 °C is due to NiO strongly interacting with the ZrO_2 support and the shoulders are due to NiO weakly interacting with the support. With increasing metal loading, a systematic growth in intensity of the peaks due to weakly interacting NiO at about 300 °C was observed. The TPR profile of Ni(15 wt%)/ZrO_2 contained the peak at 300 °C as the dominant one. The H_2 uptake values (in TPR) for ZrO_2-supported 3, 5, 10 and 15 wt% Ni are 0.59, 1.02, 1.56 and 2.26 mmol/g, respectively.

5.3.1.7. H_2-Chemisorption. Metal dispersion (MD), average metal particle size (D_a) and metal specific surface area (MSS) were determined from hydrogen chemisorptions studies (Table 5.2). The values of MD and MSS for different supported Ni catalysts decreased as follows: Ni(5 wt%)/CeO_2 > Ni(5 wt%)/CeO_2-ZrO_2 > Ni(5 wt%)/ZrO_2. The value of D_a varied in the reverse order. In other words, support CeO_2 facilitated dispersion of nickel. An enhancement in metal dispersion was observed also when Pt or Pd (0.5 wt%) was present with Ni(5 wt%) in the catalyst (Table 5.2). It should, however, be noted that under chemisorptions conditions, Pt and Pd too ad/absorb hydrogen and thereby enhanced hydrogen uptake would be observed. In other words, in those cases the estimated dispersion is more than the actual value. Discrepancy in the values of crystallite size determined from XRD and H_2 adsorption may noticed. This was due to the fact that XRD detects only those crystallites which are above its detection limit of 3 – 5 nm whereas, crystals of all dimensions contribute to H_2 adsorption and hence, discrepancy is inevitable whenever there is a mix of large and smaller crystallites of Ni present in the system.

Table 5.2. H_2 chemisorptions data of CeO_2-ZrO_2-supported catalysts

Catalyst	H_2-Chemisorbed (mmol/g)	Metal surface area (m^2/g)	Metal dispersion (%)	Av. metal particle size (nm)
Ni(5 wt%)/CeO_2	0.716	58.1	8.7	11.6
Ni(5 wt%)/ZrO_2	0.366	29.0	4.4	23.2
Ni(5 wt%)/CeO_2-ZrO_2	0.440	34.2	5.1	19.7
Ni(5 wt%)-Pt(0.5 wt%)/CeO_2-ZrO_2	0.763	61.9	9.3	10.9
Ni(5 wt%)-Pd(0.5 wt%)/CeO_2-ZrO_2	1.235	98.0	14.7	6.9

5.3.2. Catalytic Activity

Controlled, blank experiments revealed that CA conversion was negligible (1.5 wt%) in the absence of a catalyst (Table 5.3, run no. 1). The supported Ni catalysts of the present study are highly active even at 100 °C and at a hydrogen pressure of 20 bar. A small quantity of the catalyst (0.05 g; Table 5.3) is enough for quantitative conversion of CA (1 g). In general, HCA is the selective product (89.6 – 100 wt%). Support showed significant effect on the catalytic activity of Ni. Conversion of CA and turnover frequency [TOF = moles of CA converted per mole of exposed Ni (determined from chemisorption) per hour] for different supported Ni catalysts decreased in the following order: Ni(5 wt%)/ZrO_2 (100%, 573) > Ni(5 wt%)/CeO_2 (68.3%, 456) > Ni(5 wt%)/CeO_2-ZrO_2 (45.3%, 219) (Table 5.3, run nos. 2, 3 and 4). Although it appears that the selectivity for HCA at these conversions decreases in the order: Ni(5 wt%)/CeO_2-ZrO_2 (97.3%) > Ni(5 wt%)/CeO_2 (93.7%) > Ni(5 wt%)/ZrO_2 (89.6%), it should be noted that HCA selectivity is nearly the same at similar conversion levels over all these different supported Ni catalysts [Figs. 5.6(a) and 5.6(b)]. Formation of PPL through further hydrogenation of HCA was more predominant on Ni(5 wt%)/ZrO_2. The catalyst with Pt(0.5 wt%) supported on CeO_2-ZrO_2 showed weaker catalytic activity (CA conversion) than Ni(5 wt%)/CeO_2-ZrO_2 (Table 5.3, compare run no. 7 with 4). Pt catalyst, unlike others, yielded CAL with a selectivity of 8.2 wt%. Pd(0.5 wt%)/CeO_2-ZrO_2 was highly active (run no. 8). HCA was the main product with a small quantity of other products (acetals and higher molecular weight products; 2.5 wt%) formed over this catalyst.

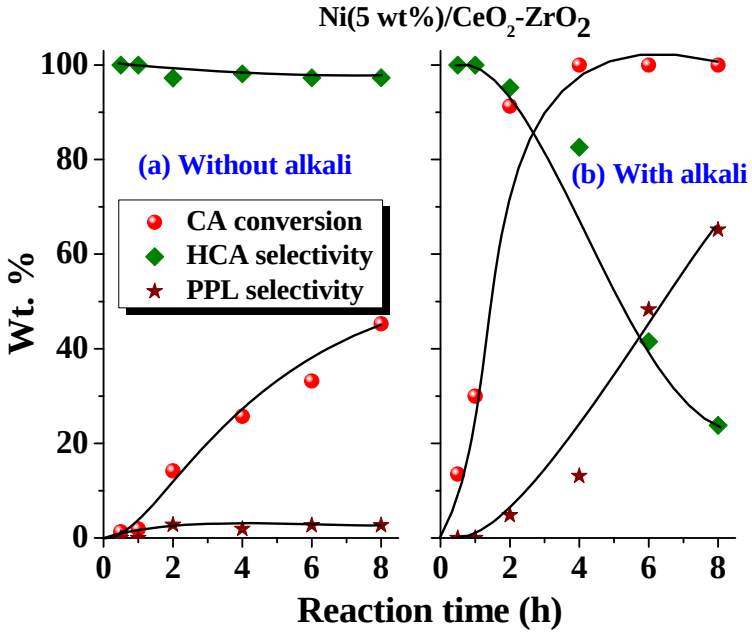

Fig. 5.6(a). Influence of alkali addition on the hydrogenation of cinnamaldehyde over Ni supported CeO_2-ZrO_2 catalysts

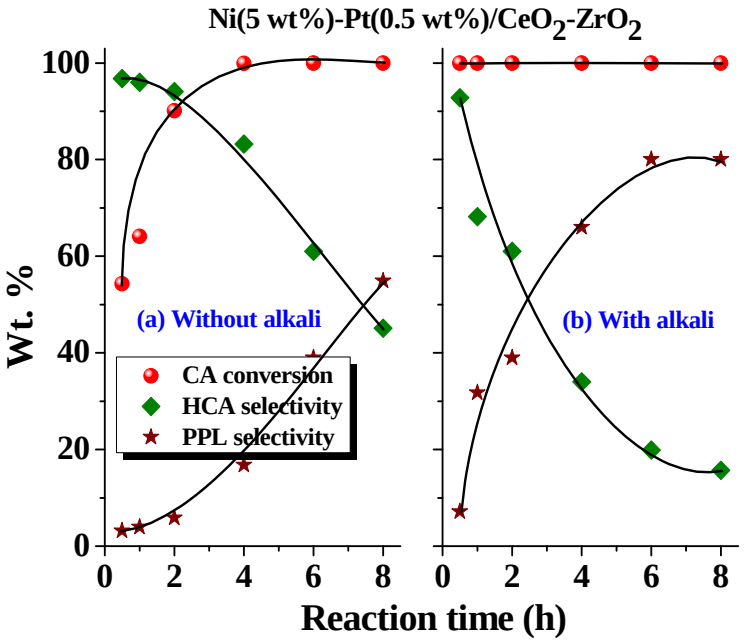

Fig. 5.6(b). Influence of alkali addition on the hydrogenation of cinnamaldehyde over Ni-Pt supported CeO_2-ZrO_2 catalysts. *Reaction conditions:* Catalyst (reduced at 400 °C for 2.5 h) = 0.05 g, CA = 1 g, iso-propanol = 25 ml, alkali = NaOH (0.01 g) in 5 ml water, H_2 pressure = 20 bar, reaction temperature = 100 °C, stirring speed = 600 rpm.

Table 5.3. Hydrogenation of cinnamaldehyde over supported Ni (5 wt%) catalysts: effect of support, noble metal and alkali promoter[a]

Run No.	Catalyst.	CA conversion (wt%)	TOF (h^{-1})	Product selectivity (%)		
				HCA	PPL	Others
Without alkali:						
1	-	1.5	-	100	0	0
2	Ni(5 wt%)/ZrO_2	100	573	89.6	10.5	0
2a	Ni(5 wt%)/ZrO_2	79.4	3643	96.1	3.9	0
3	Ni(5 wt%)/CeO_2	68.3	456	93.7	6.3	0
4	Ni(5 wt%)/CeO_2-ZrO_2	45.3	219	97.3	2.7	0
4a	Ni(5 wt%)/CeO_2-ZrO_2	14.2	275	100	0	0
5	Ni(5 wt%)-Pt(0.5 wt%)/CeO_2-ZrO_2	100	277	45.1	54.9	0
5a	Ni(5 wt%)-Pt(0.5 wt%)/CeO_2-ZrO_2	64.1	1424	96.0	4.0	0
6	Ni(5 wt%)-Pd(0.5 wt%)/CeO_2-ZrO_2	100	171	20.0	80.0	0
7	Pt(0.5 wt%)/CeO_2-ZrO_2	17.4	-	77.5	5.8	8.5(8.2)[c]
8	Pd(0.5 wt%)/CeO_2-ZrO_2	100	-	88.3	9.3	2.5
With alkali:[b]						
9	-	8.7	-	99.2	0.8	0.0

10	Ni(5 wt%)/ZrO_2	100	573	7.4	89.9	2.8
10a	Ni(5 wt%)/ZrO_2	96.7	4436	93.9	6.1	0
11	Ni(5 wt%)/CeO_2	100	668	7.7	77.7	14.6
12	Ni(5 wt%)/CeO_2-ZrO_2	100	484	23.6	65.3	11.1
13	Ni(5 wt%)-Pt(0.5 wt%)/CeO_2-ZrO_2	100	277	15.7	80.1	4.2
13a	Ni(5 wt%)-Pt(0.5 wt%)/CeO_2-ZrO_2	100	2221	68.2	31.8	0
14	Ni(5 wt%)-Pd(0.5 wt%)/CeO_2-ZrO_2	100	171	0.03	99.9	0.0
15	Pt(0.5 wt%)/CeO_2-ZrO_2	78.5	-	71.8	11.2	-(17.0)[c]
16	Pd(0.5 wt%)/CeO_2-ZrO_2	100	-	70.3	20.3	9.4

[a]*Reaction conditions:* Catalyst (reduced at 400 °C for 2.5 h) = 0.05 g, cinnamaldehyde = 1 g, solvent (iso-propanol) = 25 ml, H_2 pressure = 20 bar, reaction temperature = 100 °C, reaction time = 8 h, stirring speed = 600 rpm. CA = cinnamaldehyde, HCA = hydrocinnamaldehyde, PPL = 3-phenyl propanal, others include higher molecular weight condensation products. Turnover frequency (TOF) = moles of CA converted per mole of exposed Ni (determined from chemisorption) per hour. Run nos. 2a, 5a, 10a, 12a and 13a are those with reaction time of 1 h and 4a is with reaction time of 2 h, rest of the conditions are the same for all. [b]Alkali = NaOH (0.01 g) in 5 ml water. [c]Values in parentheses corresponds to the selectivity of cinnamyl alcohol

5.3.2.1. Influence of Noble Metal. A significant enhancement in CA conversion of CeO_2-ZrO_2-supported Ni was observed when Pd or Pt (0.5 wt%) was also a part of the catalyst composition (Table 5.3, compare run nos. 5 and 6 with 4). At 100 wt% CA conversion, HCA and PPL formed with equal weight percentage over Ni-Pt catalyst while they formed in the ratio of 20:80 wt% over Ni-Pd catalyst. Metal dispersion was higher in the case of Ni-Pd than "neat" Ni supported on CeO_2-ZrO_2. Due to this, 100% conversion of CA (with HCA selectivity of 85% and PPL selectivity of 15%) was achieved in just 1 h itself over Ni-Pd catalyst. For supported "neat" Ni catalyst, CA conversion was only 45.3% even after 8 h of reaction. Although it appears that TOF value of Ni-Pd at 8 h is lower than that of Ni, reverse is the case when it is compared at 1 h. Hence, all these observations point out that noble metal enhances the catalytic activity of supported Ni catalysts. As the individual contributions of Ni and noble metal in bimetallic systems, the H_2 chemisorption values reported in Table 5.2 have contribution from both these metals. So dispersion of Ni in bimetallic catalysts is actually lower than what is reported in Table 5.2. Taking this into consideration, TOF for run nos. 5 – 6 and 13 – 14 in Table 5.3 are the lowest values reported than the actual.

5.3.2.2. Influence of Alkali and Supports. When a small of quantify of alkali (NaOH) was added to the reaction mixture, catalytic activity (TOF) increased still further (Table 5.3, run nos. 10 to 16). PPL was the selective product in case of the supported Ni catalysts. Alkali alone couldn't catalyze this reaction to a significant extent (CA conversion = 8.7 wt%; run no. 9). When run 4a was conducted adding additionally 5 ml of water, increase in CA conversion from 14.2 to 25.4 wt% was noted [product selectivity: 97.3% (HCA) and 2.7 wt% (PPL)]. These studies, point out that both water and alkali have a role in enhancing catalytic activity of these catalysts. We believe that while water and OH^- (in alkali) alter the electronic properties of the metal, Na^+ ion facilitates polarization of carbonyl group in CA and enhance the rate of conversion of HCA to PPL. Comparison of data for runs 10 and 10a & 13 and 13a, reveals that near 100% conversion of CA is achieved in just 1 h itself when alkali promoter is added (Table 5.3). HCA is the selective product at 1 h. This product gets further hydrogenated in the due course of time and PPL becomes the main product at 8 h.

The catalyst, Ni(5 wt%)-Pd(0.5 wt%)/CeO_2-ZrO_2 gave 100 wt% conversion of CA and 99.9 wt% selectivity for PPL (run no. 14). Thus, the remarkable promotional activity of Pd and alkali is worth noting in the hydrogenation of CA over supported Ni catalysts.

While Ni(5 wt%)/ZrO_2 yielded 100 wt% CA conversion and 89.6 wt% HCA selectivity, Ni(5 wt%)-Pd(0.5 wt%)/CeO_2-ZrO_2 gave 100 wt% CA conversion and 99.9 wt% PPL selectivity in a reaction at 100 °C, 20 bar of H_2 pressure and reaction time of 8 h. By a small modification in catalyst composition, the product selectivity could be altered significantly. Upon alkali addition, even in the case of monometallic Pt catalysts, an enhancement in CA conversion from 17.4 to 78.5 wt% and increase in CAL selectivity from 8.2 to 17 wt% was observed. However, unlike with monometallic Ni, HCA is the major product on the monometallic Pt and Pd catalysts even after addition of alkali. This difference is, perhaps, due to difference in the amounts of Ni (5 wt%) and Pt/Pd (0.5 wt%) present on the catalyst surface and also due to their differences in crystallite sizes and strengths of adsorption of the product HCA molecules for them to react in further hydrogenation. Run nos. (2 & 10) and (5 & 13) for Ni(5 wt%)/ZrO_2 and Ni(5 wt%)-Pt(0.5 wt%)/CeO_2-ZrO_2 without and with alkali addition showed similar CA conversion at the end of 8 h. So, for demonstrating the influences of support and Pt on the catalytic activity of Ni (CA conversion and TOF), we have carried out reactions for shorter period of time (1 h) and the data are included in run nos. (2a & 10a) and (5a & 13a), respectively. As seen from Table 5.3, in the absence of alkali, the system is clean with only HCA and PPL as products [Pt catalyst (run no. 7) leads to alcohol as expected], however, when alkali is added, base-catalyzed aldol condensation products (others) are formed in good amount. Supported Ni-Pd (run no. 14) is highly active so that hydrogenation is more dominant than aldol condensation thus, enabled high activity and PPL selectivity is observed.

5.3.2.3. Effect of Temperature. Effect of temperature was studied in absence of alkali because the conversions were lower without alkali addition and the effect of temperature on the reaction can be monitored better. The reactions were conducted at 75, 100, 125, 150 °C. As seen from Table 5.4, Ni(5 wt%)/CeO_2-ZrO_2 is weakly active below 100 °C. TOF increased with increasing temperature; 100 wt% conversion of CA was achieved at 125 °C. Further rise in temperature changed product selectivity from HCA to PPL. So, it was found that 100 °C temperature is the optimum for these reactions.

5.3.2.4. Effect of Ni Loading. The amount of Ni loading affected the catalytic activity. CA conversion increased with increasing Ni loading indicating that there is no mass transfer limitation on the kinetics of the reaction (Table 5.5). On ZrO_2 support, nickel loading of 5 wt% was found sufficient to achieve 100 wt% CA conversion, in just, 2 h at 100 °C. At still

higher loadings, more and more amount of PPL formed due to hydrogenation of C=O on the larger crystallites of Ni formed at higher Ni loadings (XRD).

Table 5.4. Effect of temperature on hydrogenation of CA over Ni(5 wt%)/CeO_2-ZrO_2

Run No.	Reaction temperature (°C)	CA conversion (wt %)	TOF (h^{-1})	Product selectivity (%)	
				HCA	PPL
1	75	4.1	1	100	0.0
2	100	45.6	11	97.3	2.7
3	125	99.7	98.4	80.8	19.2
4	150	100	98.8	19.6	80.4

Reaction conditions: Catalyst (reduced at 400 °C for 2.5 h) = 0.05 g, CA = 1 g, solvent (iso-propanol) = 25 ml, alkali = Nil, reaction time = 8 h, stirring speed = 600 rpm.

Table 5.5. Influence of Ni loading on the hydrogenation of cinnamaldehyde over Ni/ZrO_2 catalyst

Ni loading (wt%)	CA conversion (wt%)	Product selectivity (%)	
		HCA	PPL
3	70.0	94.1	5.9
5	97.4	92.5	7.5
10	96.5	92.8	7.2
15	98.8	88.2	10.6 (1.2)[b]

Reaction conditions: Catalyst (reduced at 400 °C for 2.5 h) = 0.05 g, cinnamaldehyde (CA) = 1 g, H_2 pressure = 20 bar, solvent (iso-propanol) = 25 ml, alkali = nil, reaction temperature = 100 °C, reaction time = 2 h, stirring speed = 600 rpm. [b]Value in parentheses corresponds to that for higher molecular weight condensation (other) products.

5.3.3. Recyclability Test

The reusability of Ni(5 wt%)-Pt(0.5 wt%)/CeO_2-ZrO_2 catalyst was investigated in six recycling experiments. After each reaction, the catalyst was separated from the reaction mixture by filtration and then used without any further treatment in subsequent recycling studies. As seen from Fig. 5.7, Ni(5 wt%)-Pt(0.5 wt%)/CeO_2-ZrO_2 is more stable and no apparent loss in activity up to three recycle studies is detected.

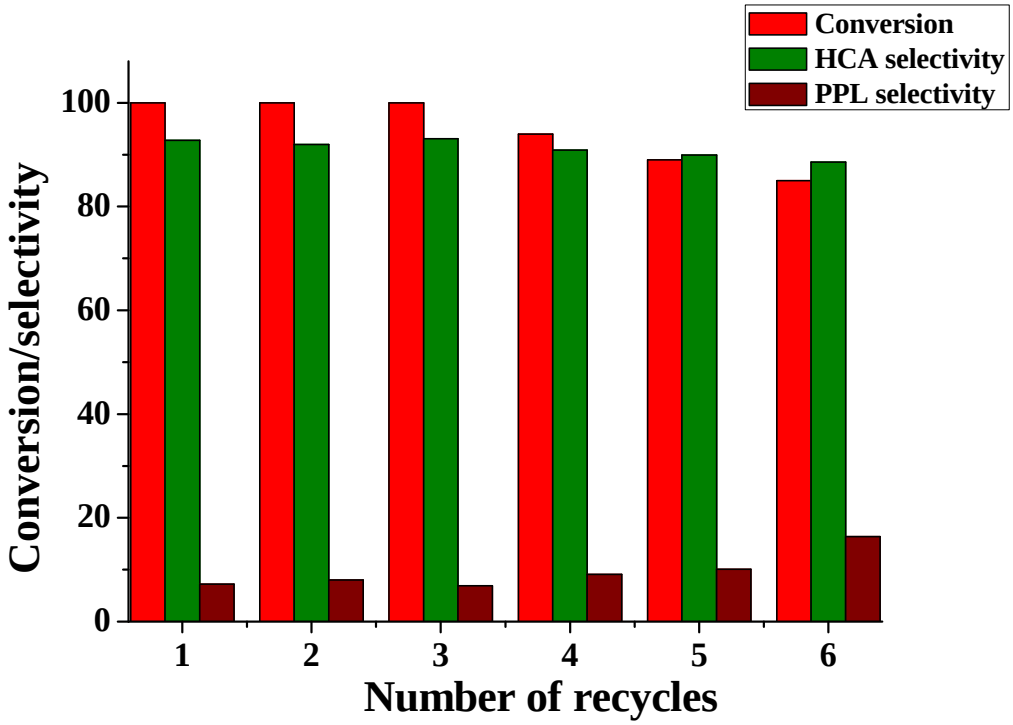

Fig. 5.7. Recyclabilty test for CA hydrogenstion over Ni-Pt/CeO_2-ZrO_2 catalyst. *Reaction conditions:* Catalyst (reduced at 400 °C for 2.5 h) = 0.1 g, cinnamaldehyde (CA) = 2 g, H_2 pressure = 40 bar, solvent (iso-propanol) = 50 ml, alkali = 0.005 g of NaOH in 10 ml of water, reaction temperature = 100 °C, reaction time = 2 h, stirring speed = 600 rpm. [b]Values in parentheses are the data at 8 h of reaction.

5.4. Structure-Activity Correlations

As seen from the catalytic data, addition of Pt has less important effect on the activity of Ni catalyst while Pd has more significant effects. This could be because of differences in the d-band width of Pt and Pd [22]. Based on theoretical calculations for adsorption of ethylene on Pt(111) and Pd(111) surfaces, Sautet and co-workers [23, 24] reported that Pd metal in bulk state has a slightly higher Fermi level than Pt metal and more importantly the d-band width significantly reduced compared to that of Pt. Hence, radial expansion of the Pd d orbitals is smaller than the Pt d-orbitals resulting in reduced overlap of the d-orbitals with the orbitals of the adsorbate on Pd (i.e., reduced $4e^-$ interactions between adsorbate and surface and reduced stabilizing $2e^-$ interactions). The direct result of this is stronger adsorbate interactions on Pd than on Pt surfaces.

As noted above alkali had a positive effect on the rate of hydrogenation. While product selectivity is nearly the same, CA conversion and TOF increased with increasing

amount of alkali-NaOH (Table 5.6). This increase was found marginal beyond an alkali amount of 0.005 g. Alkali ions modify the electronic structure of the active metal. They facilitate adsorption of CA via. polarizing the C=O group. This enhanced adsorption and effects on electronic structure of Ni (XPS) are the possible causes for the high convesion of CA in the presence of alkali ions. A strong alkali-support interaction exists and this effect could also play a role on the overall selectivity. Ni(5 wt%)/CeO_2-ZrO_2 has an acidity of 0.208 mmol/g (NH_3-TPD). The added alkali (0.005 g for 50 mg of catalyst which is equivalent to 2.5 mmol/g catalyst) neutralizes these acidic sites in the catalyst, modify the electronic structure of the active metal and facilitate adsorption polarizing the carbonyl group of CA molecule. The promotional effects observed could be explained in terms of the catalyst modifications. However, more detailed studies are needed.

Table 5.6. Influence of amount of alkali on hydrogenation of CA over Ni(5 wt%)/CeO_2-ZrO_2[a]

Run no.	Amount of NaOH (g)	CA conv. (wt%)	TOF (h^{-1})	Product selectivity (%)		
				HCA	PPL	Others
1	0	14.2	274	97.2	2.8	0
2	0.0025	38.7	748	96.2	3.9	0
3	0.005	41.4	801	95.4	4.7	0
4	0.01	49.4 (100)[b]	955	98.5 (23.6)[b]	1.5 (65.3)[b]	0 (11.1)[b]

[a]*Reaction conditions:* Catalyst (reduced at 400 °C for 2.5 h) = 0.05 g, cinnamaldehyde (CA) = 1 g, H_2 pressure = 20 bar, solvent (iso-propanol) = 25 ml, alkali = 0.0025 – 0.01 g of NaOH in 5 ml of water, reaction temperature = 100 °C, reaction time = 2 h, stirring speed = 600 rpm. [b]Values in parentheses are the data at 8 h of reaction.

Ni(5 wt%)/CeO_2–ZrO_2 was weakly active below 100 °C. TOF increased with increasing temperature; 100 wt% conversion of CA was achieved at 125 °C. Further rise in temperature changed product selectivity from HCA to PPL. Under similar conditions, conversion increased with increasing CA concentration from 0.29 to 0.9 moles/l and above that, it was unaltered. In agreement with the reports by others [25], this experiment reveals that the reaction is 1^{st} order with respect to CA up to a molar concentration of 0.9 and 0^{th} order above that concentration. CA conversion increased with increasing hydrogen pressure. HCA decreased with a growth in PPL selectivity. Based on initial rates, energy of activation

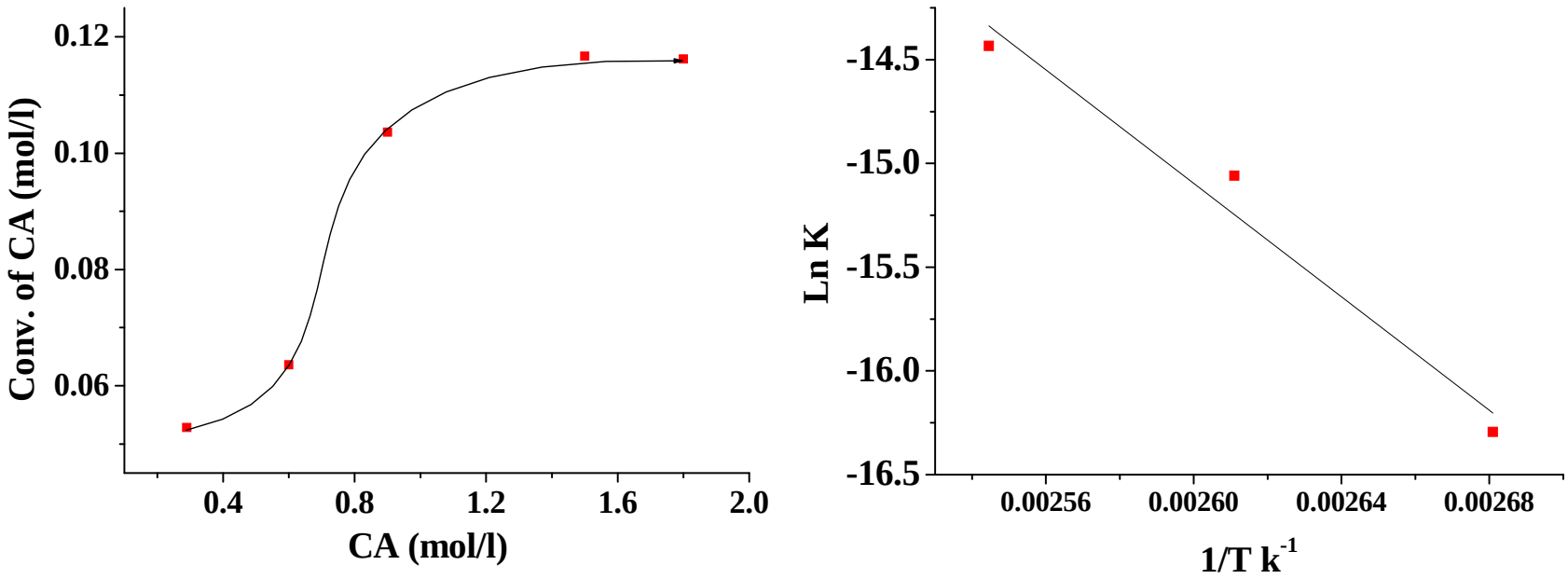

Fig. 5.8. Effect of different concentration of CA and activation energy calculations over Ni/CeO_2-ZrO_2 catalyst

was estimated and it was found to be 116 kJ/mol (Fig. 5.8). This value is higher than that for Pd/SiO_2 (30.1 kJ/mol) [25] and Co-B amorphous alloy (18.0 kJ/mol) [26, 27] indicating weaker hydrogenation activity of Ni. As such, to the best of our knowledge, there are no reports for comparison on the energy of activation of Ni catalysts for this reaction.

CA conversion increased with increasing reaction time. About 4 h was need for quantitative conversion of CA over Ni(5 wt%)/ZrO_2. This upon alkali addition could be achieved in 2 h. CA conversion was only 45.3% even after 8 h over Ni(5 wt%)/CeO_2-ZrO_2. However, on adding alkali, conversion reached 100% at the end of 4 h (Fig. 5.6(a)). The CeO_2-ZrO_2-supported Ni catalyst was less active than the ZrO_2-supported Ni catalyst. When both Pt and alkali were present, the catalytic activity of Ni was promoted and 100 wt% conversion of CA was achieved in just 0.5 h (Fig. 5.6(b)). HCA transformed into PPL on prolonging the reaction time. The S-shaped curves for HCA suggest that it is an intermediate product and two consecutive reactions (1: CA → HCA and 2: HCA → PPL) are operative at our reaction conditions. In order to confirm this further, based on the data reported in Tables 5.3 and 5.6, the conversion verses product selectivity plots for Ni(5 wt%)/CeO_2-ZrO_2 and Ni supported on all the supports were drawn (Fig. 5.9). It could be noted that irrespective of support and promoters, the selectivity for HCA decreased and PPL increased systematically with a rise in CA conversion (Fig. 5.9). This reveals that support and promoters have influenced the catalytic activity of Ni without affecting its inherent selectivity for hydrogenating C=C functionality. Although Pt alone has affinity for C=O hydrogenation, its addition did not influence the affinity of Ni for C=O over C=C hydrogenation.

The CeO_2-ZrO_2-supported Ni promoted with noble metal and alkali was found superior to most of the reported Ni catalysts (Table 5.7) [28-32]. Both CA conversion and HCA selectivity are higher over the catalyst of the present study. The reaction occurs at moderate temperature (100 °C) and pressure (20 bar). The noble metal promoted Ni catalysts showed enhanced catalytic activities than the corresponding individual mono metal catalysts. So far, Pt(0.5 wt%)-Ni(0.34 wt%)/CNT [33] (0.36 g) is known as the best Ni catalyst exhibiting CA conversion of 96% and HCA selectivity of 88% at 80 °C, 20 bar H_2 pressure and reaction time of 2 h. But, then, the present catalyst Ni(5 wt%)-Pt(0.5 wt%)/CeO_2-ZrO_2 (0.05 g) at 100 °C, 20 bar H_2 pressure and reaction time of 0.5 h showed 100 wt% CA conversion and HCA selectivity of 92.8%. This clearly demonstrates that the catalysts of the present study are more active and selective for C=C hydrogenation than the hitherto known Ni catalysts.

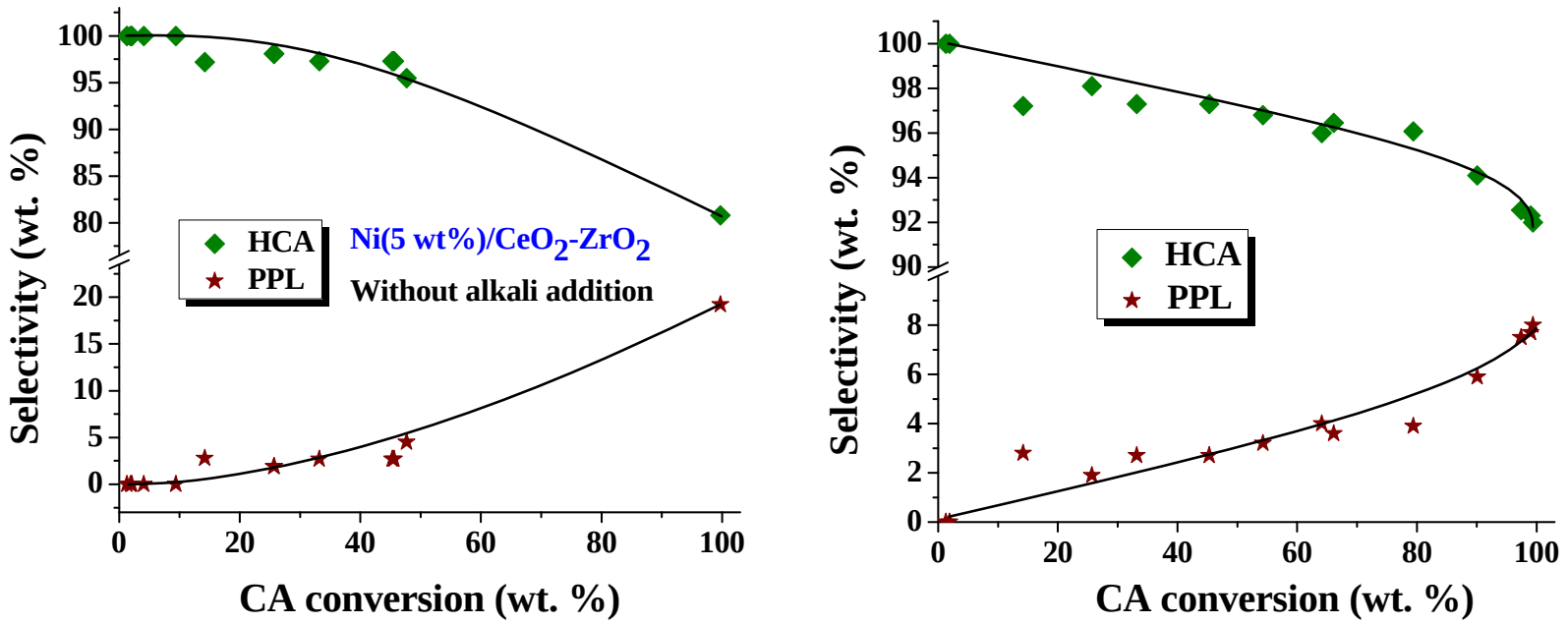

Fig. 5.9. Variation in product selectivity as a function of CA conversion in the absence of alkali addition. (Left) over Ni (5 wt%)/CeO_2- ZrO_2, and (right) over all the three supports

Table 5.7. Comparative catalytic activity data of supported Ni catalysts

Entry no.	Catalyst	Reaction conditions	CA conversion (wt%)	HCA selectivity (wt%)	Ref.
1	Ni(5 wt%)/ZrO_2	liquid phase; Catalyst = 0.05 g, CA = 1 g, iso-propanol = 25 ml, H_2 = 20 bar, T = 100 °C, t = 8 h	100	89.6	This work
2	Ni(5 wt%)-Pd(0.5 wt%)/CeO_2-ZrO_2	liquid phase; Catalyst = 0.05 g, CA = 1 g, iso-propanol = 25 ml, NaOH (0.01 g) in 5 ml water, H_2 = 20 bar, T = 100 °C, t = 8 h	100	0.03 (PPL = 99.9)	This work
3	Ni(5 wt%)-Pt(0.5 wt%)/CeO_2-ZrO_2	liquid phase; Catalyst = 0.05 g, CA = 1 g, iso-propanol = 25 ml, NaOH (0.01 g) in 5 ml water, H_2 = 20 bar, T = 100 °C, t = 0.5 h	100	92.8	This work
4	$Ni_{12}P_5/SiO_2$	liquid phase; Catalyst = 0.5 g, CA = 3 ml, cyclohexane = 115 ml, H_2 = 30 bar, T = 120 °C, t = 8 h	90	90	16
5	Pt(0.5 wt%)-Ni(0.34 wt%)/CNT	liquid phase; Catalyst = 0.36 g, CA = 1 ml, ethanol = 19 ml, H_2 = 20 bar, T = 80 °C, t = 2 h	96	88	22
6	Ni(10 wt%)/γ-Al_2O_3	vapor phase; H_2/CA = 10 ml/ml, W/F = 136 s, T = 300 °C (initial activity; catalyst deactivated with time)	87.5	73.7	18
7	Ni(15 wt%)/MCM-41	vapor phase; H_2/CA = 2.8, W/F = 0.19 g_{Ni}.h/mol, T = 200 °C, P = 1 bar (initial activity; catalyst deactivated with time)	99.5	21.3 (PPL = 26.9)	23
8	Ni(10 wt%)-Cu(10 wt%)/SiO_2	vapor phase; H_2 = 20 ml/min, CA = 1 – 3 ml/h, T = 200 °C, P = 1 bar	80	70	17

As described by Kyriakou et al [33] for Pd/Cu(111), it is likely even in the present case that the Pd atoms on Ni act as sites for facile dissociation of H_2, followed by its spillover on Ni for further hydrogenation of CA. XPS revealed that in the presence of noble metals, BE value of Ni $2p_{3/2}$ was lower indicating that Ni associated with noble metal is richer in electron density. The electron-rich Ni (in the presence of noble metals) facilitates adsorption of CA through C=C for its further hydrogenation. Likewise, alkali also is known to affect the electronic structure. Alkali ions (Na^+) facilitate adsorption of CA through polarization of the carbonyl of CA. This enhanced adsorption of CA molecules and electronic effects are the causes for more efficient activity of Ni and Ni-Pt/Pd catalysts in presence of alkali solution.

Delbecq and Sautet [23] reported that metal selectivities can be rationalized in terms of different radial expansions of their d bands; the smaller the band, stronger will be the four-electron attraction interactions with the C=C bond and higher will be the probability of its adsorption. The d-band width of Ni is much smaller than that of Pt, Ir and Os. This accounts well for the enhanced selectivities of HCA in the hydrogenations over supported Ni catalysts. Presence of noble metal enhanced the dispersion of Ni and alkali facilitated adsorption and polarization of carbonyl group of CA. All these features in turn resulted in higher catalytic activity of ZrO_2-supported Ni catalysts.

5.5. Conclusions

Physicochemical studies reveal that support and noble metal co-deposition have effects on crystallite/particle sizes, metal dispersion and electronic properties of Ni. These effects, in turn, have bearing on the activities of these catalysts. The catalytic activity of Ni supported on CeO_2, ZrO_2 and CeO_2-ZrO_2 for liquid-phase hydrogenation of CA was investigated for the first time. These catalysts showed higher activity than the hither-to-known Ni catalysts for selective hydrogenation of olefinic bonds. The catalytic activity of Ni over different supports decreased in the order: Ni(5 wt%)/ZrO_2 > Ni(5 wt%)/CeO_2 > Ni(5 wt%)/CeO_2-ZrO_2. Noble metals (Pd and Pt; 0.5 wt%) and alkali addition enhanced the catalytic activity of these supported Ni catalysts. Quantitative conversion of CA was achieved at moderate conditions (100 °C and 20 bar).

5.6. References

[1] P. Gallezot, D. Richard, Catal. Rev. Sci. Eng. 40 (1998) 81.

[2] P. Claus, Topic Catal. 5 (1998) 51.

[3] U. K. Singh, M. A. Vannice, Appl. Catal. A: Gen. 213 (2001) 1.

[4] P. Mäki Arvela, J. Hájek, T. Salmi, D. Y. Murzin, Appl. Catal. A. Gen. 292 (2005)

1.

[5] S. Mahmoud, A. Hammoudeh, S. Gharaibeh, J. Melsheimer, J. Mol. Catal. A: Chem. 178 (2002) 161.

[6] X. Chen, M. Li, J. Guan, X. Wang, C. T. Williams, C. Liang, Ind. Eng. Chem. Res. 51 (2012) 3604.

[7] B. Wu, H. Huang, J. Yand, N. Zheng, G. Fu, Angew. Chem. Int. Ed. 51 (2012) 1.

[8] R. Zheng, M. D. Porosoff, J. L. Weiner, S. Lu, Y. Zhu, J. G. Chen, Appl. Catal. A: Gen. 419 (2012) 126.

[9] A. B. Merio, B. F. Machado, V. Vetere, J. L. Faria, M. L. Casella, Appl. Catal. A: Gen. 383 (2010) 43.

[10] A. J. Plomp, D. M. P. van Asten, A. M. J. van der Eerden, P. Mäki-Arvela, D. Y. Murzin, K. P. de Jong, J. H. Bitter, J. Catal. 263 (2009) 145.

[11] J. Teddy, A. Falqui, A. Corrias, D. Carta, P. Lecante, I. Gerber, P. Serp, J. Catal. 278 (2011) 59.

[12] D. Srinivas, C. V. V. Satyanarayana, H. S. Potdar, P. Ratnasamy, Appl. Catal. A: Gen. 246 (2003) 323.

[13] C. G. Raab, J. A. Lercher, Catal. Lett: 18 (1993) 99.

[14] J. R. Croy, S. Mostafa, L. Hickman, H. Heinrich, B. Roldan Cuenya, Appl. Catal. A: Gen. 350 (2008) 207.

[15] M. Dömök M, A. Oszkó, K. Baán, I. Sarusi, A. Erdöhelyi, Appl. Catal. A: Gen. 383 (2010) 33.

[16] S. Laursen, S. Linic, Phys. Rev. Lett. 97 (2006) 26101.

[17] J. R. Croy, S. Mostafa, J. Lin, Y. Sohn, H. Heinrich, B. R. Cuenya, Catal. Lett. 119 (2007) 209.

[18] A. K. Shukla, R. K. Raman, N. A. Choudhury, K. R. Priolkar, P. R. Sarode, S. Emura, R. Kumashiro, J. Electroanalyt. Chem. 563 (2004) 181.

[19] H.-S. Roh, H. S. Potdar, K.-W. Jun, J.-W. Kim, Y.-S. Oh, Appl. Catal. A: Gen. 276 (2004) 231.

[20] P. Ratnasamy, D. Srinivas, C. V. V. Satyanarayana, P. Manikandan, R. S. Senthil Kumaran, M. Sachin and V. N. Shetti, J. Catal. 221 (2004) 455.

[21] W. Shan, M. Luo, P. Ying, W. Shen and C. Li, Appl. Catal. A: Gen. 246 (2003) 1.

[22] F. Delbecq, P. Sautet, J. Catal. 152 (1995) 217.

[23] P. Sautet, J. F. Paul, Catal. Lett. 9 (1991) 245.

[24] F. Delbecq, P. Sautet, Catal. Lett. 28 (1994) 89.

[25] H. Li, X. Chen, M. Wang, Y. Xu, Appl. Catal. A: Gen. 225 (2002) 117.

[26] D. P. Hollis, P. Selwood, J. Chem. Phys: 35 (1961) 378.

[27] L. Bonneviot, M. Che, D. Olivier, G. A. Martin, E. Freund, J. Phys. Chem. 90 (1986) 2112.

[28] H. Wang, Y. Shu, M. Zheng, T. Zhang, Catal. Lett. 124 (2008) 219.

[29] B. M. Reddy, G. M. Kumar, I. Ganesh, A. Khan, J. Mol. Catal. A: Chem. 247 (2006) 80.

[30] S. Y. Chin, F. J. Lin, A. N. Ko, Catal. Lett. 132 (2009) 389.

[31] Y. Li, C. H. Ge, J. Zhao, R. Zhou, Catal. Lett. 126 (2008) 280.

[32] K. Y. Jao, K. W. Liu, Y. H. Yang, A. N. Ko, J. Chinese. Chem. Soc. 56 (2009) 885.

[33] G. Kyriakou, M. B. Boucher, A. D. Jewell, E. A. Lewis, T. J. Lawton, A. E. Baber, H. L. Tierney, M. Flytzani-Stephanopoulos, E. C. H. Sykes, Scienc: 335 (2012) 1209.

Chapter 6

Catalytic Conversion of Furfural over Supported Pd and Pt Catalysts

6.1. Introduction

Biomass utilization has being receiving considerable interest for production of valuable chemicals and fuels towards development of a sustainable society. According to a DOE report [1], biomass conversion has a billion ton/year market. About 1,366 million tons of dry biomass per year (368 million tons from forest resources and 998 million tons from agricultural resources) is available for use. Of that, only 3 – 4% is used for food and non-food purposes and rest goes for paper industry, wood fuel and decay. In total, about 500 million tons of dry biomass is available for fuels and chemicals production. Dry cellulosic biomass contains about 75% of carbohydrates. One ton of dry biomass yields 67 gallons of biofuel. Thus, 500 million tons of dry biomass results in 32.5 billion gallons of biofuel, which is a good amount for a nation to benefit from it. India stands second in the production of sugarcane. Conversion of sugarcane bagasse into chemicals and fuels would save several thousand crores of rupees to India on the fuel import bill. Biomass is the only renewable resource that would enable production of chemicals and transportation fuels.

Furfural (FAL) is directly obtained by acid-catalyzed dehydration of xylose (Quaker Oats Technology using sulphuric acid catalyst at 153 °C for 5 h), the main building-block of hemicellulose, one of the constituents of biomass viz., corn corbs, oat hulls, wheat bran, saw dust, sugarcane bagasse, etc [2]. It is also present in the bio-oil obtained from the fast pyrolysis of biomass. Global production of FAL is about 0.8 million tons in 2012, with South Africa and China being major producers. FAL is used in fragrance industry. It is a feedstock for furan derivatives, an extracting agent for aromatics from lubricating oils, a purification solvent for C_4-C_5 hydrocarbons and a nematode control agent. FAL is a platform chemical for production of furfurylalcohol (FOL, by C=O hydrogenation), tetrahydrofurfurylalcohol (THFOL, by ring and C=O hydrogenation), methylfuran (MF, by hydrogenolysis), furan (by decarbonylation), tetrahydrofuran (THF, by decarbonylation followed by hydrogenation), n-butanol (by decarbonylation followed by hydrogenation and ring opening), diols (by hydrogenation followed by ring opening), etc. [3-5]. These furan chemicals have wide industrial applications. The production of FOL from furfural has already been industrialized using a copper-chromite catalyst, but those catalysts are environmentally hazardous. Various systems containing Ni, Co, Cu, Ru and Pd and a second metal promoter have been reported [5]. FOL can be used as an additive or solvent in resins synthesis [6]. Another product of FAL hydrogenation is THFOL. It is widely used as an environmentally benign solvent and in the production of 1, 5-pentanediols which have application in mono esters and polyurethane manufacturing [7]. Hence, the importance of production of THFOL from furfural is rapidly

growing. Most of the reports regarding the production of THFOL have been focused on the liquid-phase hydrogenation of FOL using supported Pt [8, 9], Ru [10] and Ni [11] catalysts. There are a few reports for direct hydrogenation of furfural to THFOL in the liquid-phase reaction at low reaction temperature with supported bi-metallic catalysts [12, 13]. Furan is produced by vapour-phase decarbonylation of FAL over Pd/C and Pd/Al_2O_3 catalysts. This reaction is carried out in the presence of hydrogen as carrier gas (H_2 to furfural molar ratio varies in the range 0.5 to 1), which has a role in increasing the stability of the catalyst [14]. A variety of catalysts have been reported but Pd supported on alumina or activated carbon was found to be the best catalyst for this reaction [14]. A catalytic process which can avoid the use of external hydrogen in the decarbonylation process is desirable. Furan from furfural can be produced by various other routes: (1) Furfural is first converted to furoic acid by Cannizzaro reaction which is then transformed to furan in the second step through decarboxylation, (2) conversion of furfural using fused alkali / hot alkali – this method develops huge amount of waste products and (3) pyrolysis of furfural leads to furan. But the yield is usually low [15].

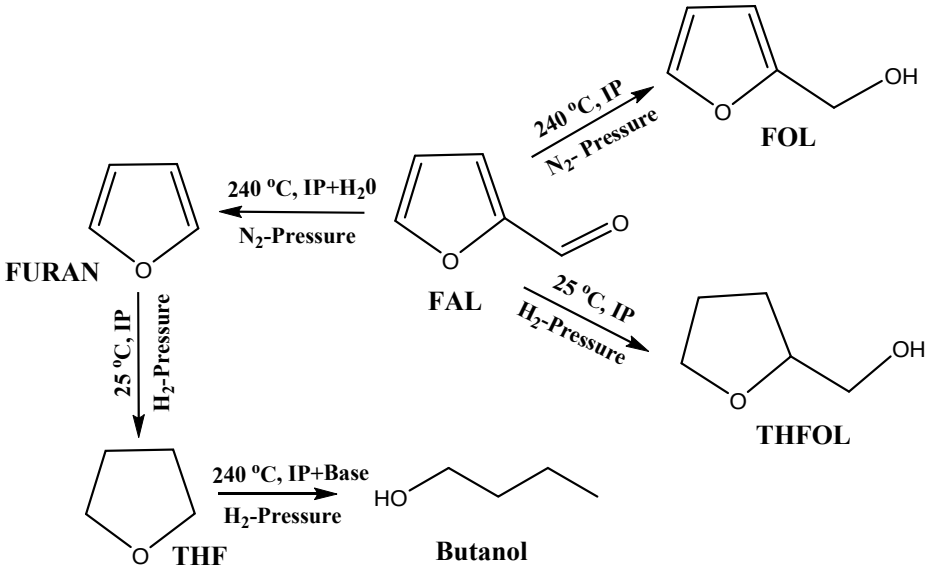

Scheme 6.1. Catalytic conversion of furfural to value-added chemicals

Cr is environmentally unfriendly. Catalysts with no Cr are recommended. Catalyst deactivation, side reactions and product selectivity, requirement of high temperatures and long contact times are some of the issues with the known catalysts. Hence, there is a need to develop more efficient and selective catalyst for transformation of FAL to a range of furan derivatives. The application of Pt and Pd supported on various oxides including Al_2O_3, CeO_2, ZrO_2, CeO_2-ZrO_2, SO_4-ZrO_2, SiO_2 and MgO for the conversion of FAL is studied in this chapter. Also the use of solvent mixture on improving the selectivity and product yield is also

investigated. The influence of reaction parameters on catalytic activity of the supported Pt and Pd catalysts is examined. The catalysts were characterized by ICP, XRD, XPS, NH_3-TPD, and H_2-TPR techniques.

6.2. Experimental Procedure and Characterization Techniques

Pd(2, 5 and 10 wt%)/Al_2O_3, Pt(2, 5 and 10 wt%)/Al_2O_3, Pd(2 wt%) supported on CeO_2, ZrO_2 and CeO_2-ZrO_2 and Pt(5 wt%) supported on sulfated-ZrO_2, SiO_2, MgO and CeO_2-ZrO_2 (Ce:Zr = 1:1 molar ratio) catalysts were synthesized and characterized as reported in Chapter 2 (sections 2.2.2. and 2.3). Prior to reaction, the Pd and Pt catalysts were reduced under H_2 (30 ml/min) flow at 250 °C and 350 °C, respectively, for 2.5 h. Procedures used in catalytic activity studies are reported in Chapter 2 (section 2.4.2.).

6.3. Results and Discussion

6.3.1. Structural Properties

6.3.1.1. Powder X-ray Diffraction. The XRD profiles of reduced 2, 5 and 10 wt% Pd and Pt supported on Al_2O_3 are shown in Fig. 6.1. The XRD pattern of "bare" γ-Al_2O_3 is also included in the figure. γ-Alumina (subjected to the same reduction treatment as of the supported Pd and Pt catalysts) showed five intense peaks at 36.6, 37.7, 39.5, 46.8 and 66.8° which were indexed to (220), (311), (322), (400) and (440) planes, respectively. The supported Pd catalysts showed three distinct additional peaks at 40.1, 46.6 and 67.6° corresponding to reflections from (111), (200) and (220) planes of metallic Pd^0. Supported Pt catalyst showed these additional peaks at 39.7, 46.1 and 67.7° corresponding to (111), (200) and (220) planes of metallic Pt^0, respectively. XRD showed no evidence for the presence of crystalline PdO and PtO phases in the reduced catalysts. Based on the positions of X-ray peaks, the cubic unit cell parameters of Pd^0 and Pt^0 (cubic closed packed structure; space group: Fm-3m) were determined (a = 0.389 and 0.392 nm, respectively) and found in good agreement with the values reported by others [16]. Using Debye-Scherrer formula, the average crystallite sizes of (2, 5 and 10 wt%) Pd and (2, 5 and 10 wt%) Pt supported on alumina were determined taking into considering of the (111) plane. The average crystallite sizes of (X-ray detectable) Pd^0 for Pd(2, 5 and 10 wt%)/Al_2O_3 were 5.8, 8.1 and 7.8 nm respectively and Pt^0 for Pt(2, 5 and 10 wt%)/Al_2O_3 were 23.2, 29.5 and 29.0 nm, respectively. Error in these estimates was ± 0.5. The crystals of Pt were bigger in size than those of Pd. Beyond a metal loading of 5 wt%, the crystallite size of the metal was nearly the same.

6.3.1.2. High Resolution Transmission Electron Microscopy. HRTEM images of Al_2O_3-supported Pd and Pt are shown in Figs. 6.2 and 6.3. Metal particle size distribution curves and lattice fringes observed at higher resolution for the Pd and Pt catalysts are also

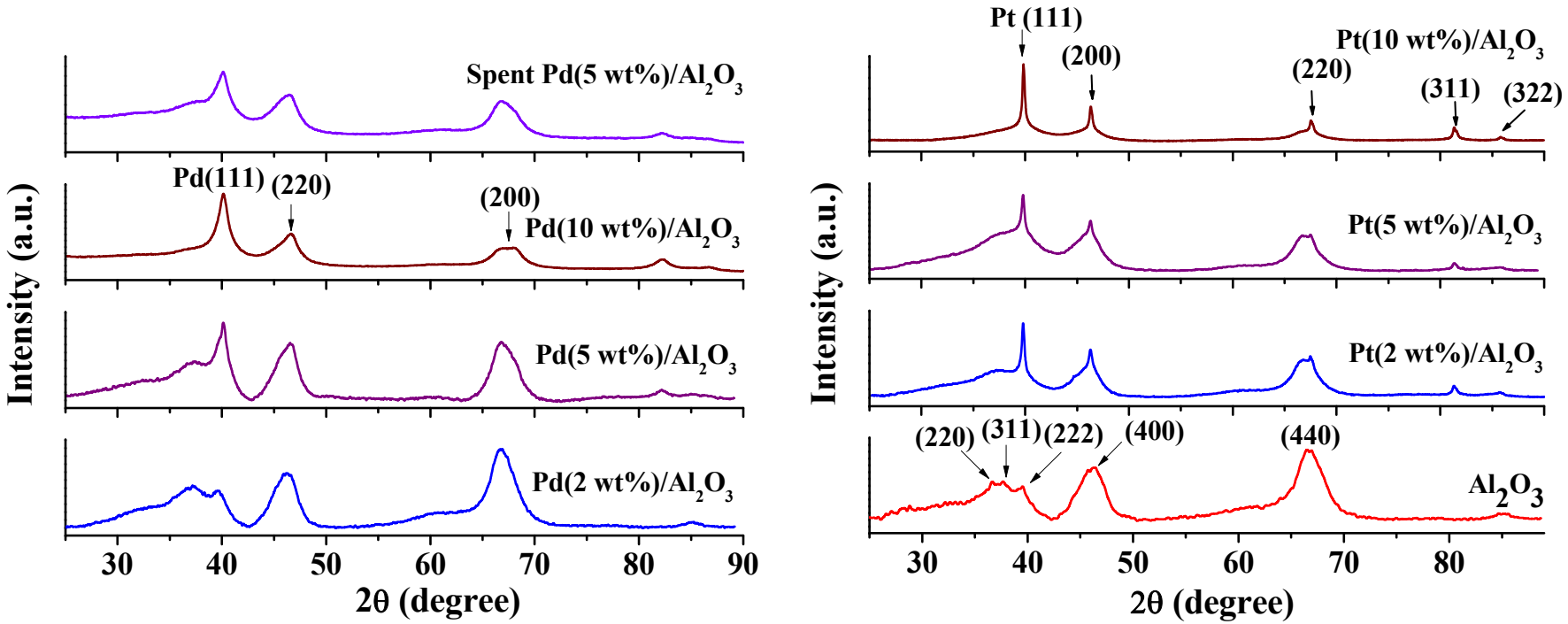

Fig. 6.1. XRD profiles of reduced Al_2O_3-supported Pd and Pt

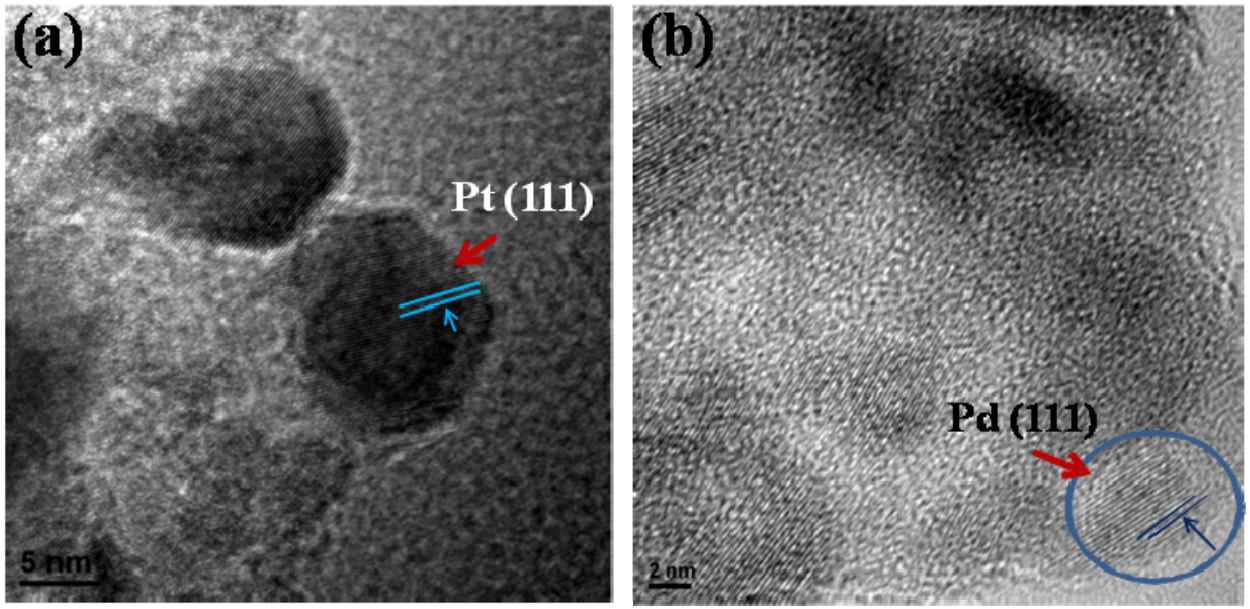

Fig. 6.2. HRTEM images of reduced (a) Pt(5 wt%)/Al_2O_3 and (b) Pd(5 wt%)/Al_2O_3 catalysts

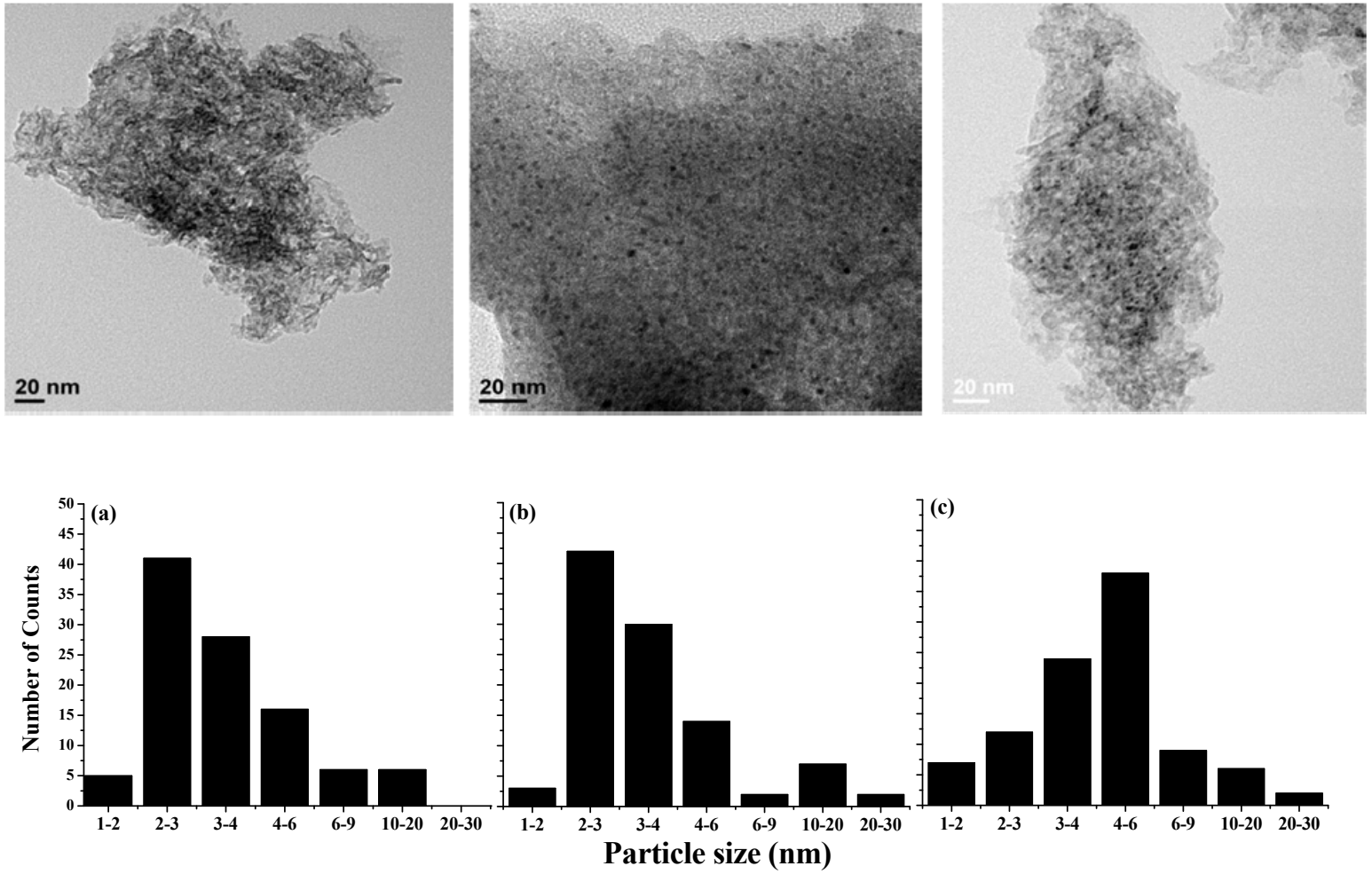

Fig. 6.3(i). HRTEM images and particle size distribution profiles of reduced (a) Pt(2 wt%)/Al_2O_3, (b) Pt(5 wt%)/Al_2O_3 and (c) Pt(10 wt%)/Al_2O_3

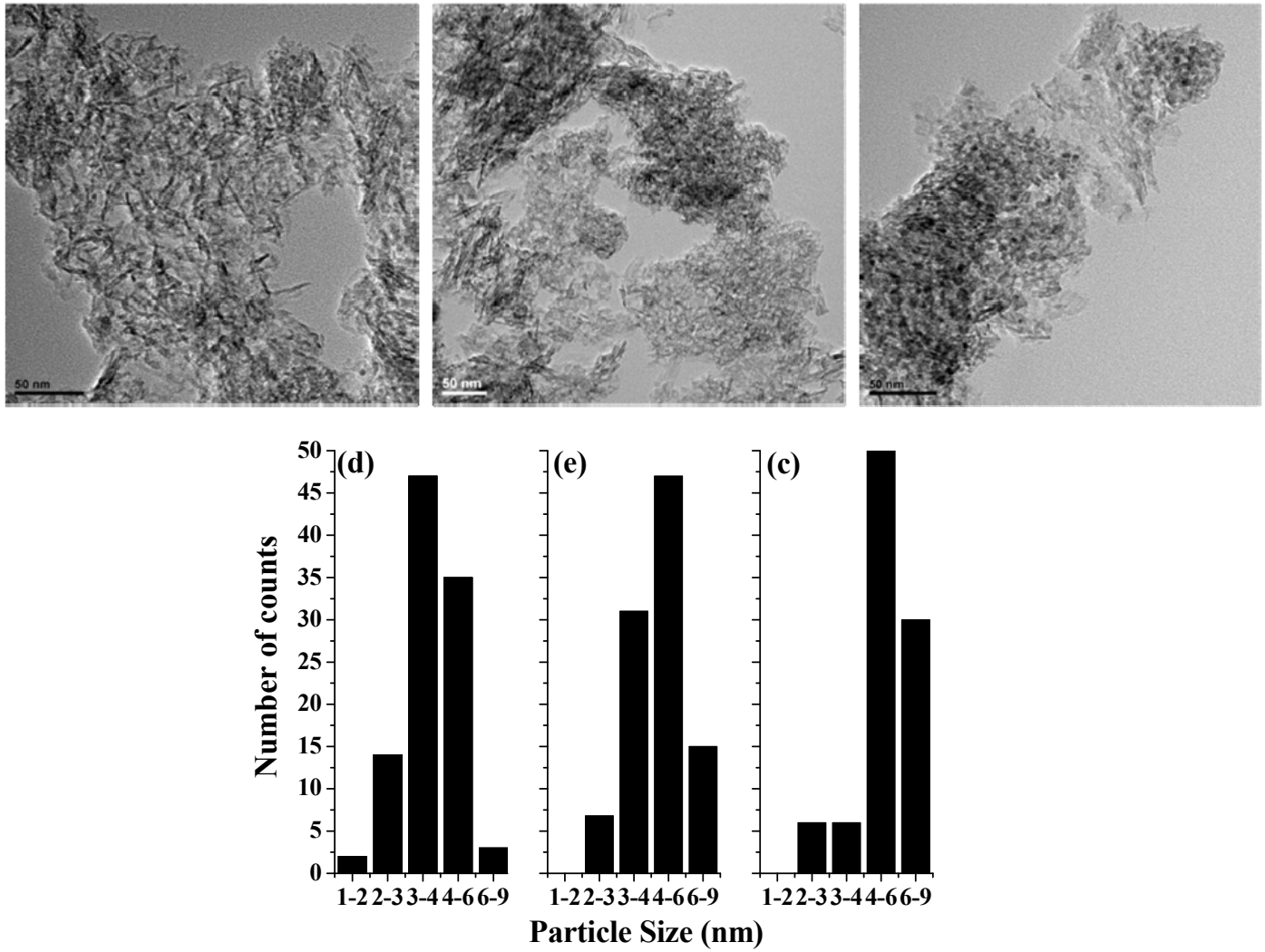

Fig. 6.3(ii). HRTEM images & particle size distribution profiles of reduced (d) Pd(2 wt%)/Al_2O_3, (e) Pd(5 wt%)/Al_2O_3 and (f) Pd(10 wt%)/Al_2O_3

shown. In general, the average particle size of the metal increased with increasing metal loading. About Pd particle of 100 numbers were considered in these calculations. The average particle sizes of Pd^0 for Pd(2, 5 and 10 wt%) on Al_2O_3 are 4.0, 4.8 and 5.5 nm, respectively. These values for 2, 5 and 10 wt% Pt on Al_2O_3 are 4.1, 4.5 and 5.9 nm, respectively. In other words, both Pd and Pt particles have nearly the same size. However, XRD showed that the crystallite size of Pt is bigger than Pd. This is because XRD views only those crystallites which are above the X-ray detection limit ca. 5-10 nm. In fact, a few particles with size in the range 20-25 nm were observed in 5 and 10 wt% Pt/Al_2O_3. Perhaps, these were the ones that were detected by XRD.

Metal dispersions (D) were calculated based on the mean particle sizes (d_{VA}) determined from HRTEM (Chapter 2, section 2.3.3). These values for Pd supported on alumina decreased in the order: Pd(2 wt%)/Al_2O_3 (24.1%) > Pd(5 wt%)/Al_2O_3 (19.8%) > Pd(10 wt%)/Al_2O_3 (17.8 %). For Pt supported on alumina, the dispersion values decreased in the order: Pt(2 wt%)/Al_2O_3 (11.4%) > Pt(10 wt%)/Al_2O_3 (8.1 %) > Pt(5 wt%)/Al_2O_3 (7.4 %). Thus, these studies reveal that the dispersion of Pd is nearly two times higher than that of Pt.

6.3.1.3. N_2-Physisorption. The specific surface area (S_{BET}) of the supported Pd and Pt catalysts are in the range 68-71 m^2/g and 73-76 m^2/g, respectively (Table 6.1). γ-Alumina has a surface area of 80 m^2/g. Pd loading decreased S_{BET} more than Pt.

The metal contents in the catalysts determined by ICP-OES were found lower than the nominal values (Table 6.1). However, it may be noted that the amount of metal in the catalyst, in a certain metal composition, is nearly the same for both Pt and Pd.

6.3.1.4. X-ray Photoelectron Spectroscopy. The electronic structure and binding energy values were determined by X-ray photoelectron spectroscopy. The XP spectra from the core level of Pd $3d_{5/2}$ and $3d_{3/2}$ and Pt $4f_{7/2}$ and $4f_{5/2}$ are shown in Fig. 6.4 (a and b). The spectra were complex. Spectral deconvolution indicated the presence of Pd and Pt in +2 and zero oxidation states. The spectral lines corresponding to + 2 oxidation state of Pd and Pd are denoted in pink and those from zero oxidation state are shown in blue color. B.E. values of different peaks are indicated in the spectra. In the case of the supported Pt catalysts, Al 2p core level peaks overlapped with those of the Pt peaks. The peak due to Al 2p for Pt/Al_2O_3 was observed in the B.E. range 73.6 – 74.3 eV. Pd/Al_2O_3 showed this peak at 73.3 – 73.4 eV. "Neat" Al_2O_3 shows this peak at 73.5 – 73.8 eV. These features indicate that Al in Pt/Al_2O_3 is poorer in electron density and has a 3+δ oxidation state. In general, B.E. values of Pt ($4f_{7/2}$) decreased with increasing metal loading suggesting that as the loading increased metal was more in a metallic state than in the oxidized form. In other words, the support-metal

Table 6.1. Physicochemical characteristics of Al_2O_3-supported Pd and Pt catalysts

Sample	Metal content (output, wt%; ICP-OES)		Average crystallite size (nm; XRD)		Specific surface area (S_{BET}; m^2/g)	Acidity (mmol/g; NH_3-TPD)	H_2-TPR (mmol/g)	Binding energy values (eV, XPS)		
								Pd	Pt	Al
	Pd	Pt	Pd	Pt						
Al_2O_3	-	-	-	-	80	2.15	-	-	-	-
Pd(2 wt%)/Al_2O_3	1.85	-	5.8	-	71	1.964	0.041	335.2	-	73.4
Pd(5 wt%)/Al_2O_3	4.7	-	8.1	-	68	1.832	0.022	335.1	-	73.3
Pd(10 wt%)/Al_2O_3	8.3	-	7.8	-	67.8	1.743	0.0994	334.6	-	73.4
Pt(2 wt%)/Al_2O_3	-	1.7	-	23.2	76	1.701	0.373	-	71.3	73.6
Pt(5 wt%)/Al_2O_3	-	4.8	-	29.5	74.1	1.652	0.232	-	71.0	73.9
Pt(10 wt%)/Al_2O_3	-	8.9	-	29.0	73.3	1.743	0.232	-	70.9	74.3
Used-Pd(5 wt%)/Al_2O_3	3.7	-	7.4	-	311	1.236	-	-	-	-

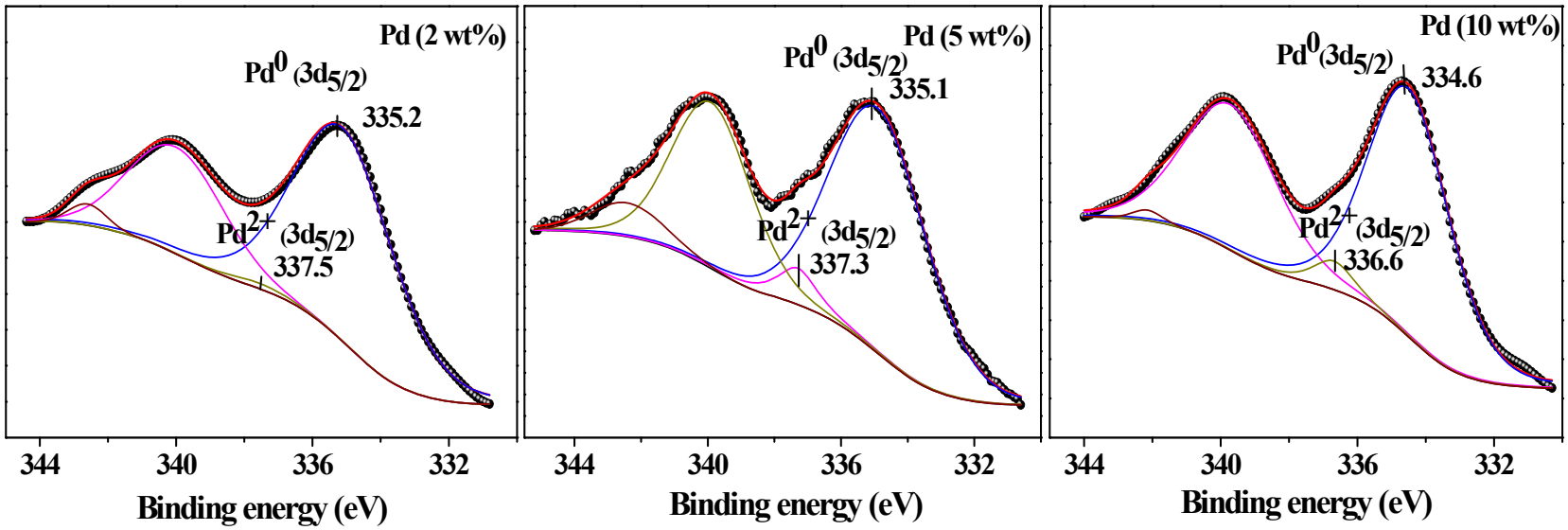

Fig. 6.4(a). X-ray photoelectron spectra of reduced Pd (2, 5 and 10 wt%) supported on alumina

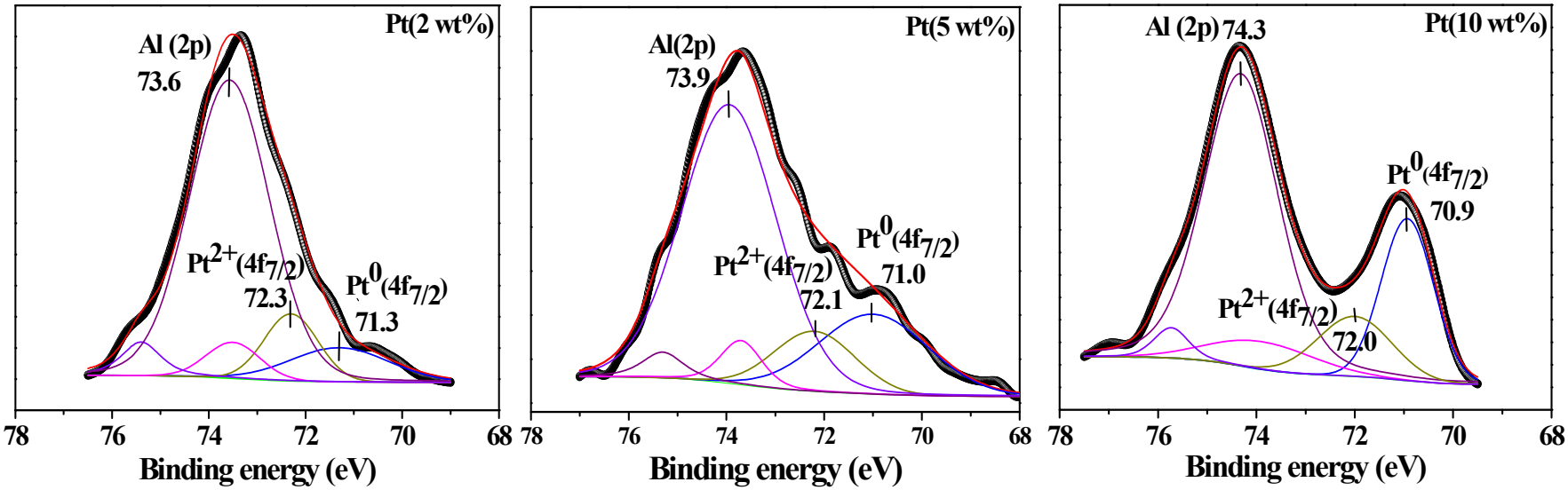

Fig. 6.4(b). X-ray photoelectron spectra of reduced Pt (2, 5 and 10 wt%) supported on alumina

interaction decreases with increasing metal loading and metal particle size. The percentage concentrations of Pt and Pd in +2 and zero oxidation states were determined and found to be: 51.7/48.3, 41.2/58.8 and 34.3/65.7 for 2, 5 and 10 wt% Pt/Al_2O_3 and 1.7/98.3, 7.4/92.6 and 6.0/94.0 for 2, 5 and 10 wt% Pd/Al_2O_3. Pt/Al ratio for 2, 5 and 10 wt% Pt/Al_2O_3 were found to be 0.011, 0.02 and 0.021, respectively. Thus, at the experimental conditions the supported Pd is more in metallic state than in +2 state while nearly 50% of Pt is in the oxidized +2 state. This correlates well with the changes in the B.E. values of Al 2p observed in these catalysts. The B.E values of $Pd(3d_{5/2})$ peak decreased in the order: Pd(2 wt%)/Al_2O_3 (335.3 eV) > Pd(5 wt%)/Al_2O_3 (335.1 eV) > Pd(10 wt%)/Al_2O_3 (334.6). Croy et al. [17] and Dömök et al. [18] reported that B.E. values of photoelectrons ejected from metal particles depend on the size of the metal particles. Smaller the particle, higher would be the binding energy. So Pd(10 wt%)/Al_2O_3 having larger size metal particles showed Pd $3d_{5/2}$ line at lower B.E value. Strong support-metal interactions could be the other reason for the higher B.E. values obtained at lower metal loadings (2 and 5 wt%). In case of Pt supported on Al_2O_3 [Fig 6.4(b)], the B.E values of Pt $4f_{7/2}$ peak decreased in the order: Pt(2 wt%)/Al_2O_3 (71.3 eV) > Pt(5 wt%)/Al_2O_3 (71.0 eV) > Pt(10 wt%)/Al_2O_3 (70.9). Normally, Pt exists in the form of Pt^0, Pt^{2+} and Pt^{4+} states on Al_2O_3 catalysts. Binding energy value of Pt^0 ($4f_{7/2}$) peak is in the range 70.5 - 71.5 eV [19]. If Pt is in metallic form, then B.E value is observed close to 70.5 eV. As the loading of Pt metal increased, the binding energy values decreased from 71.3 to 70.9 eV. Higher loading of Pt forms bigger size particles and hence, lower values of B.E. are observed.

6.3.1.5. NH_3-TPD. The acidic properties of Al_2O_3-supported Pt and Pd catalysts were determined by NH_3-TPD (Fig. 6.5). The TPD profiles of "neat" and metal supported alumina were complex and indicate the presence of several desorption peaks in the temperature range 100 – 800 °C. These peaks could be categorized under three regions (100 – 230 °C, 100 – 450 °C and 400 – 800 °C) corresponding to weak, moderate and strong acid sites. Physisorbed ammonia is included in the category of weak acid sites. While the weak and moderate sites correspond to those of Lewis type, the stronger acid sites correspond to the Brönsted sites. Neat Al_2O_3 has an acid site density of 2.15 mmol/g. Upon metal loading, a decrease in the overall acid site density was noted (Table 6.2). Further, the weak and moderately strong acid sites had increased at the expense of strong acid sites. The Pd containing catalysts contained moderately more acid sites than the Pt containing catalysts. Metal content had an effect on T_{max} of the NH_3 desorption peak.

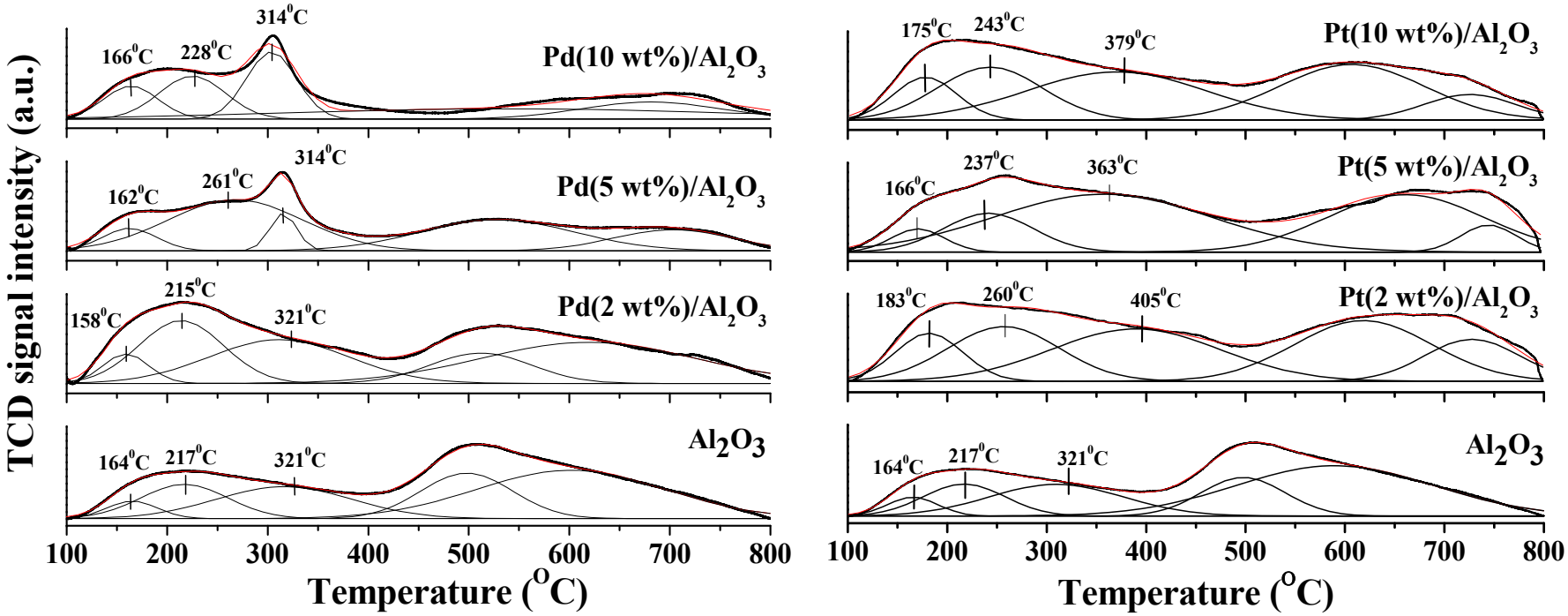

Fig. 6.5. TPD profiles of Pd and Pt supported on alumina catalysts

Table 6.2. Amount of acidity at different regions calculated by NH_3-TPD experiments

Catalyst	Acid sites (mmol/g)			Overall acidity (mmol/g)
	Weak (T_{max}: 230 °C)	Moderate (T_{max}: 100-450 °C)	Strong (T_{max}: 400-800 °C)	
Al_2O_3	0.089 (4.1 %)	0.731 (34%)	1.331 (61.9%)	2.14
Pd(2 wt%)/Al_2O_3	0.107 (5.5%)	0.907 (46.3%)	0.947 (48.3%)	1.96
Pd(5 wt%)/Al_2O_3	0.137 (7.5%)	0.880 (48.0%)	0.815 (44.5%)	1.832
Pd(10 wt%)/Al_2O_3	0.210 (12.1%)	0.727 (53.3%)	0.804 (46.2%)	1.74
Pt(2 wt%)/Al_2O_3	0.168 (9.9%)	0.885 (52.1%)	0.649 (38.2%)	1.701
Pt(5 wt%)/Al_2O_3	0.096 (5.8%)	0.922 (55.8%)	0.634 (38.4%)	1.652
Pt(10 wt%)/Al_2O_3	0.164 (10.6%)	0.758 (49.0%)	0.627 (40.%)	1.549
Used-Pd(5 wt%)/Al_2O_3	0.163 (13.2%)	0.453 (36.6%)	0.620 (50.2%)	1.236

[a]Data in parentheses corresponds to % of acidic sites.

6.3.1.6. H_2-Temperature-Programmed Reduction. Support-metal interactions and metal reduction temperature were determined by H_2-TPR experiments. Usually, bulk PdO reduces at around 25 °C and forms β-PdH [20]. These palladium hydrides decompose at higher temperature and show a negative peak. Intensity and the position of this peak depend on the size and dispersion of supported Pd metal. Bigger size particles have higher storage capacity of hydrides than the smaller ones. If the size of Pd particles is smaller, then the decomposition of β-PdH takes place at higher temperatures. Unreduced Pd(2 wt%)/Al_2O_3 showed a negative peak due to β-PdH at 84 °C. This peak for Pd(5 wt%)/Al_2O_3 and Pd(10 wt%)/Al_2O_3 appeared at 70 and 63 °C, respectively (Fig. 6.6). The hydrogen consumption values for different Pd catalysts decreased in the order: Pd(10 wt%)/Al_2O_3 (0.099 mmol/g) > Pd(2 wt%)/Al_2O_3 (0.041 mmol/g) > Pd(5 wt%)/Al_2O_3 (0.022 mmol/g). This variation in hydrogen consumption is in line with the variation in metal particle sizes determined from HRTEM. A weak high temperature peak at 363 and 355 °C due to reduction of PdO and the surface hydroxyl groups of alumina were observed for Pd(2 wt%)/Al_2O_3 and Pd(5 wt%)/Al_2O_3. This peak at high temperature was not observed for Pd(10 wt%)/Al_2O_3. Large crystals of PdO are reduced first to form Pd metal, which dissociate H_2. The hydrogen atoms spillover onto the surface of alumina hydroxyl group and finely dispersed PdO and reduce them at higher temperatures. Bare alumina reduces at temperatures above 700 °C. However, in the presence of metal the hydroxyl groups of alumina reduce below 400 °C itself [21].

Unreduced Pt(2 wt%)/Al_2O_3 showed two hydrogen reduction peaks at 231 and 415 °C, respectively (Fig. 6.6). While the former is related to PtO weakly interacting with the support, the latter is attributed to the combined effects of PtO strongly interacting with the support and reduction of surface hydroxyl groups of alumina. With increasing metal loading these peaks shifted to lower temperatures (Fig. 6.6). An third peak at 107 and 93 °C was observed in the case of Pt(5 wt%)/Al_2O_3 and Pt(10 wt%)/Al_2O_3, respectively which is corresponding to non-interacting surface PtO. Intensities of non and weakly interacting PtO peaks were higher for compositions containing higher amount of Pt. The amount of hydrogen uptake decreased in the order: Pt(2 wt%)/Al_2O_3 (0.373 mmol/g) > Pt(5 wt%)/Al_2O_3 (0.232 mmol/g) ≥ Pt(10 wt%)/Al_2O_3 (0.230 mmol/g) (Table 6.1). The uptake of hydrogen is more in the case of supported Pt than Pd. Although Pd is more dispersed than Pt (HRTEM), the lower values of hydrogen uptake for Pd indicate that some amount of hydrogen uptake might be taking place below 40 °C which could not be detected in the present experiments.

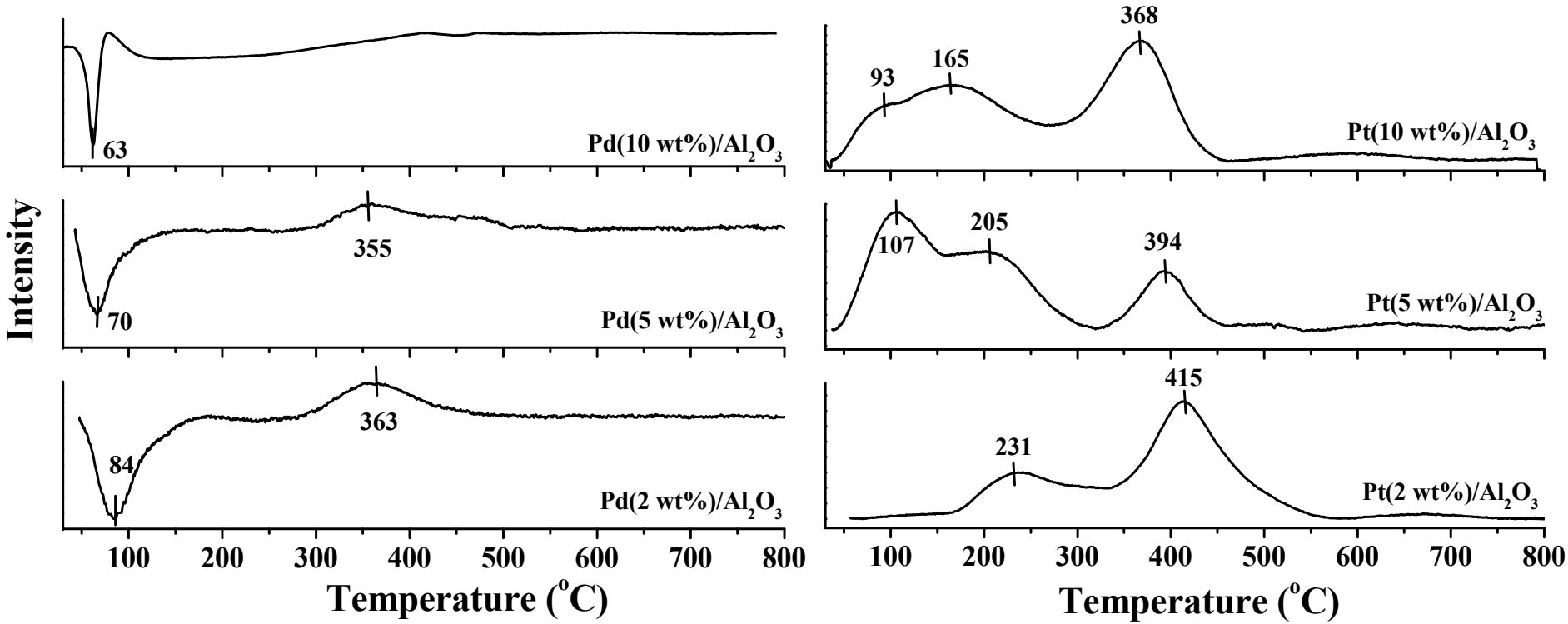

Fig. 6.6. TPR profiles of Pd and Pt supported on alumina

6.3.2. Catalytic Activity

Supported Pd and Pt catalysts of the present study are active even at room temperature (25 °C) for the hydrogenation of furfural (FAL). Fig. 6.7 shows the conversion of FAL and products selectivity for different catalysts at 8 h of reaction. This reaction usually yields different hydrogenated and decarbonylation products as shown in Scheme 6.1. Hydrogenation of carbonyl group results in furfuryl alcohol (FOL) and complete hydrogenation (both ring & carbonyl group) yields tetrahydrofurfuryl alcohol (THFOL). In the present study, supported Pd and Pt catalysts are selective for THFOL and FOL respectively, at room temperature under (20-60 bar) H_2 pressure. For decarbonylation of furfural, the supported Pd catalysts were highly selective and stable at 240 °C. Decarbonylation reaction occurs even in inert atmospheric conditions.

6.3.2.1. Effect of Metal Loading. Conversion of FAL increased with increase in the metal loading on Al_2O_3. Over different catalysts, the conversion of FAL increased in the order: Pd(2 wt%)/Al_2O_3 (22.1 wt%) < Pd(5 wt%)/Al_2O_3 (48.5 wt%) < Pd(10 wt%)/Al_2O_3 (61.6 wt%) and Pt(2 wt%)/Al_2O_3 (21.5 wt%) < Pt(5 wt%)/Al_2O_3 (30 wt%) < Pt(10 wt%)/Al_2O_3 (62.5 wt%). Supported Pt catalysts were highly selective for FOL (> 99%) while the supported Pd catalysts yielded FOL and the ring hydrogenated product THFOL. Pd(5 wt%)/Al_2O_3 formed FOL and THFOL with selectivities of 20 and 80%, respectively. Higher amount of acidity is one of the possible causes favored THFOL formation over Pd catalysts.

6.3.2.2. Effect of H_2 Pressure. H_2 pressure was varied from 20 to 60 bar while keeping the other parameters constant. FAL conversion increased with increasing H_2 pressure. At the same time, THFOL formed with 100% selectivity (Table 6.3). At 60 bar H_2 pressure the conversion of FAL was 79.8 wt% and THFOL selectivity was 100 wt%. Higher loading of palladium (10 wt%) showed less effect on the conversion (FAL, 80.3%) and THFOL selectivity (97.4%). This indicates that 5 wt% loading of Pd was optimum for better conversion and selectivity in FAL hydrogenation reaction. Conversion of FAL and product selectivity as a function of time (Fig. 6.8) revealed that it is a consecutive reaction with hydrogenation of carbonyl group forming FOL being the first step, which then in the second step gets ring hydrogenated forming THFOL. Over Pt catalysts, FOL is the main product. But at higher H_2 pressures, a marginal drop in FOL selectivity with a consequent increase in unknown products (others) selectivity was observed. While lower H_2 pressures (20 bar) is suitable for producing FOL over Pt catalysts, higher pressures (40 – 60 bar) lead to THFOL over Pd catalysts. It is interesting to note that the reaction occurs at room temperature over both Pd and Pt catalysts.

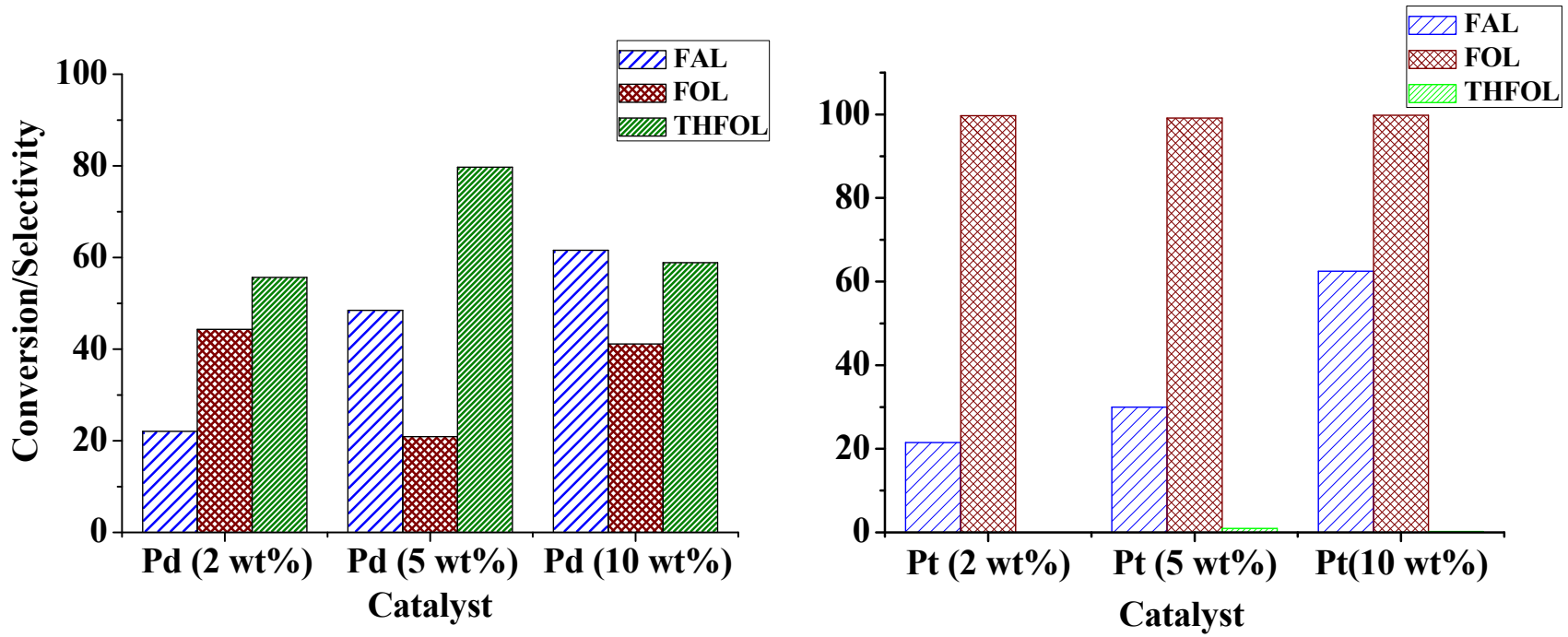

Fig. 6.7. Catalytic activity of Pd and Pt supported on alumina for FAL hydrogenation . *Reaction conditions*: Furfural = 1 g, catalyst = 0.05 g, temperature = 25 °C, solvent (iso-propanol) = 20 g, H_2-pressure = 20 bar, reaction time = 8 h, stirring speed = 600 rpm. Prior to the reaction, Pd & Pt supported catalysts were reduced under H_2 (30 ml/min) flow at 250 °C and 350 °C, respectively. FAL = furfural, FOL = furfuryl alcohol and THFOL = tetrahydrofurfuryl alcohol.

Table 6.3. Selective hydrogenation of furfural (FAL) over Pd & Pt supported on Al_2O_3 catalysts

Catalyst	H_2-Pressure (bar)	Conversion of FAL	Product Selectivity		
			FOL	THFOL	Others
Pd(2wt %)/Al_2O_3	20	22.1	44.3	55.7	0.0
Pd(5wt %)/Al_2O_3	20	48.5	20.9	79.7	0.0
Pd(5wt %)/Al_2O_3	40	66.8	0.0	100	0.0
Pd(5wt %)/Al_2O_3	60	79.5	0.0	100	0.0
Pd(10wt %)/Al_2O_3	20	61.6	41.1	58.9	0.0
Pd(10wt %)/Al_2O_3	60	80.3	2.6	97.4	0.0
Pt(2wt %)/Al_2O_3	20	21.5	99.7	0.0	0.3
Pt(5wt %)/Al_2O_3	20	30.0	99.1	0.9	0.0
Pt(5wt %)/Al_2O_3	40	35.5	95.2	0.5	1.4
Pt(5wt %)/Al_2O_3	60	40.5	94.7	0.5	2.1
Pt(10wt %)/Al_2O_3	20	62.5	99.8	0.2	0.0
Pt(10wt %)/Al_2O_3	60	65.6	99.7	0.3	0.0

Reaction conditions: Furfural = 1 g, catalyst = 0.05 g, temperature = 25 °C, solvent (iso-propanol) = 20 g, reaction time = 8 h, stirring speed = 600 rpm. Prior to the reaction, Pd & Pt supported catalysts were reduced under H_2 (30 ml/min) flow at 250 °C and 350 °C, respectively.

6.3.2.3. Effect of Temperature. The effect of reaction temperature on the hydrogenation of FAL over Pt(5 wt%)/Al_2O_3 was studied (Table 6.4). FAL conversion increased with increasing temperature up to 120 °C. FOL was the major product at these conditions. A small fraction of unknown products (others) were also dectected at higher temperatures (> 60 °C). At still higher temperatures (> 180 °C), both deoxygenation (yielding 2-methyl furan) and decarbonylation (yielding furan) were observed. At 240 °C, complete conversion of FAL and higher selectivity for 2-methyl furan (6.0 wt%) + furan (50.4 wt%) was observed. Decarbonylation was effective at higher temperatures, while hydrogenation was facilitated at ambient temperature conditions.

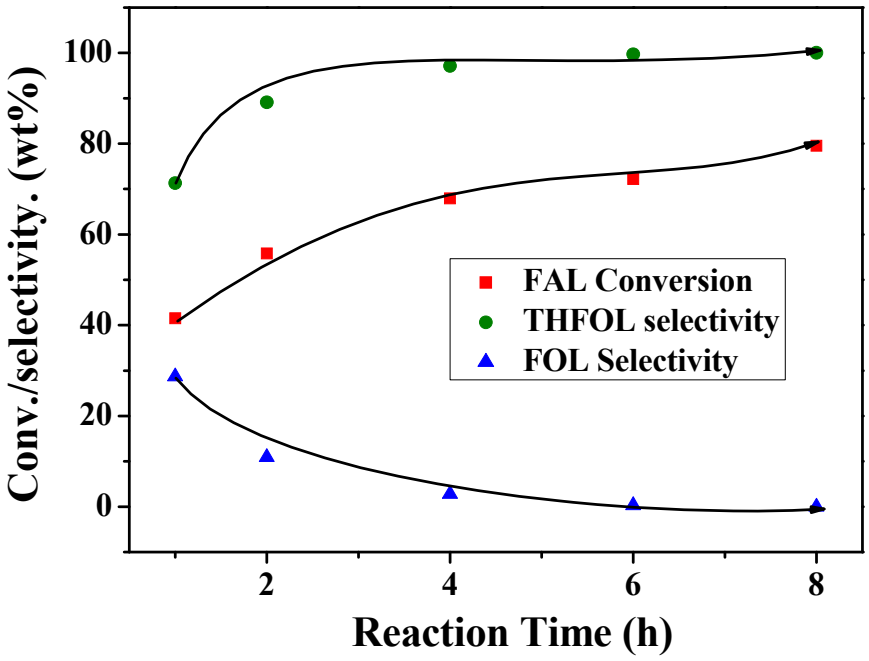

Fig. 6.8. Hydrogenation of FAL over Pd(5 wt%)/Al_2O_3 as a function of reaction time *Reaction conditions:* Furfural = 1g, catalyst = 0.05 g, temperature = 25 °C, solvent (iso-propanol) = 20 g, reaction time = 8 h, stirring speed = 600 rpm. Prior to the reaction, catalyst was reduced under H_2 (30 ml/min) flow at 250 °C.

Table 6.4. Temperature effect on hydrogenation of furfural over Pt/Al_2O_3 catalysts

Temp(°C)	FAL	Product Selectivity (%)				
	Conv. (wt %)	FOL	THFOL	2-Me-Furan	Furan	Others
25	17.5	100	0.0	0.0	-	0.0
60	45.7	98.1	0.0	0.0	-	1.9
90	52.1	97.4	0.0	0.0	-	2.6
120	75.5	95.5	0.0	0.0	-	4.5
120[a]	95.5	95.0	0.0	0.0	0.0	5.0
180	91.0	89.1	0.9	2.6	5.5	1.9
210	97.2	81.4	0.6	2.9	9.7	5.4
240	100	30.7	0.7	6.0	50.4	12.2

Reaction conditions: Furfural = 1 g, solvent (iso-propanol) = 20 g, catalyst Pt(5 wt%) /Al_2O_3) = 0.05 g, reaction time = 5 h, H_2 pressure = 20 bar, stirring speed = 600 rpm. Prior to reaction, catalyst was reduced under H_2 (30 ml/min) flow at 350 °C.
[a] Reaction time 10 h.

6.3.2.4. Effect of Solvent Mixture. Decarbonylation of furfural was conducted in iso-propanol, iso-propanol - de-ionized water (1:1, 2:1 and 4:1 weight ratio), toluene and toluene - de-ionized water (4:1 weight ratio) medium. As noted from Table 6.5, when water was added to the reaction mixture, the side reactions were suppressed and furan formed selectively. A significant enhancement in catalytic activity was observed for both Pd and Pt catalysts at 240 °C (Table 6.5). In case of Pt/Al_2O_3 catalysts, conversion and selectivity increased from 43.5 to 93.5% and 18.2 to 76.5% respectively, whereas on Pd/Al_2O_3, they increased from 77.7 to 99.7 % and 71 to 82.2% respectively, in 2 h under N_2 pressure. In the case of toluene-water medium, conversions were poor but selectivity of furan was higher. Among different composiotion, iso-propanol : water in 4:1 weight ratio showed higher catalytic activity and furan selectivity (Table 6.5).

6.3.2.5. Effect of Different Supports. Table 6.6 demonstrates the influence of support on the catalytic activity and product selectivity. Pt(5 wt%) supported on SO_4-ZrO_2, Al_2O_3, MgO, CeO_2-ZrO_2 and SiO_2 have been investigated. Al_2O_3 was found to be the best support. Over $Pt(5\%)/Al_2O_3$, furfural conversion of 30 wt% with FOL selectivity of 99.1% was obtained at 25 °C and at the end of 8 h while these conversions were only 10, 6, 2.1 and 23.9% on Pt(5 wt%)/SO_4-ZrO_2, Pt(5 wt%)/SiO_2, Pt(5 wt%)/MgO and Pt(5 wt%)/CeO_2-ZrO_2, respectively; FOL was the selective product with all these catalysts. Although, FAL conversion was 100% at 240 °C over all these catalysts, FOL is the major product over Pt supported on SiO_2, MgO and CeO_2-ZrO_2 whereas furan compounds (furan and 2-Me-Furan) were the major products over Pt supported on Al_2O_3 and SO_4-ZrO_2. Selectivity for furan compounds more than 56% was obtained over these two catalysts.

The supported Pd exhibited 100% selectivity for hydrogenation of furan to THF at 25 °C and 60 bar H_2 pressure (Table 6.7). Pd(5 wt%) supported on alumina was found to be better catalyst than that supported on ZrO_2, CeO_2, and CeO_2-ZrO_2. Pt(5 wt%)/Al_2O_3 exhibited lower conversion and selectivity for THF compared to Pd(5 wt%)/Al_2O_3. Over Pd(2 wt%)/Al_2O_3, furan conversion of 54.4 wt% and THF selectivity of 100% was obtained within 1 h of reaction time while Pd(2 wt%) supported on CeO_2, ZrO_2 and CeO_2-ZrO_2 gave furan conversions of 19.9, 25 and 20.5 wt%. respectively.

Table 6.5. Solvent effect on furfural decarbonylation

Run. no	Solvent	FAL Conv (wt%)	Product Selectivity			
			FOL	Furan	Others	Mass balance %
Pd(5 wt%)/Al_2O_3 & under 5 bar N_2 Pressure						
1	iso-Propanol	77.7	29	71	0.0	89.2
2	H_2O	35.1	0.0	100	0.0	85.0
3	iso-Propanol & H_2O (4:1)	99.7	17.9	82.2	0.0	86.2
4	iso-Propanol & H_2O (2:1)	60	8.2	82.6	9.2	87.5
5	iso-Propanol & H_2O (1:1)	30.0	0.0	83.3	13.2	88.0
6	Toluene	3.6	0.0	100	0.0	92.1
7	Toluene & H_2O (4:1)	50.3	0.0	100	0.0	90.1
Pt(5 wt%)/Al_2O_3 & under 5 bar N_2 pressure						
8	iso-Propanol	43.5	48.5	18.2	33.3[a]	89.5
9	H_2O	29.2	0.0	43.1	56.8	87.1
10	iso-Propanol & H_2O (4:1)	93.5	0.0	76.5	23.5	87.3
11[d]	iso-Propanol & H_2O	19.8	93.4	6.6	0.0	89.3
Pt(5 wt%)/Al_2O_3 & under 20 bar H_2 pressure						
12	iso-Propanol & H_2O (4:1)	100	18.6	53.0	15.6, 1.5[a], 11.3[b]	94.5
13[e]	iso-Propanol & H_2O (4:1)	100	0.0	2.3, 5.1[c]	17.3[a], 75.2[b]	92.6

Reaction conditions: Furfural = 1 g, catalyst = 0.05 g, temperature = 240 °C, reaction time = 2 h, stirring speed = 600 rpm. Prior to the reaction, Pd and Pt catalysts were reduced under H_2 (30 ml/min) flow at 250 °C and 350 °C respectively. Others include cyclopentanone, 2-methyl furan and n-butanol.

[a]1, 2-Pentanediols, [b]Butanol, [c]Tertahydrofuran, [d]Run without catalyst, [e]Reaction time = 5 h.

Table 6.6. Influence of support and temperature on hydrogenation of furfural

Catalyst	Reaction time 8 h at 25 °C				Reaction time 5 h at 240 °C					
	FAL Conv. (wt%)	Product selectivity (%)			FAL Conv. (wt %)	Product selectivity (%)				
		FOL	THFOL	Others		FOL	THFOL	2-Me-Furan	Furan	Others
Pt (5 wt%)/Al_2O_3	30.0	99.1	0.9	0.0	100	30.7	0.7	6.0	50.4	12.2
Pt (5 wt%)/Sul-ZrO_2	10	99.6	0.4	0.0	100	55.8	0.43	18.7	16.1	8.4
Pt (5 wt%)/Sul-ZrO_2	-	-	-	-	100[a]	3.8	0.0	47.2	33.3	15.7
Pt (5 wt%)/Sul-ZrO_2	-	-	-	-	38.2[b]	45.5	0.0	33.6	20.8	0.0
Pt (2 wt%)/ Sul-ZrO_2	-	-	-	-	95.0	66.4	0.0	4.3	24.6	4.6
Pt (5 wt%)/SiO_2	6.0	100	0.0	0.0	100	51.9	0.5	4.9	38.9	3.8
Pt (5 wt%)/MgO	2.1	100	0	0.0	100	66.1	0.3	5.8	24.0	3.8
Pt (5 wt%) /CeO_2-ZrO_2	23.9	100	0.0	0.0	100	70.3	0.3	3.0	25.2	1.3

Reaction conditions: Furfural = 1 g, solvent (iso-propanol) = 20 g, H_2 pressure = 20 bar, catalyst = 0.05 g, stirring speed = 600 rpm. Prior to the reaction, catalyst was reduced under H_2 flow (30 ml/min) at 350 °C.

[a] Reaction time 8 h. [b] Solvent = Toluene.

Table 6.7. Hydrogenation of furan to THF over supported Pd catalyst

Catalyst	H_2-Pressure (bar)	Conv. (wt%)	Product selectivity (%)	
			THF	Others
Pd(2 wt%)/CeO_2	60	19.9	100	0.0
Pd(2 wt %)/CeO_2-ZrO_2	60	20.5	100	0.0
Pd(2 wt %)/ZrO_2	60	25.0	100	0.0
Pd(2 wt %)/Al_2O_3	60	54.4	100	0.0
Pd(5 wt %)/Al_2O_3	60	100	100	0.0
Pd(5 wt %)/Al_2O_3	40	51	100	0.0
Pd(5 wt %)/Al_2O_3	20	40	100	0.0
Pt(5 wt %)/Al_2O_3	60	21.5	82.0	18.0

Reaction conditions: Furan = 2 g, catalysts = 0.05 g, temperature = 25 °C, solvent (iso-propanol) = 40 ml, reaction time = 1 h, stirring speed = 600 rpm. Prior to the reaction, catalyst was reduced under H_2 flow (30 ml/min) at 250 °C.

6.3.3. Recyclability Test

Recyclability of Pd(5 wt%)/Al_2O_3 in decarbonylation of furfural to furan and hydrogenation of furan to tetrahydrofuran (THF) was investigated (Fig. 6.9).

6.3.3.1. Catalyst Recyclability Study for FAL to Furan. 0.250 g of reduced Pd(5 wt%)/γ-Al_2O_3 was transferred into a 300 ml Parr reactor containing 5 g of furfural, 100 g of iso-propanol and 25 g of de-ionized water and then, the reactor was pressurized with nitrogen to 10 bar. The reaction was conducted for 2 h at 240 °C. Then the reactor was cooled to 25 °C, it was depressurized and the solid catalyst was separated and reused in the next cycle without any activation. Such reuses of the catalyst were done for 3 times and then in the subsequent recycles the catalyst was washed with acetone, dried at 110 °C and reused. The liquid product was analyzed by gas chromatorgraphy. It is interesting to note that there is little loss in conversion and product selectivity (Fig. 6.9 (a)). Washing of the catalyst with acetone slightly improved furan selectivity.

6.3.3.2. Catalyst Recyclability Study for Furan to THF. 0.100 g of freshly reduced Pd(5 wt%) /γ-Al_2O_3 catalyst was transferred into a 100 ml Parr reactor containing 4 g of furan and 40 ml of iso-propanol. The reactor was pressurized to 60 bar with H_2 gas. Reaction was conducted for 1 h at 25 °C. Then the rector was depressurized, catalysts was separated from the liquid products and then reused in subsequent recycles without subjecting it to any further washing or activating steps. This catalyst was used in six recycling experiments. As seen from Fig. 6.9(b), no loss in catalytic activity and THF selectivity was observed. These experiments, thus, reveal that the catalyst is recyclable.

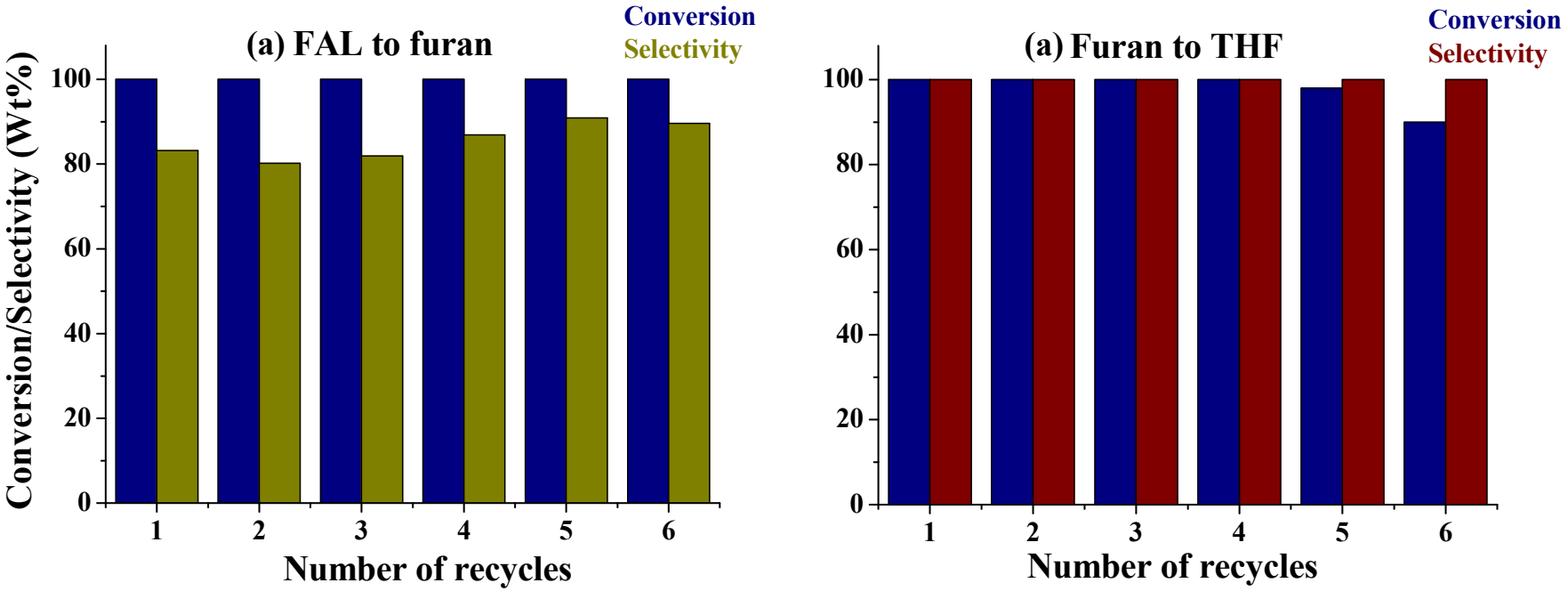

Fig. 6.9. Catalyst stability test on Pd(5 wt%)/Al_2O_3 catalysts

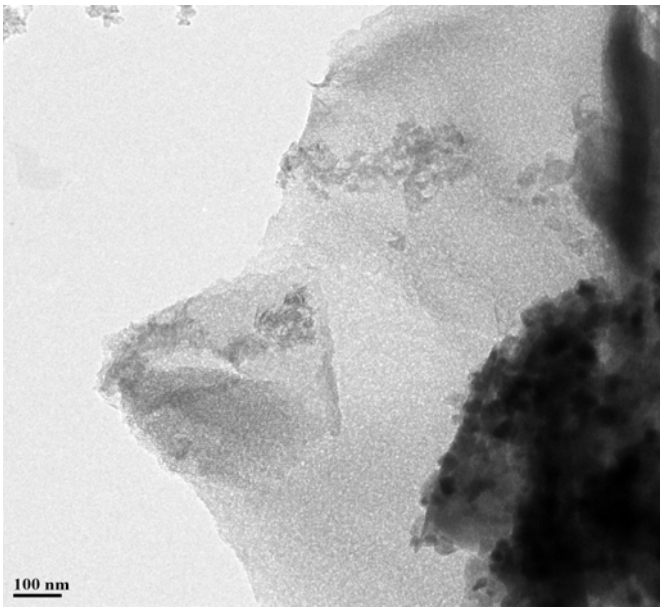

Fig. 6.10. HRTEM image of spent-Pd(5 wt%)/Al_2O_3 catalyst

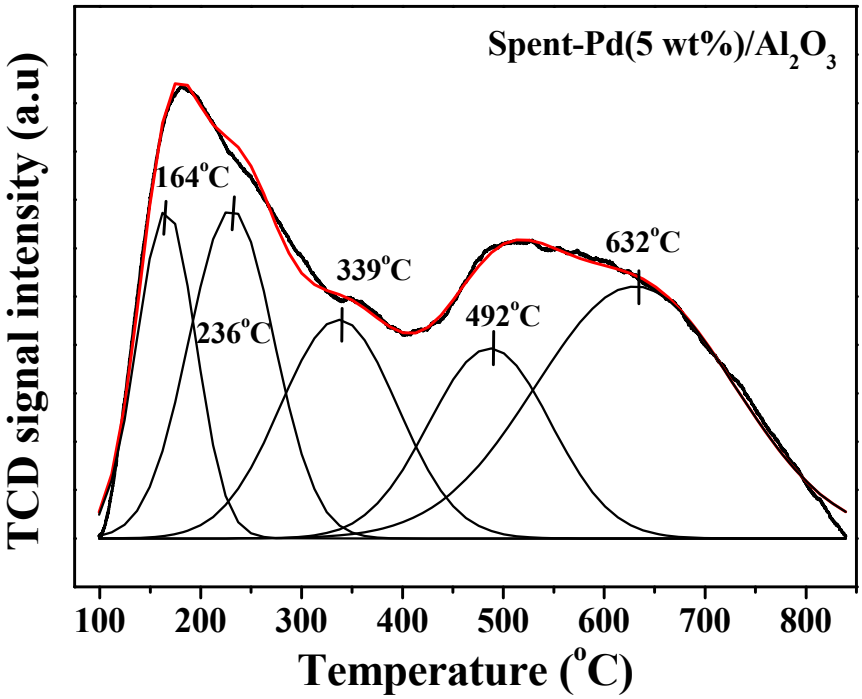

Fig. 6.11. NH_3-TPD profile of spent-Pd(5 wt%)/Al_2O_3

In order to assess the stability of the catalyst, the spent catalyst, Pd(5 wt%)/Al_2O_3 used in decarbonylation of furfural was characterized by ICP-OES, XRD, HRTEM, N_2-physisorption and NH_3-TPD. Metal estimation by ICP-OES revealed a decrease in Pd content from 4.7 wt% (in fresh catalyst) to 3.7 wt% (in the spent catalyst; Table 6.1). The XRD profile of the spent catalyst is similar to that of the fresh catalyst except that the intensities of the peaks were lower (Fig. 6.1). The average crystallite size of Pd decreased from 8.1 (for fresh catalyst) to 7.4 nm (for spent catalyst; Table 6.1). HRTEM image of the spent catalyst (Fig. 6.10) indicated the presence of some carbon material (EDAX) covering the metal particles. Upon use, the S_{BET} of the catalyst increased from 68 to 311 m^2/g (Table 6.1). A decrease in total acidity from 1.832 to 1.236 mmol/g was observed for the spent catalyst (Fig. 6.11 and Table 6.1). These studies thus, reveal that there is some loss the chemical integrity of the catalyst. Presence of carbonaceous matter could be the cause for the lower apparent values of the metal content and acidity and also for the lower intensity of XRD peaks.

6.4. Structure-Activity and Correlations

6.4.1. Selective Hydrogenation of FAL to FOL & THFOL

Hydrogenation of furfural to FOL and THFOL is reported for first time over Pd and Pt supported on Al_2O_3 at 25 °C under 20-60 bar hydrogen pressure. The supported Pd was more active than the supported Pt catalysts. Iso-propanol was found to be the best solvent for the high solubility of hydrogen in it [22]. It is known that this reaction is first order with respect to hydrogen pressure and zero order with respect to furfural [23]. Furfural can get activated on the metal either through η^1 or η^2 coordination modes. While the adsorption through η^1 mode is preferred on first-row Cu, η^2(C,O) coordination is preferred on Pd(111) and Pt(111) surfaces (Fig 6.12) [22]. In the case of platinum, hydrogenation of carbonyl group is more facile than the furan ring due to large d-band width of the metal and stronger four electronic repulsive interactions between the furan ring (C=C) π-electrons and metal d-electrons [24, 25]. The lesser d-band width of Pd compared to Pt favours closer interaction with furan ring (C=C) π-electrons so that THFOL formed as major product. At the end of 8 h, FAL conversion over these catalysts increased in the order of : Pd(2 wt%)/Al_2O_3 (22.1%) < Pd(5 wt%)/Al_2O_3 (48.5%) < Pd(10 wt%)/Al_2O_3 (61.6%); and the selectivity for THFOL increased in the order of : Pd (2 wt%)/Al_2O_3 (55.7%) < Pd (5 wt%)/ Al_2O_3 (79.7%) > Pd(10 wt%)/Al_2O_3 (58.9%). With increasing hydrogen pressure, solubility of hydrogen in IP solvent increased and hence, raise in catalytic activity of Pd was observed.

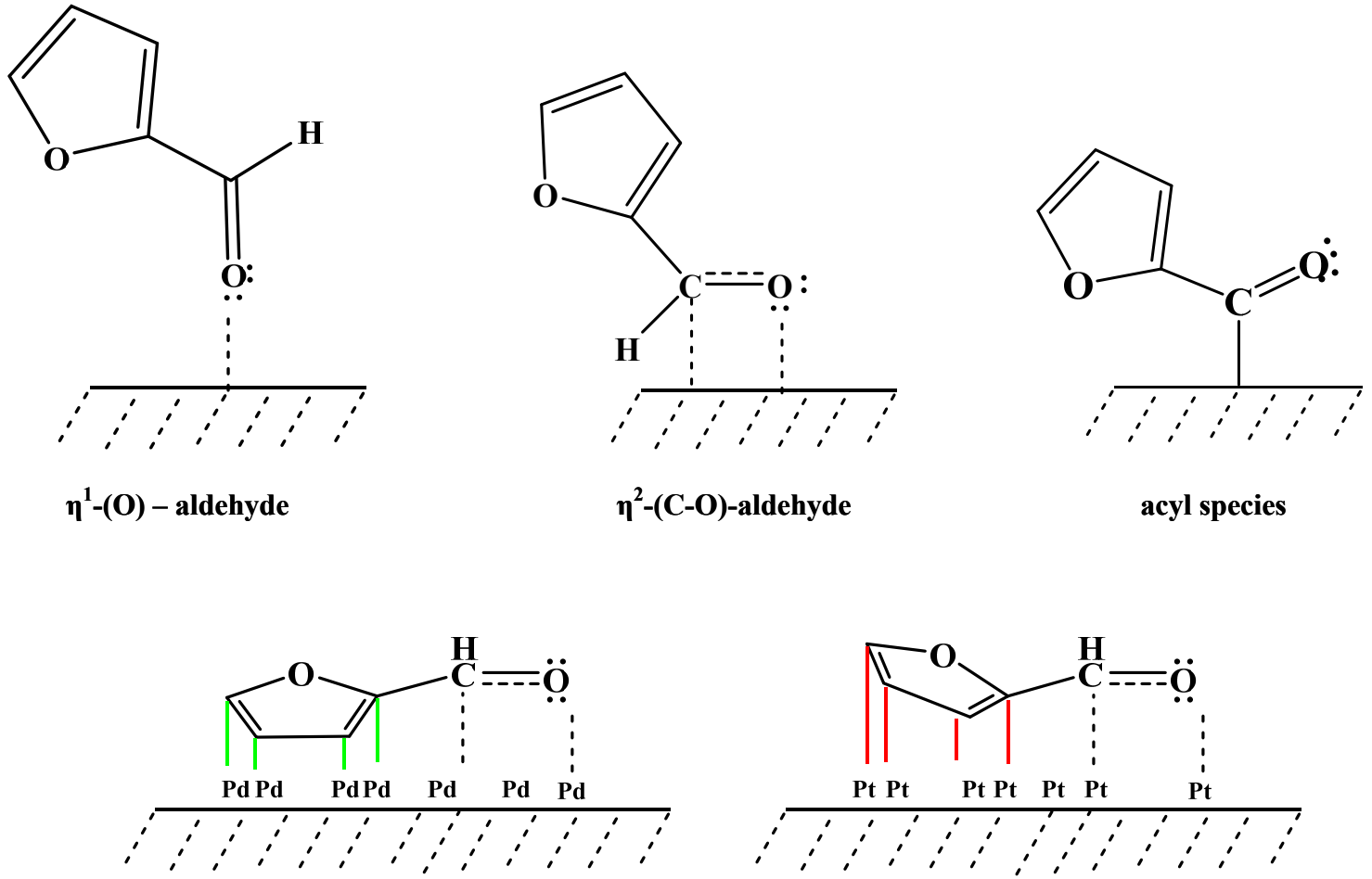

Fig. 6.12. Mode of adsorption of FAL on supported metal catalysts

Pd(5 wt%)/Al_2O_3 having high metal dispersion, higher acidity and higher support-metal interaction exhibited enhanced selectivity for THFOL (100 %) at a hydrogen pressure of 60 bar and 25 °C. Hydrogenation of furfural takes place even in the absence of external hydrogen supply. The solvent – isopropanol acts as a source for hydrogen which in turn hydrogenated furfural. At 240 °C and inert atmosphere, FAL conversions of 43.5 and 77.7 wt% and FOL selectivity of 48.5 and 29 wt% were achieved over Pt(5 wt%)/Al_2O_3 and Pd(5 wt%)/Al_2O_3. To the best of knowledge this is the first report on hydrogenation of furfural under inert atmospheric conditions over Al_2O_3-supportd Pt and Pd catalysts.

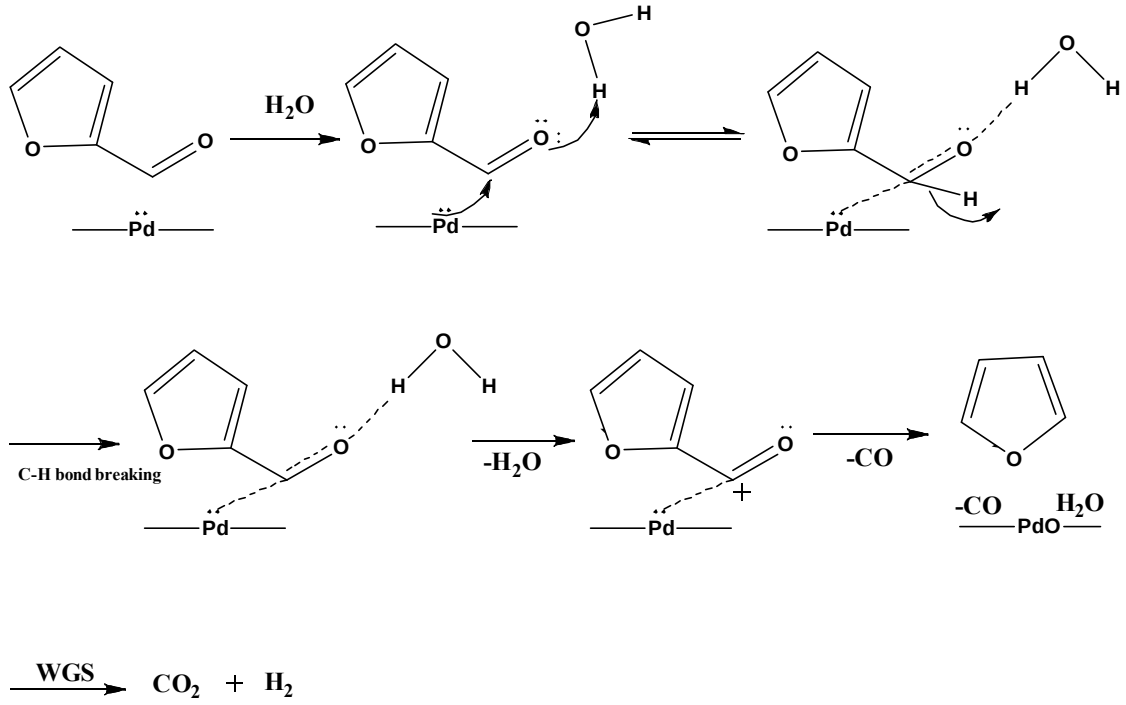

Scheme 6.2. Reaction mechanisam of furfural decarbonylation

6.4.2. Decarbonylation and Hydrogenation of Furfural

Decarbonylation reaction takes places at 180 °C and above. Higher yields of furan were obtained at 240 °C. Isopropanol-water was found to be the best solvent. Water suppressed hydrogenation reaction and promoted the selectivity for decarbonylation leading to furan. This reaction occurs without using any external hydrogen. Pushkarev et al [26] reported that Pt with 1.5 nm size particles are very selective for decorbonylation of FAL. But the conversions reported were low even at 220 °C and 0.93 bar H_2 pressure. Water polarizes the carbonyl group through formation of H-bond. The carbonyl group is activated on Pd(111) surface. C-H bond cleavage on metal surface forms an unstable acyl intermediate (Fig. 6. 12

and Scheme 6.2) which upon decomposition yields furan and CO. Water-gas shift reaction on Pd surface converts CO to CO_2. No deactivation of Pd/Al_2O_3 catalysts was observed as a consequence of this water-gas shift reaction. The supported Pd catalysts were reusable in several recycling experiments. $Pd(5\ wt\%)/Al_2O_3$ was highly active for hydrogenation of furan to THF at 25 °C and 60 bar hydrogen pressure (Table 6.7). Acidity of the support has a major influence on the hydrogenation activity.

6.5. Conclusions

Liquid-phase hydrogenation, decarbonylation and hydrogenolysis of furfural were investigated over Pd and Pt supported on Al_2O_3 catalysts. $Pt(5\ wt\%)/Al_2O_3$ was highly selective for production of furfuryl alcohol while $Pd(5\ wt\%)/Al_2O_3$ yielded tertahydrofurfuryl alcohol at 25 °C and 60 bar H_2 pressure. Decarbonylation is a prominent reaction at temperatures above 180 °C. $Pd(5\ wt\%)/Al_2O_3$ was found superior to $Pt(5\ wt\%)/Al_2O_3$. Isopropanol-water was found to be a better solvent mixture. This reaction occurs without the need of any external hydrogen. While isopropanol acts as a source for hydrogen, water suppressed undesired hydrogenation and facilitated formation of furan. Acidity, metal dispersion and solvent played an important role on the activity of supported Pd catalysts. The formed furan can be hydrogenated to THF at 25 °C over the same supported Pd catalyst.

6.6. References

[1] http://www.osti.gov/bridge/servlets/purl/885984-pH60fj

[2] 1, 2, The chemistry and technology of furfural and its many by-products, Vol. 13, 1st Ed., Elsevier, Amsterdam (2000) 34-69, Sugar Series

[3] K. An, N. Musselwhite, G. Kennedy, V. V. Pushkarev, L. Robert Baker, G. A. Somorjai, J. of Coll. and Inter. Scien. 392 (2013) 122.

[4] S.Sitthisa, D. E. Resasco, Catal Lett, 141 (2011) 784.

[5] R. S. Rao, R. T. K. Baker, M. A. Vannice, Catal. Lett. 60 (1999) 51.

[6] L. Baijun, L. Lianhai, W. Bingchun, C. Tianxi, K. Iwatani, Appl. Catal. A 171 (1998) 117.

[7] K. Chen, S. Koso, T. Kubota, Y. Nakagawa, K. Tomishige, ChemCatChem 2 (2010) 547.

[8] X. Chen, W. Sun, N. Xiao, Y. Yan, S. Liu, Chem. Eng. J. 126 (2007) 5.

[9] W. –L. Wei, H.-Y. Zhu, C.-L. Zhao, M.-Y. Huang, Y.-Y. Jiang, React. Funct. Polym. 59 (2004) 33.

[10] F.-A. Khan, A. Vallat, G. Süss-Fink, Catal. Commun. 12 (2011) 1428.

[11] N. Merat, C. Godawa, A. Gaset, J. Chem. Technol. Biotechnol. 48 (1990) 145.

[12] Y. Nakagawa, K. Tomishige, Catal. Commun. 12 (2010) 154.

[13] G. Seo, H. Chon, J. Catal. 67 (1981) 424.

[14] W. Zhanga, Y. Zhua, S. Niua, Y. Li, Journal of Molecular Catalysis A: Chemical. 335 (2011) 71.

[15] C. D. Hurd, A. R. Goldsby and E. N. Osborne, J. Am. Chem. Soc. 54 (1932) 2532.

[16] L. K. Ono, B. Yuan, H. Heinrich and B. R. Cuenya, J. Phys. Chem. C. 114 (2010) 22119.

[17] J.R. Croy, S. Mostafa, L. Hickman, H. Heinrich, B. R. Cuenya, Appl. Catal. A: Gen., 350 (2008) 207.

[18] M. Dömök, A. Oszkó, K. Baán, I. Sarusi, A. Erdöhelyi, Appl. Catal. A: Gen. 383 (2010) 33.

[19] S. Bhogeswararao, D. Srinivas, Journal of Catalysis 285 (2012) 31.

[20] S. Chandra Shekar, J. Krishna Murthy, P. Kanta Rao, K.S. Rama Rao, Journal of Molecular Catalysis A: Chemical 191 (2003) 45.

[21] N. W. Hurst, S. J. Gentry, A. Jones, B. D. Mcnicol, Catal. Rev. -Sci. Eng. 24 (1992) 233.

[22] A. T. Manoj, V. M. Vijaykumar, Ind. Eng. Chem., Res. 46 (2007) 3275.

[23] Y. Nakagawa, H. Nakazawa, H. Watanabe, and K. Tomishige, ChemCatChem 4 (2012) 1791.

[24] P. Sautet and J.F. Paul, Catal Lett. 9 (1991) 245.

[25] F. Delbecq, P. Sautet J. Catal. 152 (1995) 217.

[26] V. V. Pushkarev, N. Musselwhite, K. An, S. Alayoglu, G. A. Somorjai, Nano Lett., 12 (2012) 5196.

Chapter 7

Overall Summary and Conclusions

Catalytic hydrogenation is an important and widely investigated reaction in organic synthesis and in the manufacture of industrial chemicals. Although much understanding of the fundamentals and applications has been achieved, development of controlled/selective hydrogenation catalysts that operate at mild to moderate conditions is still a challenging task in this area of research. The effects of method of preparation, support-metal interactions, co-metals, additives, solvent etc on the activity and selectivity of noble metal catalysts is yet to be fully understood. The work presented in this thesis has addressed some of these aspects. Chemoselective transformation of two industrially important reactions, 1) hydrogenation of cinnamaldehyde (a representative α, β-unsaturated aldehyde) and 2) hydrogenation/hydrogenolysis/decarbonylation of furfural (a biomass-derived compound) to value-added chemicals have been investigated using supported Pt and Pd catalysts. CeO_2-ZrO_2 compositions and γ-Al_2O_3 were used as catalyst supports in these transformations, respectively. The supported noble metal catalysts were prepared by impregnation method. The methodology of the synthesis and the physicochemical techniques used for characterization of the metal catalysts were described in detailed in **Chapter 2**.

Chapters 3, 4 and 5 described liquid-phase hydrogenation of cinnamaldehyde (CA) over CeO_2-ZrO_2-supported Pt, Pd and Pt/Pd promoted Ni catalysts, respectively. CA was chosen as a representative α, β-unsaturated aldehyde. It is the main component of cassia (~90%) and ceylon cinnamon bark oils (~75%). It is present in smaller quantities in many other essential oils. In addition to its application in perfume and flavor industries, cinnamaldehyde is used as a starting material to produce valuable chemicals. CA has two functional groups (olefinic C=C and carbonyl C=O) in conjugation in its structure. Hydrogenation of CA yields a number of products including cinnamyl alcohol (CAL), hydrocinnamaldehyde (HCA) and 3-phenylpropanol (PPL). Condensation products like acetals are also formed. Cinnamyl alcohol (an unsaturated alcohol) has many applications, particularly in perfumery industry because of its odour characteristic properties. Moreover, cinnamyl alcohol is an important building block in organic synthesis. It is also an intermediate in the synthesis of pharmaceuticals, such as the antibiotic chloromycetin. Hydrocinnamaldehyde was found be an important intermediate in the preparation of a drug used in the treatment of HIV. Production of cinnamyl alcohol via selective hydrogenation is a difficult task as thermodynamics favour the formation of saturated aldehyde to unsaturated alcohol. Although, hydrogenation of C=C compared to C=O is easy, development of still more efficient

catalysts that operate at moderate conditions is also desirable. In view of this, the catalytic activities of supported Pt, Pd and Pt/Pd promoted Ni catalysts for this hydrogenation have been investigated for the first time in this thesis.

CeO_2-ZrO_2-supported Pt(5 wt%) catalysts were found highly active even at room temperature (25 °C) and yielded CAL, the unsaturated alcohol with selectivity as high as 97.3 wt% (**Chapter 3)**. Catalytic efficiency of this supported Pt catalyst is superior to the hitherto known Pt catalysts. CeO_2-ZrO_2-supported Pd(2 wt%) were active above 50 °C and showed selectivity mainly to saturated aldehyde (HCA; **Chapter 4**). Molar composition of CeO_2 and ZrO_2 in the support influenced the catalytic activity and HCA selectivity of Pd to some extent. ZrO_2 and CeO_2-ZrO_2-supported Ni(5 wt%) exhibited high activity above 100 °C and selectivity for HCA product (100 wt%). The Pt/Pd (0.5 wt%) promoted Ni(5 wt%) catalysts showed enhanced catalytic activity and selectivity mainly to PPL product at the end of 8 h of reaction (**Chapter 5**). The Ni catalysts of this investigation showed higher activity than the known Ni catalysts for selective hydrogenation of olefinic bonds. The study revealed that catalytic efficiencies of the catalysts of this study for hydrogenation of CA varied in the order: Pt(5 wt%)/CeO_2-ZrO_2 > Pd(2 wt%)/CeO_2-ZrO_2 > Ni(5 wt%)/CeO_2-ZrO_2. Also the selectivity for C=O hydrogenation decreased in the same order. The supportd Ni catalysts showed highest selectivity for C=C hydrogenation forming mainly HCA. Thus, type of metal influenced hydrogenation activity and selectivity.

Alkali addition to the reaction mixture enhanced catalytic activity of the supported metals to a significant extent. In the case of supported Pd caalysts, alkali addition shifted the hydrogenation activity from C=C to C=O. Further, alkali addition reduced for formation of undesired acetal products. Alkali activates the C=O group of α, β-unsaturated aldehydes and facilitates hydrogenation yielding unsaturated alcohols (CAL). The enhanced activation of C-O bond could be interpreted by the polarization of C=O bond resulting from the interaction of the alkali cation with the lone-pair electrons of the oxygen atom of the C-O group. These unsaturated alcohols (CAL) were further hydrogenated to saturated alcohols (PPL) in presence of Pd(2 wt%)/CeO_2-ZrO_2 catalyst by 1, 4 addition. Finally, the saturated alcohol (PPL) percentage increased with increasing alkali percentage. Alkali ions have suppressed the acidity of the support and thereby, decreased for formation of other products. Pd catalysts are known for selective hydrogenation of C=C. However, this study demonstrated, for the first time, that by

adding a small quantity of alkali, the electronic and redox properties of Pd could be fine-tuned and the selectivity for hydrogenation (between C=C and C=O of CA) could be controlled/altered.

Solvents showed a marked effect on catalytic activity. Ethanol and iso-propanol having higher values of Gutmann's acceptor number (AN) and high miscibility in water were found to be suitable solvents for high catalytic activity. Acetonitrile, in spite of being more polar and miscible with water, has lower value of AN. Hence, it was not of good choice. Further, the concentration of dissolved H_2 is the crucial parameter that determined the reaction rate.

Metal selectivities could be rationalized in terms of the radial expansion of d bands; the larger the band, stronger would be the four-electron repulsive interactions with the C=C bond and lower would be the probability of its adsorption. The d band width of different metals increases in the order: Ni < Pd < Pt < Ir, Os which accounts well for the selectivities observed over Ni, Pd and Pt catalysts of the present study. Larger crystals preferentially exposure the Pt (111) plane which facilitates adsorption of CA through η^1(C=O) coordination. On Pt (100), the adsorption is through both η^2(C=C) and η^1(C=O) modes. With increasing crystallite size, the fraction of steps and corners decreases and (111) planes are preferentially oriented. The particle size of Pt in the catalysts of present work was 5 – 12 nm. A few particles of 40 nm were also observed. As expected, (111) plane was more exposed and the Pt catalysts of this study were more selective for the CAL product. Polarization of C=O, high dispersion of the metal, high electron density, strong support-metal interactions and facile low-temperature reducibility are the unique features that made the supported noble metal catalyst of this work highly efficient and selective. Promotion of Ni with Pt enhanced the catalytic activity but did not alter its selectivity.

The catalytic activities of γ-alumina-supported Pt and Pd for transformation of furfural (FAL) to furfuryl alcohol (FOL), tetrahydrofurfuryl alcohol (THFOL), furan and tetrahydrofuran (THF) were investigated in **Chapter 6**. Like cinnamaldehyde, furfural is also having C=C (ring) and C=O functionalities. Pt(5 wt%)/Al_2O_3 was found highly selective for hydrogenation of C=O yielding mainly FOL. This reaction occurs at room temperature itself over the Pt catalysts of the present study. Pd(5 wt%)/Al_2O_3 was non-selective, hydrogenating both the ring and C=O groups. It yielded FOL and THFOL in near equal proportions. However, at 60 bar hydrogen pressure THFOL was the main product over the supported Pd catalyst. Both these product are of high value. FOL is widely used in polymers, fine chemicals, and farm chemicals. THFOL is preferred as a green solvent in the pharmaceutical industry and also used as significant intermediate

chemical in various industrial and agricultural fields. The supported Pd catalyst was found to be more active than the Pt catalyst for decarbonylation and hydrogenolysis (or deoxygenation) of FAL at temperatures above 180 °C. Furan and 2-methyl furan were the products of these reactions, respectively. Iso-propanol-water solvent mixture has a pronounced effect on the selectivity for furan and suppression of ring opened products. Interestingly, this reaction takes place even without the use of hydrogen. Among SO_4-ZrO_2, Al_2O_3, MgO, CeO_2-ZrO_2 and SiO_2, alumina showed superior performance as a support. Furan was hydrogenated to THF again at room temperature (60 bar hydrogen pressure) over Pd(5 wt%)/Al_2O_3 catalyst. THF yields of 100 wt% were obtained. The Pd catalyst was reusable in seven recycling experiments. High metal dispersion, acidity and support-metal interactions were found to be the cause for the high activity of Pd/Al_2O_3 catalyst in furan and THF formation reactions.

By and large, this thesis reports some novel supported noble metal catalysts for chemoselective hydrogenation of cinnamaldehyde and furfural. Factors influencing activity and selectivity of these catalysts were probed using a variety of characterization technique. This study advances the knowledge on hydrogenation reactions and contributes to the area of green and sustainable chemistry.

List of Publications

1. Chemoselective hydrogenation of cinnamaldehyde over Pd/CeO_2–ZrO_2 catalysts
   S. Bhogeswararao and D. Srinivas
   Catal. Lett. 140 (2010) 55 - 64.
2. Intramolecular selective hydrogenation of cinnamaldehyde over CeO_2–ZrO_2-supported Pt catalysts
   S. Bhogeswararao and D. Srinivas
   J. Catal. 285 (2012) 31 - 40.
3. Catalytic activity of ZIF-8 in the synthesis of styrene carbonate from CO_2 and styrene oxide
   Minqi Zhu, Darbha Srinivas, **Seemala Bhogeswararao**, Paul Ratnasamy and Moises A. Carreon
   Catal. Comm. 32 (2013) 36 - 40.
4. Noble metal promoted CeO_2-ZrO_2-supported Ni catalysts for liquid-phase hydrogenation of cinnamaldehyde
   S. Bhogeswararao, V. Pavan Kumar, K.V.R. Chary and D. Srinivas
   Catal. Lett. 143 (2013) 1266 - 1276.
5. Catalytic conversion of furfural over supported Pd and Pt catalysts
   S. Bhogeswararao and D. Srinivas
   To be communicated.

List of Patents

1. Process for preparing tetrahydrofuran
   Darbha Srinivas and **Seemala Bhogeswararao**
   India and PCT (NCL No. 2013-NCL-0088; Appln. No. 1868/DEL/2013, CSIR No. 2013-NF-0130).
2. Process for producing furan
   Darbha Srinivas and **Seemala Bhogeswararao**
   India and PCT (NCL No. 2013-NCL-0087, Appln. No. 1869/DEL/2013, CSIR No. 2013-NF-0129).